TRANSMISSION LINE PROTECTION AND FAULT LOCATING BASED ON DYNAMIC STATE ESTIMATION

A Dissertation
Presented to
The Academic Faculty

by

Yu Liu

In Partial Fulfillment
Of the Requirements for the Degree
Doctor of Philosophy in the
School of Electrical and Computer Engineering

Georgia Institute of Technology
August 2017

Transmission Line Protection and Fault Locating Based on Dynamic State Estimation

Approved by:

Dr. A. P. Meliopoulos, Advisor
School of Electrical and Computer Engineering
Georgia Institute of Technology

Dr. Thomas G Habetler
School of Electrical and Computer Engineering
Georgia Institute of Technology

Dr. Ying Zhang
School of Electrical and Computer Engineering
Georgia Institute of Technology

Dr. Maryam Saeedifard
School of Electrical and Computer Engineering
Georgia Institute of Technology

Dr. Andy Sun
School of Industrial and Systems Engineering
Georgia Institute of Technology

Date Approved: June 02 2017

To my beloved parents Baocheng, Yuanling and my wife Yiran

ACKNOWLEDGEMENTS

Ph.D study is a journey with ups and downs but also with valuable rewards. I am greatful that four years ago I made that right decision to pursue my Ph.D degree. This journey not only helped improve my academic skills, but also helped me become a better person. I would not have accomplished this without the help and support of countless people. I want to express my appreciation to all of them.

First, I would like to express my sincere gratitude to my advisor Dr. A. P. Sakis Meliopoulos. I could not have finished my Ph.D study without his patience, motivation and support. Dr. Meliopoulos is one of the smartest people that I've ever met. He is enthusiastic, sharp and extremely knowldegable. When dealing with a problem, he always guided me to understand the way of analyzing the problem instead of directly show me the conclusion. He helped me learn the most important thing during my Ph.D study: to use rigorous logic thinking to deal with all kinds of problems; specifically, all theories and applications are based on and can be proved by rigorous math derivations. Additionally, he provided me valuable opportunities to apply the knowledge I learnt to actual power systems, so I could have grounded understanding of how the power system works. Furthermore, when I told him that I would like to enhance my communicating and teaching skills, he kindly presented me the Teaching Assistant position for the course power system engineering, through which I really improved myself. I could not have imagined having a better advisor and mentor for my Ph.D. study.

I also would like to give my special thanks to Dr. George Cokkinides. He is indeed an expert in the area of power system, especially in software and hardware implementations of power system functions. He taught me many implementation details including phasor/sampled value protocols, GPS protocols and relay/device wiring, which helped connecting the ivory tower to the main street. Also, I learnt lots of hardware development skills which were and will be very valuable for my research.

Besides, I would like to express my appreciation to Dr. Guotong Zhou, the director of Georgia Tech Shanghai campus. She provided me the great chance to be a master student in Georgia Tech Shanghai campus so I could have the opportunity to be a visiting scholar in Georgia Tech and to prove my qualification as a Ph.D student to my advisor Dr. Meliopoulos. Also, I would like to thank her for giving advises and the support on my application to Ph.D studies in Georgia Tech.

In addition, I would like to thank the members of my committee, Dr. Thomas G Habetler, Dr. Maryam Saeedifard, Dr. Andy Sun and Dr. Ying Zhang. Their time, commitment and valuable feedback greatly contribute to the completion of my dissertation.

My sincere thanks also go to my fellow labmates in PSCAL (Power System Control and Automation Laboratory), including Dr. Renke Huang, Dr. Liangyi Sun, Dr. Rui Fan, Dr. Zhenyu Tan, Dr. Dongbo Zhao, Dr. Aniemi Umana, Dr. Yonghee Lee, Bai Cui, Sanghun Choi, Wenlu Fu, Boqi Xie, Chiyang Zhong, Yuan Kong, Yi Du as well as other lab students. Specifically, I would like to thank Dr. Renke Huang who led me to the right track of the research, Dr. Liangyi Sun who helped me with software programs, and Dr. Rui Fan who enlightened me with parameter identification ideas. Besides, I also would like to thank many other friends in Georgia Tech including Dr. Jiaming Li, Dr. Kai Ying, Dr. Hongteng Xu, Xiaochen Zhang, Xinwei Chen, Hao Wu, He Xiao and Zhen Wang for all their support and the fun we have had in the last four years.

Lastly, I would like to thank my family for all their love and encouragement. Specifically, I want to thank my parents Baocheng Liu and Yuanling Gu who raised me with a love of science and truth, for their unconditional love and support through all these years. Also, I would like to thank my loving wife Yiran An, for her great support and encouragement during hard times of my Ph.D. study and for always being there for me during the most difficult days.

TABLE OF CONTENTS

LIST OF TABLES

LIST OF FIGURES

SUMMARY

Transmission lines are important devices since they can transmit large amount of power over large distances. In the U.S., the voltage level of transmission line can vary from 69 kV up to 765 kV. The rated current can be up to several kA. The total length of the transmission line can also vary from several miles to several hundred miles. Sometimes a fault may occur inside a transmission line system. Without proper responses, the fault could potentially cause major damage (fire, explosion), power system stability issues and even a large-scale power outage. To prevent above issues, there are mainly two steps that the utilities need to do about this fault. First, the line with fault needs to be isolated from the rest of the system as soon as possible (transmission line protection). Second, the exact location of the fault needs to be identified to minimize the time searching for the fault (transmission line fault locating).

For the first step, nowadays the transmission lines are protected by numerical relays integrated with many legacy protection functions. The main challenges are: (a) the coordinations and the settings for the numerical relay functions are very complex, which increase the possibility of human error; and (b) for high impedance faults, the existing numerical relays would fail to detect them, or these faults will be detected with a relatively long delay. For the second step, legacy transmission line fault locating schemes are utilized to find the location of the fault. The main challenges are: (a) for fundamental frequency phasor based methods, the accuracy is limited due to phasor approximation and inaccurate modeling of transmission lines; (b) for traveling wave based methods, very high sampling rates are needed to ensure sufficient accuracy.

To solve above problems, **D**ynamic **S**tate **E**stimation (DSE) based algorithm is proposed. It utilizes a high-fidelity dynamic model of transmission lines and instantaneous measurements (sampled values). The DSE based algorithm is implemented in an object-oriented way. The device dynamic model of the component of interest is expressed in a standard syntax referred to as State Control and Parameter Algebraic Quadratic Companion Form (SCPAQCF). Subsequently, the method utilizes the device SCPAQCF object and the model of measurements to generate measurement SCPAQCF object. Finally, the computations are directly based on the measurement SCPAQCF object. Note that all of above applications, including EBP, EBFL and EBPI, utilize the SCPAQCF object.

Specifically, for protection application (Dynamic State **E**stimation **B**ased **P**rotection, **EBP**), the main idea is to monitor the consistency between the measurements and the dynamic model and quantify this consistency with the probability of goodness of fit (or confidence level). The fault is detected by a low confidence level, which indicates inconsistency between the measurements and the model. Simulation results prove the advantages of the proposed EBP method such as the simplified settings and the ability to reliably and quickly detect high impedance faults.

For fault locating application (Dynamic State **E**stimation **B**ased **F**ault **L**ocating, **EBFL**), the main idea is to treat the fault location as a parameter of the dynamic line model and estimate the fault location via a DSE algorithm. Simulation results prove the advantages of the proposed EBFL method such as improved accuracy of the estimated fault location compared to phasor based algorithms and relatively low sampling rate compared to traveling wave based methods.

Moreover, to ensure high fidelity models for EBP and EBFL, Dynamic State **E**stimation **B**ased **P**arameter **I**dentification (**EBPI**) during normal operating conditions of the transmission line is proposed to carefully validate the parameters of the interested transmission line. The high-fidelity dynamic model can be established by (a) physically measuring the average height of phase conductors and the average distance between phase conductors, and (b) estimate the total length of the line as the only parameter.

CHAPTER 1 Introduction

1.1 Problem Statement

Transmission lines are important components of modern power systems. Sometimes a fault may happen inside transmission lines, and there are mainly two necessary steps that the utilities should do about this fault. The first step is protection, which isolates the fault from the rest of the electrical network as soon as possible, to ensure personnel safety, minimize the damage to electric equipment and prevent power system stability issues. The second step is fault locating, which identifies the exact location of the fault, to minimize the time spend searching for the fault, reduce the overall outage time and reduce operating costs.

To protect classic transmission lines, legacy relaying protection schemes with high degree of sophistication have been designed. They trip the line if the calculated results enter the relay characteristics. Due to large number of different fault conditions, the relay characteristics need to be carefully designed with complex settings to cover all faults that may occur inside the line. Nevertheless, the relay characteristic does not precisely depict the entire fault zone. Additionally, complex settings and coordination among protection functions may cause possible improper actions. As a result, these schemes cannot guarantee 100% deopendability and security, especially when they are applied to high impedance faults. Moreover, legacy relaying protection schemes would encounter more challenges when dealing with complex transmission lines such as series compensated lines, since the continuity of inductive impedance through the line is interrupted by series capacitors.

To locate faults in two-terminal transmission lines, legacy fault locating techniques were introduced and can be mainly classified into two groups: fundamental frequency phasor based methods and traveling wave based methods. For the first group, the fault locating results may not be accurate for the following reasons: (a) the methods are based on fundamental frequency phasors; if the system experiences transients these methods are inaccurate; (b) some of the methods utilize a sequence line model which is an approximate model; (c) grounding of the line is typically neglected and this can generate errors depending on the fault type. For the second group, the disadvantages include: (a) traveling waves may not be reliably detected since the intensity of traveling wave highly depends on the fault initiation time; (b) the methods require special instrumentation since the usual CTs will filter out the high frequency content of traveling waves; (c) the accuracy of the fault locator highly depends upon the sampling rate of the measurements. Moreover, legacy fault locating schemes would encounter additional challenges when dealing with three-terminal lines. For fundamental frequency phasor based methods, the basic idea is to transform a three-terminal fault locating problem into a two-terminal fault locating problem, which would generate additional errors. For traveling wave based methods, the additional reflections and transmissions of the fault initiated waves at the tap point make it difficult to determine the arrival time of the wavefronts.

1.2 Research Objectives

The objective of the proposed research is to (a) develop a reliable scheme to quickly protect transmission lines from internal faults, with immunity to external faults; (b) for any internal faults, develop a fault locating scheme to accurately find the location of the fault.

To realize above objectives, a new **D**ynamic **S**tate **E**stimation (DSE) based algorithm is proposed. The algorithm requires a device dynamic model, a model of measurements and a dynamic state estimation process. The overall **D**ynamic **S**tate **E**stimation based algorithm is implemented in an object-oriented way. The device dynamic model of the component of interest is expressed in a standard syntax referred to as State Control and Parameter Algebraic Quadratic Companion Form (SCPAQCF). Afterwards, the method utilizes the device SCPAQCF object and the model of measurements to generate measurement SCPAQCF object. Finally, the computations are directly based on the measurement SCPAQCF object.

Specifically, for the protection application (Dynamic State **E**stimation **B**ased **P**rotection, **EBP**), the method finds internal faults by evaluating the consistency between the measurements and the dynamic model of the transmission line. The proposed **EBP** scheme has the following advantages: (a) it requires very few settings and no coordination with other relays; (b) it can be easily applied to both classic and complex transmission lines such as series compensated lines since it utilizes an object-oriented algorithm; (c) it can detect internal high impedance faults faster and more reliably than legacy schemes.

For the fault locating application (Dynamic State **E**stimation **B**ased **F**ault **L**ocating, **EBFL**), the method estimates fault location as a parameter of the dynamic model of transmission line. The proposed **EBFL** can be applied to both two-terminal and three-terminal transmission lines. It has the following advantages: (a) it uses a high fidelity physically based three phase dynamic model with explicit grounding representation; (b) it utilizes instantaneous values instead of phasors; (c) it only requires relatively low sampling rate; (d) it has higher accuracy than legacy fault locating schemes.

Furthermore, to build high-fidelity dynamic models for EBP and EBFL applications, parameters of the components of interests are carefully identified during normal operating conditions (Dynamic State **E**stimation **B**ased **P**arameter **I**dentification, **EBPI**). These parameters are selected based on the physical structure of the transmission line, including the total length of the transmission line, the average distance between phase conductors and the average height of phase conductors. The dissertation proves that the high-fidelity dynamic model can be established by physically measuring the distance and the height parameter on the tower, and estimate the total length of the line as the only parameter.

1.3 Thesis Outline

The outline of the remaining parts of this dissertation is as follows.

Chapter 2 presents a thorough literature survey on transmission line legacy protection schemes and legacy fault locating schemes. For legacy protection schemes, the dissertation first describes classic protection schemes for transmission lines and their limitations; second, the additional challenges on complex transmission lines such as series compensated lines are explained in detail. For legacy fault locating schemes, the dissertation first demonstrates the fault locating schemes on two-terminal transmission lines, including fundamental frequency phasor based methods, traveling wave based methods and their disadvantages; second, the additional challenges on three-terminal transmission lines are provided.

Chapter 3 presents the proposed DSE based algorithm. The DSE based algorithm is introduced in an object-oriented way. First, a standard SCPAQCF syntax is utilized to represent the device dynamic model. Note that here the parameters are considered as extended states in the DSE procedure. Second, the method utilizes the device SCPAQCF object and the model of measurements to generate the measurement SCPAQCF object. Finally, different methods of solving the DSE problem are introduced.

Chapter 4 presents the simulation results of transmission line EBP. A series compensated transmission line is utlizied as an example and two different installations of relays are considered. The proposed EBP method is compared to legacy protection methods such as distance protection and line differential protection. The advantages of the proposed EBP method are demonstrated.

Chapter 5 presents the simulation results of transmission line EBFL. A two-terminal transmission line and a three-terminal transmission line are utilized as examples to find the location of the fault. For each example, the proposed EBFL method is compared to legacy fault locating methods such as fundamental frequency phasor based single-ended and dual-ended algorithms. The advantages of the proposed EBFL method are demonstrated.

Chapter 6 presents the simulation results of transmission line EBPI during normal operating conditions. Three parameters are selected based on the physical structure of the transmission line. Next, 7 combinations of these parameters are considered to demonstrate the characteristics of the selected parameters. Afterwards, the characteristics of these parameters are further explained via mathematical proofs. Finally, the way of building a high-fidelity dynamic model for EBP and EBFL application is concluded.

Finally, Chapter 7 summarizes the research work and outlines the results and contributions of this dissertation.

There are also four appendices in this dissertation. Appendix A describes the SCPQDMs of transmission lines without fault, including classic transmission lines and series compensated lines. Appendix B describes the SCPQDMs of transmission lines integrated with fault, including two-terminal transmission lines and three-terminal transmission lines. Appendix C describes the SCPQDMs of transmission lines with parameters during normal operating conditions. Appendix D describes the quadratic integration method. Appendix E validates the accuracy of multi-section transmission line model compared to the fully distributed frequency dependent model.

CHAPTER 2 Literature Survey

This chapter provides the background information of existing technologies related to the proposed research along with literature review of legacy schemes. Section 2.1 provides legacy protection functions of transmission lines. Section 2.2 demonstrates legacy fault locating techniques.

2.1 Legacy Protection Functions of Transmission Lines

Legacy protection functions of transmission lines can be classified into two groups: **single-ended methods** and **dual-ended methods** (also known as pilot protections). **Single-ended methods** mainly include: (1) Overcurrent protection; (2) Distance protection; **Dual-ended methods** mainly include: (3) Directional comparison pilot protection; (4) Pilot distance protection; and (5) Line differential protection. Section 2.1.1 describes the details of legacy functions on classic transmission lines [47-48]. Section 2.1.2 shows the additional challenges on complex transmission lines [49-50] such as series compensated lines.

Details of Legacy Functions on Classic Transmission Lines

(1) Overcurrent protection

Overcurrent protection scheme was first introduced without directional elements, which uses three-phase currents at the location of the relay. It can be further classified into instantaneous overcurrent protection and time overcurrent protection according to trip delays. For instantaneous overcurrent relays, they will instantaneously trip the line if one of the phase currents or sequence currents (negative, zero) exceeds the corresponding current setting. For time overcurrent relays, inverse-time characteristics are utilized to allow different tripping delays for different magnitudes of phase or sequence currents. The main disadvantage is that it cannot identify the direction of the fault and therefore it fails to ensure selectivity in the system with bi-directional power flow. To overcome the above disadvantages, directional elements are added to the overcurrent relay to form **directional overcurrent protection** [1-2]. It uses three phase currents and voltages at the location of the relay. The relays will trip if (a) the overcurrent function is activated and (b) the directional element identifies that the current direction is from the bus to the protected line. The main disadvantages include: (a) it is sensitive to the change of source impedance; (b) it uses same setting for all kinds of faults therefore the protection zone will be shortened; (c) it is general impossible to coordinate directional overcurrent relays in a network transmission system; (d) it is sensitive to fault impedances.

(2) Distance protection

Distance protection method [3-4] uses three phase currents and voltages at the location of the relay to calculate the impedance between the fault and the relay. Compared with directional overcurrent protection, distance protection (a) immunes to the changes of source outputs; (b) uses different calculation methods for different fault types; (c) can be used in a network transmission system; and (d) has some tolerance towards fault impedances. Three-step (three zones) distance protection is usually adopted. The tripping characteristics of zone 1, 2 and 3 are shown in Figure 2.1, where each zone is a circle including the origin point (0,0) with the diameter of the selected setting (here for zone 1, 2 and 3, the example settings are 80%, 120% and 260% of the positive sequence impedance of the protected line). The disadvantages of distance protection include: (a) it cannot protect short lines since in this case the relay characteristics is very small; (b) it cannot protect the whole length of the line instantaneously; (c) for high impedance faults, it will trip with large delay or even fails to trip.

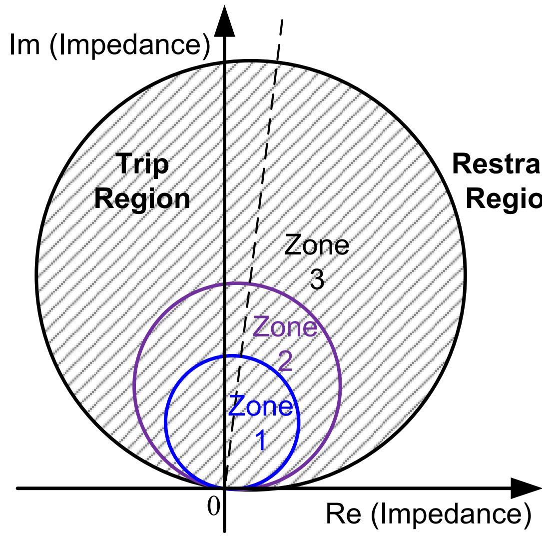

Figure 2.1. Characteristics of distance protection

(3) Directional comparison pilot protection

The method [5] uses three-phase voltages and currents at both sides of the line. The relay monitors the direction of the current at both terminals and will trip the line if both directional elements operate. The directional element is the same as introduced in directional overcurrent protection. The disadvantages include: (a) it cannot recognize internal faults near terminals where the measured voltages of the faulted phases are near zero; (b) it has limited sensitivity towards high impedance faults.

(4) Pilot distance protection

The method [6-7] uses three-phase voltages and currents at both sides of the line. The relay will trip the line if at least for one terminal the calculated impedance enters zone 1 of the corresponding distance relay. The main disadvantage is that it has limited sensitivity towards high impedance faults.

(5) Line differential protection

The method uses three-phase currents at both sides of the line. It is based on the assumption that the sum of two-side current phasors of any phase is zero under normal operations, and non-zero with internal faults. Usually the alpha-plane line differential protection [8] is adopted to test this zero sum. The relay trips only when (a) one of the thresholds of phase current or sequence current (negative, zero) is exceeded; (b) the phasor ratio exits the restraint region described in Figure 2.2. The main disadvantages of line differential protection include: (a) long transmission lines exhibit large capacitance and corresponding large capacitive current, which decreases the sensitivity of differential protection and makes it difficult to detect high impedance faults [9]; (b) To improve sensitivity, use of negative or zero sequence current has been applied as well as compensation for line charging current [15, 38]. These methods and settings are based on sequence models which are approximate and may result in less sensitivity.

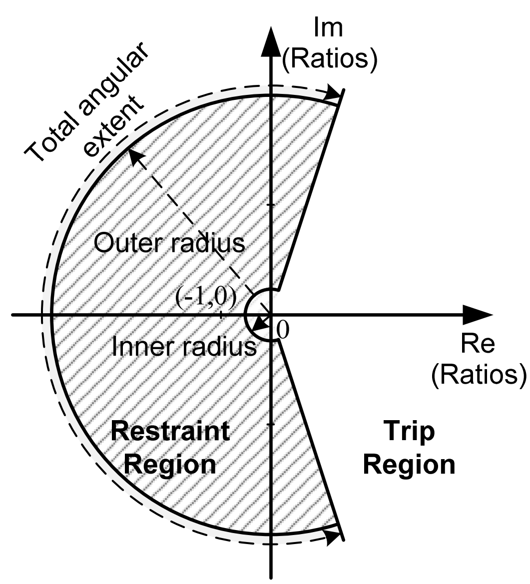

Figure 2.2. Characteristics of line differential protection

Challenges in Series Compensated Lines

Appropriately designed, **series compensated lines** can increase transmission capability, improve stability, reduce losses and damp sub-synchronous oscillations [10-11]. However, other than above disadvantages in 2.1.1, legacy protection functions confront **additional challenges** when dealing with complex transmission lines such as series compensated lines. A series compensated transmission system is shown in Figure 2.3, with Series Capacitors (SCs) at M side of MN line. Two faults F_1 and F_2 are considered as examples. There are two possible locations of the relay near SCs [12, 15]: bus-side relay installation (relay II) and line-side relay installation (relay II'). Legacy protections of the series compensated transmission line MN will experience different limitations as follows.

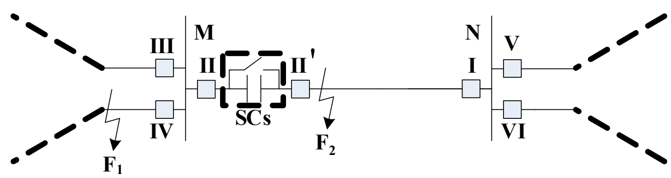

Figure 2.3. Series compensated transmission system

(1) For **single-ended** algorithms such as overcurrent and distance protection, relay I will incorrectly trip fault F_1, because SCs reduce impedance between F_1 and relay I. For example, a distance protective relay at relay I will "see" the fault at the middle of the line and it will incorrectly trip the line if the line is 50% compensated. To avoid this type of mis-operation, the protection zone of overcurrent protection and distance protection will be shortened [13] thus desensitizing the relays. Additionally, both relay II and relay II' with both protection schemes cannot distinguish between fault F_1 and F_2, therefore relay

II cannot operate during fault F_2 and relay II' will mis-operate during fault F_1. For similar reasons, directional element of directional overcurrent protection at relay II will wrongly miss fault F_2, because of current inversion caused by the capacitive impedance between relay II and F_2 [14]; directional element at relay II' will wrongly trip fault F_1.

(2) Dual-ended algorithms would also confront limitations. **Directional comparison protection scheme** will confront similar current inversion problem. For bus-side relay installation, internal fault F_2 will be neglected since relay I and II have the same direction results; for line-side relay installation, external F_1 will be wrongly captured since relay I and II' have different direction results. **Pilot distance protection scheme** cannot fully protect the compensated line as well. For bus-side relay installation, the scheme cannot trip fault F_2, because relay I cannot cover the total length of the line and relay II will 'see' a capacitive impedance; for line-side relay installation, the scheme will mis-operate during fault F_1. **Line differential protection** may also fail to operate because of current inversion [15].

2.2 Legacy Fault Locating Techniques

Legacy fault locating techniques can be mainly classified into two groups: fundamental frequency phasor based methods and traveling wave based methods. A brief survey of the two classes of methods is provided for two-terminal lines with commentary on the challenges when applied to three-terminal lines.

(1) Fundamental frequency phasor based methods

These methods use voltage and current phasors of fundamental frequency to calculate the impedance and afterwards the distance between the fault location and the terminals of the line [16-18]. They can be further classified into single-ended and dual-ended algorithms. (a) Single-ended algorithms calculate the location of the fault from voltage and current phasors at one end. The main advantage is that it does not require communication channels from the remote end. The accuracy of these methods largely depends on the fault type and fault impedance, as well as the line model accuracy, presence of mutually coupled circuits, and grounding parameters of the line [19-20]. (b) Dual-ended algorithms use voltage and current phasors at both ends of the line. They can be further subdivided into methods that use GPS synchronized measurements or non-synchronized measurements. These methods are in general more accurate than single ended methods as the influence of fault impedance and mutually coupled circuits is mitigated. [21-22]. There is a variety of algorithms depending on the available data, for example, dual-ended voltages only, dual-ended voltages and single-ended currents, dual-ended voltages and currents [23-25]. The main disadvantages of fundamental frequency phasor based single-ended or dual-ended methods are: (a) the algorithms are based on fundamental frequency phasors, so fault locating results may not be accurate if the system is experiencing transients; (b) some of these methods utilize a sequence line model (positive, negative and zero sequence) which is an approximate model and therefore increases the fault locating error; (c) the grounding of the line is typically neglected and this can potentially generate larger errors depending on the fault type.

(2) Traveling wave based methods

When a fault initiates in a transmission line, high frequency traveling waves are generated and propagate away towards both terminals of the line approximately with the speed of light. At each discontinuity, for example a bus with multiple lines, the fault, etc., they reflect and transmit generating more traveling waves. Traveling wave based methods [26-27, 57] monitor the traveling time of these waves to determine the fault location. They can be classified into two groups: single-ended algorithms and dual-ended algorithms. (a) Single-ended algorithms use subsequent time signals at one terminal to identify the fault location, including Type A, C, E and F fault locator [28-30]. Type A measures the time difference between the arrival of the first wave front and its reflection; Type C injects a high frequency impulse from one terminal and measures the time difference between the arrival of the reflection and the injection; Type E and F are quite similar with Type C expect that the injected impulses are generated by closing/opening the circuit breaker at one terminal. (b) Dual-ended algorithms use the time differences between the arrival of first wave front at both terminals to identify fault location, including Type B and D fault locator [29, 31-32]. Type B measures the time differences by sending stop signals from one end to another; Type D is quite similar with Type B except using synchronized time tagging to increase accuracy. Because the traveling waves are modulated by the frequency dependent characteristics of the line, digital signal processing is required to identify the actual arrival time of the wave. Different methods are applied for this, including Wavelet Transformation (WT) [33-34]. Traveling wave based methods have the following disadvantages. (a) The intensity of traveling waves is greatly influenced by the fault initiation time relative to the power frequency cycle. This generates the issue of detection reliability of the traveling waves. (b) They require special instrumentation since the usual CTs will filter out the high frequency content of the traveling waves. Related to this issue is the need to sample at very high rates. (c) The accuracy of the fault locator is also dependent upon the sampling rate of the measurements [35]. For example, a system with a 100 kilo-samples per second (ks/s) sampling rate could cause up to 0.93 miles systematic error with Type D fault locator.

(3) Additional challenges for three-terminal lines

Further, researchers have been studying fault locating methods for three-terminal lines. The methods can also be categorized into fundamental frequency phasor based methods and traveling wave based methods. (a) **Fundamental frequency phasor based methods.** One method transforms the three-terminal line into a two-terminal equivalent line, and then directly applies standard two-terminal line fault locating algorithms [39-40]. The method first determines the faulted branch by estimating the voltage phasor at the tap point from terminal voltage and current phasors; the faulted branch is the one providing a different estimated tap voltage from the other two branches. Next, the three-terminal line is transformed into a two-terminal line with measured voltage and current phasor at one terminal and the calculated voltage and current phasors at the tap point. Finally, usual two-terminal methods (single-ended, dual-ended) are applied to estimate the location of the fault. These methods can be further categorized according to data synchronization and availability, including three-ended GPS synchronized data [41], non-synchronized terminal voltages and currents [42], dual-ended synchronized measurements [43], three-ended synchronized currents and one-terminal voltages [44], etc. The fault location error of these methods is in general larger than that of two-terminal lines. (b) **Traveling wave based methods.** They also first determine the faulted branch: the intensity of the traveling wave obtained at the terminal of the faulted branch will be significantly higher than those obtained at the terminals of the non-faulted branches [34]. Next, the fault location is computed by either single-ended or three-ended algorithms, with principles similar to two-terminal lines. It is noted that algorithmic challenges are generated by the additional reflections and transmissions of the fault initiated waves at the tap point, making it difficult to determine the arrival time of the wavefronts [45].

CHAPTER 3 Proposed Research

In this chapter, the principles of the proposed **D**ynamic **S**tate **E**stimation (DSE) based methods are addressed. The DSE requires a device dynamic model, a model of measurements and a dynamic state estimation process. The overall DSE is implemented in an object-oriented way. The object orientation starts with an object that represents the device dynamic model of the component of interest. The object has a specific syntax referred to as State Control and Parameter Algebraic Quadratic Companion Form (SCPAQCF). Afterwards, the method utilizes the device SCPAQCF object and the model of measurements to generate the measurement SCPAQCF object. Finally, the computations are directly based on the measurement SCPAQCF object. Note that this algorithm with the standard syntax can be used in both transmission line protection (Dynamic State **E**stimation **B**ase **P**rotection, **EBP**) and fault locating (Dynamic State **E**stimation **B**ase **F**ault **L**ocating, **EBFL**). However, the matrices corresponding to the dynamic model would be different for different applications.

This chapter is arranged as follows. Section 3.1 provides the methods to generate the dynamic models in SCPAQCF standard syntax; section 3.2 describes the overall DSE procedure.

3.1 Dynamic Model with SCPAQCF syntax

The object orientation starts with an object that represents the device dynamic model of the transmission line of interest. The object has a specific syntax. In general, the object of the device dynamic model is developed by first expressing the mathematical description of the component as a set of algebraic and differential equations in terms of the states ($\boldsymbol{x}$), the controls ($\boldsymbol{u}$) and the parameters ($\boldsymbol{p}$) of the component. Subsequently we convert these equations into a set of algebraic and first order differential equations with nonlinearities not greater than two. In general, this is achieved by introducing additional variables. We refer to this as the quadratization procedure. If the model is linear or quadratic, the quadratization procedure is not needed. Afterwards, the equations are cast into a specific syntax, which has been named State, Control and Parameter Quadratic Dynamic Model (SCPQDM). The syntax is:

$$
\begin{aligned}
\mathbf{i}(t) &= \mathbf{Y}_{eqx1}\mathbf{x}(t) + \mathbf{Y}_{equ1}\mathbf{u}(t) + \mathbf{Y}_{eqp1}\mathbf{p}(t) + \mathbf{D}_{eqxd1}\frac{d\mathbf{x}(t)}{dt} + \mathbf{C}_{eqc1} \\
\mathbf{0} &= \mathbf{Y}_{eqx2}\mathbf{x}(t) + \mathbf{Y}_{equ2}\mathbf{u}(t) + \mathbf{Y}_{eqp2}\mathbf{p}(t) + \mathbf{D}_{eqxd2}\frac{d\mathbf{x}(t)}{dt} + \mathbf{C}_{eqc2} \\
\mathbf{0} &= \mathbf{Y}_{eqx3}\mathbf{x}(t) + \mathbf{Y}_{equ3}\mathbf{u}(t) + \mathbf{Y}_{eqp3}\mathbf{p}(t) + \begin{Bmatrix} \vdots \\ \mathbf{x}(t)^T \left\langle \mathbf{F}^i_{eqxx3} \right\rangle \mathbf{x}(t) \\ \vdots \end{Bmatrix} + \begin{Bmatrix} \vdots \\ \mathbf{u}(t)^T \left\langle \mathbf{F}^i_{equu3} \right\rangle \mathbf{u}(t) \\ \vdots \end{Bmatrix} \\
&\quad + \begin{Bmatrix} \vdots \\ \mathbf{p}(t)^T \left\langle \mathbf{F}^i_{eqpp3} \right\rangle \mathbf{p}(t) \\ \vdots \end{Bmatrix} + \begin{Bmatrix} \vdots \\ \mathbf{u}(t)^T \left\langle \mathbf{F}^i_{equx3} \right\rangle \mathbf{x}(t) \\ \vdots \end{Bmatrix} + \begin{Bmatrix} \vdots \\ \mathbf{p}(t)^T \left\langle \mathbf{F}^i_{eqpx3} \right\rangle \mathbf{x}(t) \\ \vdots \end{Bmatrix} + \begin{Bmatrix} \vdots \\ \mathbf{u}(t)^T \left\langle \mathbf{F}^i_{equp3} \right\rangle \mathbf{p}(t) \\ \vdots \end{Bmatrix} + \mathbf{C}_{eqc3}
\end{aligned}
\tag{3.1}
$$

where $\mathbf{x}(t)$, $\mathbf{u}(t)$, $\mathbf{p}(t)$ represent the state, control, parameter vectors of the component, respectively; terminal currents are represented by $\mathbf{i}(t)$, and terminal voltages are usually included in $\mathbf{x}(t)$. Additionally, the first equation may correspond to actual measurements $\mathbf{i}(t)$; the second and third equations correspond to internal constraints that describe the relationship among states, controls and parameters of the component.

Sometimes the component of interest consists of several parts. We need to combine them together to form an overall device SCPQDM. Next, the way to combine interconnected models will be introduced. Figure 3.1 depicts an example of combining three components which share the same node (marked as red). Besides including the original device SCPQDMs of three components, two additional steps are necessary: (a) substitute the voltage states at the common node ($v_1^{(2)}$, $v_2^{(1)}$, $v_3^{(1)}$) with one state (e.g. $v_1^{(2)}$) in all equations; (b) substitute all equations corresponding to terminal current at the common node ($i_1^{(2)}$, $i_2^{(1)}$, $i_3^{(1)}$) with one internal constraint equation ($0 = i_1^{(2)} + i_2^{(1)} + i_3^{(1)}$), i.e. apply KCL. After these steps, the combined component still has the same device SCPQDM format of as shown in equation (3.1). The detailed device SCPQDMs of line protection, fault locating and parameter identification during normal operating conditions are provided in Appendix A, B and C, respectively. Note that a multi-section time-domain transmission line model is adopted for all transmission line applications. This model is a close approximation of the fully distributed transmission line model with explicit grounding representation [46], as shown in Appendix E. The multi-section model is computational preferable for fault locating purposes.

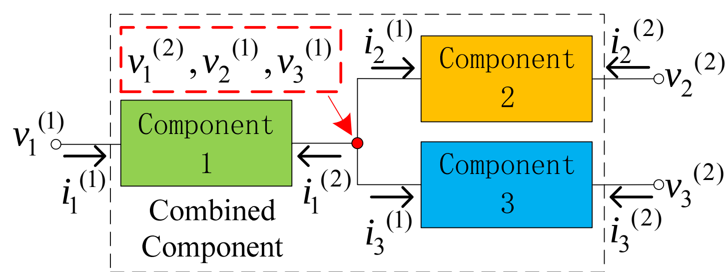

Figure 3.1. Combination of interconnected components

In order to numerically solve the unknown variables of the system, the device SCPQDM equations are integrated using the quadratic integration method [36]. Details of quadratic integration method are derived in Appendix D. The integration converts the model into a set of algebraic quadratic equations in terms of the state, control and parameter variables. We refer to this model as the device State, Control and Parameter Algebraic Quadratic Companion Form (SCPAQCF) model. Also, since the parameter variables are constants, additional equations that describe this property also need to be added into the device SCPAQCF model as shown in equation (3.2) (same parameters inside each time step) and (3.3) (same parameters between two consecutive time steps).

$$\mathbf{0} = \mathbf{p}(t) - \mathbf{p}(t_m) \tag{3.2}$$

$$\mathbf{0} = \mathbf{p}(t) - \mathbf{p}(t - 2\Delta t) \tag{3.3}$$

After above procedure, the device SCPAQCF model has the format shown in equation (3.4) where all the matrices can be expressed by the matrices defined in device SCPQDM.

$$\begin{aligned}
\begin{Bmatrix} \mathbf{i}(t) \\ \mathbf{0} \\ \mathbf{0} \\ \mathbf{i}(t_m) \\ \mathbf{0} \\ \mathbf{0} \end{Bmatrix} &= \mathbf{Y}_{eqx}\mathbf{x}(t,t_m) + \mathbf{Y}_{equ}\mathbf{u}(t,t_m) + \mathbf{Y}_{eqp}\mathbf{p}(t,t_m) + \begin{Bmatrix} \vdots \\ \mathbf{x}(t,t_m)^T \left\langle \mathbf{F}^i_{eqxx} \right\rangle \mathbf{x}(t,t_m) \\ \vdots \end{Bmatrix} \\
&+ \begin{Bmatrix} \vdots \\ \mathbf{u}(t,t_m)^T \left\langle \mathbf{F}^i_{equu} \right\rangle \mathbf{u}(t,t_m) \\ \vdots \end{Bmatrix} + \begin{Bmatrix} \vdots \\ \mathbf{p}(t,t_m)^T \left\langle \mathbf{F}^i_{eqpp} \right\rangle \mathbf{p}(t,t_m) \\ \vdots \end{Bmatrix} + \begin{Bmatrix} \vdots \\ \mathbf{u}(t,t_m)^T \left\langle \mathbf{F}^i_{equx} \right\rangle \mathbf{x}(t,t_m) \\ \vdots \end{Bmatrix} \\
&+ \begin{Bmatrix} \vdots \\ \mathbf{p}(t,t_m)^T \left\langle \mathbf{F}^i_{eqpx} \right\rangle \mathbf{x}(t,t_m) \\ \vdots \end{Bmatrix} + \begin{Bmatrix} \vdots \\ \mathbf{u}(t,t_m)^T \left\langle \mathbf{F}^i_{equp} \right\rangle \mathbf{p}(t,t_m) \\ \vdots \end{Bmatrix} - \mathbf{b}\left(t - 2\Delta t\right)
\end{aligned} \tag{3.4}$$

$$\mathbf{b}(t-2\Delta t) = -\mathbf{N}_{eqx} \cdot \mathbf{x}(t-2\Delta t) - \mathbf{N}_{equ} \cdot \mathbf{u}(t-2\Delta t) - \mathbf{N}_{eqp} \cdot \mathbf{p}(t-2\Delta t) - \mathbf{M}_{eq} \cdot \mathbf{i}(t-2\Delta t) - \mathbf{K}_{eq}$$

Afterwards, from the device SCPAQCF object and the model of measurements, we express all the measurements as algebraic quadratic expressions of state, control and parameter variables. We refer to this as the measurement SCPAQCF object. The measurement SCPAQCF object has the following format:

$$
\begin{aligned}
\mathbf{z}(t,t_m) &= h(\mathbf{x}(t,t_m),\mathbf{u}(t,t_m),\mathbf{p}(t,t_m)) \\
&= \mathbf{Y}_{m,x}\mathbf{x}(t,t_m)+\mathbf{Y}_{m,u}\mathbf{u}(t,t_m)+\mathbf{Y}_{m,p}\mathbf{p}(t,t_m)+\begin{Bmatrix} \vdots \\ \mathbf{x}(t,t_m)^T\left\langle \mathbf{F}^i_{m,xx}\right\rangle \mathbf{x}(t,t_m) \\ \vdots \end{Bmatrix} \\
&+\begin{Bmatrix} \vdots \\ \mathbf{u}(t,t_m)^T\left\langle \mathbf{F}^i_{m,uu}\right\rangle \mathbf{u}(t,t_m) \\ \vdots \end{Bmatrix}+\begin{Bmatrix} \vdots \\ \mathbf{p}(t,t_m)^T\left\langle \mathbf{F}^i_{m,pp}\right\rangle \mathbf{p}(t,t_m) \\ \vdots \end{Bmatrix}+\begin{Bmatrix} \vdots \\ \mathbf{u}(t,t_m)^T\left\langle \mathbf{F}^i_{m,ux}\right\rangle \mathbf{x}(t,t_m) \\ \vdots \end{Bmatrix} \\
&+\begin{Bmatrix} \vdots \\ \mathbf{p}(t,t_m)^T\left\langle \mathbf{F}^i_{m,px}\right\rangle \mathbf{x}(t,t_m) \\ \vdots \end{Bmatrix}+\begin{Bmatrix} \vdots \\ \mathbf{u}(t,t_m)^T\left\langle \mathbf{F}^i_{m,up}\right\rangle \mathbf{p}(t,t_m) \\ \vdots \end{Bmatrix}-\mathbf{b}_z\left(t-h\right)
\end{aligned}
\tag{3.5}
$$

$$
\mathbf{b}_z(t-2\Delta t)=-\mathbf{N}_{m,x}\cdot\mathbf{x}(t-2\Delta t)-\mathbf{N}_{m,u}\cdot\mathbf{u}(t-2\Delta t)-\mathbf{N}_{m,p}\cdot\mathbf{p}(t-2\Delta t)-\mathbf{M}_m\cdot\mathbf{i}(t-2\Delta t)-\mathbf{K}_m
$$

Here the measurements $\mathbf{z}(t,t_m)$ can be categorized into the following three types: actual measurements, pseudo measurements and virtual measurements. (a) Actual measurements are measured by actual meters such as terminal three-phase voltages and currents, with standard deviation determined by installed meters; (b) pseudo measurements are introduced to ensure observability of the system without actual meter installation, such as terminal neutral voltages. These measurements are often chosen as the best guess (eg. zeros for neutral voltages) with large standard deviations; (c) virtual measurements correspond to internal constraints of the system such as zero sum of currents of specific nodes.

3.2 Dynamic State Estimation Algorithm

In this section, we will introduce the standard procedure of Dynamic State Estimation (DSE) [51-56] to solve for the best estimate of states and parameters $\mathbf{xp}(t,t_m)=\left[\mathbf{x}(t,t_m),\mathbf{p}(t,t_m)\right]^T$ from the measurements $\mathbf{z}(t,t_m)$ and the SCPAQCF model described in equation (3.5). Note that the control variables $\mathbf{u}(t,t_m)$ in equation (3.5) are typically constants during the DSE algorithm and are treated as such. The flow chart of the DSE with parameters is provided in Figure 3.2. For some cases the value of parameters will influence the SCPAQCF model, so the model may need to be updated every DSE time step. An example is the application on fault locating where the fault location is considered as a parameter and the model might need to be updated to ensure accuracy.

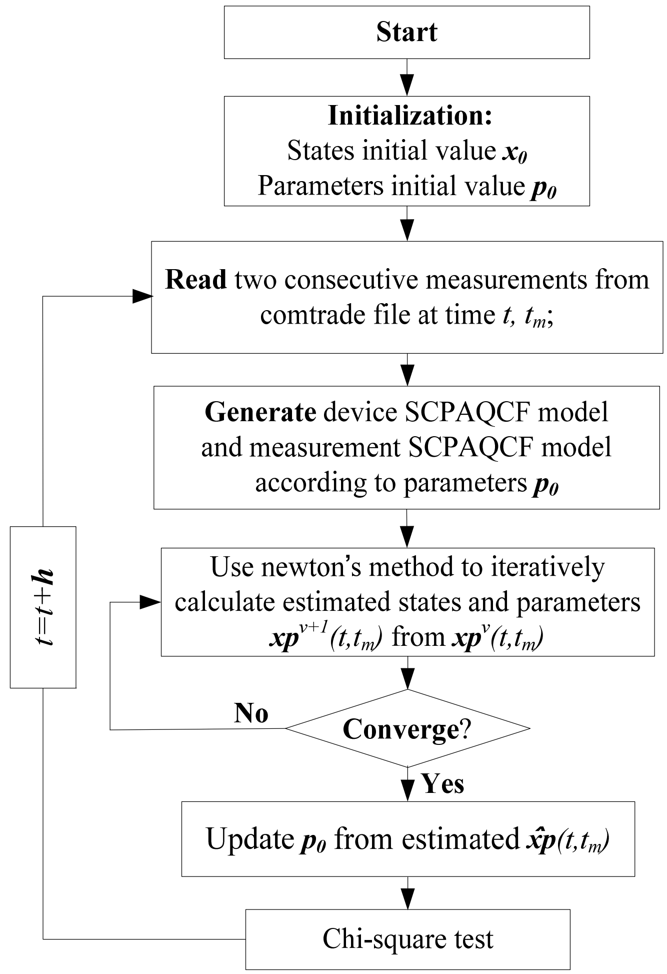

Figure 3.2. Flow chart of standard procedure of Dynamic State Estimation

Additionally, the effectiveness of the estimated $\mathbf{x\hat{p}}(t,t_m)$ is validated by the confidence level $P_{conf}(t)$ from the chi-square test [37]. A high confidence level (near 100%) means the estimated results are trustworthy, i.e. the measurements fit the model quite well. The confidence level $P_{conf}(t)$ can be calculated by,

$$P_{conf}(t) = P\left(\chi^2 \geq \zeta(t)\right) = 1 - P\left(\zeta(t), m\right) \tag{3.6}$$

$$\zeta(t) = \left(h(\mathbf{x\hat{p}}(t,t_m)) - \mathbf{z}(t,t_m)\right)^T \mathbf{W}\left(h(\mathbf{x\hat{p}}(t,t_m)) - \mathbf{z}(t,t_m)\right) \tag{3.7}$$

where $P\left(\zeta(t),m\right)$ is the probability of χ^2 distribution given $\chi^2 \le \zeta(t)$ with degree of freedom m, $\mathbf{W}=\text{diag}\left\{1/\sigma_1^2, 1/\sigma_2^2, \cdots\right\}$ where σ_i is the measurement error standard deviation, and $h(\mathbf{x}\hat{\mathbf{p}}(t,t_m))$ is defined as in equation (3.5) with control variables substituted.

The results of the chi-square test will be used differently for different applications. For the application of protection (EBP), the confidence level is used for trip decision, since a low confidence level implies inconsistency between measurements and model and therefore a fault. To dependably and securely protect the component, we use the following integral equation to decide the trip signal:

$$Trip(\text{t})=\begin{cases}1, \text{ if } TripValue(\text{t}) \ge K_{set} \\ 0, \text{ if } TripValue(\text{t}) < K_{set}\end{cases} \tag{3.8}$$

$$TripValue(\text{t})=\int_{t-\Delta\tau_{set}}^{t}\left(1-P_{conf}\left(t\right)\right)dt \tag{3.9}$$

where $\Delta\tau_{set}$ and K_{set} are the settings of the EBP relay. Usually they are chosen as $20\ cycles$ and $0.5\ cycles$, respectively.

For the application of fault locating (EBFL), the confidence level is used for verifying the effectiveness of estimated fault location. A high confidence level indicates a trustworthy fault location result.

There are different ways to solve the best estimated states and parameters. The algorithm differs according to how to handle the virtual measurements, past history $\mathbf{b}_z(t-2\Delta t)$ and DSE time step h. Details are provided as follows.

(a) Virtual Measurements

Unconstraint Optimization

This method treats virtual measurements the same as all other measurements but it assigns a small standard deviation for the measurement error. The unconstraint optimization problem is:

$$Min\ J = \left(h(\mathbf{xp}(t,t_m)) - \mathbf{z}(t,t_m)\right)^T \mathbf{W} \left(h(\mathbf{xp}(t,t_m)) - \mathbf{z}(t,t_m)\right) \tag{3.10}$$

The best estimated solution $\hat{\mathbf{xp}}(t,t_m)$ is provided by the following iterative algorithm until convergence:

$$\mathbf{xp}(t,t_m)^{\nu+1} = \mathbf{xp}(t,t_m)^{\nu} - (\mathbf{H}^T\mathbf{W}\mathbf{H})^{-1}\mathbf{H}^T\mathbf{W}(h(\mathbf{xp}(t,t_m)^{\nu}) - \mathbf{z}(t,t_m)) \tag{3.11}$$

where the Jacobian matrix $\mathbf{H} = \partial h(\mathbf{xp}(t,t_m)) / \partial \mathbf{xp}(t,t_m)$

Constraint Optimization

This method treats virtual measurements as equality constraints. Note that for virtual measurements corresponding to parameters (as shown in equation (3.2) and (3.3)), the parameters $\mathbf{p}(t,t_m)$ would stuck at initial values if these virtual measurements are also treated as equality constraints. In order to proceed the DSE process, here equation (3.2) and (3.3) are treated as measurements with small standard deviation (similar as unconstraint method), to make the parameters gradually converge to actual values. The constraint optimization problem is:

$$\begin{aligned} &Min\ J = \left(h_c(\mathbf{xp}(t,t_m)) - \mathbf{z}_c(t,t_m)\right)^T \mathbf{W}_c \left(h_c(\mathbf{xp}(t,t_m)) - \mathbf{z}_c(t,t_m)\right) \\ &Subject\ To: \qquad \mathbf{0} = g_c(\mathbf{xp}(t,t_m)) \end{aligned} \tag{3.12}$$

where $g_c(\mathbf{xp}(t,t_m))$ corresponds to the expression of equality constraints inside equation (3.5); $h_c(\mathbf{xp}(t,t_m))$, $\mathbf{z}_c(\mathbf{x}(t,t_m))$ and $\mathbf{W}_c$ are similar as $h(\mathbf{xp}(t,t_m))$, $\mathbf{z}(\mathbf{x}(t,t_m))$ and $\mathbf{W}$ but without the entries corresponding to equality constraints.

The best estimated solution $\mathbf{x\hat{p}}(t,t_m)$ is provided by the method of Lagrangian multipliers given with the following iterative algorithm until convergence:

$$\begin{bmatrix} \mathbf{xp}(t,t_m)^{v+1} \\ \boldsymbol{\lambda}(t,t_m)^{v+1} \end{bmatrix} = \begin{bmatrix} \mathbf{xp}(t,t_m)^{v} \\ \boldsymbol{\lambda}(t,t_m)^{v} \end{bmatrix} - \begin{bmatrix} \mathbf{H}_c{}^T\mathbf{W}_c\mathbf{H}_c & \mathbf{G}_c{}^T \\ \mathbf{G}_c & \mathbf{0} \end{bmatrix}^{-1} \begin{bmatrix} \mathbf{H}_c{}^T\mathbf{W}_c\left(h_c(\mathbf{xp}(t,t_m)^v) - \mathbf{z}_c(t,t_m)\right) + \mathbf{G}_c{}^T\boldsymbol{\lambda}(t,t_m)^v \\ g_c(\mathbf{xp}(t,t_m)^v) \end{bmatrix} \quad (3.13)$$

where the Jacobian matrices $\mathbf{H}_c = \partial h_c(\mathbf{xp}(t,t_m))/\partial\mathbf{xp}(t,t_m)$, $\mathbf{G}_c = \partial g_c(\mathbf{xp}(t,t_m))/\partial\mathbf{xp}(t,t_m)$, and $\boldsymbol{\lambda}(t,t_m)$ is the Lagrangian multiplier.

(b) Past history

Estimated values

This method uses estimated values from the previous DSE time step for $\mathbf{x}(t-2\Delta t)$, $\mathbf{i}(t-2\Delta t)$, $\mathbf{u}(t-2\Delta t)$, and $\mathbf{p}(t-2\Delta t)$ in the calculation of past history vector $\mathbf{b}_z(t-2\Delta t)$.

Measured values

This method uses measured values for $\mathbf{x}(t-2\Delta t)$, $\mathbf{i}(t-2\Delta t)$, $\mathbf{u}(t-2\Delta t)$, and $\mathbf{p}(t-2\Delta t)$ in the calculation of past history vector $\mathbf{b}_z(t-2\Delta t)$, if the corresponding actual measurement exist. Estimated values are used for all other variables that do not have corresponding actual measurements.

(c) DSE time step h

Two Sampling Intervals

This method performs DSE every two sampling intervals ($h = 2\Delta t$), as shown in Figure 3.3. For example, DSE at time t_k provides past history information for DSE at time $t_k + 2\Delta t$.

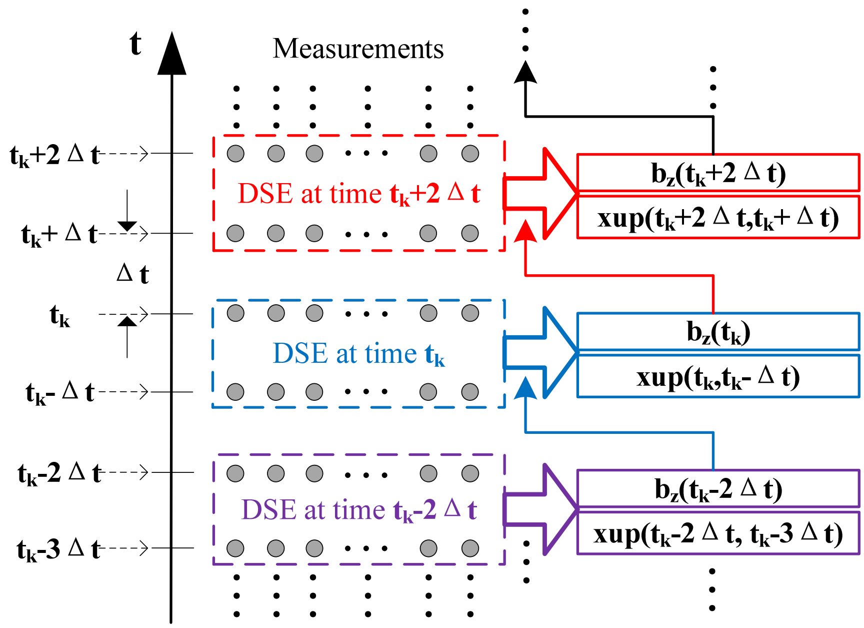

Figure 3.3. DSE procedure with time step $h=2\Delta t$

One Sampling Interval

This method performs DSE per sampling interval ($h=\Delta t$), as shown in Figure 3.4. For example, DSE at time t_k provide past history information for DSE at time $t_k+\Delta t$.

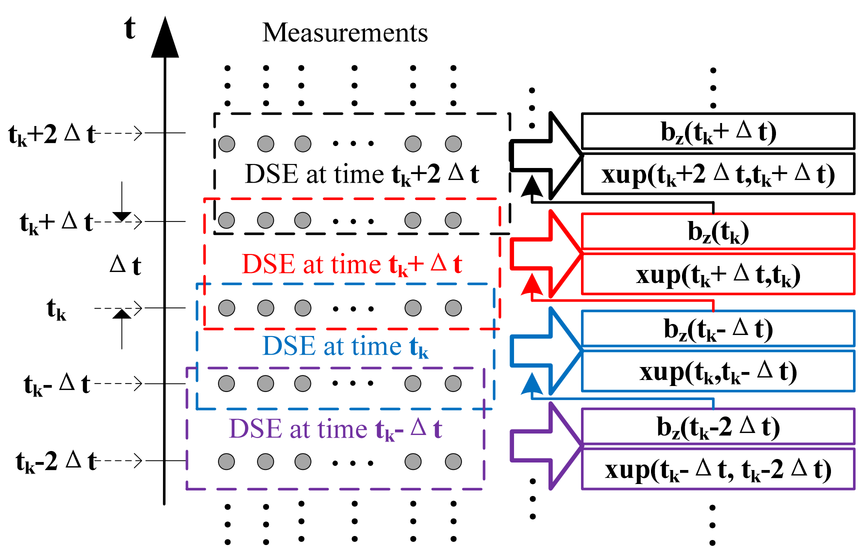

Figure 3.4. DSE procedure with time step $h=\Delta t$

CHAPTER 4 Numerical Experiments of Transmission Line EBP

This chapter describes the application on transmission line protection (Dynamic State **E**stimation **B**ased **P**rotection, **EBP**). A series compensated transmission line is chosen as an example to compare the performance of the proposed EBP with typical legacy protection schemes [49]. Section 4.1 provides the example test system; section 4.2 describes all relays and their settings; section 4.3 shows event studies in which the performances of EBP and legacy protection schemes are evaluated; section 4.4 concludes the proposed EBP scheme.

4.1 Example Test System

In this research, we compare the performance of the proposed EBP with typical legacy protection schemes for a series compensated power line. The compensation is located at one terminal of the line. We consider two possible installations of the relay: bus-side installation and line-side installation. Figure 4.1 illustrates the power line and the two possible locations of the measurements; the rest of the network is not shown. The line ratings are: 500kV, 83-mile long, 4330 MVA. The series capacitors are 0.148 mF representing a 42.4% compensation.

The source impedance is shown in Table 4.1. The tower structure is provided in Figure 4.2. The tower footing resistance is 25 ohms and the ground impedance of the substations at the two ends of the line is one ohm. The R, L and C matrices of the transmission line are provided in Table 4.2. The sequence parameters are shown in Table 4.3. The sampling rate is 4800 samples/second. The dynamic state estimation for each time step executes in a fraction of the time between two consecutive samples of streaming data, 416 μs. The typical execution time for this system is 120 μs on a high end personal computer.

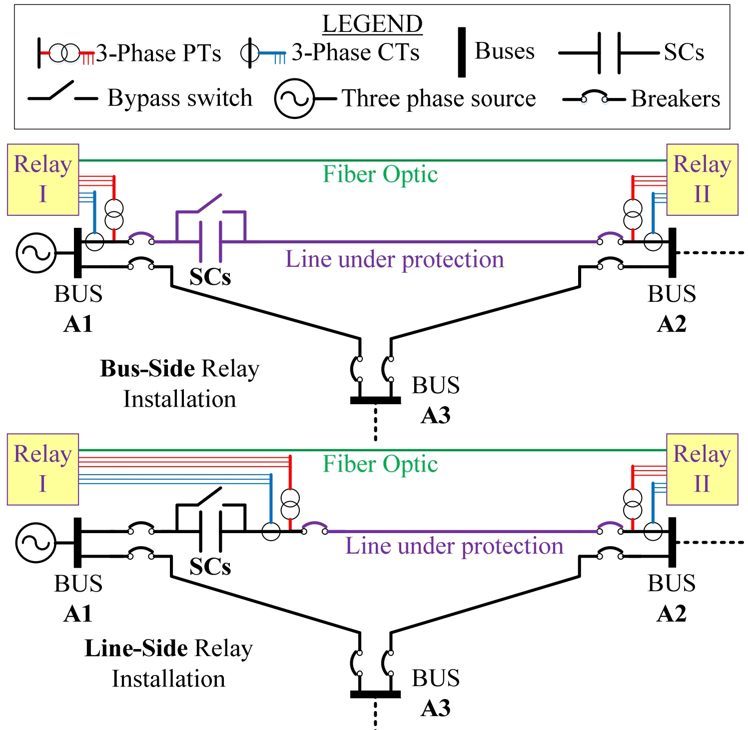

Figure 4.1. Numerical example test system for EBP: series compensated line, with bus side relay installation and line side relay installation

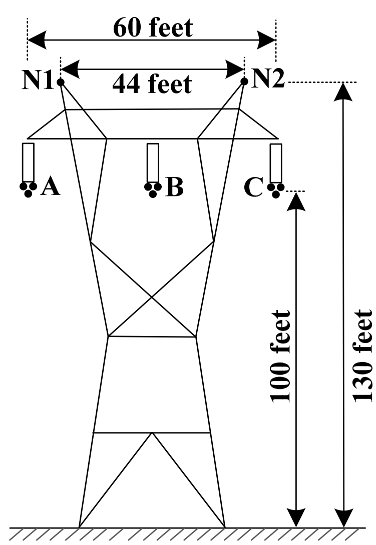

Figure 4.2. Tower structure of the transmission line

Table 4.1. Source impedances

Parameter	*Value*
Positive sequence impedance	$13.59\angle 86.99^\circ\ \Omega$
Negative sequence impedance	$12.88\angle 86.82^\circ\ \Omega$
Zero sequence impedance	$5.76\angle 82.88^\circ\ \Omega$

Table 4.2. R, L and C matrices of the line

Parameter matrices	*Value*
Series resistance (per mile)	$\begin{bmatrix} 0.104 & 0.089 & 0.089 & 0.088 & 0.088 \\ 0.089 & 0.104 & 0.089 & 0.088 & 0.088 \\ 0.089 & 0.089 & 0.104 & 0.088 & 0.088 \\ 0.088 & 0.088 & 0.088 & 2.357 & 0.087 \\ 0.088 & 0.088 & 0.088 & 0.087 & 2.357 \end{bmatrix} \Omega / mile$
Series inductance (per mile)	$\begin{bmatrix} 2.79 & 1.48 & 1.26 & 1.47 & 1.26 \\ 1.48 & 2.89 & 1.48 & 1.41 & 1.41 \\ 1.26 & 1.48 & 2.79 & 1.26 & 1.47 \\ 1.47 & 1.41 & 1.26 & 5.55 & 1.36 \\ 1.26 & 1.41 & 1.47 & 1.36 & 5.55 \end{bmatrix} mH / mile$
Shunt capacitance (per mile)	$\begin{bmatrix} 9.01 & -2.11 & -0.75 & -1.33 & -0.50 \\ -2.11 & 9.55 & -2.11 & -0.94 & -0.94 \\ -0.75 & -2.11 & 9.01 & -0.50 & -1.33 \\ -1.33 & -0.94 & -0.50 & 5.52 & -0.58 \\ -0.50 & -0.94 & -1.33 & -0.58 & 5.52 \end{bmatrix} nF / mile$
Shunt conductance (per mile)	$\boldsymbol{0}_{5\times 5}\ mho / mile$

Table 4.3. Sequence parameters of the line

Parameter	*Value*
Positive (Negative) sequence series impedance (Z_1)	$42.53\angle 88.34^\circ\ \Omega$
Zero sequence series impedance (Z_0)	$142.71\angle 74.56^\circ\ \Omega$
Positive (Negative) sequence shunt susceptance (Y_1)	$0.341\angle 90.0^\circ\ m\Omega$
Zero sequence shunt susceptance (Y_0)	$0.186\angle 90.0^\circ\ m\Omega$

4.2 Settings of Relays

We assumed the line is protected with only two legacy protection functions: (a) distance protection (at side A1), and (b) line differential protection (alpha plane). The settings of the legacy protection functions as well as EBP are provided corresponding to two possible locations of the relay.

(a) Bus-side relay installation, distance protection settings

The distance relay settings are summarized in Table 4.4.

Table 4.4. Distance relay settings (bus side)

Function	*Settings*
Line and Ground Distance, Zone 1	$19.72\angle 87.13°\ \Omega$, $0.015s$ delay, compensation factor $k = 2.39\angle\text{-}19.48°\ \Omega$
Line and Ground Distance, Zone 2	$30.80\angle 87.13°\ \Omega$, $0.15s$ delay, compensation factor $k = 2.39\angle\text{-}19.48°\ \Omega$
Line and Ground Distance, Zone 3	$64.08\angle 87.13°\ \Omega$, $0.5s$ delay, compensation factor $k = 2.39\angle\text{-}19.48°\ \Omega$

(b) Bus-side relay installation, line differential protection (alpha plane) [14] settings

Here the zero sequence current differential protection scheme with capacitive charging current compensation is used. The restraint region is between 1/6 to 6, with total angular extent 195°. The relay trip logic is activated when at least one of the following thresholds is exceeded (a) phase current 6 kA, (b) $3I_0$ (zero-sequence) current 500 A, (c) $3I_2$ (negative-sequence) current 500 A. The relay will trip when the trip logic is activated and the ratio falls outside the restraint region, with a delay of 0.015s.

(c) Bus-side relay installation, EBP settings

For consistency, the intentional delay for the EBP relay is also selected as $\tau_{delay} = 0.015s$ and the reset time is $\tau_{reset} = 0.03\ s$.

(d) Line-side relay installation, distance protection settings

The distance relay settings are shown in Table 4.5.

Table 4.5 Distance relay settings (line side)

Function	*Settings*
Line and Ground Distance, Zone 1	$34.02\angle 88.34°\ \Omega$, $0.015s$ delay, compensation factor $k = 2.39\angle\text{-}19.48°\ \Omega$
Line and Ground Distance, Zone 2	$53.16\angle 88.34°\ \Omega$, $0.15s$ delay, compensation factor $k = 2.39\angle\text{-}19.48°\ \Omega$
Line and Ground Distance, Zone 3	$110.58\angle 88.34°\ \Omega$, $0.5s$ delay, compensation factor $k = 2.39\angle\text{-}19.48°\ \Omega$

(e) Line-side relay installation, line differential protection settings

The settings of the line-side line differential relay are exactly the same as the bus-side line differential relay.

(f) Line-side relay installation, EBP settings

The settings of line-side EBP relay are exactly same as bus-side EBP relay.

4.3 Event Studies

We compare the performance of the legacy protection functions to the EBP relay performance for three specific events described below.

Event 1: Low Impedance Phase A-G Internal Fault near Bus A1.

A phase A to ground internal fault with 0.4 Ω impedance happens at 1 mile from the side A1 and time 0.5s. The results are shown in Figure 4.3 for the period [0.45 s to 0.55 s].

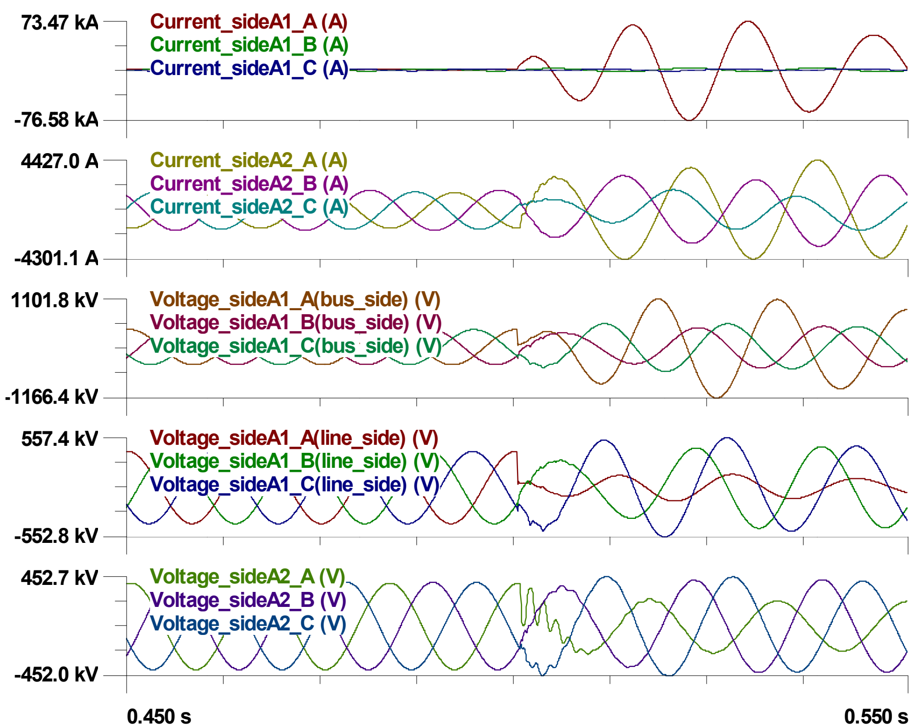

Figure 4.3. Current and voltage results of a phase A to ground internal fault near SCs

(a) Performance of Bus-side Relay Installation

Distance relay: the trace of the impedance "seen" by the relay, superimposed on its characteristic, is shown in Figure 4.4. It can be observed that the impedance stays outside the tripping characteristics during the fault due to the capacitive reactance of SCs. Therefore, the distance relay fails to detect this fault.

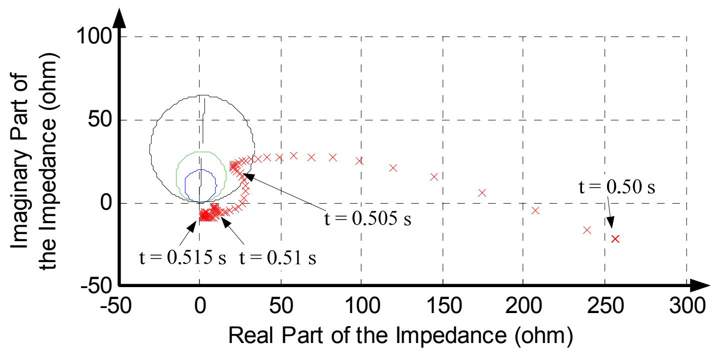

Figure 4.4. Trace of impedance during a phase A to ground internal fault near SCs, bus-side relay installation

Line differential protection relay: the phasor ratio trace of zero sequence current, superimposed on the relay characteristic, is shown in Figure 4.5. Along the trace, the character 'o' means the thresholds are not exceeded while the character 'x' means the thresholds are exceeded. Prior to the fault, the ratio is near the ideal point (-1,0), and none of the thresholds are exceeded (with the character 'o'). During the fault, the thresholds are gradually exceeded (transition 'o' to 'x') with the ratio already in the trip zone. The transition (detection) occurs at 0.504 s. The line differential relay trips the line at 0.504 + 0.015 s = 0.519 s.

EBP relay: The results are depicted in Figure 4.6. The first two sets of traces show the residuals and normalized residuals of three-phase currents of side A2. The confidence level and the trip signal are given in the next two traces. The confidence level drops to zero at time 0.5002 s. Thus the fault is detected at 0.5002 s and the line is tripped at 0.5152 s.

Summary: For event 1 and **bus-side relay installation**, the distance relay fails to detect the fault; the line differential relay detects the fault at 0.504 s and trips the line at 0.519 s; the EBP relay detects the fault at 0.5002 s and trips the line at 0.5152 s.

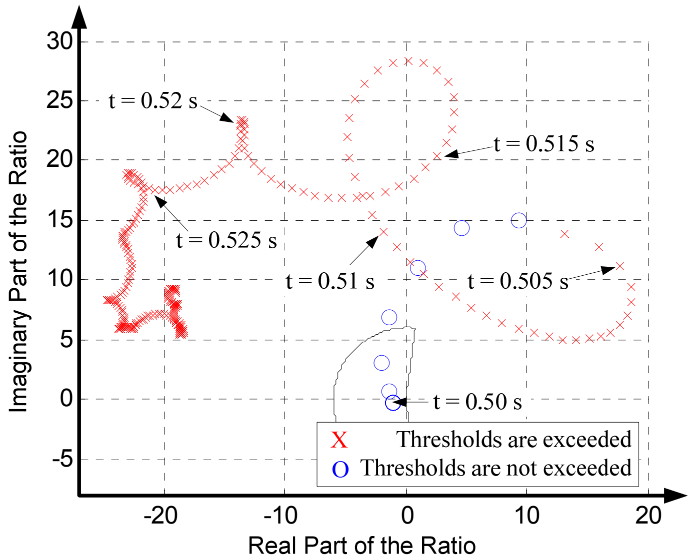

Figure 4.5. Trace of the ratios during a phase A to ground internal fault near SCs, bus-side relay installation

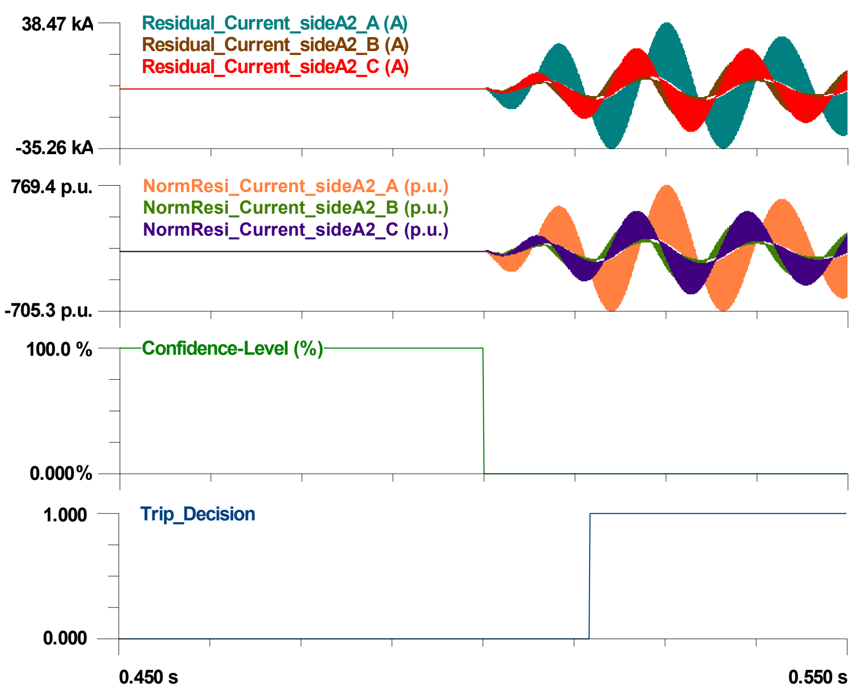

Figure 4.6. EBP results of a phase A to ground internal fault near SCs, bus-side relay installation

(b) Performance of Line-side relay installation

Distance protection relay: the trace of impedance "seen" by the relay, superimposed on its characteristic, is shown in Figure 4.7. It can be observed that the impedance enters zone 1 of the tripping characteristics during the fault. Thus, the distance relay trips the line at 0.509 + 0.015 s=0.524 s.

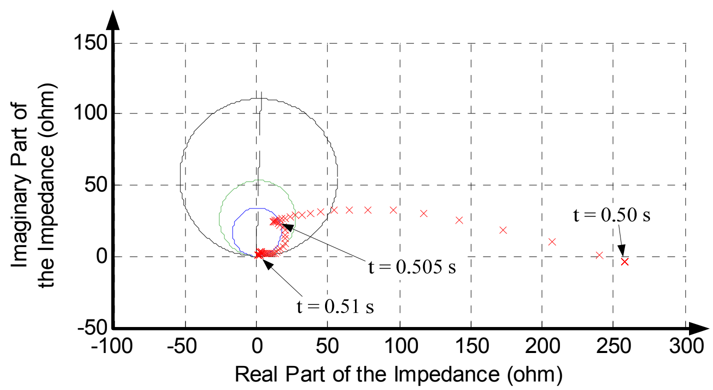

Figure 4.7. Trace of impedance during a phase A to ground internal fault near SCs, line-side relay installation

Line differential protection relay: the performance is the same as in Figure 4.5. The relay detects the fault at 0.504 s and trips the line at 0.519 s.

EBP relay: The results are depicted in Figure 4.8. The detection of the fault happens at 0.5002 s and the relay trips the line at 0.5152 s.

Summary: For event 1 and **line-side relay installation**, the distance relay correctly detects the fault at 0.509 s and trips the line at 0.524 s; the line differential relay correctly detects the fault at 0.504 s and trips the line at 0.519 s; the EBP relay detects the fault at 0.5002 s and trips the line at 0.5152 s.

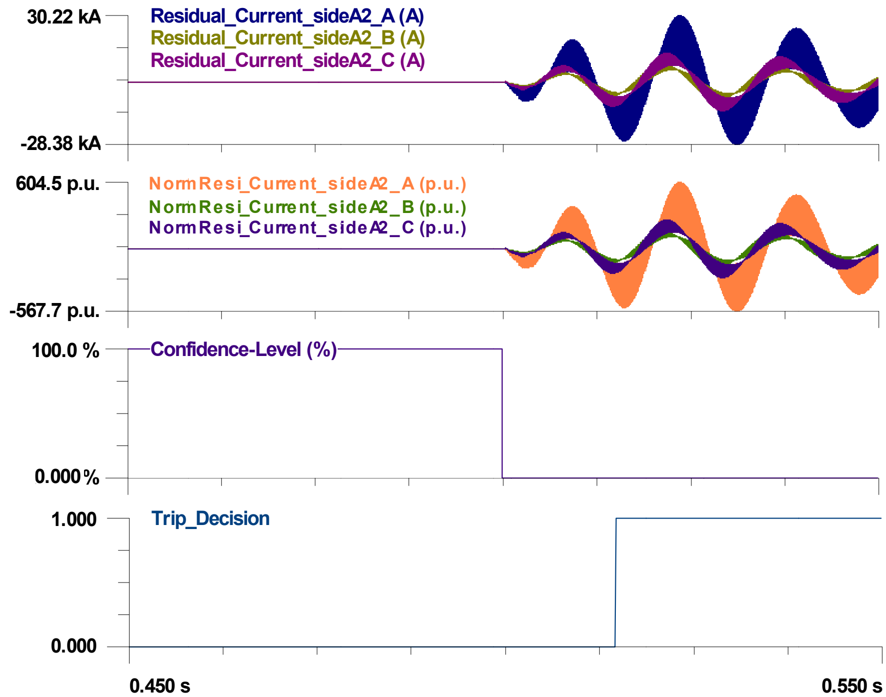

Figure 4.8. EBP results of a phase A to ground internal fault near SCs, line-side relay installation

Event 2: Low Impedance Phase A-G External Fault at Bus A1

A phase A to ground fault with 0.9 Ω impedance occurs at bus A1 and time 0.5 s. The results are shown in Figure 4.9 for the period [0.45 s to 0.55 s].

(a) Performance of Bus-side Relay Installation

Distance protection relay: the impedance "seen" by the relay, superimposed on its characteristic, is shown in Figure 4.10. The impedance stays outside the tripping characteristics. Thus, the distance relay correctly ignores this external fault.

Line differential protection relay: the phasor ratio trace of zero sequence current, superimposed on the relay characteristic, is shown in Figure 4.11. Prior to the fault, the ratio of zero sequence current is near the ideal point (-1,0), and none of the thresholds are exceeded (with the character ‘o’). During the fault, the ratio remains in the restraint region, with some thresholds exceeded (with the character ‘x’). Thus, line differential relay correctly ignores this external fault.

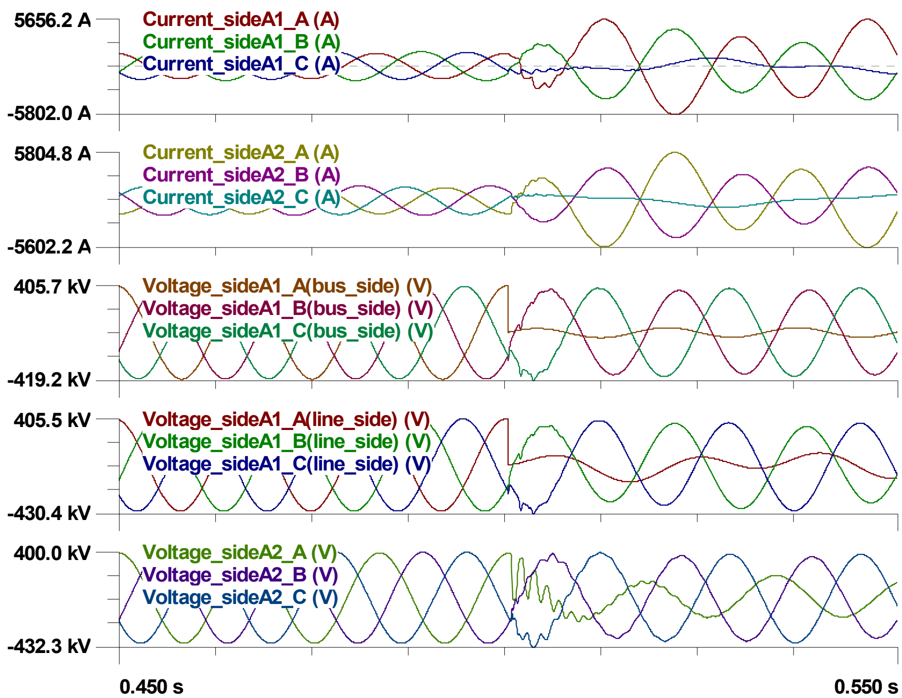

Figure 4.9. Current and voltage results of a phase A to ground external fault at bus A1

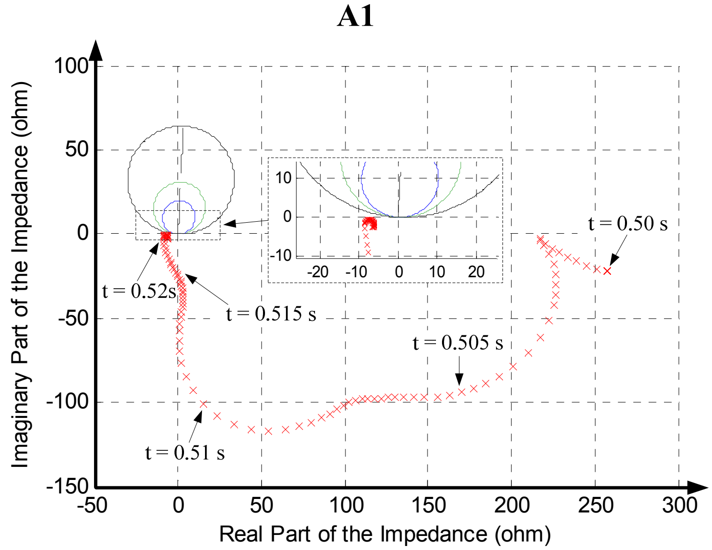

Figure 4.10. Trace of impedance during a phase A to ground external fault at bus A1, bus-side relay installation

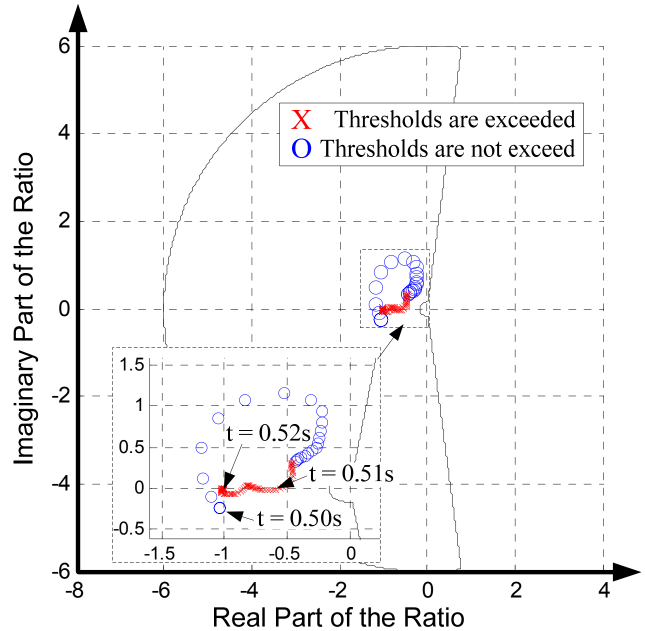

Figure 4.11. Trace of the ratios during a phase A to ground external fault at bus A1, bus-side relay installation

EBP relay: The results are depicted in Figure 4.12. The confidence level stays at 100% except some transients for a short period (around 1.5 ms). The trip signal remains at zero. Thus, the EBP relay correctly ignores this external fault.

Summary: For event 2 and **bus-side relay installation**, legacy protection relays and EBP relay correctly ignore the external fault.

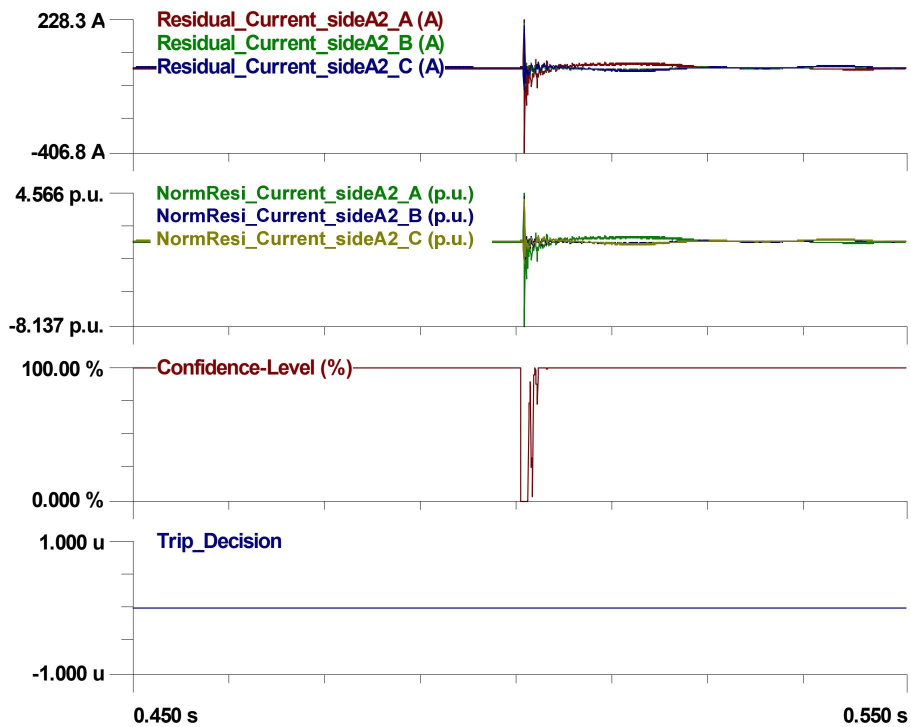

Figure 4.12. EBP results of a phase A to ground external fault at bus A1, bus-side relay installation

(b) Performance of Line-side Relay Installation

Distance protection relay: the impedance "seen" by the relay, superimposed on its characteristic, is shown in Figure 4.13. The impedance enters zone 1 of the characteristic. Thus, the distance relay will wrongly trip the line at 0.519 + 0.015 s = 0.534 s.

Line differential protection relay: the performance is the same as in Figure 4.11. The relay will correctly ignore this external fault.

EBP relay: The results are depicted in Figure 4.14. The confidence level stays at 100% except some transients for a short period (around 1.5 ms). Thus, the EBP relay correctly ignores this external fault.

Summary: For event 2 and **line-side relay installation**, distance protection incorrectly trips the line at 0.534 s, while line differential and the EBP relay correctly ignore the external fault.

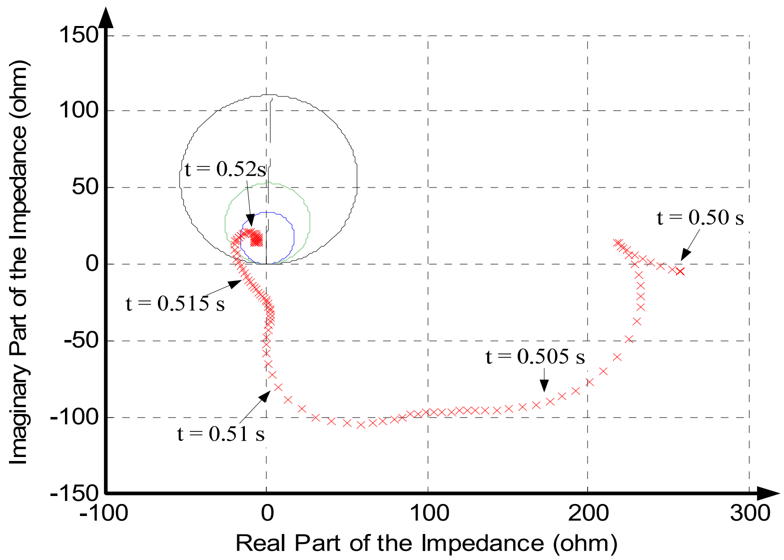

Figure 4.13. Trace of impedance during a phase A to ground internal fault near SCs, line-side relay installation

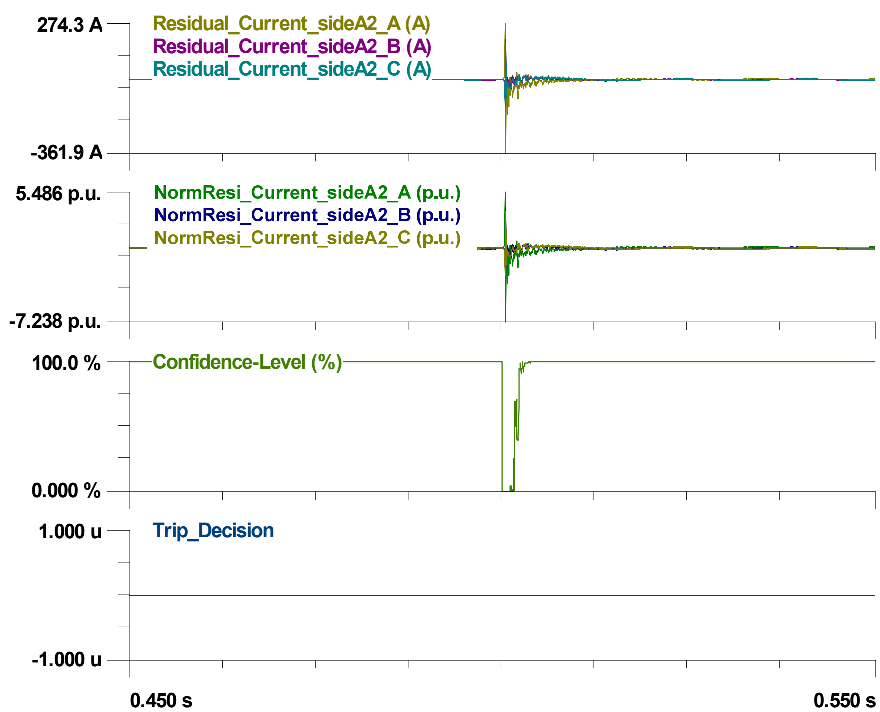

Figure 4.14. EBP results of a phase A to ground external fault at bus A1, line-side relay installation

Event 3: High Impedance Phase A-G Internal Fault

A phase A to ground internal fault with 300 Ω impedance occurs at 60 miles from the side A1 and time 0.5 s. The results are shown in Figure 4.15 for the period [0.45 s to 0.55 s].

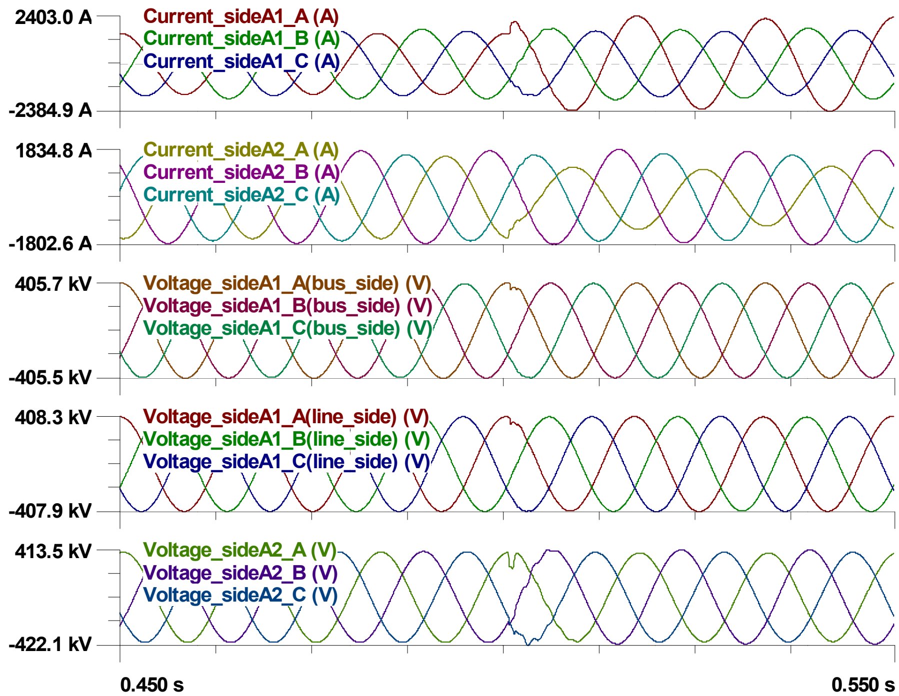

Figure 4.15. Current and voltage results of a phase A to ground high impedance internal fault

(a) Performance of Bus-side Relay Installation

Distance protection relay: the impedance "seen" by the relay, superimposed on its characteristic, is shown in Figure 4.16. The impedance stays outside of the relay characteristic. Thus, the distance relay fails to detect this fault.

Line differential protection relay: the phasor ratio trace of zero sequence current, superimposed on the relay characteristic, is shown in Figure 4.17. Prior to the fault, the ratio is in the restraint region, and none of the thresholds are exceeded (character 'o').

During the fault, the ratio exits the restraint region at 0.504 s and the threshold asserts (character ‘x’) at 0.520 s. The line is tripped at 0.520 + 0.015 s = 0.535 s.

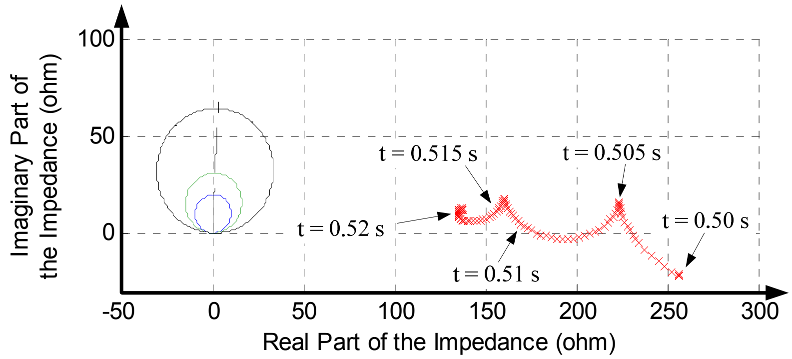

Figure 4.16. Trace of impedance during a phase A to ground high impedance internal fault, bus-side relay installation

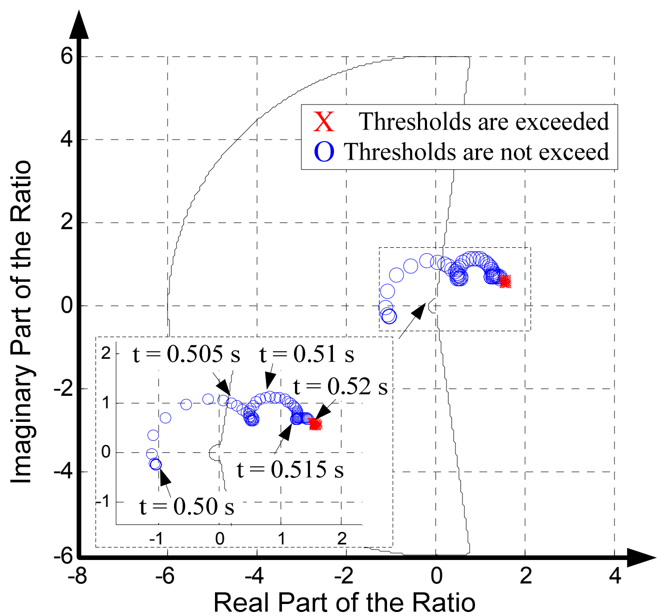

Figure 4.17. Trace of ratio during a phase A to ground high impedance internal fault, bus-side relay installation

EBP relay: The results are depicted in Figure 4.18. The confidence level drops to near zero 0.2 ms after the fault initiation. The trip command is issued at 0.5154 s.

Summary: For event 3 and **bus-side relay installation**, distance relay fails to detect the fault; differential relay and EBP relay issue a trip command at 0.535 s and 0.5154 s respectively.

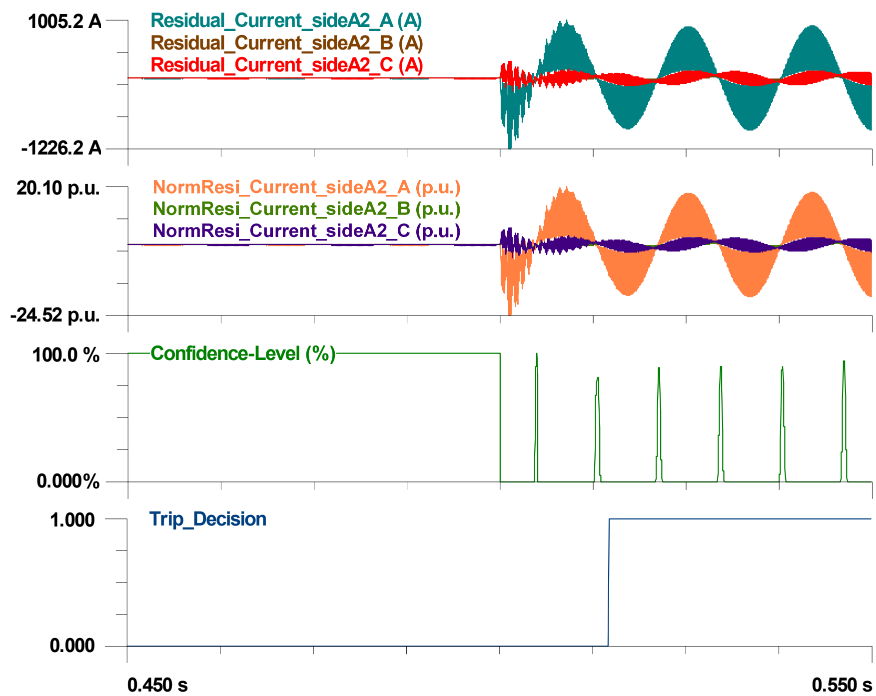

Figure 4.18. EBP results of a phase A to ground high impedance internal fault, bus-side relay installation

(b) Performance of Line-side Relay Installation

Distance protection relay: the impedance "seen" by the relay, superimposed on its characteristic, is shown in Figure 4.19. The impedance stays outside the tripping characteristic. Thus, the distance relay fails to detect this fault.

Line differential protection relay: the performance is the same as in Figure 4.17. The relay issues a trip at time 0.535 s.

EBP relay: The results are depicted in Figure 4.20. The EBP relay detects the fault at 0.5002 s and issues a trip at 0.5153 s.

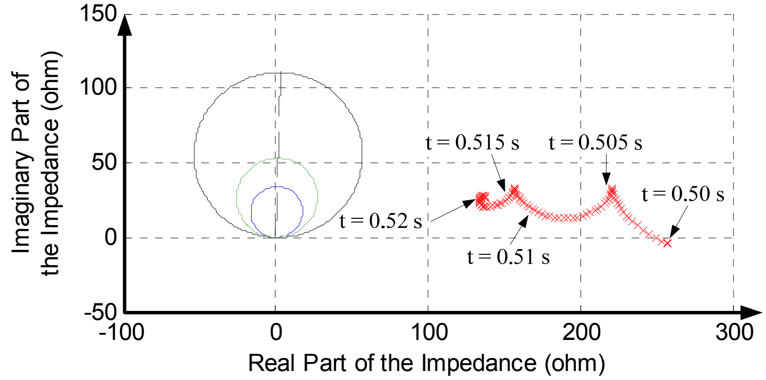

Figure 4.19. Trace of impedance during a phase A to ground high impedance internal fault, line-side relay installation

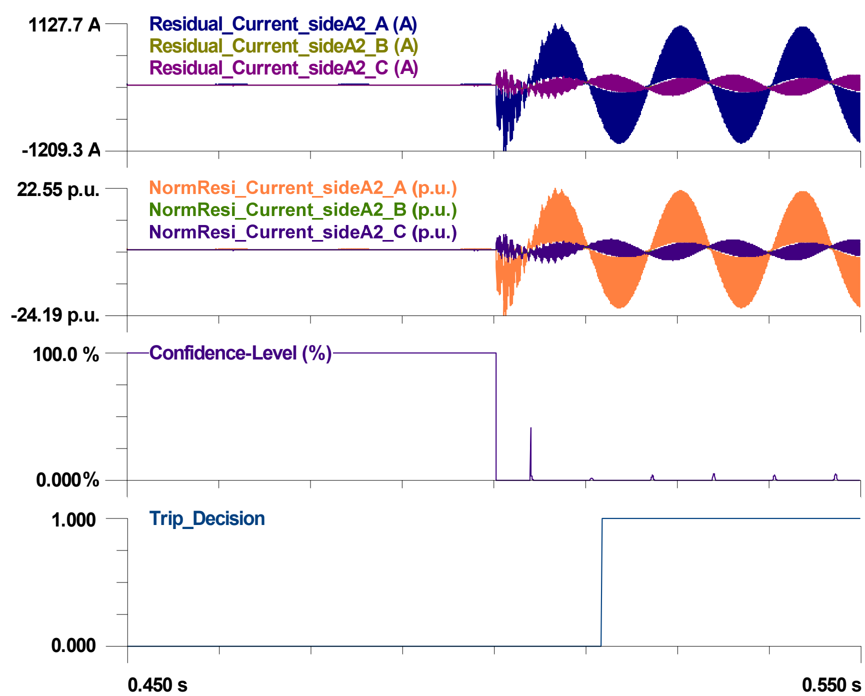

Figure 4.20. EBP results of a phase A to ground high impedance internal fault, line-side relay installation

Summary: For event 3 and **line-side relay installation**, distance protection relay fails detect the fault; line differential relay detects the fault at 0.520 s and issues a trip at 0.535 s; EBP relay detects the fault at 0.5002 s and issues a trip at 0.5153 s.

4.4 Summary of Proposed EBP Scheme

In this chapter the EBP method is compared to legacy protection functions for a series compensated transmission line. The proposed **EBP** scheme has the following advantages: (a) it simplifies the settings of the protection and does not need coordination with other protection functions; (b) it detects faults faster than legacy protection schemes (within sub-millisecond); (c) it is immune to current inversion due to SCs; and (d) it reliably detects high impedance faults.

CHAPTER 5 Numerical Experiments of Transmission Line EBFL

This chapter describes the application on transmission line fault locating (Dynamic State **E**stimation **B**ased **F**ault **L**ocating, **EBFL**).

We compare the performance of the proposed EBFL with legacy fault locating schemes using two example test systems: a two-terminal transmission line system and a three-terminal transmission line system. Section 5.1 provides a two-terminal transmission line example test system; section 5.2 describes legacy fault locating schemes of two-terminal transmission lines; section 5.3 shows event studies of two-terminal transmission lines; section 5.4 provides a three-terminal transmission line example test system; section 5.5 describes legacy fault locating schemes of three-terminal transmission lines; section 5.6 shows event studies of three-terminal transmission lines; section 5.7 concludes the proposed EBFL scheme.

5.1 Two-terminal Transmission Line Example Test System

The two-terminal line example test system is partially illustrated in Figure 5.1. The full network used for the simulations is not shown. The line of interest (A1-A2) is a 500kV, 135.22 mile-long, 4330 MVA transmission line. Three phase voltage and current measurements are installed at both terminals of the transmission line. The sequence parameters of the transmission line are shown in Table 5.1. The tower structure and R, L and C matrices of the transmission line are the same as those in Chapter 4 (in Figure 4.2 and Table 4.2). A number of events have been simulated and the results have been stored in COMTRADE files, with standard 4800 samples/second according to IEC 61850-9-2LE standard.

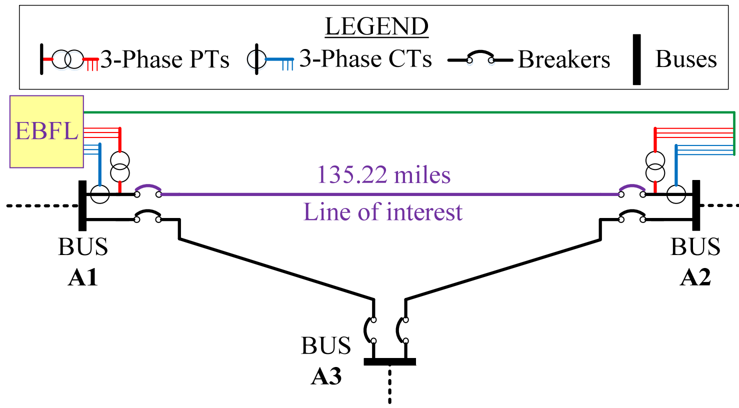

Figure 5.1. 500kV, two-terminal line example test system

Table 5.1. Sequence parameters of the line

Parameter	*Value*
Positive (Negative) sequence impedance (Z_{1L})	$68.75\angle 88.16°\Omega$
Zero sequence impedance (Z_{0L})	$230.65\angle 74.69°\Omega$

5.2 Legacy Fault Locating Schemes of Two-terminal Transmission Lines

We assumed that legacy fundamental frequency phasor based single-ended and dual-ended fault locating schemes are applied to this line to estimate the fault distance *m* from side A1. Note we do not consider traveling wave based methods because the sampling rate is too low for estimating the fault location with reasonable accuracy. The two legacy methods for comparison are as follows:

(a) Single-ended fundamental frequency phasor based method,

$$m = \frac{\mathrm{Im}(V_{\mathrm{A1}} / I_{\mathrm{A1}})}{\mathrm{Im}(Z_{\mathrm{1L}})}$$

(b) Dual-ended fundamental frequency phasor based method,

$$m = \frac{\left(V_{\mathrm{A1}} - V_{\mathrm{A2}} + Z_{\mathrm{1L}} I_{\mathrm{A2}}\right)}{\left(Z_{\mathrm{1L}}\left(I_{\mathrm{A1}} + I_{\mathrm{A2}}\right)\right)}$$

where Z_{1L} is the positive (negative) sequence impedance of the line; the values of V_{Ai} and I_{Ai} (i = 1, 2 for side A1 and side A2 respectively) are chosen according to different type of faults, as shown in the following table.

Table 5.2. Values of V_{Ai} and I_{Ai} for different fault types

Fault Type	V_{Ai}	I_{Ai}
a-n	$V_{\mathrm{Ai,a}}$	$I_{\mathrm{Ai,a}} + k_0 I_{\mathrm{Ai,0}}$
b-n	$V_{\mathrm{Ai,b}}$	$I_{\mathrm{Ai,b}} + k_0 I_{\mathrm{Ai,0}}$
c-n	$V_{\mathrm{Ai,c}}$	$I_{\mathrm{Ai,c}} + k_0 I_{\mathrm{Ai,0}}$
a-b, a-b-n	$V_{\mathrm{Ai,a}}$ - $V_{\mathrm{Ai,b}}$	$I_{\mathrm{Ai,a}}$ - $I_{\mathrm{Ai,b}}$
b-c, b-c-n	$V_{\mathrm{Ai,b}}$ - $V_{\mathrm{Ai,c}}$	$I_{\mathrm{Ai,b}}$ - $I_{\mathrm{Ai,c}}$
a-c, a-c-n	$V_{\mathrm{Ai,a}}$ - $V_{\mathrm{Ai,c}}$	$I_{\mathrm{Ai,a}}$ - $I_{\mathrm{Ai,c}}$
a-b-c, a-b-c-n	$V_{\mathrm{Ai,a}}$	$I_{\mathrm{Ai,a}}$

where for side Ai $(i = 1, 2)$ $V_{\mathrm{Ai,a}}$, $V_{\mathrm{Ai,b}}$, $V_{\mathrm{Ai,c}}$, $I_{\mathrm{Ai,a}}$, $I_{\mathrm{Ai,b}}$ and $I_{\mathrm{Ai,c}}$ are voltage and current phasors of each phase, $I_{\mathrm{Ai,0}} = (I_{\mathrm{Ai,a}} + I_{\mathrm{Ai,b}} + I_{\mathrm{Ai,c}})/3$ is the zero sequence current; $k_0 = \left(Z_{\mathrm{0L}} - Z_{\mathrm{1L}}\right)/Z_{\mathrm{1L}}$ is the zero sequence compensation factor; and Z_{0L} is the zero sequence impedance of the line.

5.3 Event Studies of Two-terminal Transmission Lines

We compare the performance of the above legacy fault locating schemes to EBFL method with different test cases as described below. Here we will only present results for phase A to neutral faults and phase A to B faults. Results for other fault types are similar.

Test Case 1: Bolt Phase A to N Faults

A bolt phase A to neutral fault occurred on line A1-A2, 50 miles from bus A1. Figure 5.2 and Figure 5.3 depict the fault locating results of legacy single-ended and dual-ended fundamental frequency phasor based methods. The fault locating results are 51.2722 miles from bus A1 for the legacy single-ended method and 49.6947 miles from bus A1 for the legacy dual-ended method.

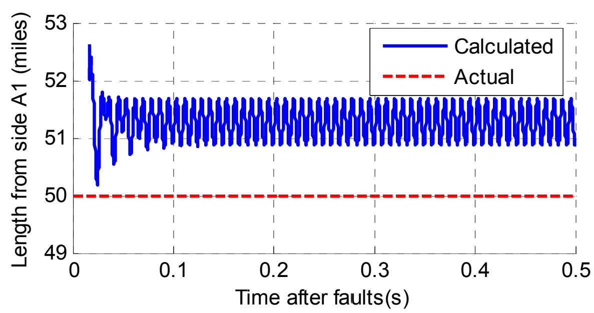

Figure 5.2. Fault locating results, legacy single-ended method, bolt phase A to neutral fault, 50 miles from bus A1

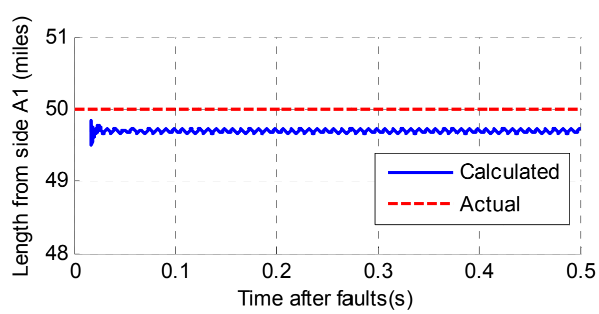

Figure 5.3. Fault locating results, legacy dual-ended method, bolt phase A to neutral fault, 50 miles from bus A1

Figure 5.4 shows the fault locating results of the proposed EBFL method. The fault is computed to be at 50.0461 miles from bus A1. Note that the average error is 0.0461 miles, which is much smaller compared to legacy methods (1.2722 miles for legacy single-ended method and 0.3053 miles for legacy dual-ended method). Figure 5.5 demonstrates the chi-square test results of the DSE process. A 100% confidence level proves that all the states and parameters of the system are consistent with the model, and the fault locating results are trustworthy. Figure 5.6 provides the standard deviation of the calculated fault location (0.0878 miles), which proves the stability of the method. From these figures, we can see that for this fault the proposed EBFL method is more accurate than both legacy methods.

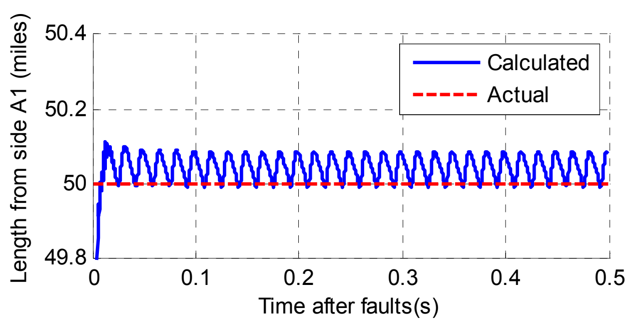

Figure 5.4. Fault locating results, EBFL method, bolt phase A to neutral fault, 50 miles from bus A1

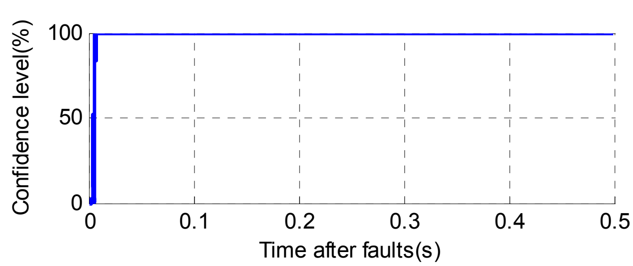

Figure 5.5. Chi-square test results, EBFL method, bolt phase A to neutral fault, 50 miles from bus A1

To further validate the effectiveness of the proposed EBFL method, bolt phase A to neutral faults at different fault locations are tested. Table 5.3 and Figure 5.7 provide the fault locating error of legacy single-ended method, legacy dual-ended method and the proposed EBFL method. It is noted that the EBFL method is more accurate than both legacy methods.

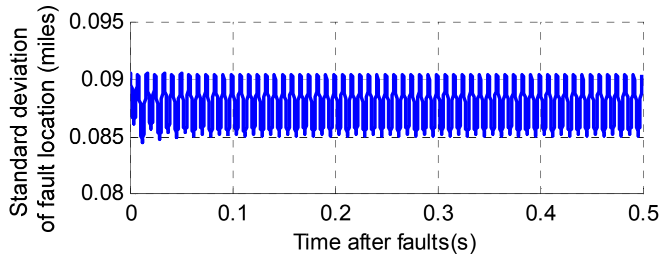

Figure 5.6. Standard deviation of fault location, EBFL method, bolt phase A to neutral fault, 50 miles from bus A1

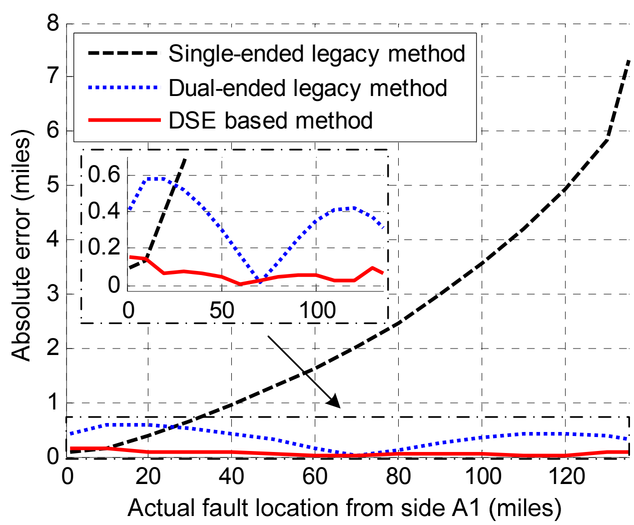

Figure 5.7. Fault locating results comparison, bolt phase A to neutral faults, variable fault location

Table 5.3. Fault locating error of bolt phase A to N faults (in miles)

Fault Location	*Single-Ended*	*Dual-Ended*	*EBFL*
1	0.0993	-0.4084	0.1541
10	0.1388	-0.5739	0.1457
20	0.3927	-0.5742	0.0683
30	0.662	-0.5212	0.0747
40	0.9528	-0.4278	0.0695
50	1.2722	-0.3053	0.0461
60	1.6276	-0.1653	0.0124
70	2.0259	-0.0188	-0.024
80	2.476	0.1228	-0.0475
90	2.9855	0.2488	-0.0597
100	3.5622	0.3476	-0.0535
110	4.2151	0.4087	-0.0276
120	4.9499	0.4206	-0.0287
130	5.8396	0.3713	-0.0939
135	7.307	0.3157	-0.0675

Test Case 2: Impedance Phase A to N Faults

10 ohm phase A to neutral faults at different fault locations are tested. The results are provided in Table 5.4 and Figure 5.8. It is observed that the EBFL method is more accurate than both legacy methods.

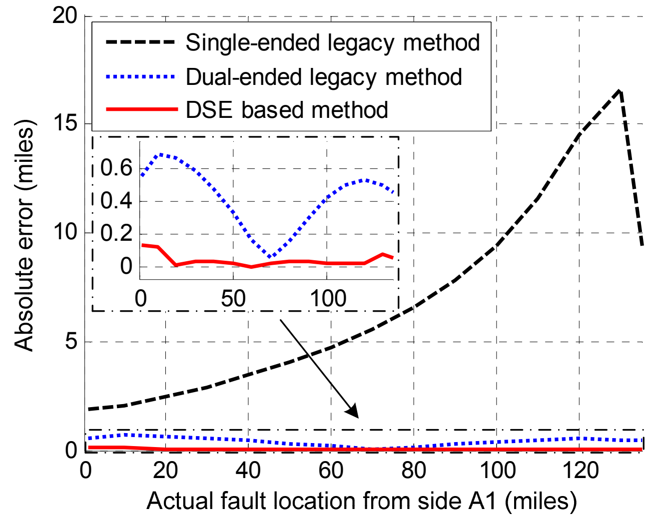

Figure 5.8. Fault locating results comparison, impedance phase A to neutral faults, 10 ohm fault impedance, variable fault location

Table 5.4. Fault locating error of impedance phase A to N faults (in miles)

Fault Location	*Single-Ended*	*Dual-Ended*	*EBFL*
1	1.8609	-0.5535	0.1386
10	2.0251	-0.6785	0.1169
20	2.446	-0.658	0.0155
30	2.9106	-0.5855	0.0323
40	3.4327	-0.4726	0.0386
50	4.0315	-0.3307	0.0247
60	4.7295	-0.1713	0.0008
70	5.5571	-0.0575	-0.0271
80	6.5625	0.1551	-0.0382
90	7.8119	0.3	-0.0372
100	9.4179	0.4178	-0.0181
110	11.5729	0.4975	0.0215
120	14.5393	0.5277	0.0185
130	16.6275	0.4962	-0.0783
135	9.4413	0.4476	-0.0538

Test Case 3: Bolt Phase A to B Faults

Bolt phase A to B faults at different fault locations are tested. The results are provided in Table 5.5 and Figure 5.9. We can observe that, EBFL method is more accurate than both legacy methods.

Table 5.5. Fault locating error of bolt phase A to B faults (in miles)

Fault Location	*Single-Ended*	*Dual-Ended*	*EBFL*
1	-0.0253	0.592	0.2143
10	-0.2338	0.59	0.2668
20	-0.4283	0.6345	0.2897
30	-0.576	0.711	0.2779
40	-0.6677	0.8068	0.2402
50	-0.695	0.9083	0.186
60	-0.6492	1.0024	0.1231
70	-0.5206	1.0764	0.0599
80	-0.3003	1.1168	0.0015
90	0.0214	1.1116	-0.0464
100	0.4532	1.0482	-0.0801
110	1.0041	0.9152	-0.0964
120	1.6791	0.7012	-0.0923
130	2.4705	0.3959	-0.065
135	2.806	0.2459	-0.0473

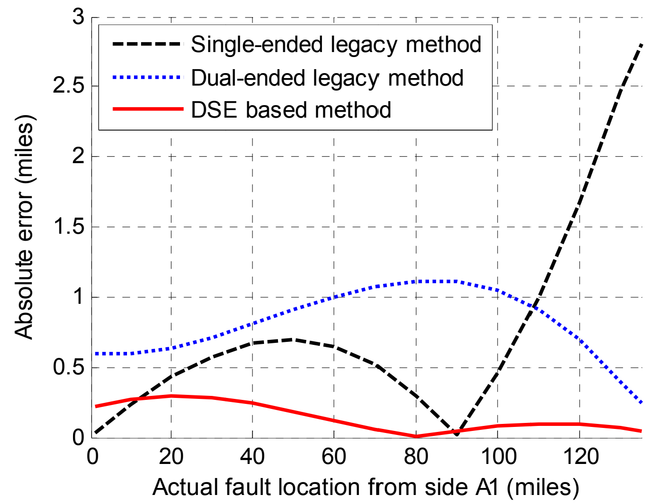

Figure 5.9. Fault locating results comparison, bolt phase A to B faults, variable fault location

Test Case 4: Impedance Phase A to B Faults

10 ohm phase A to B faults at different fault locations are tested. The results are provided in Table 5.6 and Figure 5.10. We can observe that, EBFL method is more accurate than both legacy methods.

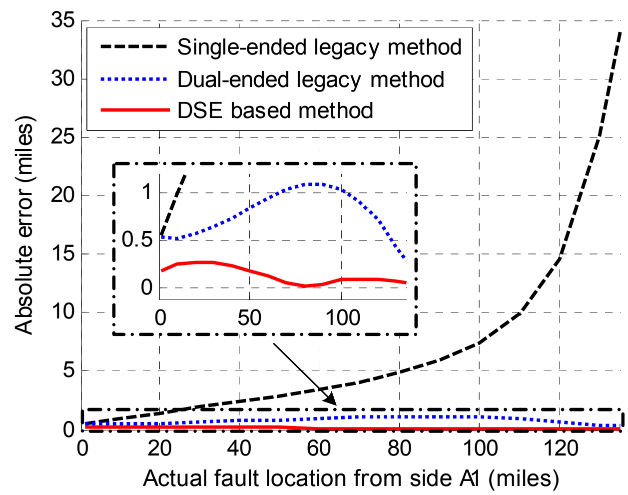

Figure 5.10. Fault locating results comparison, impedance phase A to B faults, 10 ohm fault impedance, variable fault location

Table 5.6. Fault locating error of impedance phase A to B faults (in miles)

Fault Location	*Single-Ended*	*Dual-Ended*	*EBFL*
1	-0.5576	0.5316	0.1858
10	-0.9825	0.5262	0.247
20	-1.4551	0.5687	0.2771
30	-1.9307	0.6454	0.2706
40	-2.4154	0.7432	0.2365
50	-2.9212	0.8487	0.1846
60	-3.4697	0.9492	0.1241
70	-4.0982	1.0309	0.0617
80	-4.8709	1.0815	0.0316
90	-5.9041	1.0882	-0.0454
100	-7.4213	1.0384	-0.0985
110	-9.8947	0.9206	-0.0995
120	-14.5007	0.7235	-0.0985
130	-25.1046	0.4363	-0.0741
135	-34.0185	0.2941	-0.0563

5.4 Three-terminal Transmission Line Example Test System

The three-terminal line example test system is partially illustrated in Figure 5.11. The line of interest is a 500kV, 4330 MVA three-terminal transmission line. The lengths of branch 1 (A1-T), branch 2 (A2-T) and branch 3 (A3-T) are shown in the figure. Here three phase voltage and current measurements are installed at all three terminals of the transmission line (A1, A2 and A3). The rest of the network is not shown. The sequence parameters of the transmission line are shown in Table 5.1. The tower structure and R, L and C matrices of the transmission line are the same as those in Chapter 4 (in Figure 4.2

and Table 4.2). A number of events have been simulated and the results have been stored in COMTRADE files, with standard 4800 samples/second according to IEC 61850-9-2LE standard.

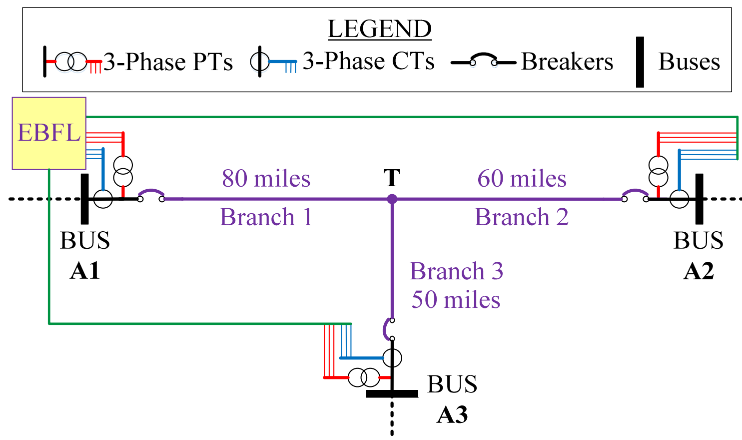

Figure 5.11. 500kV, three-terminal line example test system

5.5 Legacy Fault Locating Schemes of Three-terminal Transmission Lines

We assumed that legacy fundamental frequency phasor based fault locating schemes are applied to this line to estimate the location of the fault. The legacy method first estimates the branch that the fault locates in, and next finds the location of the fault inside that specific branch. It simply estimates the voltage phasor at tap T from the terminal voltage and current phasors of two healthy branches; the branch with fault is the branch which has different estimation of the voltage phasor at tap T. Afterwards, the three-terminal line fault locating problem is equivalently transferred into a two-terminal line fault locating problem. Similarly as in section 5.2, single-ended and dual-ended methods can be utilized to determine the location of the fault.

The reason we do not consider traveling wave based legacy methods is that, (a) the sampling rate here is too low for an estimated fault location with reasonable accuracy, and (b) traveling wave based methods have limitations in three-terminal lines since they cannot differentiate the reflection from the tap point and from the terminal of lines.

For our proposed EBFL on three-terminal lines, one important step is to determine the branch that the fault locates in. This is achieved by building three different models where each model corresponds to the fault inside each branch. Three models are running simultaneously with all available measurements and two of the fault locating results will generally converge to unrealistic values (less than zero or larger than the whole length of the branch) or simply diverge.

5.6 Event Studies of Three-terminal Transmission Lines

We compare the performance of the legacy fault locating schemes to EBFL method with different test cases as described below. Here we will only present results for phase A to neutral faults and phase A to B faults, inside branch 1. Nevertheless, the results are similar for other fault types and fault locations.

Test Case 5: Bolt Phase A to N Faults in Branch 1

Bolt phase A to neutral faults at different fault locations in Branch 1 are tested. The results are provided in Table 5.7 and Figure 5.12. We can observe that, EBFL method is more accurate than both legacy methods.

Table 5.7. Fault locating error of bolt phase A to N faults, variable fault location in Branch 1 (in miles)

Fault Location	*Single-Ended*	*Dual-Ended*	*EBFL*
1	0.2303	0.0309	-0.0839
10	0.0773	0.0496	-0.1329
20	0.1623	0.1726	-0.1872
30	0.2992	0.32	-0.2606
40	0.4628	0.4735	-0.2875
50	0.6561	0.6294	-0.2599
60	0.8811	0.7847	-0.2106
70	1.1368	0.9346	-0.15
80	1.4244	1.076	-0.0757
90	1.7476	1.2053	0.0137
100	2.1047	1.3187	0.1177
110	2.4959	1.4123	0.2293
120	2.9239	1.4829	0.3333
130	3.3876	1.527	0.4051
135	3.8833	1.5412	0.4294

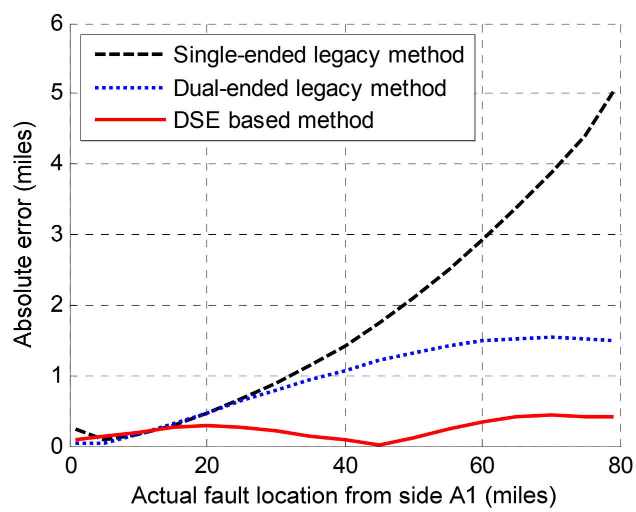

Figure 5.12. Fault locating results comparison, bolt phase A to neutral faults, variable fault location in Branch 1

Test Case 6: Impedance Phase A to N Faults in Branch 1

10 ohm phase A to neutral faults at different fault locations in Branch 1 are tested. The results are provided in Table 5.8 and Figure 5.13. We can observe that, EBFL method is more accurate than both legacy methods.

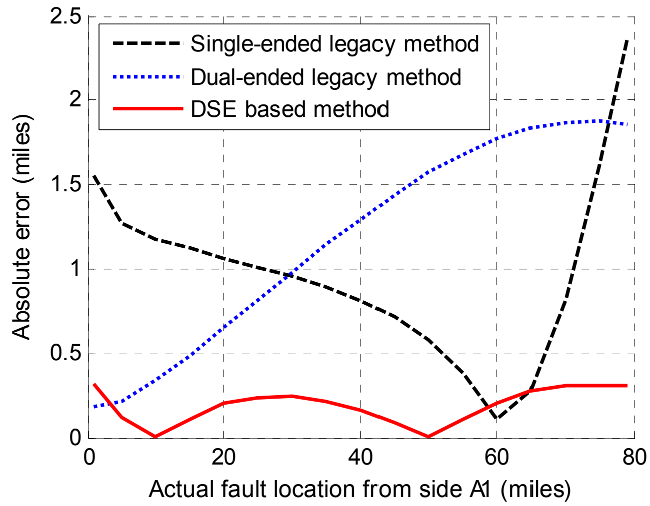

Figure 5.13. Fault locating results comparison, impedance phase A to neutral faults, 10 ohm fault impedance, variable fault location in Branch 1

Table 5.8. Fault locating error of impedance phase A to N faults, variable fault location in Branch 1 (in miles)

Fault Location	*Single-Ended*	*Dual-Ended*	*EBFL*
1	1.5564	0.1847	0.3186
10	1.269	0.2106	0.1244
20	1.1799	0.3387	0.0002
30	1.1205	0.4912	-0.1141
40	1.0644	0.6513	-0.2019
50	1.0109	0.8155	-0.2399
60	0.9558	0.9803	-0.2413
70	0.8928	1.1419	-0.2124

Table 5.8. continued

80	0.8146	1.2965	-0.1645
90	0.7141	1.4406	-0.0919
100	0.5758	1.5702	0.0007
110	0.3826	1.6816	0.106
120	0.1113	1.7715	0.2081
130	-0.2737	1.8361	0.2824
135	-0.826	1.8723	0.3128

Test Case 7: Bolt Phase A to B Faults in Branch 1

Bolt phase A to B faults at different fault locations in Branch 1 are tested. The results are provided in Table 5.9 and Figure 5.14. We can observe that, EBFL method is more accurate than both legacy methods.

Table 5.9. Fault locating error of bolt phase A to B faults, variable fault location in Branch 1 (in miles)

Fault Location	*Single-Ended*	*Dual-Ended*	*EBFL*
1	-0.0307	0.567	-0.0314
10	-0.1443	0.5492	-0.0293
20	-0.2717	0.557	-0.0144
30	-0.3817	0.5851	0.008
40	-0.4733	0.6294	0.0293
50	-0.5455	0.6867	0.0467
60	-0.5973	0.753	0.06
70	-0.6274	0.8249	0.0716
80	-0.6352	0.8983	0.0827

Table 5.9. continued

90	-0.6195	0.9695	0.0949
100	-0.5798	1.0341	0.1088
110	-0.5144	1.0888	0.1249
120	-0.4235	1.1291	0.1409
130	-0.3061	1.1513	0.1515
135	-0.1619	1.1517	0.1496

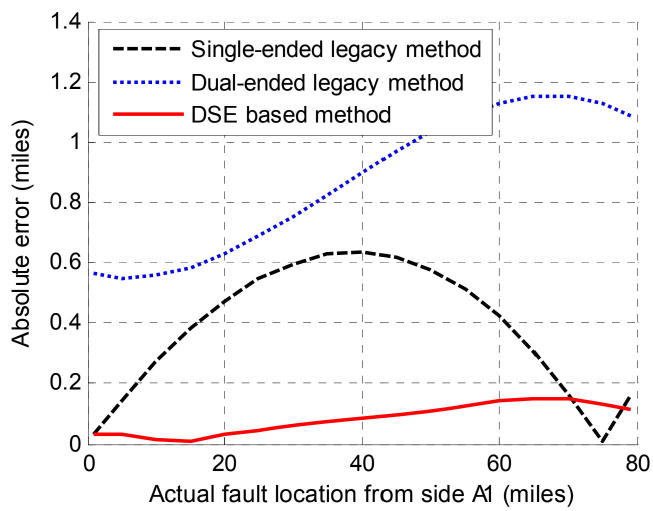

Figure 5.14. Fault locating results comparison, bolt phase A to B faults, variable fault location in Branch 1

Test Case 8: Impedance Phase A to B Faults in Branch 1

10 ohm phase A to B faults at different fault locations in Branch 1 are tested. The results are provided in Table 5.10 and Figure 5.15. We can observe that, EBFL method is more accurate than both legacy methods.

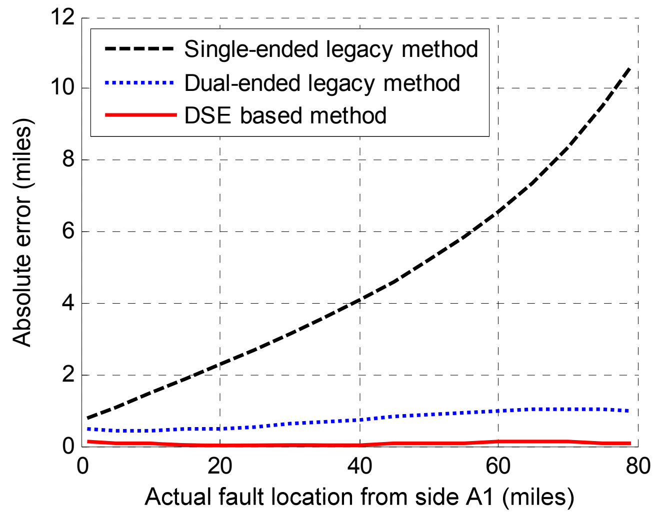

Figure 5.15. Fault locating results comparison, impedance phase A to B faults, 10 ohm fault impedance, variable fault location in Branch 1

Table 5.10. Fault locating error of impedance phase A to B faults, variable fault location in Branch 1 (in miles)

Fault Location	*Single-Ended*	*Dual-Ended*	*EBFL*
1	-0.7752	0.4543	-0.1118
10	-1.0836	0.4357	-0.0986
20	-1.4742	0.4349	-0.0718
30	-1.8722	0.4547	-0.0397
40	-2.2799	0.4922	-0.0122
50	-2.7008	0.544	0.0092
60	-3.1389	0.6067	0.0252
70	-3.5994	0.6764	0.0375
80	-4.0889	0.7497	0.049
90	-4.6159	0.8222	0.0606
100	-5.1914	0.8902	0.074
110	-5.8296	0.9498	0.0887
120	-6.5491	0.9968	0.1032
130	-7.3748	1.0275	0.1126
135	-8.341	1.0377	0.1098

5.7 Summary of Proposed EBFL Scheme

This chapter compares the performance of EBFL to legacy fault locating schemes. The proposed **EBFL** has the following advantages: (a) it uses a high-fidelity multi-section transmission line dynamic model; (b) it utilizes instantaneous values (sampled values) instead of phasors enabling estimation of the fault location in the presence of transients, which is very important when the fault duration is short; (c) it demonstrates higher accuracy compared with legacy fault locating schemes; (d) the sampling rate it requires is relatively low (in this case 4.8 kilo-samples per second) and therefore it can be used with existing instrumentation in substations.

CHAPTER 6 Numerical Experiments of Transmission Line EBPI during Normal Operating Conditions

This chapter describes the application on transmission line parameter identification (Dynamic State **E**stimation **B**ased **P**arameter **I**dentification, **EBPI**) during normal operating conditions. The reason for the parameter identification is to make sure high-fidelity dynamic models for transmission line EBP and EBFL applications. Section 6.1 introduced the interested parameters of transmission line EBPI; section 6.2 describes an example transmission line test system; section 6.3 demonstrates EBPI results; section 6.4 concludes the proposed transmission line EBPI.

6.1 Parameters of Interest in Transmission Line EBPI

Traditional parameters for transmission lines could include series resistance ($\mathbf{R}_1$), series inductance ($\mathbf{L}_1$), shunt capacitance ($\mathbf{C}_1$) and shunt conductance ($\mathbf{G}_1$) matrices of the transmission line per mile. However, there are extensive entries inside these matrices and some of these entries are dependent on each other. Therefore, it is desirable to find parameters that are independent from each other.

Here three parameters are selected based on the physical structure of the transmission line: the total length of the line (l), the average height of the phase conductors (h) and the average distance between phase conductors (d), as shown in Figure 6.1. These parameters could have approximate values based on physical measurements. However, transmission lines always have sags, which may cause the fact that these physically measured values may not be accurate. As shown in Figure 6.1, for example, the average height of phase conductors may be smaller than the height of phase conductors measured at towers; the total length of the line may be longer than the length that is geographically measured; the distance between phase conductors could also be different compared to the distance between phase conductors measured at towers. Detail SCPQDMs of transmission line EBPI are provided in Appendix C.

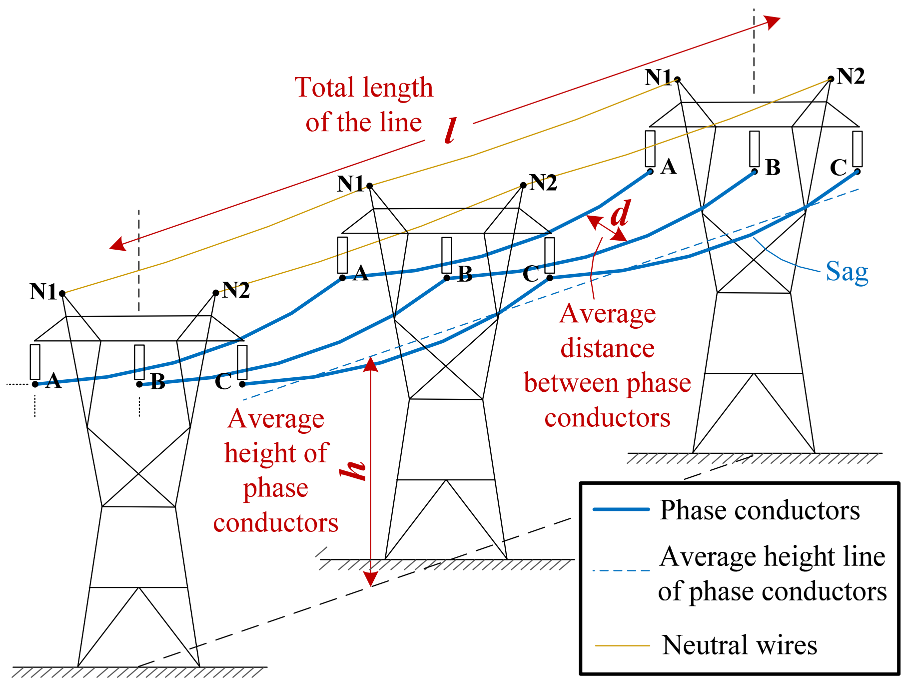

Figure 6.1. Example tower structure of the transmission line

6.2 Transmission Line Example Test System

The transmission line example test system is partially illustrated in Figure 6.2. The full network used for the simulations is not shown. The line of interest (A1-A2) is a 500kV, 135.22 mile-long, 4330 MVA transmission line. Three phase voltage and current measurements are installed at both terminals of the transmission line. The tower is the same as shown in Figure 6.1. Different combinations of the total length of the line, the distance between phase conductors and the height of phase conductors are considered. The simulation results (during normal operating conditions) have been stored in

COMTRADE files, with standard 4800 samples/second according to IEC 61850-9-2LE standard.

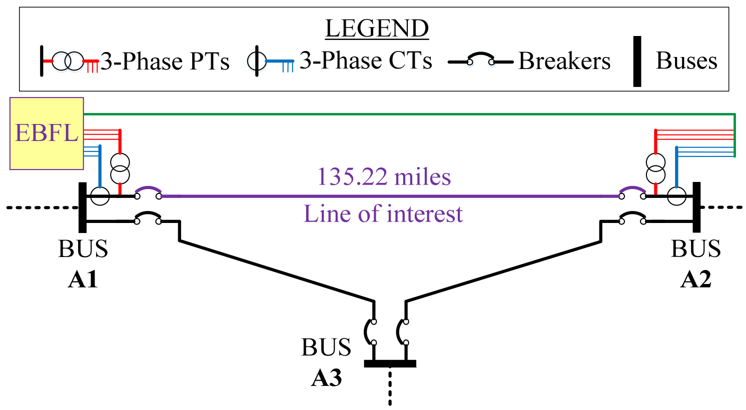

Figure 6.2. 500kV transmission line example test system

6.3 Calculation of Linearization Coefficients

From Appendix C, the models are built based on linearization near the present parameters. This is because the mathematically relationship between the parameters (l, h and d) and the matrices ($\mathbf{R}_1, \mathbf{L}_1, \mathbf{C}_1$, and $\mathbf{G}_1$) series resistance, series inductance, shunt capacitance and shunt conductance) are highly nonlinear. In this section, examples of calculating linearization coefficients are introduced.

For height linearization coefficients $\boldsymbol{\alpha}_R^{(h_0)}$, $\boldsymbol{\alpha}_L^{(h_0)}$, $\boldsymbol{\alpha}_C^{(h_0)}$ and $\boldsymbol{\alpha}_G^{(h_0)}$,where

$$\mathbf{R}_1 = \mathbf{R}_1^{(h_0)} + \boldsymbol{\alpha}_R^{(h_0)} \cdot (h - h_0) \tag{6.1}$$

$$\mathbf{L}_1 = \mathbf{L}_1^{(h_0)} + \boldsymbol{\alpha}_L^{(h_0)} \cdot (h - h_0) \tag{6.2}$$

$$\mathbf{C}_1 = \mathbf{C}_1^{(h_0)} + \boldsymbol{\alpha}_C^{(h_0)} \cdot (h - h_0) \tag{6.3}$$

$$\mathbf{G}_1 = \mathbf{G}_1^{(h_0)} + \boldsymbol{\alpha}_G^{(h_0)} \cdot (h - h_0) \tag{6.4}$$

Therefore, select one h_1 (with corresponding matrices $\mathbf{R}_1^{(h_1)}$, $\mathbf{L}_1^{(h_1)}$, $\mathbf{C}_1^{(h_1)}$, $\mathbf{G}_1^{(h_1)}$) that is near the initial value h_0 (with corresponding matrices $\mathbf{R}_1^{(h_0)}$, $\mathbf{L}_1^{(h_0)}$, $\mathbf{C}_1^{(h_0)}$, $\mathbf{G}_1^{(h_0)}$) to calculate $\boldsymbol{\alpha}_R^{(h_0)}$, $\boldsymbol{\alpha}_L^{(h_0)}$, $\boldsymbol{\alpha}_C^{(h_0)}$ and $\boldsymbol{\alpha}_G^{(h_0)}$,

$$\boldsymbol{\alpha}_R^{(h_0)} = \frac{\mathbf{R}_1^{(h_1)} - \mathbf{R}_1^{(h_0)}}{h_1 - h_0} \tag{6.5}$$

$$\boldsymbol{\alpha}_L^{(h_0)} = \frac{\mathbf{L}_1^{(h_1)} - \mathbf{L}_1^{(h_0)}}{h_1 - h_0} \tag{6.6}$$

$$\boldsymbol{\alpha}_C^{(h_0)} = \frac{\mathbf{C}_1^{(h_1)} - \mathbf{C}_1^{(h_0)}}{h_1 - h_0} \tag{6.7}$$

$$\boldsymbol{\alpha}_G^{(h_0)} = \frac{\mathbf{G}_1^{(h_1)} - \mathbf{G}_1^{(h_0)}}{h_1 - h_0} \tag{6.8}$$

For distance linearization coefficients $\boldsymbol{\beta}_R^{(d_0)}$, $\boldsymbol{\beta}_L^{(d_0)}$, $\boldsymbol{\beta}_C^{(d_0)}$ and $\boldsymbol{\beta}_G^{(d_0)}$,where

$$\mathbf{R}_1 = \mathbf{R}_1^{(d_0)} + \boldsymbol{\beta}_R^{(d_0)} \cdot (d - d_0) \tag{6.9}$$

$$\mathbf{L}_1 = \mathbf{L}_1^{(d_0)} + \boldsymbol{\beta}_L^{(d_0)} \cdot (d - d_0) \tag{6.10}$$

$$\mathbf{C}_1 = \mathbf{C}_1^{(d_0)} + \boldsymbol{\beta}_C^{(d_0)} \cdot (d - d_0) \tag{6.11}$$

$$\mathbf{G}_1 = \mathbf{G}_1^{(d_0)} + \boldsymbol{\beta}_G^{(d_0)} \cdot (d - d_0) \tag{6.12}$$

Therefore, select one d_1 (with corresponding matrices $\mathbf{R}_1^{(d_1)}$, $\mathbf{L}_1^{(d_1)}$, $\mathbf{C}_1^{(d_1)}$, $\mathbf{G}_1^{(d_1)}$) that is near the initial value d_0 (with corresponding matrices $\mathbf{R}_1^{(d_0)}$, $\mathbf{L}_1^{(d_0)}$, $\mathbf{C}_1^{(d_0)}$, $\mathbf{G}_1^{(d_0)}$) to calculate $\boldsymbol{\alpha}_R^{(d_0)}$, $\boldsymbol{\alpha}_L^{(d_0)}$, $\boldsymbol{\alpha}_C^{(d_0)}$ and $\boldsymbol{\alpha}_G^{(d_0)}$,

$$\boldsymbol{\beta}_R^{(d_0)} = \frac{\mathbf{R}_1^{(d_1)} - \mathbf{R}_1^{(d_0)}}{d_1 - d_0} \tag{6.13}$$

$$\boldsymbol{\beta}_L^{(d_0)} = \frac{\mathbf{L}_1^{(d_1)} - \mathbf{L}_1^{(d_0)}}{d_1 - d_0} \tag{6.14}$$

$$\boldsymbol{\beta}_C^{(d_0)} = \frac{\mathbf{C}_1^{(d_1)} - \mathbf{C}_1^{(d_0)}}{d_1 - d_0} \tag{6.15}$$

$$\boldsymbol{\beta}_G^{(d_0)} = \frac{\mathbf{G}_1^{(d_1)} - \mathbf{G}_1^{(d_0)}}{d_1 - d_0} \tag{6.16}$$

For example, here we calculate the linearization coefficient at height $h_0 = 100$ feet and distance $d_0 = 40$ feet. Select $h_1 = 110$ feet and $d_1 = 30$ feet.

Matrices with h_0 = 100 feet, d_0 = 40 feet

$\mathbf{R}_1^{(100,40)} =$

[0.104347590176 0.088583249026 0.088520253655 0.087708846378 0.087665381084

0.088583249026 0.104347590176 0.088583249026 0.087706865179 0.087706865179

0.088520253655 0.088583249026 0.104347590176 0.087665381084 0.087708846378

0.087708846378 0.087706865179 0.087665381084 2.356843656902 0.086821105107

0.087665381084 0.087706865179 0.087708846378 0.086821105107 2.356843656902]

/1609.344 ohm/m

$\mathbf{L}_1^{(100,40)} =$

[0.002787891873 0.001385703060 0.001162707720 0.001431639815 0.001213702381

0.001385703060 0.002787891873 0.001385703060 0.001411874608 0.001411874608

0.001162707720 0.001385703060 0.002787891873 0.001213702381 0.001431639815

0.001431639815 0.001411874608 0.001213702381 0.005546572070 0.001360715345

0.001213702381 0.001411874608 0.001431639815 0.001360715345 0.005546572070]

/1609.344 H/m

$\mathbf{C}_1^{(100,40)}$ =

$$\left[\begin{array}{ccccc} 0.008673213756 & -0.001702280372 & -0.000570448536 & -0.001271058847 & -0.000467020645 \\ -0.001702280372 & 0.009188610795 & -0.001702280372 & -0.001041558379 & -0.001041558379 \\ -0.000570448536 & -0.001702280372 & 0.008673213756 & -0.000467020645 & -0.001271058847 \\ -0.001271058847 & -0.001041558379 & -0.000467020645 & 0.005506436407 & -0.000597139505 \\ -0.000467020645 & -0.001041558379 & -0.001271058847 & -0.000597139505 & 0.005506436407 \end{array}\right]$$

/1609.344 uF/ m

$\mathbf{G}_1^{(100,40)}$ =

$$\left[\begin{array}{ccccc} 0.0000 & 0.0000 & 0.0000 & 0.0000 & 0.0000 \\ 0.0000 & 0.0000 & 0.0000 & 0.0000 & 0.0000 \\ 0.0000 & 0.0000 & 0.0000 & 0.0000 & 0.0000 \\ 0.0000 & 0.0000 & 0.0000 & 0.0000 & 0.0000 \\ 0.0000 & 0.0000 & 0.0000 & 0.0000 & 0.0000 \end{array}\right]$$ mho/m

Matrices with h = 110 feet, d_0 = 40 feet:

$\mathbf{R}_1^{(110,40)}$ =

$$\left[\begin{array}{ccccc} 0.103750690896 & 0.087987262362 & 0.087926935707 & 0.087416782473 & 0.087374196810 \\ 0.087987262362 & 0.103750690896 & 0.087987262362 & 0.087414841703 & 0.087414841703 \\ 0.087926935707 & 0.087987262362 & 0.103750690896 & 0.087374196810 & 0.087416782473 \\ 0.087416782473 & 0.087414841703 & 0.087374196810 & 2.356843656902 & 0.086821105107 \\ 0.087374196810 & 0.087414841703 & 0.087416782473 & 0.086821105107 & 2.356843656902 \end{array}\right]$$

/1609.344 ohm/m

$\mathbf{L}_1^{(110,40)}$=

[0.002789794873 0.001387605846 0.001164609867 0.001517071845 0.001232567659
0.001387605846 0.002789794873 0.001387605846 0.001484947578 0.001484947578
0.001164609867 0.001387605846 0.002789794873 0.001232567659 0.001517071845
0.001517071845 0.001484947578 0.001232567659 0.005546572070 0.001360715345
0.001232567659 0.001484947578 0.001517071845 0.001360715345 0.005546572070]
/1609.344 H/m

$\mathbf{C}_1^{(110,40)}$=

[0.008718638097 -0.001646366405 -0.000583065500 -0.001526953216 -0.000455366401
-0.001646366405 0.009293927180 -0.001646366405 -0.001240030942 -0.001240030942
-0.000583065500 -0.001646366405 0.008718638097 -0.000455366401 -0.001526953216
-0.001526953216 -0.001240030942 -0.000455366401 0.005666947543 -0.000490141322
-0.000455366401 -0.001240030942 -0.001526953216 -0.000490141322 0.005666947543]
/1609.344 uF/m

$\mathbf{G}_1^{(110,40)}$=

[0.0000 0.0000 0.0000 0.0000 0.0000
0.0000 0.0000 0.0000 0.0000 0.0000
0.0000 0.0000 0.0000 0.0000 0.0000
0.0000 0.0000 0.0000 0.0000 0.0000
0.0000 0.0000 0.0000 0.0000 0.0000] mho/m

Matrices with h_0 = 100 feet, d = 30 feet

$\mathbf{R}_1^{(100,30)}$ =

[0.104347590176 0.088592486771 0.088556927835 0.087712066960 0.087679430362

0.088592486771 0.104347590176 0.088592486771 0.087706865178 0.087706865179

0.088556927835 0.088592486771 0.104347590176 0.087679430362 0.087712066960

0.087712066960 0.087706865178 0.087679430362 2.356843656902 0.086821105107

0.087679430362 0.087706865179 0.087712066960 0.086821105107 2.356843656902]

/1609.344 ohm/m

$\mathbf{L}_1^{(100,30)}$ =

[0.002787891873 0.001478270483 0.001255249151 0.001470057663 0.001257909658

0.001478270483 0.002787891873 0.001478270483 0.001411874608 0.001411874608

0.001255249151 0.001478270483 0.002787891873 0.001257909658 0.001470057663

0.001470057663 0.001411874608 0.001257909658 0.005546572070 0.001360715345

0.001257909658 0.001411874608 0.001470057663 0.001360715345 0.005546572070]

/1609.344 H/m

$\mathbf{C}_1^{(100,30)}$ =

[0.009012027914 -0.002110249121 -0.000744939125 -0.001333986086 -0.000498877545

-0.002110249121 0.009550679371 -0.002110249121 -0.000938850151 -0.000938850151

-0.000744939125 -0.002110249121 0.009012027914 -0.000498877545 -0.001333986086

-0.001333986086 -0.000938850151 -0.000498877548 0.005523972166 -0.000581144150

-0.000498877545 -0.000938850151 -0.001333986086 -0.000581144150 0.005523972166]

/1609.344 uF/ m

$\mathbf{G}_1^{(100,30)}$ =

[0.0000 0.0000 0.0000 0.0000 0.0000

0.0000 0.0000 0.0000 0.0000 0.0000

0.0000 0.0000 0.0000 0.0000 0.0000

0.0000 0.0000 0.0000 0.0000 0.0000

0.0000 0.0000 0.0000 0.0000 0.0000] mho/m

Therefore, the linearization coefficients (at h_0 = 100 feet, d_0 = 40 feet) $\boldsymbol{\alpha}_R^{(h_0,d_0)}$, $\boldsymbol{\alpha}_L^{(h_0,d_0)}$, $\boldsymbol{\alpha}_C^{(h_0,d_0)}$, $\boldsymbol{\alpha}_G^{(h_0,d_0)}$, $\boldsymbol{\beta}_R^{(h_0,d_0)}$, $\boldsymbol{\beta}_L^{(h_0,d_0)}$, $\boldsymbol{\beta}_C^{(h_0,d_0)}$ and $\boldsymbol{\beta}_G^{(h_0,d_0)}$ are calculated as follows.

For $\boldsymbol{\alpha}_R^{(h_0,d_0)}$, $\boldsymbol{\alpha}_L^{(h_0,d_0)}$, $\boldsymbol{\alpha}_C^{(h_0,d_0)}$, $\boldsymbol{\alpha}_G^{(h_0,d_0)}$, they are calculated by the value of (h_0 = 100 feet, d_0 = 40 feet) and (h = 110 feet, d_0 = 40 feet).

$$\boldsymbol{\alpha}_R^{(h_0,d_0)} = \frac{\mathbf{R}_1^{(h_1,d_0)} - \mathbf{R}_1^{(h_0,d_0)}}{h_1 - h_0} = \frac{\mathbf{R}_1^{(110,40)} - \mathbf{R}_1^{(100,40)}}{110-100} =$$

[-5.96899280	-5.95986664	-5.93317948	-2.92063905	-2.91184274
-5.95986664	-5.96899280	-5.95986664	-2.92023476	-2.92023476
-5.93317948	-5.95986664	-5.96899280	-2.91184274	-2.92063905
-2.92063905	-2.92023476	-2.91184274	0	0
-2.91184274	-2.92023476	-2.92063905	0	0]

/1609.344/0.3048*10^{-5} ohm/m^2

$$\boldsymbol{\alpha}_L^{(h_0,d_0)} = \frac{\mathbf{L}_1^{(h_1,d_0)} - \mathbf{L}_1^{(h_0,d_0)}}{h_1 - h_0} = \frac{\mathbf{L}_1^{(110,40)} - \mathbf{L}_1^{(100,40)}}{110-100} =$$

[0.01903000	0.01902786	0.01902147	0.85432030	0.18865278
0.01902786	0.01903000	0.01902786	0.73072970	0.73072970
0.01902147	0.01902786	0.01903000	0.18865278	0.85432030

0.85432030 0.7307297 0.18865278 0 0

0.18865278 0.7307297 0.85432030 0 0]

/1609.344/0.3048*10^{-5} H/m^2

$$\boldsymbol{\alpha}_C^{(h_0,d_0)} = \frac{\mathbf{C}_1^{(h_1,d_0)} - \mathbf{C}_1^{(h_0,d_0)}}{h_1 - h_0} = \frac{\mathbf{C}_1^{(110,40)} - \mathbf{C}_1^{(100,40)}}{110-100} =$$

[0.45424341	0.55913967	-0.12616964	-2.55894369	0.11654244
0.55913967	1.05316385	0.55913967	-1.98472563	-1.98472563
-0.12616964	0.55913967	0.45424341	0.11654244	-2.55894369
-2.55894369	-1.98472563	0.11654244	1.60511136	1.06998183
0.11654244	-1.98472563	-2.55894369	1.06998183	1.60511136]

/1609.344/0.3048*10^{-5} uF/m^2

$$\boldsymbol{\alpha}_G^{(h_0,d_0)} = \frac{\mathbf{G}_1^{(h_1,d_0)} - \mathbf{G}_1^{(h_0,d_0)}}{h_1 - h_0} = \frac{\mathbf{G}_1^{(110,40)} - \mathbf{G}_1^{(100,40)}}{110-100} =$$

[0	0	0	0	0
0	0	0	0	0
0	0	0	0	0
0	0	0	0	0
0	0	0	0	0]

mho/m^2

For $\boldsymbol{\beta}_R^{(h_0,d_0)}$, $\boldsymbol{\beta}_L^{(h_0,d_0)}$, $\boldsymbol{\beta}_C^{(h_0,d_0)}$ and $\boldsymbol{\beta}_G^{(h_0,d_0)}$, they are calculated by the value of (h_0 = 100 feet, d_0 = 40 feet) and (h_0 = 100 feet, d = 30 feet).

$$\boldsymbol{\beta}_R^{(h_0,d_0)} = \frac{\mathbf{R}_1^{(h_0,d_1)} - \mathbf{R}_1^{(h_0,d_0)}}{d_1 - d_0} = \frac{\mathbf{R}_1^{(100,30)} - \mathbf{R}_1^{(100,40)}}{30-40} =$$

[0	-0.9237745	-3.6674180	-0.3220582	-1.4049278
-0.9237745	0	-0.9237745	0	0
-3.6674180	-0.9237745,	0	-1.4049278	-0.3220582
-0.3220582	0	-1.4049278	0	0
-1.4049278	0	-0.3220582	0	0]

/1609.344/0.3048*10^{-6} ohm/m^2

$$\boldsymbol{\beta}_L^{(h_0,d_0)} = \frac{\mathbf{L}_1^{(h_0,d_1)} - \mathbf{L}_1^{(h_0,d_0)}}{d_1 - d_0} = \frac{\mathbf{L}_1^{(100,30)} - \mathbf{L}_1^{(100,40)}}{30-40} =$$

[0	-9.2567423	-9.2541431	-3.8417848	-4.4207277
-9.2567423	0	-9.2567423	0	0
-9.2541431	-9.2567423	0	-4.4207277	-3.8417848
-3.8417848	0	-4.4207277	0	0
-4.4207277	0	-3.8417848	0	0]

/1609.344/0.3048*10^{-6} H/m^2

$$\boldsymbol{\beta}_C^{(h_0,d_0)} = \frac{\mathbf{C}_1^{(h_0,d_1)} - \mathbf{C}_1^{(h_0,d_0)}}{d_1 - d_0} = \frac{\mathbf{C}_1^{(100,30)} - \mathbf{C}_1^{(100,40)}}{30-40} =$$

[-3.38814158 4.07968749 1.74490589 0.62927239 0.31856900]

4.07968749 -3.62068576 4.07968749 -1.02708228 -1.02708228]

1.74490589 4.07968749 -3.38814158 0.31856900 0.62927239]

0.62927239 -1.02708228 0.31856903 -0.17535759 -0.15995355]

0.31856900 -1.02708228 0.62927239 -0.15995355 -0.17535759]

$/1609.344/0.3048*10^{-5}$ uF/m^2

$$\boldsymbol{\beta}_G^{(h_0,d_0)} = \frac{\mathbf{G}_1^{(h_0,d_1)} - \mathbf{G}_1^{(h_0,d_0)}}{d_1 - d_0} = \frac{\mathbf{G}_1^{(100,30)} - \mathbf{G}_1^{(100,40)}}{30-40} =$$

$$\begin{bmatrix} 0 & 0 & 0 & 0 & 0 \\ 0 & 0 & 0 & 0 & 0 \\ 0 & 0 & 0 & 0 & 0 \\ 0 & 0 & 0 & 0 & 0 \\ 0 & 0 & 0 & 0 & 0 \end{bmatrix} \text{ mho/m}^2$$

6.4 Simulation Results

This section provides 4 groups of results. The first group shows the results with one parameter: the total length of the line *l* (model: based on Appendix C.1); the second group shows the results with one parameter: the average distance between phase conductors *d* (model: based on Appendix C.2); the third group shows the results with one parameter: average height of phase conductors *h* (model: based on Appendix C.3); the forth group shows the results with two parameters: length *l* and distance *d* (model: based on Appendix C.4); the fifth group shows the results with two parameters: length *l* and height *h* (model: based on Appendix C.5); the sixth group shows the results with two parameters: distance *d* and height *h* (model: based on Appendix C.6); the seventh group shows the results with three parameters: length l, distance d and height h (model: based on Appendix C.7).

Group 1: with One Parameter (Length)

Test Case 1:

Initial Length: 135.22 miles; **Actual Length**: **134.5** miles;

Initial Distance: 32 feet (9.7536 meters) **Actual Distance**: 32 feet (9.7536 meters)

Initial Height: 100 feet (30.48 meters) **Actual Height**: 100 feet (30.48 meters)

Here the distance and the height are not estimated as a parameter. The actual length differs from the initial length. The estimated length is:

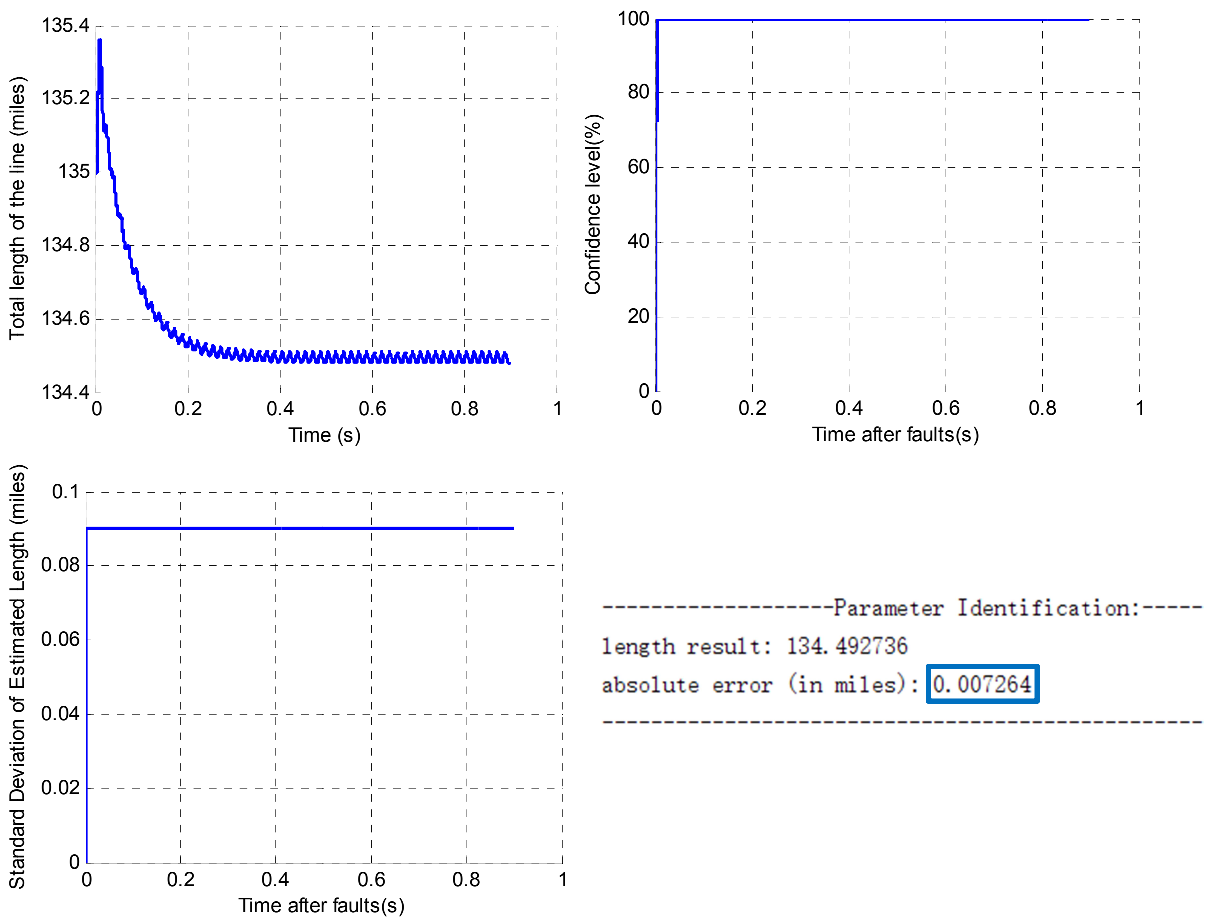

Figure 6.3. Results with one parameter (length) and with actual length 134.5 miles

Test Case 2:

Initial Length: 135.22 miles; **Actual Length**: **136.5** miles;

Initial Distance: 32 feet (9.7536 meters) **Actual Distance**: 32 feet (9.7536 meters)

Initial Height: 100 feet (30.48 meters) **Actual Height**: 100 feet (30.48 meters)

Here the distance and the height are not estimated as a parameter. The actual length differs from the initial length. The estimated length is:

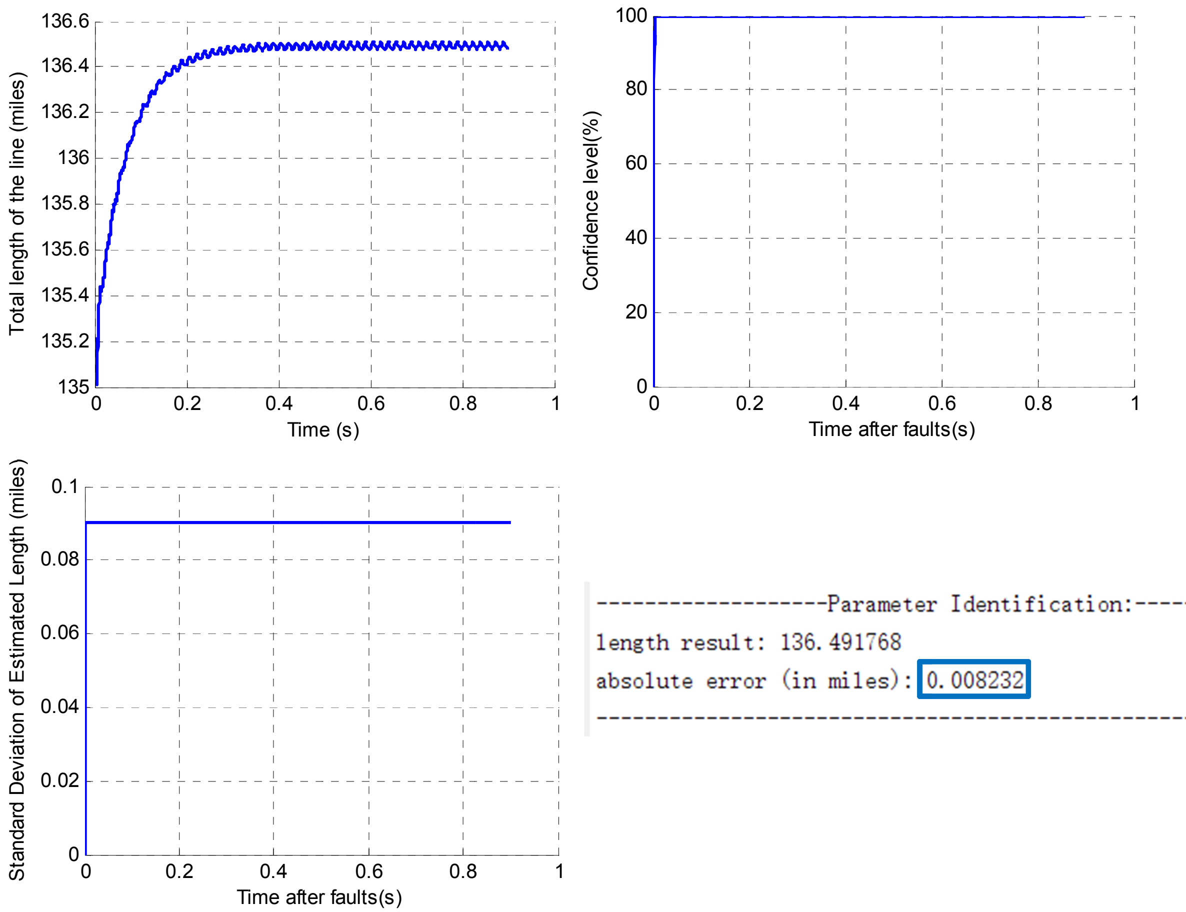

Figure 6.4. Results with one parameter (length) and with actual length 136.5 miles

Test Case 3:

Initial Length: 135.22 miles;	**Actual Length**: **<u>138.5</u>** miles;
Initial Distance: 32 feet (9.7536 meters)	**Actual Distance**: 32 feet (9.7536 meters)
Initial Height: 100 feet (30.48 meters)	**Actual Height**: 100 feet (30.48 meters)

Here the distance and the height are not estimated as a parameter. The actual length differs from the initial length. The estimated length is:

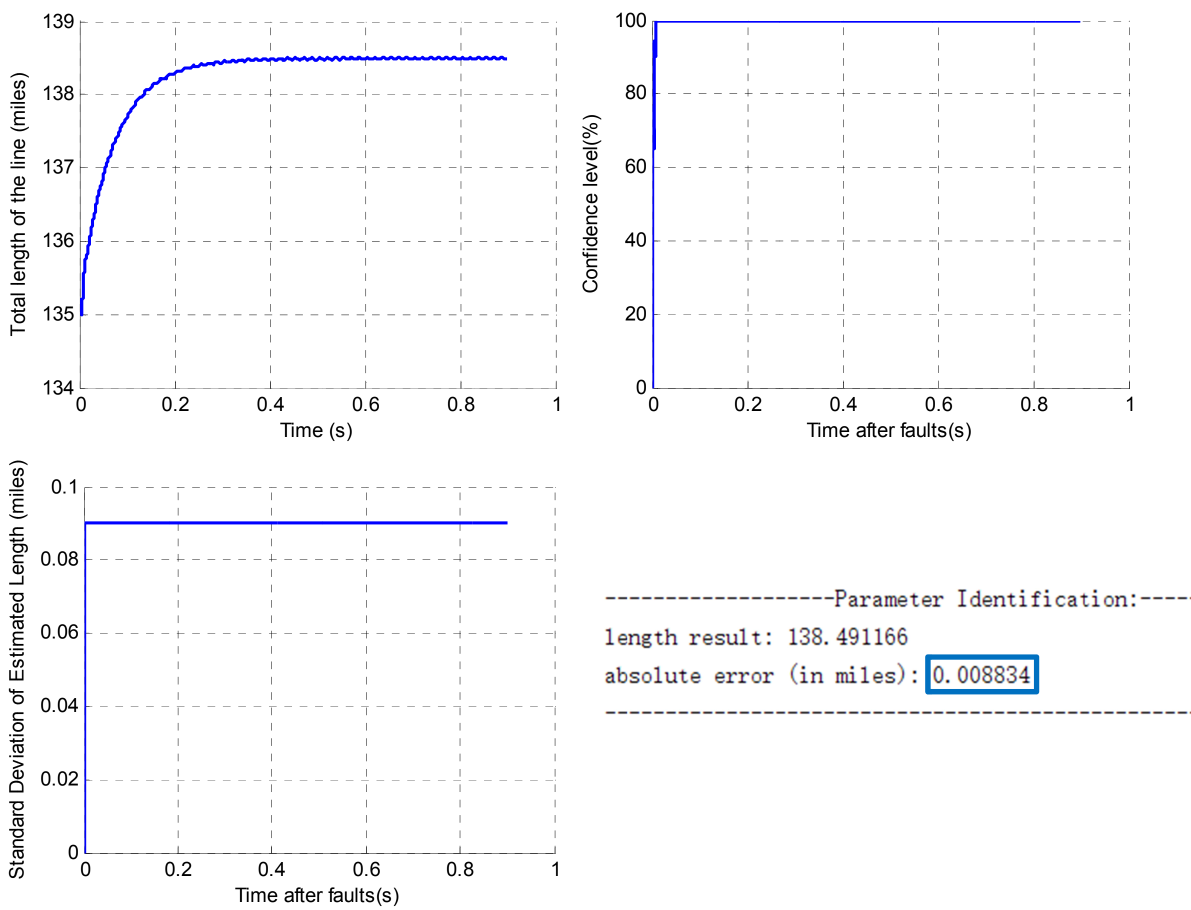

Figure 6.5. Results with one parameter (length) and with actual length 138.5 miles

Test Case 4:

Initial Length: 135.22 miles; **Actual Length**: 140.5 miles;

Initial Distance: 32 feet (9.7536 meters) **Actual Distance**: 32 feet (9.7536 meters)

Initial Height: 100 feet (30.48 meters) **Actual Height**: 100 feet (30.48 meters)

Here the distance and the height are not estimated as a parameter. The actual length differs from the initial length. The estimated length is:

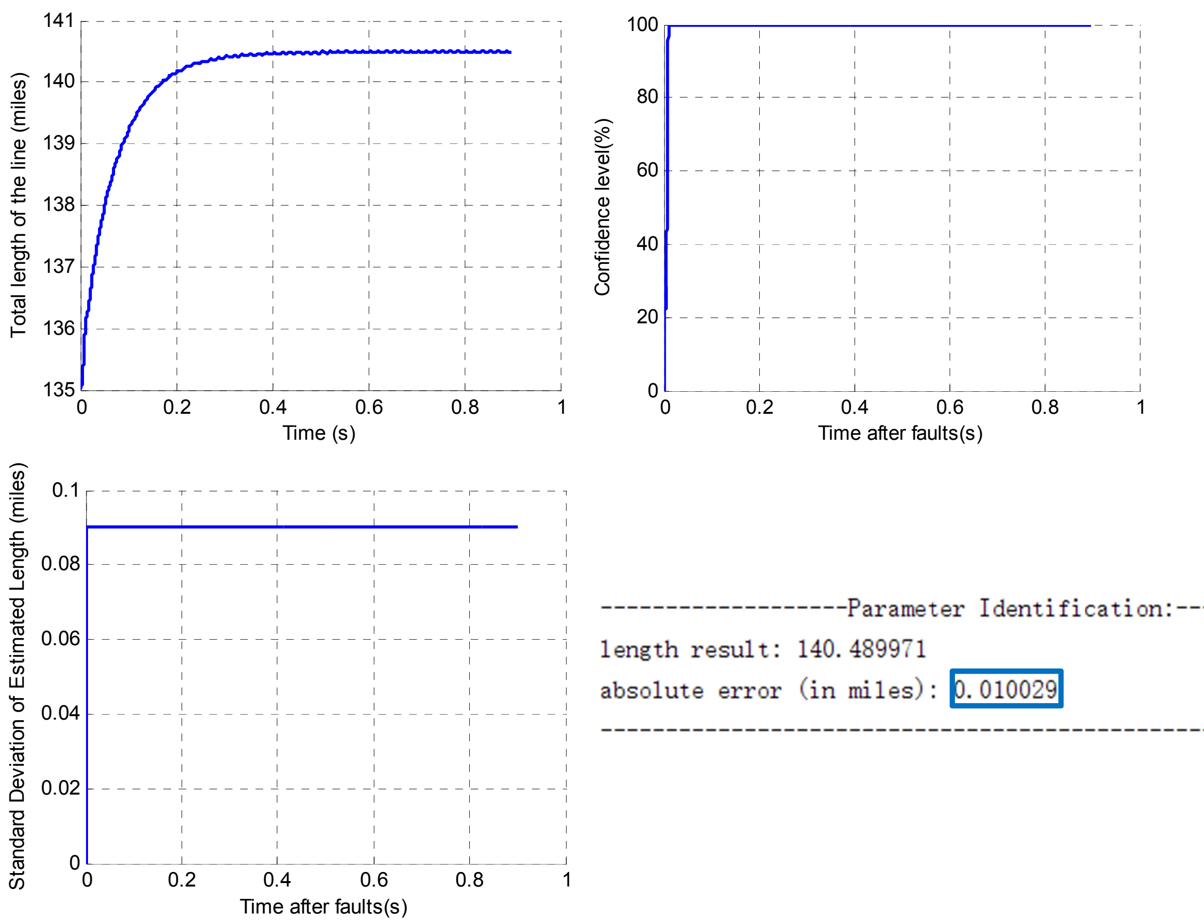

Figure 6.6. Results with one parameter (length) and with actual length 140.5 miles

Test Case 5:

Initial Length: 135.22 miles; **Actual Length**: <u>**142.5**</u> miles;

Initial Distance: 32 feet (9.7536 meters) **Actual Distance**: 32 feet (9.7536 meters)

Initial Height: 100 feet (30.48 meters) **Actual Height**: 100 feet (30.48 meters)

Here the distance and the height are not estimated as a parameter. The actual length differs from the initial length. The estimated length is:

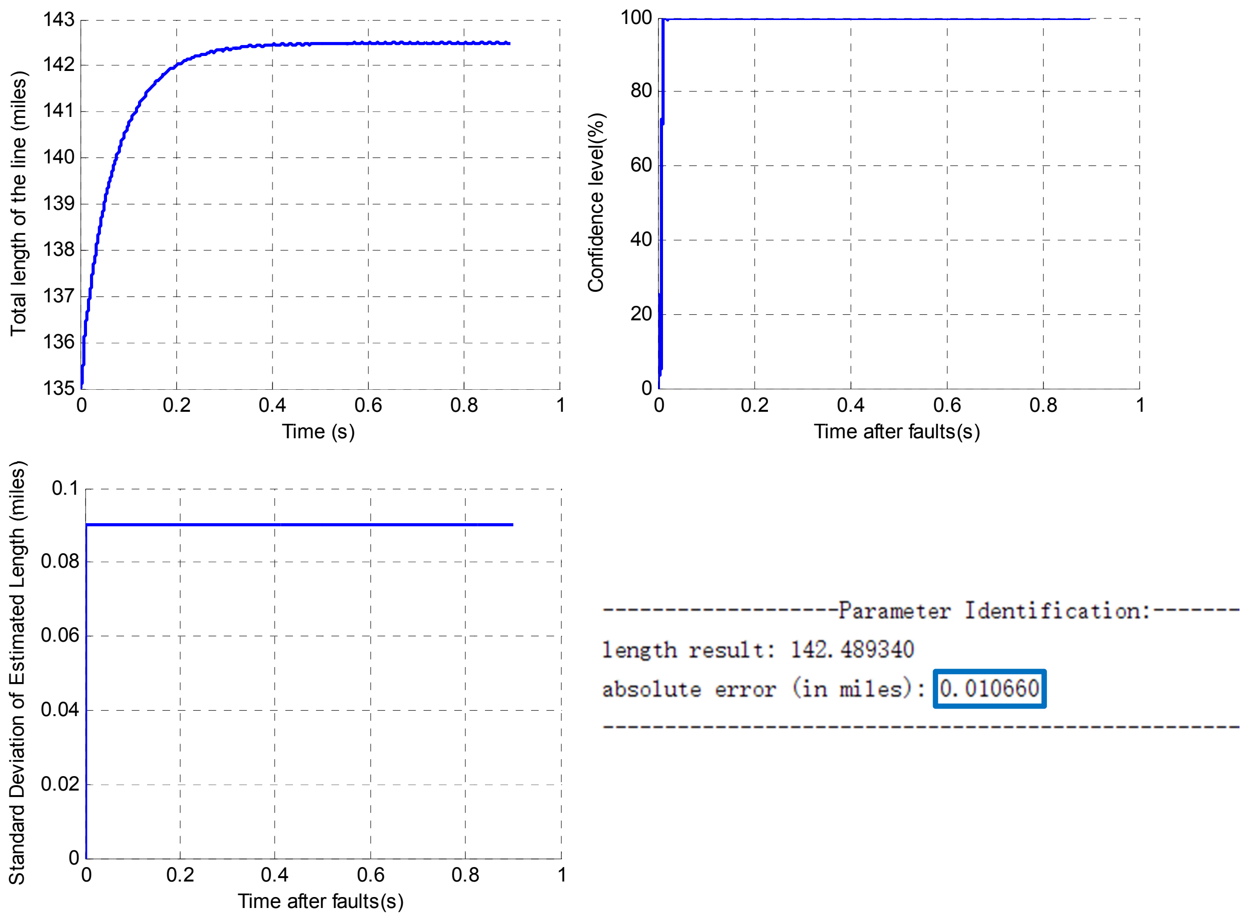

Figure 6.7. Results with one parameter (length) and with actual length 142.5 miles

Summary of Results, Group 1:

From the above simulation results, we can conclude that, for the model with one parameter (length), the length parameter is estimated with very high accuracy, as shown in Table 6.1. As shown in the following table, the length parameter is estimated with very high accuracy.

Table 6.1. Conlusion of results, group 1

Case number	*Actual length (miles)*	*Estimated length (miles)*	*Error (miles)*	*Standard deviation (miles)*	*Error percentage*
1	134.5	134.492736	- 0.007264	0.090	- 0.0054%
2	136.5	136.491768	- 0.008232	0.090	- 0.0060%
3	138.5	138.491166	- 0.008834	0.090	- 0.0064%
4	140.5	140.489971	- 0.010029	0.090	- 0.0071%
5	142.5	142.489340	- 0.010660	0.090	- 0.0075%

Group 2: with One Parameter (Inter-phase Distance)

Test Case 1:

Initial Length: 136.5 miles; **Actual Length**: 136.5 miles;

Initial Distance: 40 feet (12.192 meters) **Actual Distance**: **40 feet** (12.192 meters)

Initial Height: 100 feet (30.48 meters) **Actual Height**: 100 feet (30.48 meters)

Here the length and the height are not estimated as a parameter, and the actual values are exactly the same as the initial values. The estimated distance between the phase conductors is:

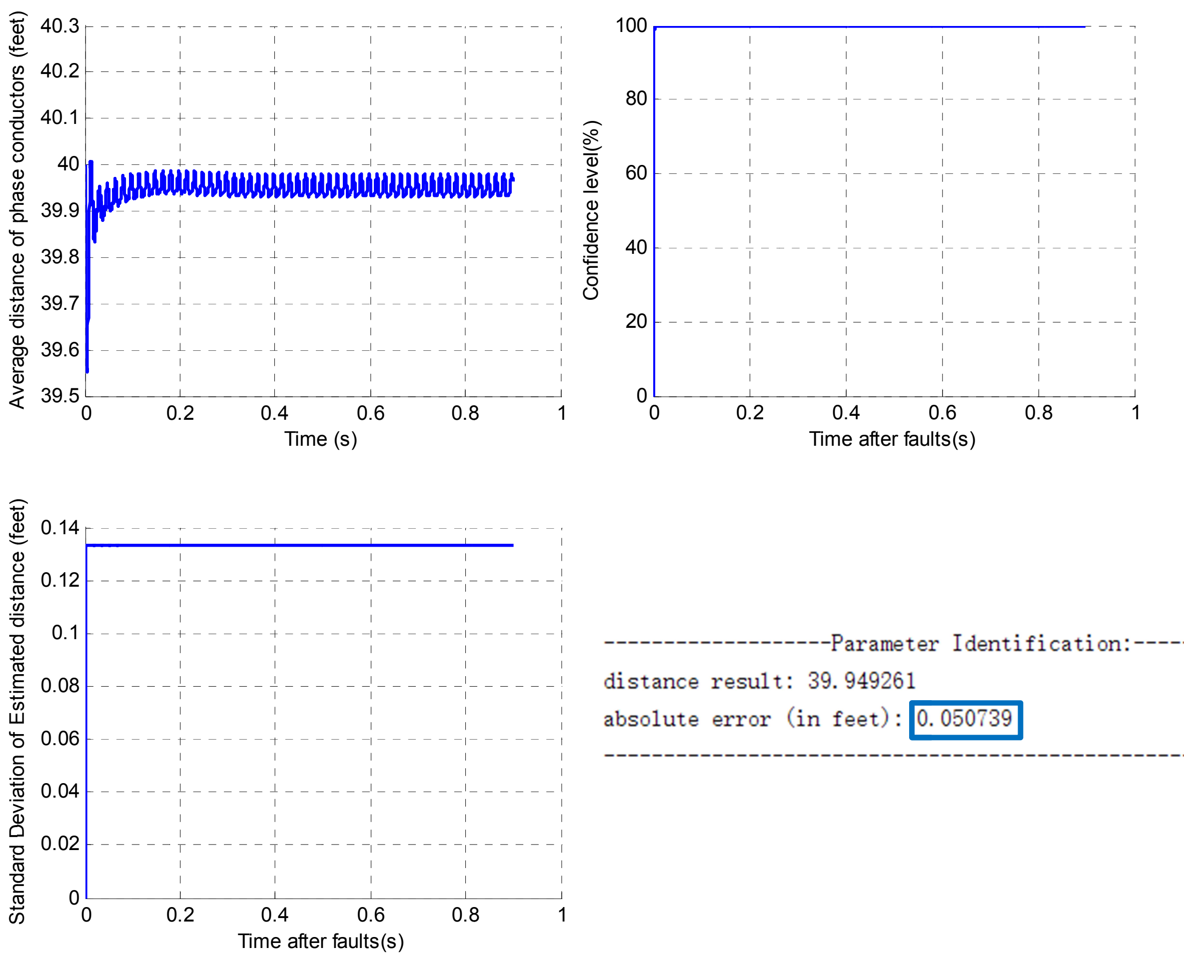

Figure 6.8. Results with one parameter (distance) and with actual distance 40 feet

Test Case 2:

Initial Length: 136.5 miles; **Actual Length**: 136.5 miles;

Initial Distance: 40 feet (12.192 meters) **Actual Distance**: **38 feet** (11.5824 meters)

Initial Height: 100 feet (30.48 meters) **Actual Height**: 100 feet (30.48 meters)

Here the length and the height are not estimated as a parameter. The actual distance differs from the initial distance. The estimated distance between the phase conductors is:

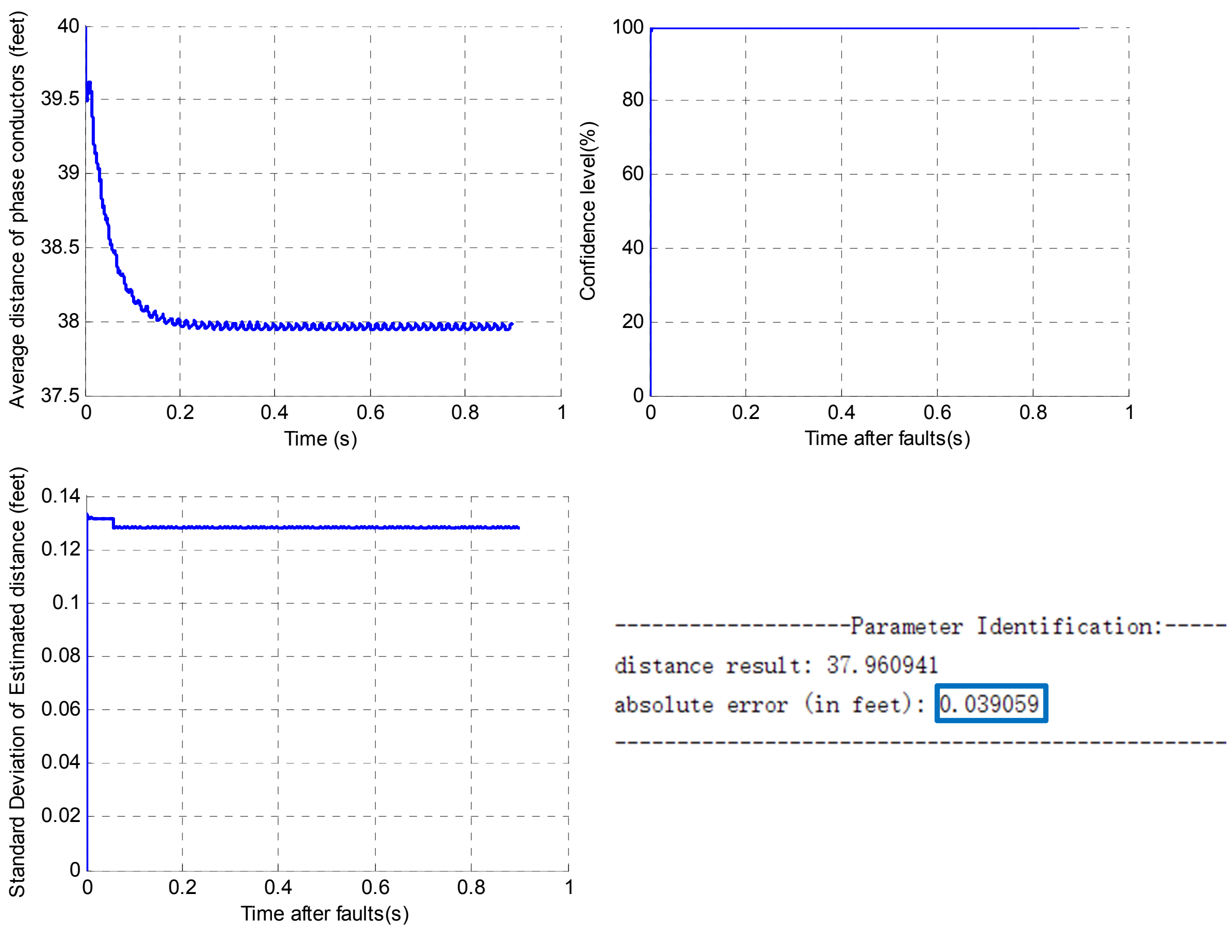

Figure 6.9. Results with one parameter (distance) and with actual distance 38 feet

Test Case 3:

Initial Length: 136.5 miles; **Actual Length**: 136.5 miles;

Initial Distance: 40 feet (12.192 meters) **Actual Distance**: **36 feet** (10.9728 meters)

Initial Height: 100 feet (30.48 meters) **Actual Height**: 100 feet (30.48 meters)

Here the length and the height are not estimated as a parameter. The actual distance differs from the initial distance. The estimated distance between the phase conductors is:

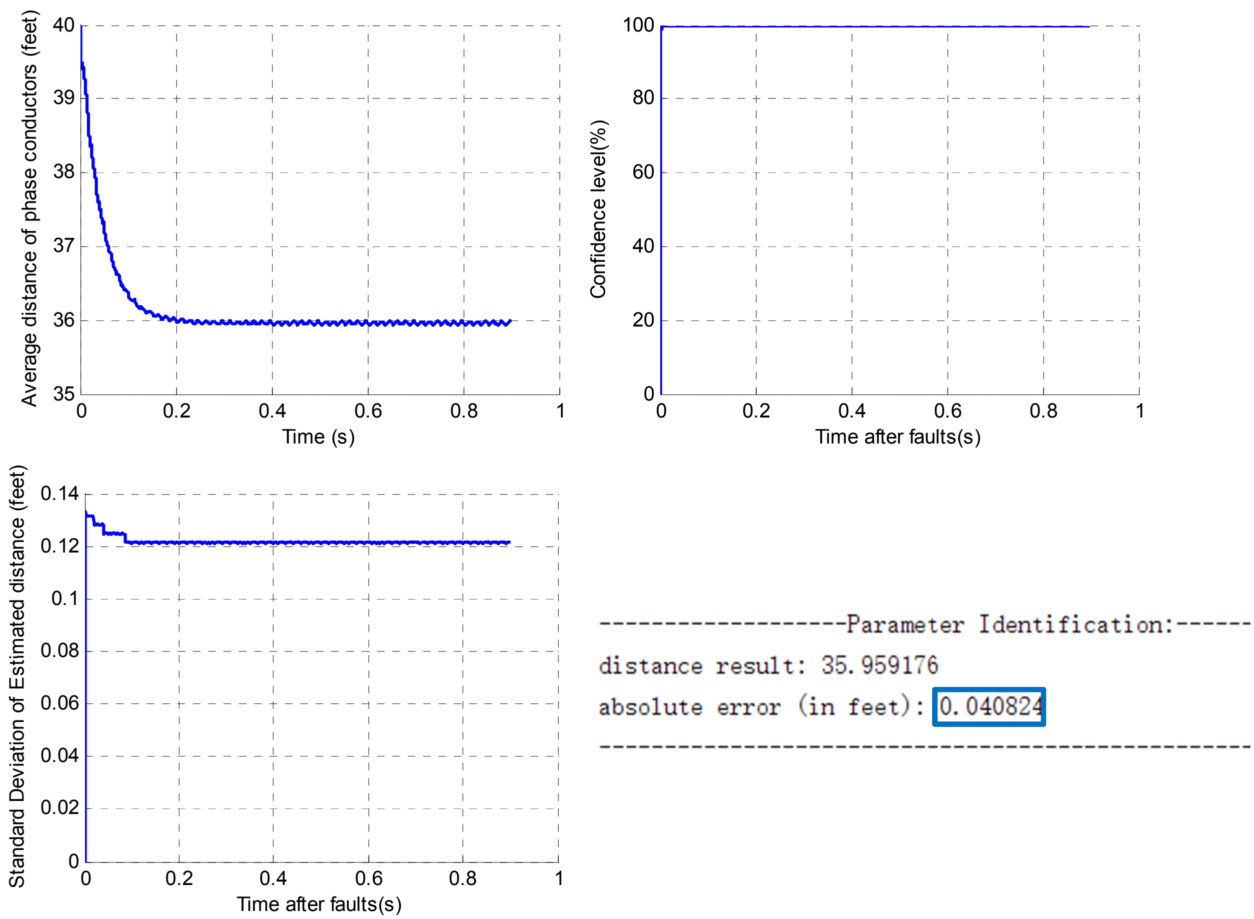

Figure 6.10. Results with one parameter (distance) and with actual distance 36 feet

Test Case 4:

Initial Length: 136.5 miles; **Actual Length**: 136.5 miles;

Initial Distance: 40 feet (12.192 meters) **Actual Distance**: **<u>34 feet</u>** (10.3632 meters)

Initial Height: 100 feet (30.48 meters) **Actual Height**: 100 feet (30.48 meters)

Here the length and the height are not estimated as a parameter. The actual distance differs from the initial distance. The estimated distance between the phase conductors is:

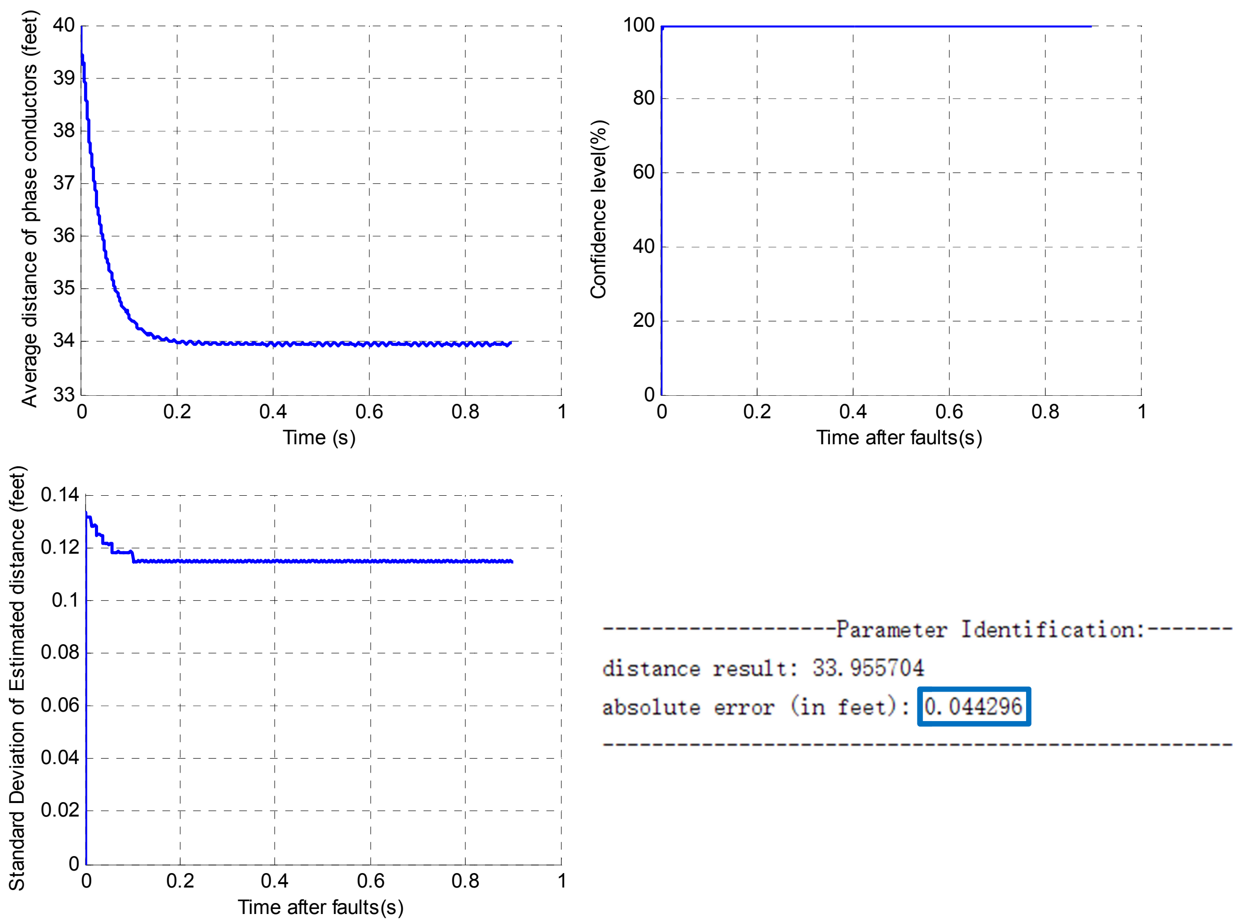

Figure 6.11. Results with one parameter (distance) and with actual distance 34 feet

Test Case 5:

Initial Length: 136.5 miles; **Actual Length**: 136.5 miles;

Initial Distance: 40 feet (12.192 meters) **Actual Distance**: **32 feet** (9.7536 meters)

Initial Height: 100 feet (30.48 meters) **Actual Height**: 100 feet (30.48 meters)

Here the length and the height are not estimated as a parameter. The actual distance differs from the initial distance. The estimated distance between the phase conductors is:

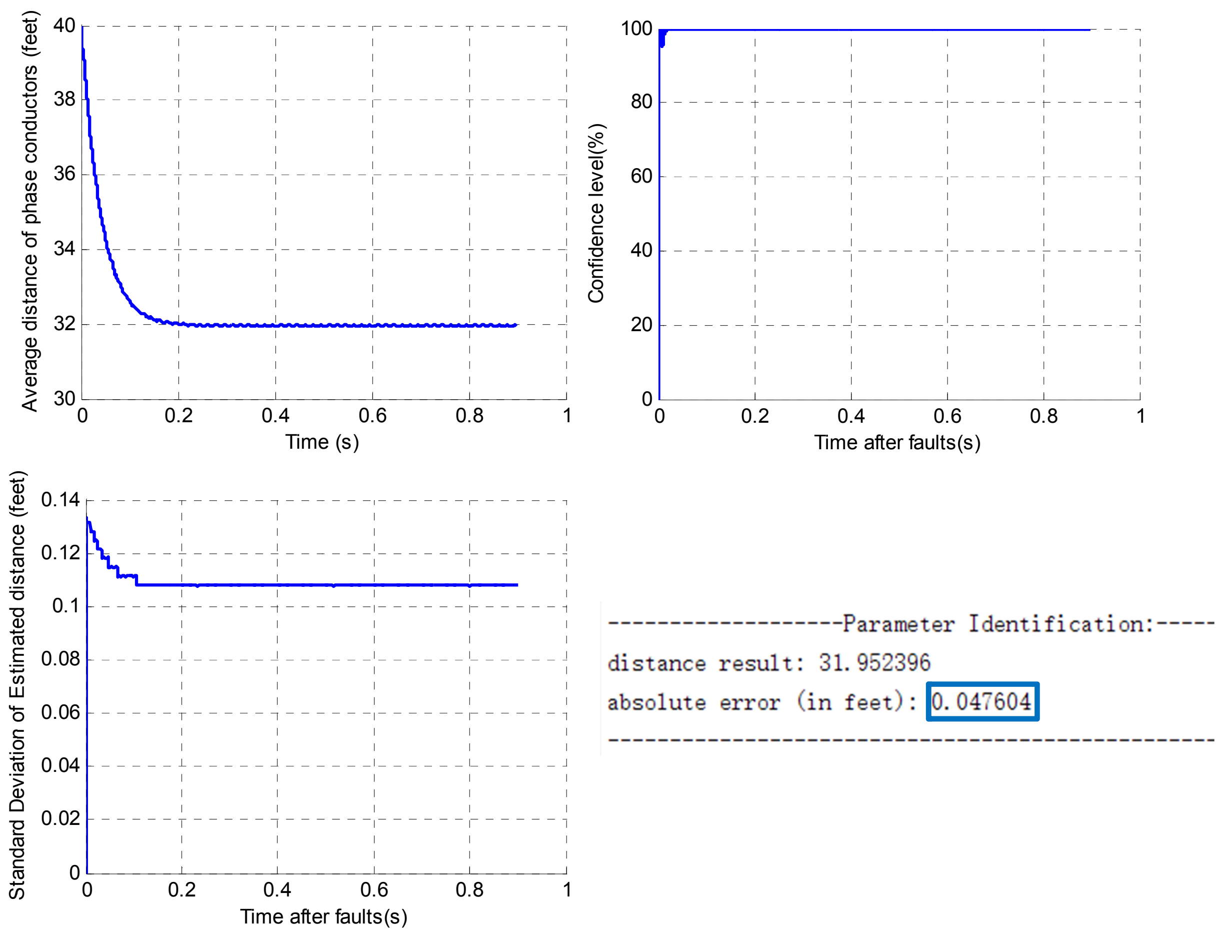

Figure 6.12. Results with one parameter (distance) and with actual distance 32 feet

Summary of Results, Group 2:

From the above simulation results, we can conclude that, for the model with one parameter (distance), the distance parameter is estimated with very high accuracy, as shown in Table 6.2.

Table 6.2. Conlusion of results, group 2

Case number	*Actual distance (feet)*	*Estimated distance (feet)*	*Error (feet)*	*Standard deviation (feet)*	*Error percentage*
1	40	39.949261	- 0.050739	0.135	- 0.127%
2	38	37.960941	- 0.039059	0.130	- 0.103%
3	36	35.959176	- 0.040824	0.121	- 0.113%
4	34	33.955704	- 0.044296	0.118	- 0.130%
5	32	31.952396	- 0.047604	0.109	- 0.149%

Group 3: with One Parameter (Height)

Test Case 1:

Initial Length: 136.5 miles; **Actual Length**: 136.5 miles;

Initial Distance: 30 feet (9.144 meters) **Actual Distance**: 30 feet (9.144 meters)

Initial Height: 100 feet (30.48 meters) **Actual Height**: <u>**100**</u> feet (30.48 meters)

The actual height (100 feet) is exactly the same as the initial height value. The estimated height of the phase conductors is:

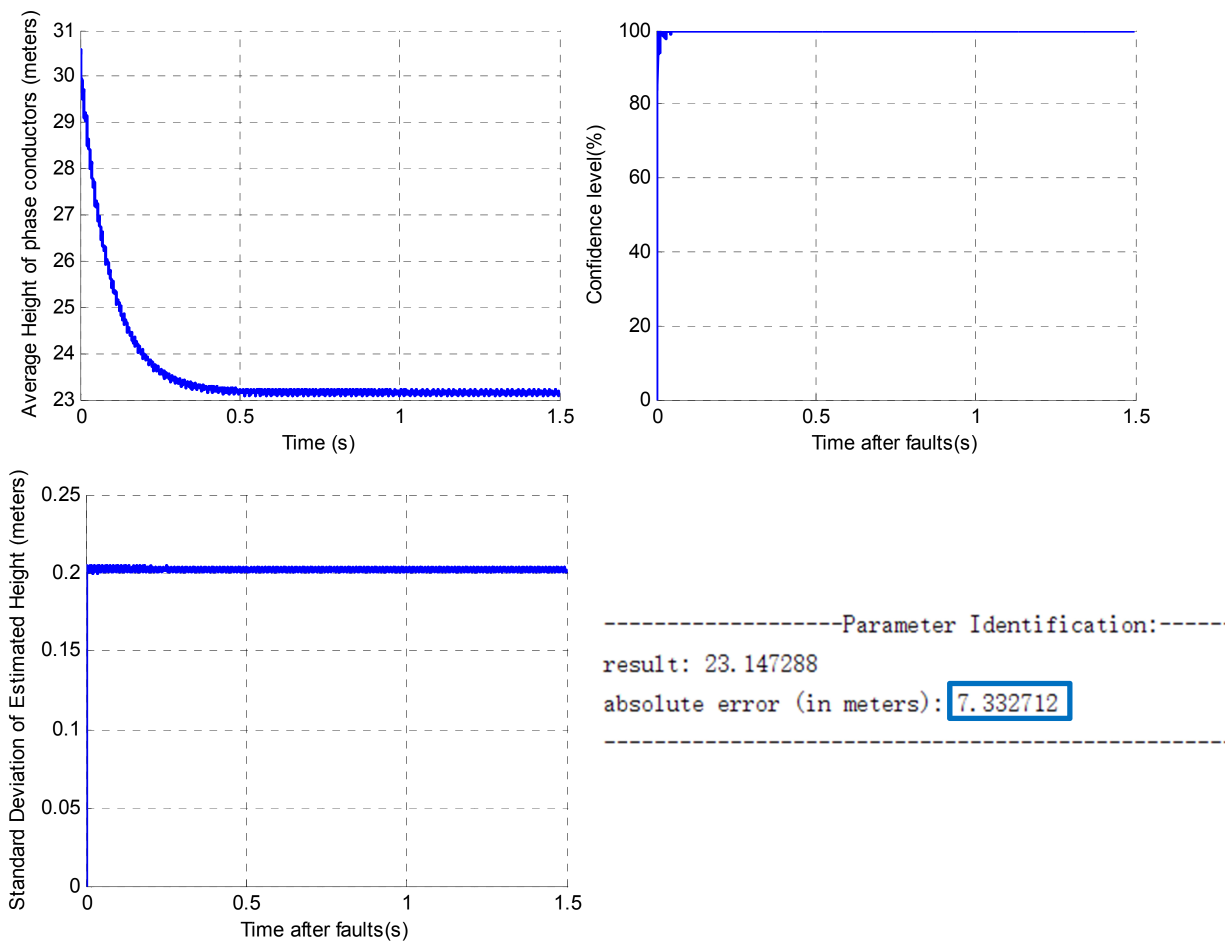

Figure 6.13. Results with one parameter (height) and with actual height 100 feet

We can see that, still the error for this estimation is large, even we have a perfect initial guess.

Test Case 2:

Initial Length: 136.5 miles; **Actual Length**: 136.5 miles;

Initial Distance: 30 feet (9.144 meters) **Actual Distance**: 30 feet (9.144 meters)

Initial Height: 100 feet (30.48 meters) **Actual Height**: 85 feet (30.48 meters)

The actual height (85 feet) differs from the initial height value. The estimated height of the phase conductors is:

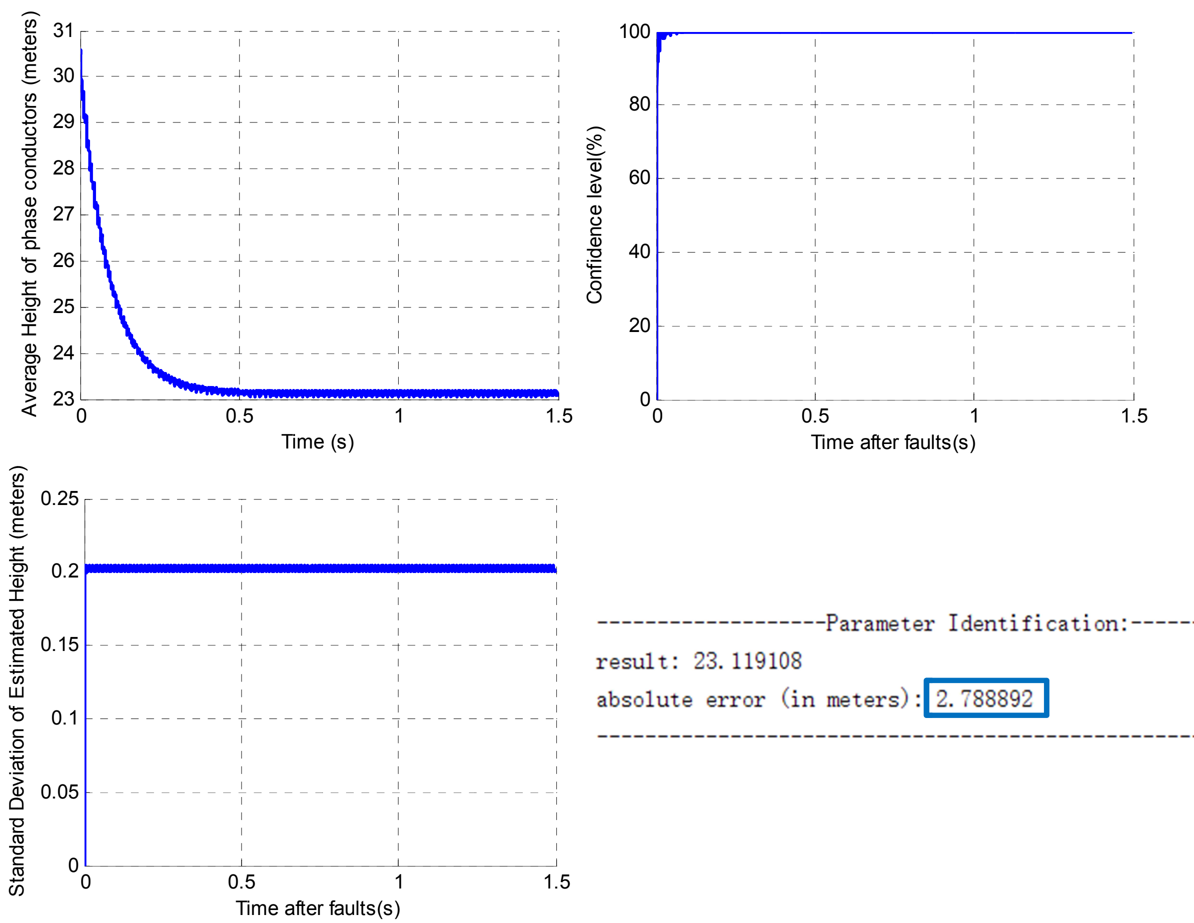

Figure 6.14. Results with one parameter (height) and with actual height 85 feet

We can see that, still the error for this estimation is large.

Summary of Results, Group 3:

From the above simulation results, we can conclude that, for the model with one parameter (height), the height parameter is estimated with very large errors, as shown in Table 6.3.

Table 6.3. Conlusion of results, group 3

Case number	*Actual height (feet)*	*Estimated height (feet)*	*Error (feet)*	*Standard deviation (feet)*	*Error percentage*
1	100	75.942546	- 24.057454	0.663	- 24.057%
2	85	75.850092	- 9.149908	0.663	- 10.765%

Group 4: with Two Parameters (Length and Distance)

Test Case 1:

Initial Length: 135.22 miles; **Actual Length**: <u>**135.22**</u> miles;

Initial Distance: 40 feet (12.192 meters) **Actual Distance**: <u>**40**</u> feet (12.192 meters)

Initial Height: 100 feet (30.48 meters) **Actual Height**: 100 feet (30.48 meters)

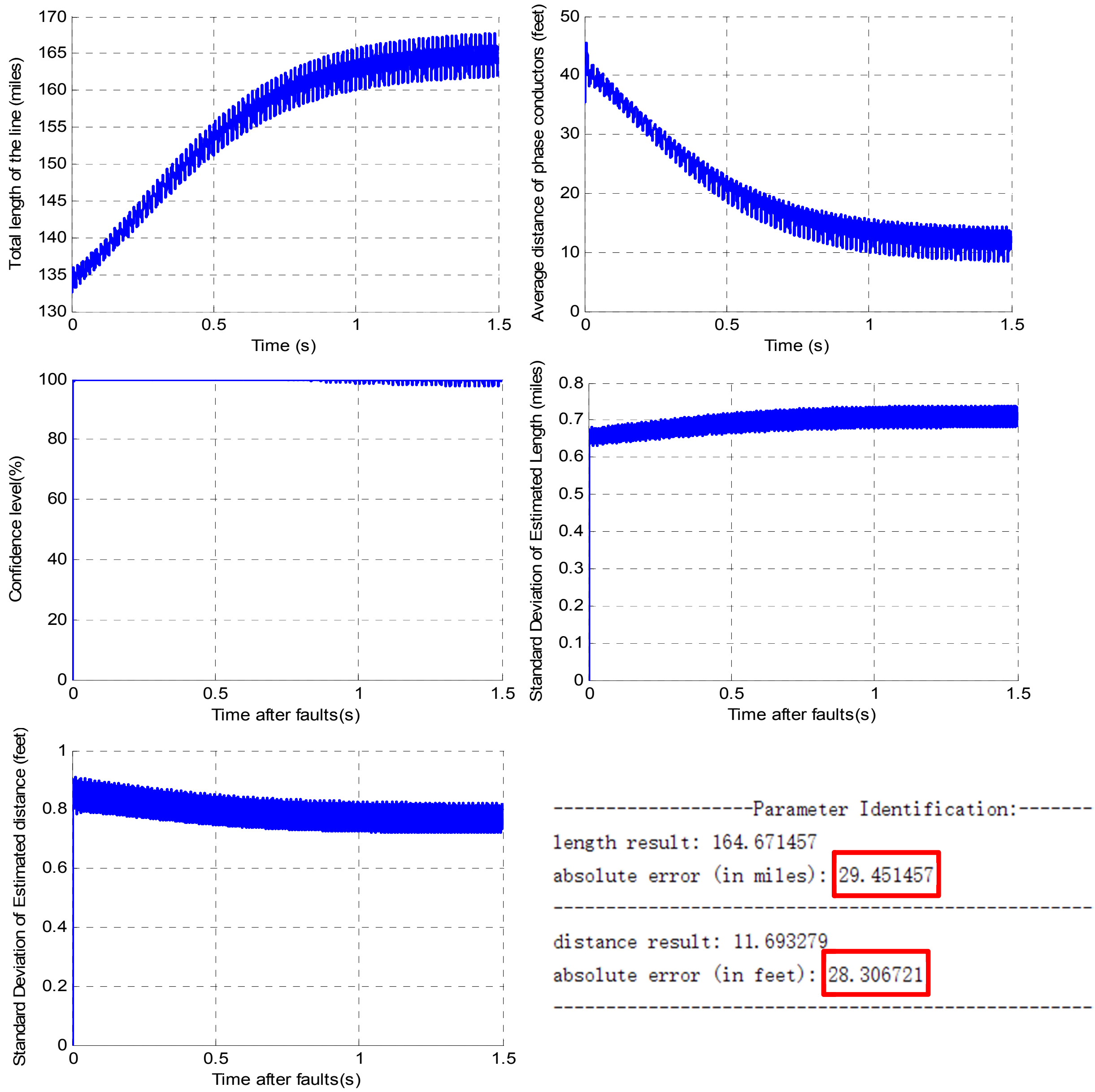

Figure 6.15. Results with two parameters (length and distance) and with actual length 135.22 miles and distance 40 feet

From the results here we can observe that both length and distance are not accurate.

Test Case 2:

Initial Length: 135.22 miles; **Actual Length**: 136.5 miles;

Initial Distance: 40 feet (12.192 meters) **Actual Distance**: 40 feet (12.192 meters)

Initial Height: 100 feet (30.48 meters) **Actual Height**: 100 feet (30.48 meters)

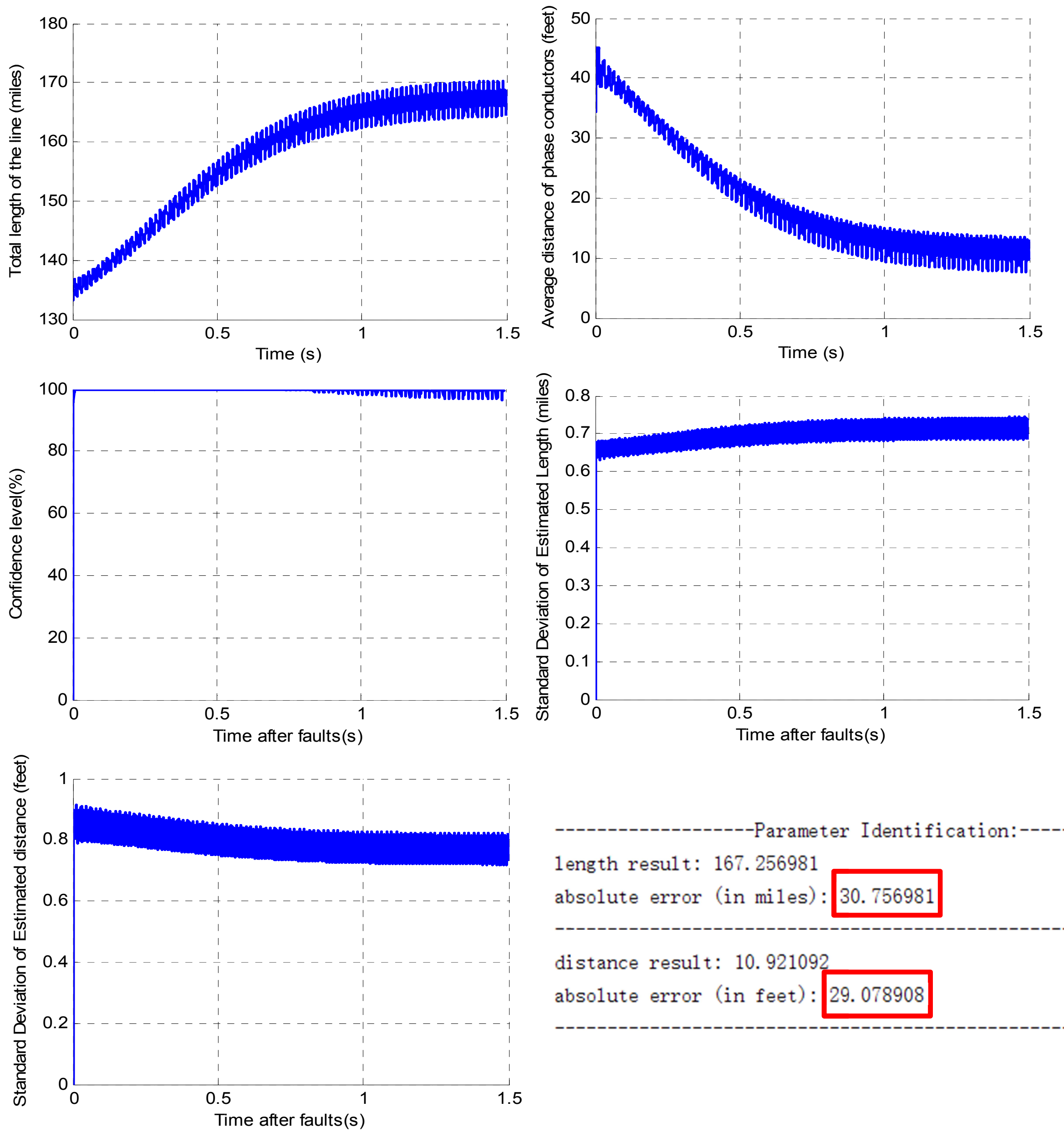

Figure 6.16. Results with two parameters (length and distance) and with actual length 136.5 miles and distance 40 feet

From the results here we can observe that both length and distance are not accurate.

Test Case 3:

Initial Length: 135.22 miles; **Actual Length**: <u>**136.5**</u> miles;

Initial Distance: 40 feet (12.192 meters) **Actual Distance**: <u>**32**</u> feet (9.7536 meters)

Initial Height: 100 feet (30.48 meters) **Actual Height**: 100 feet (30.48 meters)

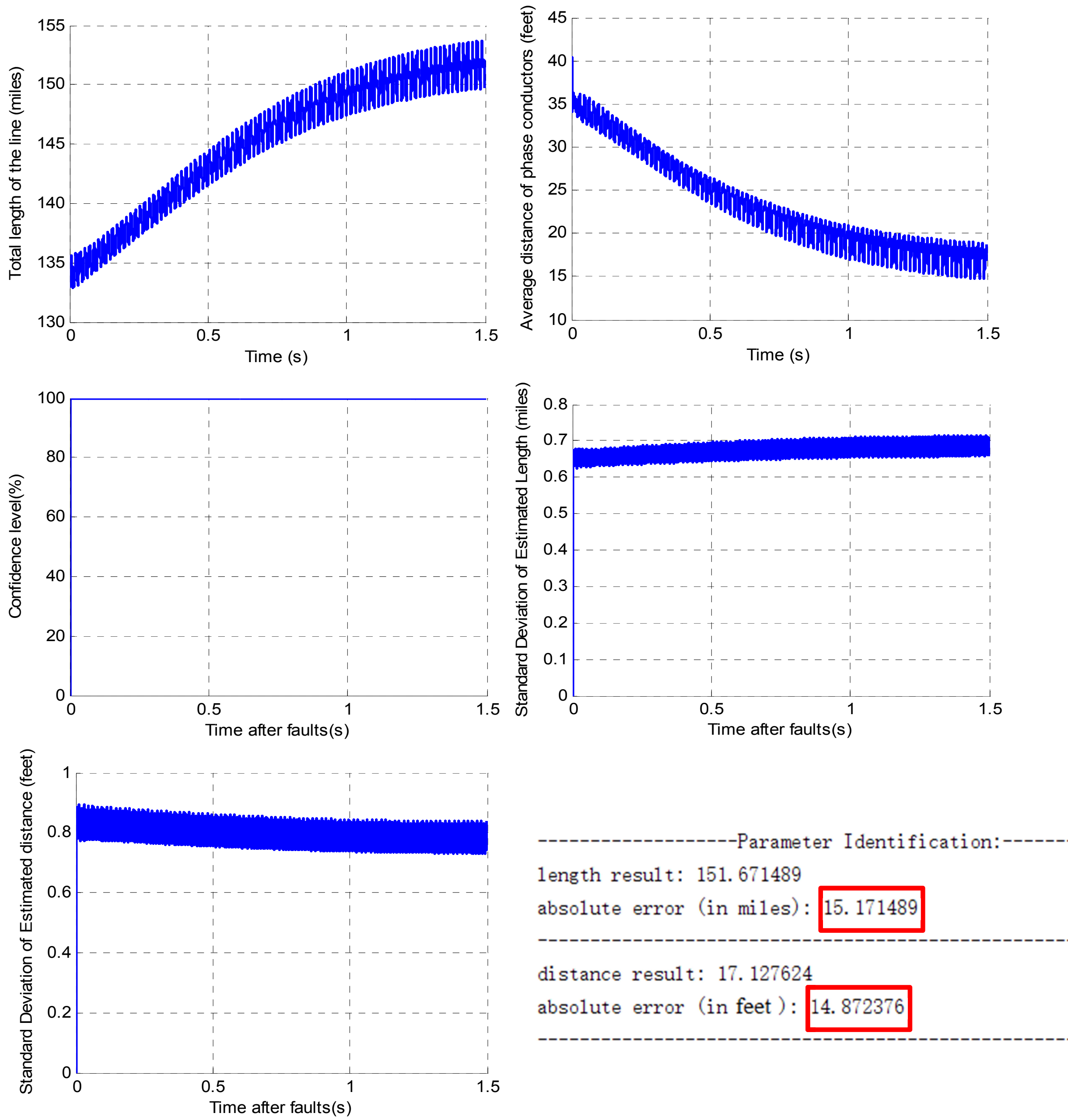

Figure 6.17. Results with two parameters (length and distance) and with actual length 136.5 miles and distance 32 feet

From the results here we can observe that both length and distance are not accurate.

Summary of Results, Group 4:

From the above simulation results, we can conclude that, for the model with two parameters (length and distance), both the length parameter and the distance parameter are estimated with large errors, as shown in Table 6.4.

Table 6.4. Conlusion of results, group 4

Case number	*Actual length (miles)*	*Actual distance (feet)*	*Estimated length (miles)*	*Estimated distance (feet)*	*Length error (miles)*	*Distance error (feet)*
1	135.22	40	164.671457	11.693279	- 29.451457	- 28.306721
2	136.5	40	167.256981	10.921092	- 30.756981	- 29.078908
3	136.5	32	151.671489	17.127624	- 15.171489	- 14.872376

Case number	*Length standard deviation (miles)*	*Distance standard deviation (feet)*	*Length error percentage*	*Distance error percentage*
1	0.712	0.787	- 21.780 %	- 70.767 %
2	0.715	0.772	- 22.533 %	- 72.697 %
3	0.687	0.791	- 11.115 %	- 46.476 %

Group 5: with Two Parameters (Length and Height)

To save space, the simulation results are omitted. The results are similar as the combination of the results of group 1 and group 3. For the model with two parameters (length and height), the estimated length parameter is quite accurate; the estimated height parameter is with large errors.

Group 6: with Two Parameters (Distance and Height)

To save space, the simulation results are omitted. The results are similar as the combination of the results of group 2 and group 3. For the model with two parameters (length and height), the estimated distance parameter is quite accurate; the estimated height parameter is with large errors.

Group 7: with Three Parameters (Length, Distance and Height)

To save space, the simulation results are omitted. The results are similar as the combination of the results of group 1, group 2 and group 3. For the model with three parameters (length, distance and height), all estimated parameters (length, distance and height) are with large errors.

Summary of Results from Above 7 Groups

From above 7 groups of selected estimated parameters, the absolute error percentages of estimated parameters are summarized in Table 6.5. From the table, we can observe that the estimation of one parameter (length or distance) has a very good accuracy. However, there exist two following issues:

(a) The estimation of height parameter (with or without other parameters such as length and distance, as shown in group 3, group 5, group 6 and group 7) has a large error;

(b) The estimation of length parameter and distance parameter together (with or without the other parameter height, as shown in group 4 and group 7) has a large error.

Table 6.5. Conlusion of results, 7 groups

Group Number	*Absolute Error percentage*		
	Length	*Distance*	*Height*
1	< 0.001 % (**Good accuracy**)	N/A	N/A
2	N/A	< 0.15 % (**Good accuracy**)	N/A
3	N/A	N/A	> 20 % (**Large error**)
4	> 20% (**Large error**)	> 70 % (**Large error**)	N/A
5	< 0.001 % (**Good accuracy**)	N/A	> 20 % (**Large error**)
6	N/A	< 0.15 % (**Good accuracy**)	> 20 % (**Large error**)
7	> 20 % (**Large error**)	> 70 % (**Large error**)	> 20 % (**Large error**)

The reasons of the above large errors are: (1) limited sensitivity of the height parameter; (2) distance parameter and length parameter are dependent on each other. Details proofs are provided in section 6.5.

Also, notice that the measured distance between phase conductors has much less error than the total length of the line. Therefore, for the EBPI of the transmission line, the height of the phase conductors and the distance between phase conductors are selected as measured values, and the length of the transmission line can be accurately estimated.

6.5 Proofs of Limited Sensitivity of Height Parameter and Linear Dependence of Distance/Length Parameters

System Simplification for Analysis

Detail three-phase and neutral matrices are utilized in EBPI to represent the physical laws that the transmission line should satisfy. Here some approximations are introduced to simplify the proving process.

These approximations are:

(a) Since we are estimating parameters during normal operations, we assume symmetrical three phase voltages, currents and parameters. Here we use phasors and positive-sequence network to do the analysis.

(b) The line to ground/ line to line capacitance is neglected;

(c) The currents and voltages inside neutral lines are neglected;

Therefore, the transmission line positive-sequence equivalent circuit is shown in the following Figure 2, where v_1 and v_2 are positive-sequence voltage phasors at the left and the right side, i is the positive-sequence current phasor through the transmission line, R and L are the positive-sequence resistance and inductance of the line. Also, assume that three parameters: length, distance and height are considered.

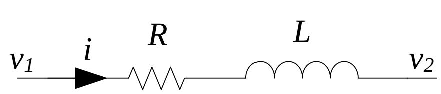

Figure 6.18. Transmission line simplified positive-sequence equivalent circuit

The physical laws can be expressed as,

$$
\begin{aligned}
\frac{v_1 - v_2}{i} &= R + j\omega L \\
&= \left(R_1 + j\omega L_1\right)\cdot l \\
&= \Big\{R_1^{(h_0,d_0)} + \alpha_R^{(h_0,d_0)}\cdot\left(h - h_0\right) + \beta_R^{(h_0,d_0)}\cdot\left(d - d_0\right) \\
&\quad + j\omega\Big[L_1^{(h_0,d_0)} + \alpha_L^{(h_0,d_0)}\cdot\left(h - h_0\right) + \beta_L^{(h_0,d_0)}\cdot\left(d - d_0\right)\Big]\Big\}\cdot l \\
&= \Big\{\Big[R_1^{(h_0,d_0)} - \alpha_R^{(h_0,d_0)}\cdot h_0 - \beta_R^{(h_0,d_0)}\cdot d_0 + j\omega\Big(L_1^{(h_0,d_0)} - \alpha_L^{(h_0,d_0)} h_0 - \beta_L^{(h_0,d_0)} d_0\Big)\Big] \\
&\quad + \Big(\alpha_R^{(h_0,d_0)} + j\omega\alpha_L^{(h_0,d_0)}\Big)\cdot h + \Big(\beta_R^{(h_0,d_0)} + j\omega\beta_L^{(h_0,d_0)}\Big)\cdot d\Big\}\cdot l
\end{aligned}
\tag{6.1}
$$

where l as the total length of the line, R_1 and L_1 as the actual positive-sequence resistance and inductance per mile (with height h and distance d), $R_1^{(h_0,d_0)}$ and $L_1^{(h_0,d_0)}$ as the original positive-sequence resistance and inductance per mile (with height h_0 and distance d_0), $\alpha_R^{(h_0,d_0)}$ and $\alpha_L^{(h_0,d_0)}$ are positive sequence height linearization coefficients of resistance and inductance; $\beta_R^{(h_0,d_0)}$ and $\beta_L^{(h_0,d_0)}$ are positive sequence distance linearization coefficients of resistance and inductance.

The typical values of $R_1^{(h_0,d_0)}$, $j\omega L_1^{(h_0,d_0)}$, $\alpha_R^{(h_0,d_0)}$, $j\omega\alpha_L^{(h_0,d_0)}$, $\beta_R^{(h_0,d_0)}$ and $j\omega\beta_L^{(h_0,d_0)}$ can be calculated from the corresponding matrices. For example, select h_0 = 100 feet and d_0 = 40 feet shown in section 6.3. Recall these matrices are:

$\mathbf{R}_1^{(h_0,d_0)} =$

[0.104347590176 0.088583249026 0.088520253655 0.087708846378 0.087665381084

0.088583249026 0.104347590176 0.088583249026 0.087706865179 0.087706865179

0.088520253655 0.088583249026 0.104347590176 0.087665381084 0.087708846378
0.087708846378 0.087706865179 0.087665381084 2.356843656902 0.086821105107
0.087665381084 0.087706865179 0.087708846378 0.086821105107 2.356843656902]
/1609.344 ohm/m

$\mathbf{L}_1^{(h_0,d_0)} =$

[0.002787891873 0.001385703060 0.001162707720 0.001431639815 0.001213702381
0.001385703060 0.002787891873 0.001385703060 0.001411874608 0.001411874608
0.001162707720 0.001385703060 0.002787891873 0.001213702381 0.001431639815
0.001431639815 0.001411874608 0.001213702381 0.005546572070 0.001360715345
0.001213702381 0.001411874608 0.001431639815 0.001360715345 0.005546572070]
/1609.344 H/m

$\boldsymbol{\alpha}_R^{(h_0,d_0)} =$

[-5.96899280 -5.95986664 -5.93317948 -2.92063905 -2.91184274
-5.95986664 -5.96899280 -5.95986664 -2.92023476 -2.92023476
-5.93317948 -5.95986664 -5.96899280 -2.91184274 -2.92063905
-2.92063905 -2.92023476 -2.91184274 0 0
-2.91184274 -2.92023476 -2.92063905 0 0]
/1609.344/0.3048*10^{-5} ohm/m^2

$\boldsymbol{\alpha}_L^{(h_0,d_0)} =$

[0.01903000 0.01902786 0.01902147 0.85432030 0.18865278
0.01902786 0.01903000 0.01902786 0.73072970 0.73072970

0.01902147	0.01902786	0.01903000	0.18865278	0.85432030
0.85432030	0.7307297	0.18865278	0	0
0.18865278	0.7307297	0.85432030	0	0]

/1609.344/0.3048*10^{-5} H/m^2

$\boldsymbol{\beta}_R^{(h_0,d_0)} =$

[0	-0.9237745	-3.6674180	-0.3220582	-1.4049278
-0.9237745	0	-0.9237745	0	0
-3.6674180	-0.9237745,	0	-1.4049278	-0.3220582
-0.3220582	0	-1.4049278	0	0
-1.4049278	0	-0.3220582	0	0]

/1609.344/0.3048*10^{-6}ohm/m^2

$\boldsymbol{\beta}_L^{(h_0,d_0)} =$

[0 -9.2567423	-9.2541431	-3.8417848		-4.4207277
-9.2567423	0	-9.2567423	0	0
-9.2541431	-9.2567423	0	-4.4207277	-3.8417848
-3.8417848	0	-4.4207277	0	0
-4.4207277	0	-3.8417848	0	0]

/1609.344/0.3048*10^{-6} H/m^2

From the above matrices, we can calculate the value of $R_1^{(0)}$, $j\omega L_1^{(0)}$, α_R, $j\omega\alpha_L$, β_R and $j\omega\beta_L$:

$$R_1^{(0)} \approx 0.015785/1609.344 = 9.8086\times10^{-6}\ ohm/m$$

$$j\omega L_1^{(0)} \approx j120\pi \times 0.0014765/1609.344 = j3.4588\times 10^{-4}\ ohm/m$$

$$\alpha_R = -0.018022/1609.344/0.3048\times 10^{-5} = -3.6740\times 10^{-10}\ ohm/m^2$$

$$j\omega\alpha_L = j120\pi \times 0.00000427/1609.344/0.3048\times 10^{-5} = j3.2817\times 10^{-11}\ ohm/m^2$$

$$\beta_R = 1.8383/1609.344/0.3048\times 10^{-5} = 3.7476\times 10^{-8}\ ohm/m^2$$

$$j\omega\beta_L = j120\pi \times 9.2559/1609.344/0.3048\times 10^{-5} = j7.1135\times 10^{-5}\ ohm/m^2$$

Therefore, equation (6.1) can be rewritten by substituting above values,

$$\begin{aligned}
&\frac{v_1 - v_2}{i} \\
&= \Big\{\Big[R_1^{(h_0,d_0)} - \alpha_R^{(h_0,d_0)}\cdot h_0 - \beta_R^{(h_0,d_0)}\cdot d_0 + j\omega\Big(L_1^{(h_0,d_0)} - \alpha_L^{(h_0,d_0)} h_0 - \beta_L^{(h_0,d_0)} d_0\Big)\Big] \\
&\quad + \Big(\alpha_R^{(h_0,d_0)} + j\omega\alpha_L^{(h_0,d_0)}\Big)\cdot h + \Big(\beta_R^{(h_0,d_0)} + j\omega\beta_L^{(h_0,d_0)}\Big)\cdot d\Big\}\cdot l \\
&= \Big[\Big(9.8086\times 10^{-6} + 3.6740\times 10^{-10}\times 100\times 0.3048 - 3.7476\times 10^{-8}\times 40\times 0.3048 \\
&\quad + j3.4588\times 10^{-4} - j3.2817\times 10^{-11}\times 100\times 0.3048 - j7.1135\times 10^{-5}\times 40\times 0.3048\Big) \\
&\quad + \Big(-3.6740\times 10^{-10} + j3.2817\times 10^{-11}\Big)\cdot h + \Big(3.7476\times 10^{-8} + j7.1135\times 10^{-5}\Big)\cdot d\Big]\cdot l \\
&= \Big(9.3629\times 10^{-6} - j5.2140\times 10^{-4}\Big) + \Big(-3.6740\times 10^{-10} + j3.2817\times 10^{-11}\Big)\cdot h \\
&\quad + \Big(3.7476\times 10^{-8} + j7.1135\times 10^{-5}\Big)\cdot d \\
&= \Big[\Big(5.2148\times 10^{-4}\Big)e^{-j88.971^\circ} + \Big(3.6886\times 10^{-10}\Big)e^{j174.90^\circ}\cdot h + \Big(7.1135\times 10^{-5}\Big)e^{j89.970^\circ}\cdot d\Big]\cdot l
\end{aligned} \tag{6.2}$$

where h, d and l are in meters.

Explanation of Limited Sensitivity of Height Parameter

Recall equation (6.2),

$$\frac{v_1 - v_2}{i} = \left[\left(5.2148\times10^{-4}\right)e^{-j88.971^\circ} + \left(3.6886\times10^{-10}\right)e^{j174.90^\circ}\cdot h + \left(7.1135\times10^{-5}\right)e^{j89.970^\circ}\cdot d\right]\cdot l$$

As we can observe from above, the height parameter h does not influence much the physical laws of the transmission line. Even the height parameter changes 1000 meters, which is too large to be realistic, the overall influence on the physical laws would still be neglectable. Therefore, the height parameter has neglectable influence on the physical laws of the transmission line. Also, it has limited sensitivity and could not be accurately estimated via the proposed EBPI process.

Explanation of Linear Dependence of Distance/Length Parameters

Recall equation (6.2),

$$\frac{v_1 - v_2}{i} = \left[\left(5.2148\times10^{-4}\right)e^{-j88.971^\circ} + \left(3.6886\times10^{-10}\right)e^{j174.90^\circ}\cdot h + \left(7.1135\times10^{-5}\right)e^{j89.970^\circ}\cdot d\right]\cdot l$$

By neglecting the influence of parameter h (the coefficient before h is less than $1/10^5$ of the other coefficients) and approximating $-88.971^\circ \approx -90^\circ$ and $89.970^\circ \approx 90^\circ$, we have

$$\frac{v_1 - v_2}{i} = j\left[-5.2148\times10^{-4} + 7.1135\times10^{-5}\cdot d\right]\cdot l \tag{6.3}$$

As we can observe from above, if the length of the line l increases, the distance parameter d will decrease to maintain the physical laws (this is consistent with the results in section 6.4, group 4). Also, there are infinite combinations of parameter l and d that can satisfy the above equation. In other words, the parameter l and d are linearly dependent on each other and cannot be accurately estimated together.

6.6 Summary

This chapter introduces EBPI of transmission lines. Three parameters are selected based on the physical structure of the transmission line: the total length of the line, the average height of the phase conductors and the average distance between phase conductors. From the simulation results and the proofs, it can be concluded that: (a) the height parameter has limited sensitivity; and (b) the distance parameter and the length parameter are dependent on each other. Therefore, the preferable way for the parameter identification of transmission lines is to (a) physically measure the distance between phase conductors and the height of phase conductors; (b) generate series resistance, series inductance, shunt conductance and shunt capacitance matrices based on the above distance and height; and (c) estimate the length parameter of the line as the only parameter. This provides the high-fidelity three-phase physically based models for transmission lines.

CHAPTER 7 Conclusions and Future Work Direction

7.1 Conclusion

The contributions of this dissertation are as follows. (1) A new transmission line Dynamic State **E**stimation **B**ased **P**rotection (**EBP**) scheme has been proposed. The new scheme is secure, reliable, more sensitive and faster than legacy protection functions. (2) A new transmission line Dynamic State **E**stimation **B**ased **F**ault **L**ocating (**EBFL**) scheme has been proposed. The new scheme is more accurate than traditional fault locating schemes. (3) A new transmission line Dynamic State **E**stimation **B**ased **P**arameter **I**dentification (**EBPI**) scheme during normal operating conditions has been proposed. The new scheme enables high-fidelity dynamic models for EBP and EBFL applications. (4) Accurate transmission line modeling by the introduction of SCPAQCF standard is accomplished, including EBP, EBFL and EBPI applications. Next, each contribution is explained in detail.

The proposed EBP method has been compared to legacy protection functions for a series compensated transmission line (with two possible installations of relays). The proposed EBP scheme has the following advantages: (a) it simplifies the settings of the protection and does not need coordination with other protection functions; (b) it detects faults faster than legacy protection schemes (within sub-millisecond); (c) it is immune to current inversion due to SCs; and (d) it reliably detects high impedance faults.

For the proposed transmission line fault locating (EBFL) method is compared to legacy fault locating schemes via a two-terminal transmission line and a three-terminal transmission line, respectively. The proposed EBFL has the following advantages: (a) it uses a high-fidelity multi-section transmission line dynamic model; (b) it utilizes instantaneous values (sampled values) instead of phasors enabling estimation of the fault location in the presence of transients, which is very important when the fault duration is short; (c) it demonstrates higher accuracy compared with legacy fault locating schemes; (d) the sampling rate it requires is relatively low (in this case 4.8 kilo-samples per second) and therefore it can be used with existing instrumentation in substations.

Third, for transmission line EBPI during normal operating conditions, three parameters are selected based on the physical structure of the transmission line: the total length of the line, the average height of the phase conductors and the average distance between phase conductors. It can be concluded that, the preferable way for the parameter identification of transmission lines is to (a) physically measure the distance between phase conductors and the height of phase conductors; (b) generate series resistance, series inductance, shunt conductance and shunt capacitance matrices based on the measured distance and height; and (c) estimate the length parameter of the line as the only parameter. This provides the high-fidelity three-phase physically based models for transmission lines.

Finally, accurate transmission line modeling by the introduction of SCPAQCF standard has been accomplished. For EBP application, the modeling of transmission line without fault in SCPAQCF syntax has been completed and demonstrated. For EBFL application, the modeling of transmission line with fault in SCPAQCF syntax has been completed and demonstrated. For EBPI application, the modeling of transmission line with parameters during normal operating conditions in SCPAQCF syntax has been completed and demonstrated.

7.2 Future Work Directions

The dissertation focuses on detecting faults in transmission lines and protecting transmission lines. The method is based on DSE. The thesis also addressed the related problems of fault locating and line parameter identification. The presented research can be extended to additional related problems. Details are provided as follows.

First, the research can be extended to DC devices. In recent years, DC devices have demonstrated their advantages in certain applications. For example, the new High Voltage Direct Current (HVDC) transmission lines have fully-controlled power flow, are free of line to ground charging current, and are more economic beneficial when applied to long distance power transmission. However, most popular line protection and fault locating methods are based on AC systems and cannot be directly applied to HVDC lines. The proposed EBP/EBFL methods can be applied to solve the protection and fault locating problem in HVDC lines.

Second, the present research does not addrees the issue of instrumentation errors which can compromise the operation of the EBP relay. Power system operates with high voltages and currents. In order to measure the voltages and currents of devices, instrumentation transformers such as CTs and VTs are utilized to transform the primary voltages/currents (several kA, several hundred kV) to a relatively low level (5A, 69V). The introduction of CTs and VTs brings both random and systematic errors. In practice, these errors always sacrifice the sensitivity of the protective relays and the accuracy of fault locating results. Therefore, for protection and fault locating applications, it will be advantageous to accurately model CTs and VTs and then integrate these models into the EBP/EBFL to improve the performance of the proposed EBP/EBFL method.

Third, I want to further investigate characteristics of different DSE methods. There exist many DSE methods, including but not limited to Unconstraint Weighted Least Square (UWLS), Constraint Weighted Least Square (CWLS), Extended Kalman Filter (EKF), Ensemble Kalman Filter (EnKF), Unscented Kalman Filter (UKF) and Particle Filter (PF). Some of them may be computational efficient with fair accuracy and are suitable for time-sensitive applications (such as protection). Others may have better accuracy or convergence properties with relatively higher computational burden and are suitable for highly nonlinear applications (such as fault locating and parameter identification). Full investigation of their characteristics will benefit their applications in related research topics.

PUBLICATIONS

1. **Y. Liu**, S. Meliopoulos, R. Fan, L. Sun and Z. Tan, "Dynamic State Estimation Based Protection on Series Compensated Transmission Lines", *IEEE Transactions on Power Delivery*, in press.

2. S. Meliopoulos, G. J. Cokkinides, P. Myrda, **Y. Liu**, R. Fan, L. Sun, R. Huang and Z. Tan, "Dynamic State Estimation Based Protection: Status and Promise", *IEEE Transactions on Power Delivery*, Vol 32, Issue 1, pp 320-330, Feb. 2017.

3. **Y. Liu**, S. Meliopoulos, L. Sun and R. Fan, "Dynamic State Estimation Based Protection on Mutually Coupled Transmission Lines", *CSEE Journal of Power and Energy Systems*, Vol.2, No.4, pp 6- 14, Dec. 2016.

4. **Y. Liu**, S. Meliopoulos, Z. Tan, L. Sun and R. Fan, "Dynamic State Estimation Based Fault Locating in Transmission Lines", *IET Generation, Transmission & Distribution* (2^{nd} Round Review).

5. **Y. Liu**, S. Meliopoulos, N. Tai, L. Sun and B. Xie, "Protection and Fault Locating Method of Series Compensated Lines by Wavelet Based Energy Traveling Wave", in *IEEE Power and Energy Society (PES) General Meeting*, 2017.

6. L. Sun, S. Meliopoulos, **Y. Liu** and B. Xie, "Dynamic State Estimation Based Synchronous Generator Model Calibration Using PMU Data", in *IEEE Power and Energy Society (PES) General Meeting*, 2017.

7. **Y. Liu**, S. Choi, S. Meliopoulos, R. Fan, L. Sun and Z. Tan, "Dynamic State Estimation Enabled Predictive Inverter Control", in *IEEE Power and Energy Society (PES) General Meeting*, 2016.

8. S. Meliopoulos, G. Cokkinides, **Y. Liu**, R. Fan, S. Choi and P. Myrda, "Protection and Control of Systems with Converter Interfaced Generation (CIG)", in *49th Hawaii International Conference on System Sciences (HICSS)*, 2016.

9. L. Sun, R. Fan, S. Meliopoulos, **Y. Liu** and Z. Tan, "Capacitor Bank Protection via Constraint WLS Dynamic State Estimation Method (CWLS-DSE) ", in *North American Power Symposium (NAPS)*, 2016.

10. R. Fan, S. Meliopoulos, L. Sun, Z. Tan and **Y. Liu**, "Transformer Inter-turn Faults Detection by Dynamic State Estimation Method", in *North American Power Symposium (NAPS)*, 2016.

11. **Y. Liu**, S. Meliopoulos, R. Fan and L. Sun, "Dynamic State Estimation Based Protection of Microgrid Circuits", in *IEEE Power and Energy Society (PES) General Meeting*, 2015.

12. R. Fan, S. Meliopoulos, G. J. Cokkinides, L, Sun and **Y. Liu**, "Dynamic State Estimation-based Protection of Power Transformers", in *IEEE Power and Energy Society (PES) General Meeting*, 2015.

APPENDICES

Appendix A. SCPQDM of Transmission Lines for EBP

This Appendix describes SCPQDMs of transmission lines for EBP application (without faults). For **classic transmission lines** (as shown in Figure A.1), a multi-section model is applied, where each section is a π-equivalent model, and the section number is chosen in such a way that the traveling length of electro-magnetic wave during one sampling interval is comparable to the length of each section. Also, for **series compensated lines** (as shown in Figure A.2), the overall SCPQDM of them can be generated by combining the SCPQDMs of the series capacitors (SCs) and the classic transmission line. The SCPQDM of π-equivalent model for each section and the SCPQDM of SCs are introduced respectively.

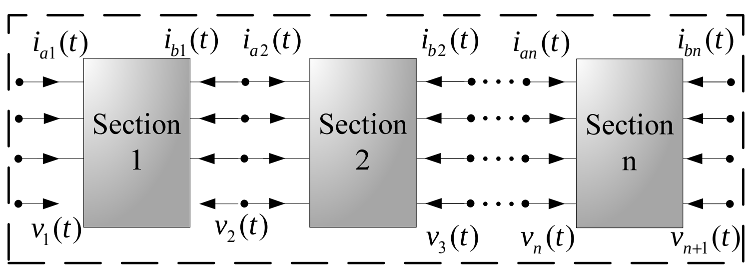

Figure A.1. Classic multi-section transmission line model without fault

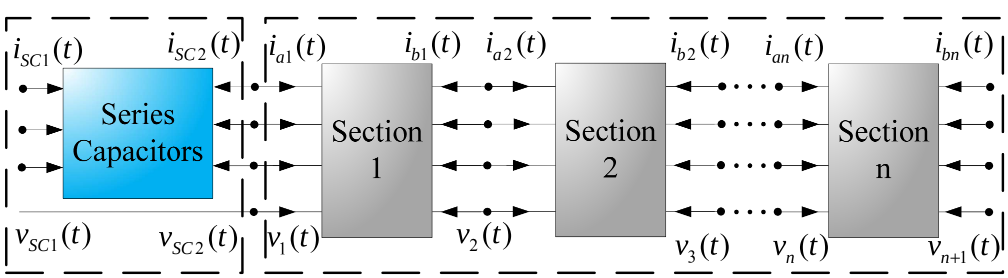

Figure A.2. Series compensated multi-section transmission line model without fault

The variables in Figure A.1 and Figure A.2 are defined as follows. $\boldsymbol{i}_{ak}(t)$ and $\boldsymbol{i}_{bk}(t)$ are three phase and neutral current vectors at each terminal of transmission line section *k*; $\boldsymbol{v}_{k}(t)$ and $\boldsymbol{v}_{k+1}(t)$ are three phase and neutral voltage vectors at each terminal of transmission line section *k*; $\boldsymbol{i}_{SC1}(t)$ and $\boldsymbol{i}_{SC2}(t)$ are three phase current vectors at each terminal of SCs; $\boldsymbol{v}_{SC1}(t)$ and $\boldsymbol{v}_{SC2}(t)$ are three phase voltage vectors at each terminal of SCs.

Next, the detailed SCPQDMs are introduced, including (a) section *k*, two-terminal transmission line model without fault, and (b) the model of SCs.

A.1 Section *k*, Two-terminal Transmission Line Model without Fault

The model of section k is described in Figure A.3.

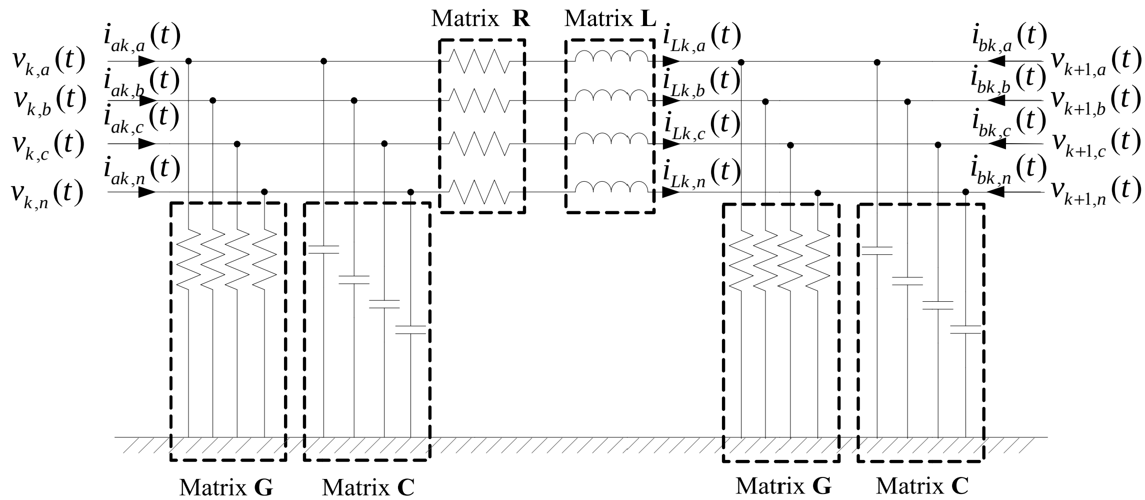

Figure A.3. Section *k*, transmission line model without fault

where $\mathbf{R}$, $\mathbf{L}$, $\mathbf{G}$ and $\mathbf{C}$ are series resistance, series inductance, shunt conductance and shunt capacitance of each section; all states and through variables are defined in Table A.1 and Table A.2, respectively.

Table A.1. States of section *k*, transmission line model without fault

Index	Variable	Description
0	$v_{k,a}(t)$	phase A voltage, left terminal
1	$v_{k,b}(t)$	phase B voltage, left terminal
2	$v_{k,c}(t)$	phase C voltage, left terminal
3	$v_{k,n}(t)$	phase N voltage, left terminal
4	$v_{k+1,a}(t)$	phase A voltage, right terminal
5	$v_{k+1,b}(t)$	phase B voltage, right terminal
6	$v_{k+1,c}(t)$	phase C voltage, right terminal
7	$v_{k+1,n}(t)$	phase N voltage, right terminal
8	$i_{Lk,a}(t)$	phase A current through inductance
9	$i_{Lk,b}(t)$	phase B current through inductance
10	$i_{Lk,c}(t)$	phase C current through inductance
11	$i_{Lk,n}(t)$	phase N current through inductance

Table A.2. **Through variables of section *k*, transmission line model without fault**

Index	Variable	Description
0	$i_{ak,a}(t)$	phase A current, left terminal
1	$i_{ak,b}(t)$	phase B current, left terminal
2	$i_{ak,c}(t)$	phase C current, left terminal
3	$i_{ak,n}(t)$	phase N current, left terminal
4	$i_{bk,a}(t)$	phase A current, left terminal
5	$i_{bk,b}(t)$	phase B current, left terminal
6	$i_{bk,c}(t)$	phase C current, left terminal
7	$i_{bk,n}(t)$	phase N current, left terminal

Define $\mathbf{i}_{Lk}(t)$ as the three phase and neutral current through the series inductance; recall the definitions of $\mathbf{i}_{ak}(t)$, $\mathbf{v}_k(t)$, $\mathbf{i}_{bk}(t)$ and $\mathbf{v}_{k+1}(t)$: three phase and neutral current and voltage vectors at each terminal of section *k*. That means,

$$\mathbf{v}_k(t)=\begin{bmatrix} v_{k,a}(t) \\ v_{k,b}(t) \\ v_{k,c}(t) \\ v_{k,n}(t) \end{bmatrix}, \mathbf{v}_{k+1}(t)=\begin{bmatrix} v_{k+1,a}(t) \\ v_{k+1,b}(t) \\ v_{k+1,c}(t) \\ v_{k+1,n}(t) \end{bmatrix}, \mathbf{i}_{Lk}(t)=\begin{bmatrix} i_{Lk,a}(t) \\ i_{Lk,b}(t) \\ i_{Lk,c}(t) \\ i_{Lk,n}(t) \end{bmatrix}, \mathbf{i}_{ak}(t)=\begin{bmatrix} i_{ak,a}(t) \\ i_{ak,b}(t) \\ i_{ak,c}(t) \\ i_{ak,n}(t) \end{bmatrix}, \ \mathbf{i}_{bk}(t)=\begin{bmatrix} i_{bk,a}(t) \\ i_{bk,b}(t) \\ i_{bk,c}(t) \\ i_{bk,n}(t) \end{bmatrix}.$$

The transmission line section *k* model can be formulated in compact form as follows:

$$\mathbf{i}_{ak}(t)=\mathbf{G}\cdot\mathbf{v}_k(t)+\mathbf{C}\cdot\frac{d\mathbf{v}_k(t)}{dt}+\mathbf{i}_{Lk}(t) \tag{A.1}$$

$$\mathbf{i}_{bk}(t)=\mathbf{G}\cdot\mathbf{v}_{k+1}(t)+\mathbf{C}\cdot\frac{d\mathbf{v}_{k+1}(t)}{dt}-\mathbf{i}_{Lk}(t) \tag{A.2}$$

$$\mathbf{0}=-\mathbf{v}_k(t)+\mathbf{v}_{k+1}(t)+\mathbf{R}\cdot\mathbf{i}_{Lk}(t)+\mathbf{L}\cdot\frac{d\mathbf{i}_{Lk}(t)}{dt} \tag{A.3}$$

The matrices corresponding to the SCPQDM of transmission line section *k* are:

$\mathbf{x}(t)=\left[\mathbf{v}_k(t) \quad \mathbf{v}_{k+1}(t) \quad \mathbf{i}_{Lk}(t)\right]^T$; $\mathbf{p}(t)=null$; $\mathbf{u}(t)=null$; $\mathbf{i}(t)=\left[\mathbf{i}_{ak}(t) \quad \mathbf{i}_{bk}(t)\right]^T$;

$$\mathbf{Y}_{eqx1}=\begin{bmatrix}\mathbf{G} & \mathbf{0} & \mathbf{I}_4\\ \mathbf{0} & \mathbf{G} & -\mathbf{I}_4\end{bmatrix};\ \mathbf{D}_{eqxd1}=\begin{bmatrix}\mathbf{C} & \mathbf{0} & \mathbf{0}\\ \mathbf{0} & \mathbf{C} & \mathbf{0}\end{bmatrix};\ \mathbf{Y}_{equ1}=null;\ \mathbf{Y}_{eqp1}=null;\ \mathbf{C}_{eqc1}=\mathbf{0};$$

$$\mathbf{Y}_{eqx2}=\begin{bmatrix}-\mathbf{I}_4 & \mathbf{I}_4 & \mathbf{R}\end{bmatrix};\ \mathbf{D}_{eqxd2}=\begin{bmatrix}\mathbf{0} & \mathbf{0} & \mathbf{L}\end{bmatrix};\ \mathbf{Y}_{equ2}=null;\ \mathbf{Y}_{eqp2}=null;\ \mathbf{C}_{eqc2}=\mathbf{0};$$

$$\mathbf{Y}_{eqx3}=null;\ \mathbf{Y}_{equ3}=null;\ \mathbf{Y}_{eqp3}=null;\ \mathbf{C}_{eqc3}=null;\ \left\langle\mathbf{F}^i_{eqxx3}\right\rangle=null;\ \left\langle\mathbf{F}^i_{equu3}\right\rangle=null;$$

$$\left\langle\mathbf{F}^i_{eqpp3}\right\rangle=null;\ \left\langle\mathbf{F}^i_{eqxu3}\right\rangle=null;\left\langle\mathbf{F}^i_{equp3}\right\rangle=null;\left\langle\mathbf{F}^i_{eqxp3}\right\rangle=null;$$

where $\mathbf{I}_4$ is the identity matrix with the dimension of 4.

A.2 Model of Series Capacitors (SCs)

The model of SCs described in Figure A.4.

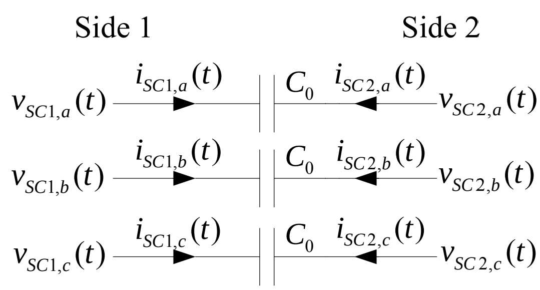

Figure A.4. Series capacitors model

where C_0 is the capacitance per phase; all states and through variables are defined in Table A.3 and Table A.4, respectively.

Table A.3. States of the series capacitors

Index	Variable	Description
0	$v_{SC1,a}(t)$	phase A voltage, left terminal
1	$v_{SC1,b}(t)$	phase B voltage, left terminal
2	$v_{SC1,c}(t)$	phase C voltage, left terminal
3	$v_{SC2,a}(t)$	phase A voltage, right terminal
4	$v_{SC2,b}(t)$	phase B voltage, right terminal
5	$v_{SC2,c}(t)$	phase C voltage, right terminal

Table A.4. Through variables of the series capacitors

Index	Variable	Description
0	$i_{SC1,a}(t)$	phase A current, left terminal
1	$i_{SC1,b}(t)$	phase B current, left terminal
2	$i_{SC1,c}(t)$	phase C current, left terminal
3	$i_{SC2,a}(t)$	phase A current, right terminal
4	$i_{SC2,b}(t)$	phase B current, right terminal
5	$i_{SC2,c}(t)$	phase C current, right terminal

Recall the definitions of $\boldsymbol{i}_{SC1}(t)$ and $\boldsymbol{i}_{SC2}(t)$: three phase current vectors at each terminal of SCs; $\boldsymbol{v}_{SC1}(t)$ and $\boldsymbol{v}_{SC2}(t)$: three phase voltage vectors at each terminal of SCs. That means,

$$\mathbf{v}_{SC1}(t)=\begin{bmatrix} v_{SC1,a}(t) \\ v_{SC1,b}(t) \\ v_{SC1,c}(t) \end{bmatrix},\ \mathbf{v}_{SC2}(t)=\begin{bmatrix} v_{SC2,a}(t) \\ v_{SC2,b}(t) \\ v_{SC2,c}(t) \end{bmatrix},\ \mathbf{i}_{SC1}(t)=\begin{bmatrix} i_{SC1,a}(t) \\ i_{SC1,b}(t) \\ i_{SC1,c}(t) \end{bmatrix},\ \mathbf{i}_{SC2}(t)=\begin{bmatrix} i_{SC2,a}(t) \\ i_{SC2,b}(t) \\ i_{SC2,c}(t) \end{bmatrix}.$$

The series capacitors model can be formulated in compact form as follows:

$$\mathbf{i}_{SC1}(t)=\mathbf{C}_{SC}\cdot\mathbf{v}_{SC1}(t)-\mathbf{C}_{SC}\cdot\mathbf{v}_{SC2}(t) \tag{A.4}$$

$$\mathbf{i}_{SC2}(t)=-\mathbf{C}_{SC}\cdot\mathbf{v}_{SC1}(t)+\mathbf{C}_{SC}\cdot\mathbf{v}_{SC2}(t) \tag{A.5}$$

The matrices corresponding to the SCPQDM of SCs are:

$\mathbf{x}(t)=\left[\mathbf{v}_{SC1}(t)\quad \mathbf{v}_{SC2}(t)\right]^T$; $\mathbf{p}(t)=null$; $\mathbf{u}(t)=null$; $\mathbf{i}(t)=\left[\mathbf{i}_{SC1}(t)\quad \mathbf{i}_{SC2}(t)\right]^T$;

$\mathbf{Y}_{eqx1}=\mathbf{0}$; $\mathbf{D}_{eqxd1}=\begin{bmatrix} \mathbf{C}_{SC} & -\mathbf{C}_{SC} \\ -\mathbf{C}_{SC} & \mathbf{C}_{SC} \end{bmatrix}$; $\mathbf{Y}_{equ1}=null$; $\mathbf{Y}_{eqp1}=null$; $\mathbf{C}_{eqc1}=\mathbf{0}$; $\mathbf{Y}_{eqx2}=\mathbf{0}$;

$\mathbf{D}_{eqxd2}=\mathbf{0}$; $\mathbf{Y}_{equ2}=null$; $\mathbf{Y}_{eqp2}=null$; $\mathbf{C}_{eqc2}=\mathbf{0}$; $\mathbf{Y}_{eqx3}=null$; $\mathbf{Y}_{equ3}=null$; $\mathbf{Y}_{eqp3}=null$;

$\mathbf{C}_{eqc3}=null$; $\left\langle\mathbf{F}^i_{eqxx3}\right\rangle=null$; $\left\langle\mathbf{F}^i_{equu3}\right\rangle=null$; $\left\langle\mathbf{F}^i_{eqpp3}\right\rangle=null$; $\left\langle\mathbf{F}^i_{eqxu3}\right\rangle=null$; $\left\langle\mathbf{F}^i_{equp3}\right\rangle=null$;

$\left\langle\mathbf{F}^i_{eqxp3}\right\rangle=null$;

where $\mathbf{C}_{SC}=diag\left[C_0\quad C_0\quad C_0\right]$.

Appendix B. SCPQDMs of Transmission Lines for EBFL

This Appendix describes SCPQDMs of transmission lines for EBFL application, including a two-terminal transmission line integrated with a fault and a three-terminal transmission line integrated with a fault. For **two-terminal transmission lines with a fault** (as shown in Figure B.1), similar as in Appendix A, multi-section models are adopted for both the left and the right side part, with *m* and *n* sections respectively, where each section represents a π-equivalent short line model. For **three-terminal transmission lines with a fault** (as shown in Figure B.2), the model consists of three parts: a two-terminal transmission line model with a fault (same as the model introduced in Figure B.1) and two multi-section transmission line models without faults (same as the classic transmission line model introduced in Appendix A), with section number $m+n$, p, and q, respectively. All section numbers are chosen in such a way that the traveling length of electro-magnetic wave during one sampling interval is comparable to the length of each section. The overall model can be obtained by combining the models of all sections.

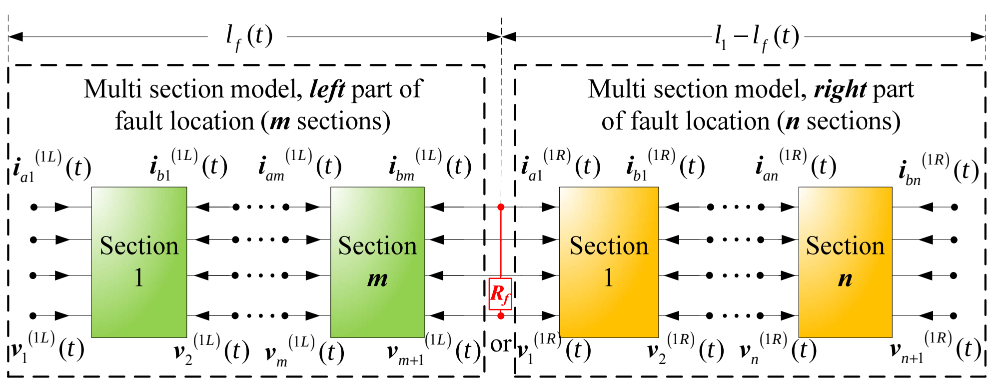

Figure B.1. Model of two-terminal faulted line

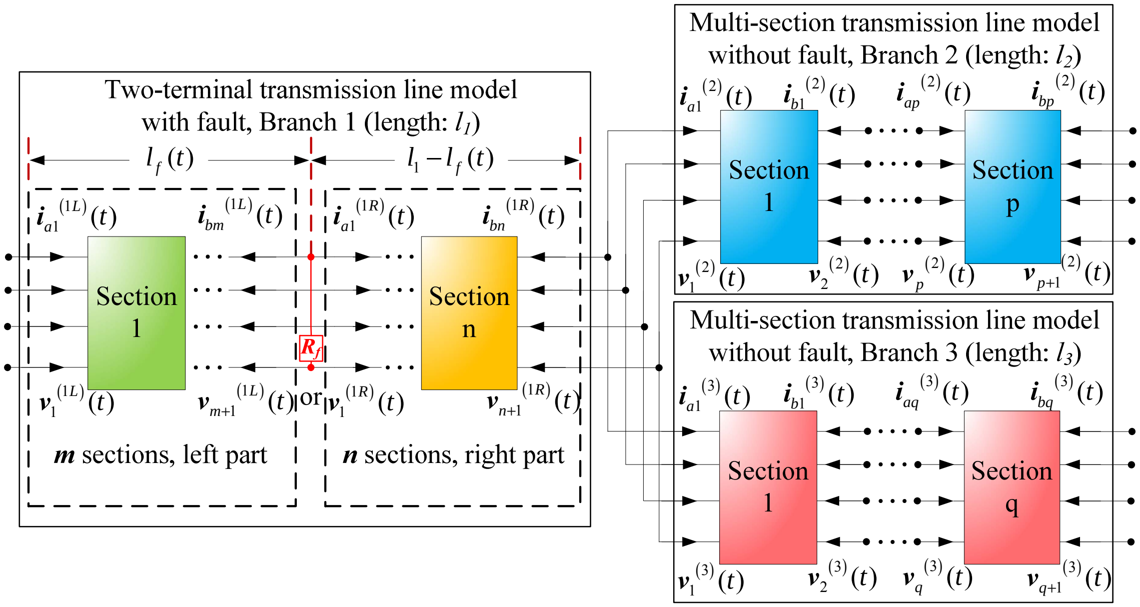

Figure B.2. Model of three-terminal line with fault

The variables in Figure B.1 and Figure B.2 are defined as follows. $\boldsymbol{i}_{ak}^{(1L)}(t)$ and $\boldsymbol{i}_{bk}^{(1L)}(t)$ are three phase and neutral current vectors at each terminal of section k, two-terminal transmission line model with fault, left part; $\boldsymbol{i}_{ak}^{(1R)}(t)$ and $\boldsymbol{i}_{bk}^{(1R)}(t)$ are three phase and neutral current vectors at each terminal of section k, two-terminal transmission line model with fault, right part; $\boldsymbol{v}_{k}^{(1L)}(t)$ and $\boldsymbol{v}_{k+1}^{(1L)}(t)$ are three phase and neutral voltage vectors at each terminal of section k, two-terminal transmission line model with fault, left part; $\boldsymbol{v}_{k}^{(1R)}(t)$ and $\boldsymbol{v}_{k+1}^{(1R)}(t)$ are three phase and neutral voltage vectors at each terminal of section k, two-terminal transmission line model with fault, right part; $\boldsymbol{i}_{ak}^{(j)}(t)$ and $\boldsymbol{i}_{bk}^{(j)}(t)$ $(j=2,\ 3)$ are three phase and neutral current vectors at each terminal of section k, two-terminal transmission line model without fault (branch 2 and 3); $\boldsymbol{v}_{ak}^{(j)}(t)$ and $\boldsymbol{v}_{bk}^{(j)}(t)$ $(j=2,\ 3)$ are three phase and neutral voltage vectors at each terminal of section k, two-terminal transmission line model without fault (branch 2 and 3); $l_f(t)$ is the distance between the left terminal of the line and the fault; l_1 is the total length of the two-terminal transmission line with fault; l_2 and l_3 are the total length of branch 2 and 3, respectively.

For different fault types, the model of the fault is different. Therefore, the way of combining models between the left part and the right part inside the two-terminal multi-section transmission line model is different. Specifically, the currents between the aforementioned left and the right part would satisfy:

$$\mathbf{0} = \mathbf{T}_{type} \cdot \mathbf{i}_{bm}{}^{(1L)}(t) + \mathbf{T}_{type} \cdot \mathbf{i}_{a1}{}^{(1R)}(t) \tag{B.1}$$

where $\mathbf{T}_{type}$ is a matrix whose value and dimension correspond to different fault types, as shown in Table. B.1.

Table B.1. Values and dimension of matrix $\mathbf{T}_{type}$ for different fault type

Fault Type	*Value of matrix* $\mathbf{T}_{type}$	*Dimension of matrix* $\mathbf{T}_{type}$
A-N	$\begin{bmatrix} 1 & 0 & 0 & 1 \\ 0 & 1 & 0 & 0 \\ 0 & 0 & 1 & 0 \end{bmatrix}$	3×4
B-N	$\begin{bmatrix} 1 & 0 & 0 & 0 \\ 0 & 1 & 0 & 1 \\ 0 & 0 & 1 & 0 \end{bmatrix}$	3×4
C-N	$\begin{bmatrix} 1 & 0 & 0 & 0 \\ 0 & 1 & 0 & 0 \\ 0 & 0 & 1 & 1 \end{bmatrix}$	3×4
A-B	$\begin{bmatrix} 1 & 1 & 0 & 0 \\ 0 & 0 & 1 & 0 \\ 0 & 0 & 0 & 1 \end{bmatrix}$	3×4

Table B.1. continued

B-C	$\begin{bmatrix} 1 & 0 & 0 & 0 \\ 0 & 1 & 1 & 0 \\ 0 & 0 & 0 & 1 \end{bmatrix}$	3×4
C-A	$\begin{bmatrix} 1 & 0 & 1 & 0 \\ 0 & 1 & 0 & 0 \\ 0 & 0 & 0 & 1 \end{bmatrix}$	3×4
AB-N	$\begin{bmatrix} 1 & 1 & 0 & 1 \\ 0 & 0 & 1 & 0 \end{bmatrix}$	2×4
BC-N	$\begin{bmatrix} 0 & 1 & 1 & 1 \\ 1 & 0 & 0 & 0 \end{bmatrix}$	2×4
CA-N	$\begin{bmatrix} 1 & 0 & 1 & 1 \\ 0 & 1 & 0 & 0 \end{bmatrix}$	2×4
ABC	$\begin{bmatrix} 1 & 1 & 1 & 0 \\ 0 & 0 & 0 & 1 \end{bmatrix}$	2×4
ABC-N	$\begin{bmatrix} 1 & 1 & 1 & 1 \end{bmatrix}$	1×4

Next, the detailed SCPQDMs of each parts are introduced, including (a) section k, two-terminal transmission line model with fault, left part; (b) section k, two-terminal transmission line model with fault, right part; (c) section k, two-terminal transmission line model without fault.

B.1 Section *k*, Two-terminal Transmission Line Model with Fault, Left Part

The π-equivalent model for section k inside the left part of two-terminal transmission line with fault is described in Figure B.3.

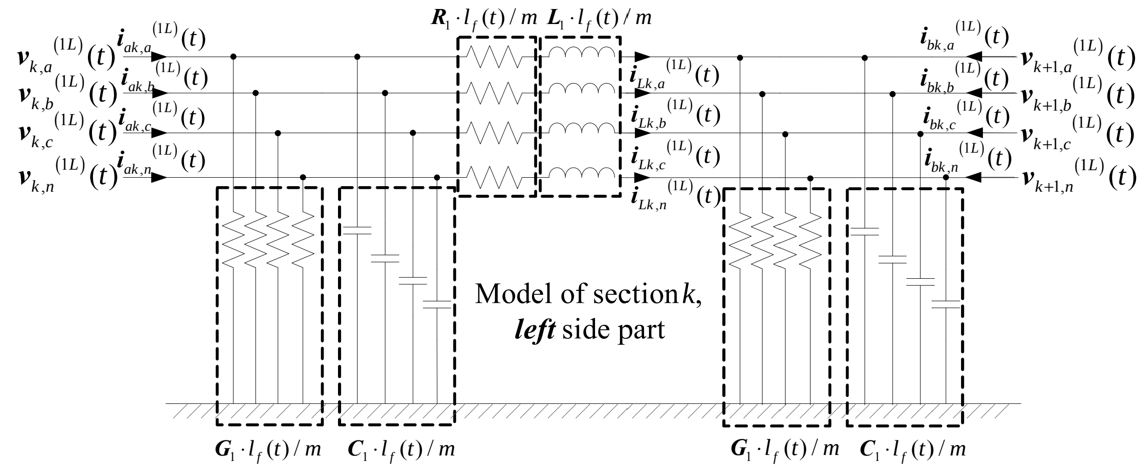

Figure B. 3. Section *k*, two-terminal transmission line model with fault, left part

where $\boldsymbol{R}_1$, $\boldsymbol{L}_1$, $\boldsymbol{G}_1$ and $\boldsymbol{C}_1$ are series resistance, series inductance, shunt conductance and shunt capacitance per mile; all states, parameters and through variables are defined in Table B.2, Table B.3 and Table B.4, respectively.

Table B.2. States of section *k*, two-terminal transmission line model with fault, left part

Index	Variable	Description
0	$v_{k,a}^{(1L)}(t)$	phase A voltage, left terminal
1	$v_{k,b}^{(1L)}(t)$	phase B voltage, left terminal
2	$v_{k,c}^{(1L)}(t)$	phase C voltage, left terminal
3	$v_{k,n}^{(1L)}(t)$	phase N voltage, left terminal
4	$v_{k+1,a}^{(1L)}(t)$	phase A voltage, right terminal
5	$v_{k+1,b}^{(1L)}(t)$	phase B voltage, right terminal
6	$v_{k+1,c}^{(1L)}(t)$	phase C voltage, right terminal

Table B.2. continued

7	$v_{k+1,n}^{(1L)}(t)$	phase N voltage, right terminal
8	$i_{Lk,a}^{(1L)}(t)$	phase A current through inductance
9	$i_{Lk,b}^{(1L)}(t)$	phase B current through inductance
10	$i_{Lk,c}^{(1L)}(t)$	phase C current through inductance
11	$i_{Lk,n}^{(1L)}(t)$	phase N current through inductance
12	$y_{vk,a}^{(1L)}(t)$	Introduced state for quadratization, phase A voltage times $l_f(t)$, left terminal
13	$y_{vk,b}^{(1L)}(t)$	Introduced state for quadratization, phase B voltage times $l_f(t)$, left terminal
14	$y_{vk,c}^{(1L)}(t)$	Introduced state for quadratization, phase C voltage times $l_f(t)$, left terminal
15	$y_{vk,n}^{(1L)}(t)$	Introduced state for quadratization, phase N voltage times $l_f(t)$, left terminal
16	$y_{v(k+1),a}^{(1L)}(t)$	Introduced state for quadratization, phase A voltage times $l_f(t)$, right terminal
17	$y_{v(k+1),b}^{(1L)}(t)$	Introduced state for quadratization, phase B voltage times $l_f(t)$, right terminal
18	$y_{v(k+1),c}^{(1L)}(t)$	Introduced state for quadratization, phase C voltage times $l_f(t)$, right terminal
19	$y_{v(k+1),n}^{(1L)}(t)$	Introduced state for quadratization, phase N voltage times $l_f(t)$, right terminal
20	$y_{Lk,a}^{(1L)}(t)$	Introduced state for quadratization, phase A current through inductance times $l_f(t)$
21	$y_{Lk,b}^{(1L)}(t)$	Introduced state for quadratization, phase B current through inductance times $l_f(t)$
22	$y_{Lk,c}^{(1L)}(t)$	Introduced state for quadratization, phase C current through inductance times $l_f(t)$
23	$y_{Lk,n}^{(1L)}(t)$	Introduced state for quadratization, phase N current through inductance times $l_f(t)$

Table B.3. Parameters of section *k*, two-terminal transmission line model with fault, left part

Index	Variable	Description
0	$l_f(t)$	Length between the fault and left terminal of the line

Table B.4. Through variables of section *k*, two-terminal transmission line model with fault, left part

Index	Variable	Description
0	$i_{ak,a}^{(1L)}(t)$	phase A current, left terminal
1	$i_{ak,b}^{(1L)}(t)$	phase B current, left terminal
2	$i_{ak,c}^{(1L)}(t)$	phase C current, left terminal
3	$i_{ak,n}^{(1L)}(t)$	phase N current, left terminal
4	$i_{bk,a}^{(1L)}(t)$	phase A current, left terminal
5	$i_{bk,b}^{(1L)}(t)$	phase B current, left terminal
6	$i_{bk,c}^{(1L)}(t)$	phase C current, left terminal
7	$i_{bk,n}^{(1L)}(t)$	phase N current, left terminal

Define $\mathbf{i}_{Lk}^{(1L)}(t)$ as the three phase and neutral current through the series inductance; $\boldsymbol{y}_{vk}^{(1L)}(t)$, $\boldsymbol{y}_{v(k+1)}^{(1L)}(t)$, and $\boldsymbol{y}_{Lk}^{(1L)}(t)$ are introduced states for quadratization; recall the definitions of $\mathbf{i}_{ak}^{(1L)}(t)$, $\mathbf{v}_{k}^{(1L)}(t)$, $\mathbf{i}_{bk}^{(1L)}(t)$ and $\mathbf{v}_{k+1}^{(1L)}(t)$: three phase and neutral current and voltage vectors at each terminal of section *k*. That means,

$$\mathbf{v}_k^{(1L)}(t)=\begin{bmatrix} v_{k,a}^{(1L)}(t) \\ v_{k,b}^{(1L)}(t) \\ v_{k,c}^{(1L)}(t) \\ v_{k,n}^{(1L)}(t) \end{bmatrix},\quad \mathbf{v}_{k+1}^{(1L)}(t)=\begin{bmatrix} v_{k+1,a}^{(1L)}(t) \\ v_{k+1,b}^{(1L)}(t) \\ v_{k+1,c}^{(1L)}(t) \\ v_{k+1,n}^{(1L)}(t) \end{bmatrix},\quad \mathbf{i}_{Lk}^{(1L)}(t)=\begin{bmatrix} i_{Lk,a}^{(1L)}(t) \\ i_{Lk,b}^{(1L)}(t) \\ i_{Lk,c}^{(1L)}(t) \\ i_{Lk,n}^{(1L)}(t) \end{bmatrix},$$

$$\mathbf{y}_{vk}^{(1L)}(t)=\begin{bmatrix} y_{vk,a}^{(1L)}(t) \\ y_{vk,b}^{(1L)}(t) \\ y_{vk,c}^{(1L)}(t) \\ y_{vk,n}^{(1L)}(t) \end{bmatrix},\ \mathbf{y}_{v(k+1)}^{(1L)}(t)=\begin{bmatrix} y_{v(k+1),a}^{(1L)}(t) \\ y_{v(k+1),b}^{(1L)}(t) \\ y_{v(k+1),c}^{(1L)}(t) \\ y_{v(k+1),n}^{(1L)}(t) \end{bmatrix},\ \mathbf{y}_{Lk}^{(1L)}(t)=\begin{bmatrix} y_{Lk,a}^{(1L)}(t) \\ y_{Lk,b}^{(1L)}(t) \\ y_{Lk,c}^{(1L)}(t) \\ y_{Lk,n}^{(1L)}(t) \end{bmatrix},$$

$$\mathbf{i}_{ak}^{(1L)}(t)=\begin{bmatrix} i_{ak,a}^{(1L)}(t) \\ i_{ak,b}^{(1L)}(t) \\ i_{ak,c}^{(1L)}(t) \\ i_{ak,n}^{(1L)}(t) \end{bmatrix},\ \mathbf{i}_{bk}^{(1L)}(t)=\begin{bmatrix} i_{bk,a}^{(1L)}(t) \\ i_{bk,b}^{(1L)}(t) \\ i_{bk,c}^{(1L)}(t) \\ i_{bk,n}^{(1L)}(t) \end{bmatrix}.$$

The transmission line section *k* model can be formulated in compact form as follows:

$$\mathbf{i}_{ak}^{(1L)}(t)=\frac{\mathbf{G}_1}{m}\cdot\mathbf{y}_{vk}^{(1L)}(t)+\frac{\mathbf{C}_1}{m}\cdot\frac{d\mathbf{y}_{vk}^{(1L)}(t)}{dt}+\mathbf{i}_{Lk}^{(1L)}(t) \tag{B.1}$$

$$\mathbf{i}_{bk}^{(1L)}(t)=\frac{\mathbf{G}_1}{m}\cdot\mathbf{y}_{v(k+1)}^{(1L)}(t)+\frac{\mathbf{C}_1}{m}\cdot\frac{d\mathbf{y}_{v(k+1)}^{(1L)}(t)}{dt}-\mathbf{i}_{Lk}^{(1L)}(t) \tag{B.2}$$

$$\mathbf{0}=-\mathbf{v}_{k}^{(1L)}(t)+\mathbf{v}_{k+1}^{(1L)}(t)+\frac{\mathbf{R}_1}{m}\cdot\mathbf{y}_{Lk}^{(1L)}(t)+\frac{\mathbf{L}_1}{m}\cdot\frac{d\mathbf{y}_{Lk}^{(1L)}(t)}{dt} \tag{B.3}$$

$$\mathbf{0}=\mathbf{y}_{vk}^{(1L)}(t)-\mathbf{v}_{k}^{(1L)}(t)\cdot l_f(t) \tag{B.4}$$

$$\mathbf{0}=\mathbf{y}_{v(k+1)}^{(1L)}(t)-\mathbf{v}_{k+1}^{(1L)}(t)\cdot l_f(t) \tag{B.5}$$

$$\mathbf{0}=\mathbf{y}_{Lk}^{(1L)}(t)-\mathbf{i}_{Lk}^{(1L)}(t)\cdot l_f(t) \tag{B.6}$$

The matrices corresponding to the SCPQDM of section *k*, two-terminal transmission line model with fault, left part are:

$$\boldsymbol{x}(t)=\begin{bmatrix}\boldsymbol{v}_{k}^{(1L)}(t) & \boldsymbol{v}_{k+1}^{(1L)}(t) & \boldsymbol{i}_{Lk}^{(1L)}(t) & \boldsymbol{y}_{vk}^{(1L)}(t) & \boldsymbol{y}_{v(k+1)}^{(1L)}(t) & \boldsymbol{y}_{Lk}^{(1L)}(t)\end{bmatrix}^T;$$

$$\boldsymbol{i}(t)=\begin{bmatrix}\boldsymbol{i}_{ak}^{(1L)}(t) & \boldsymbol{i}_{bk}^{(1L)}(t)\end{bmatrix}^{\mathrm{T}};\ \boldsymbol{p}(t)=l_f(t);$$

$$\boldsymbol{Y}_{eqx1} = \begin{bmatrix} \mathbf{0} & \mathbf{0} & \boldsymbol{I}_4 & \boldsymbol{G}_1/m & \mathbf{0} & \mathbf{0} \\ \mathbf{0} & \mathbf{0} & -\boldsymbol{I}_4 & \mathbf{0} & \boldsymbol{G}_1/m & \mathbf{0} \end{bmatrix};\ \boldsymbol{D}_{eqxd1} = \begin{bmatrix} \mathbf{0} & \mathbf{0} & \mathbf{0} & \boldsymbol{C}_1/m & \mathbf{0} & \mathbf{0} \\ \mathbf{0} & \mathbf{0} & \mathbf{0} & \boldsymbol{0} & \boldsymbol{C}_1/m & \mathbf{0} \end{bmatrix};$$

$$\boldsymbol{Y}_{eqx2} = \begin{bmatrix} -\boldsymbol{I}_4 & \boldsymbol{I}_4 & \mathbf{0} & \mathbf{0} & \mathbf{0} & \boldsymbol{R}_1/m \end{bmatrix};\ \boldsymbol{D}_{eqxd2} = \begin{bmatrix} \mathbf{0} & \mathbf{0} & \mathbf{0} & \mathbf{0} & \mathbf{0} & \boldsymbol{L}_1/m \end{bmatrix};$$

$$\boldsymbol{Y}_{eqx3} = \begin{bmatrix} \mathbf{0} & \mathbf{0} & \mathbf{0} & \boldsymbol{I}_4 & \mathbf{0} & \mathbf{0} \\ \mathbf{0} & \mathbf{0} & \mathbf{0} & \mathbf{0} & \boldsymbol{I}_4 & \mathbf{0} \\ \mathbf{0} & \mathbf{0} & \mathbf{0} & \mathbf{0} & \mathbf{0} & \boldsymbol{I}_4 \end{bmatrix};\ \boldsymbol{F}^i_{eqpx3} : f_{eq[1][i]} = -1,\ \textit{others are } 0,\ \textit{for } i = 1 \sim 12;$$

$$\mathbf{Y}_{equ1} = null;\ \mathbf{Y}_{eqp1} = null;\ \mathbf{C}_{eqc1} = \mathbf{0};\ \mathbf{Y}_{equ2} = null;\ \mathbf{Y}_{eqp2} = null;\ \mathbf{C}_{eqc2} = \mathbf{0};\ \mathbf{Y}_{equ3} = null;$$

$$\mathbf{Y}_{eqp3} = null;\ \boldsymbol{C}_{eqc3} = \mathbf{0};\ \left\langle \mathbf{F}^i_{eqxx3} \right\rangle = null;\ \left\langle \mathbf{F}^i_{equu3} \right\rangle = null;\ \left\langle \mathbf{F}^i_{eqpp3} \right\rangle = null;\ \left\langle \mathbf{F}^i_{eqxu3} \right\rangle = null;$$

$$\left\langle \mathbf{F}^i_{equp3} \right\rangle = null;$$

where $\mathbf{I}_4$ is the identity matrix with the dimension of 4.

B.2 Section *k*, Two-terminal Transmission Line Model with Fault, Right Part

The π-equivalent model for section k inside the right part of two-terminal transmission line with fault is described in Figure B.4.

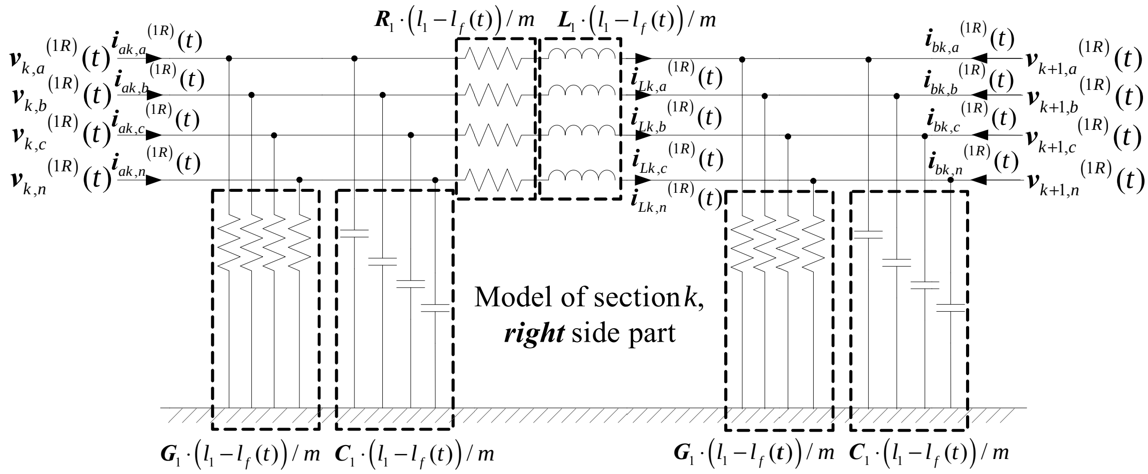

Figure B.4. Section *k*, two-terminal transmission line model with fault, right part

where $\boldsymbol{R}_1$, $\boldsymbol{L}_1$, $\boldsymbol{G}_1$ and $\boldsymbol{C}_1$ are series resistance, series inductance, shunt conductance and shunt capacitance per mile; all states and through variables are defined in Table B.5 Table B.6 and Table B.7, respectively.

Table B.5. States of section *k*, two-terminal transmission line model with fault, right part

Index	Variable	Description
0	$v_{k,a}^{(1R)}(t)$	phase A voltage, left terminal
1	$v_{k,b}^{(1R)}(t)$	phase B voltage, left terminal
2	$v_{k,c}^{(1R)}(t)$	phase C voltage, left terminal
3	$v_{k,n}^{(1R)}(t)$	phase N voltage, left terminal
4	$v_{k+1,a}^{(1R)}(t)$	phase A voltage, right terminal
5	$v_{k+1,b}^{(1R)}(t)$	phase B voltage, right terminal
6	$v_{k+1,c}^{(1R)}(t)$	phase C voltage, right terminal

Table B.5. continued

7	$v_{k+1,n}{}^{(1R)}(t)$	phase N voltage, right terminal
8	$i_{Lk,a}{}^{(1R)}(t)$	phase A current through inductance
9	$i_{Lk,b}{}^{(1R)}(t)$	phase B current through inductance
10	$i_{Lk,c}{}^{(1R)}(t)$	phase C current through inductance
11	$i_{Lk,n}{}^{(1R)}(t)$	phase N current through inductance
12	$y_{vk,a}{}^{(1R)}(t)$	Introduced state for quadratization, phase A voltage times $l_f(t)$, left terminal
13	$y_{vk,b}{}^{(1R)}(t)$	Introduced state for quadratization, phase B voltage times $l_f(t)$, left terminal
14	$y_{vk,c}{}^{(1R)}(t)$	Introduced state for quadratization, phase C voltage times $l_f(t)$, left terminal
15	$y_{vk,n}{}^{(1R)}(t)$	Introduced state for quadratization, phase N voltage times $l_f(t)$, left terminal
16	$y_{v(k+1),a}{}^{(1R)}(t)$	Introduced state for quadratization, phase A voltage times $l_f(t)$, right terminal
17	$y_{v(k+1),b}{}^{(1R)}(t)$	Introduced state for quadratization, phase B voltage times $l_f(t)$, right terminal
18	$y_{v(k+1),c}{}^{(1R)}(t)$	Introduced state for quadratization, phase C voltage times $l_f(t)$, right terminal
19	$y_{v(k+1),n}{}^{(1R)}(t)$	Introduced state for quadratization, phase N voltage times $l_f(t)$, right terminal
20	$y_{Lk,a}{}^{(1R)}(t)$	Introduced state for quadratization, phase A current through inductance times $l_f(t)$
21	$y_{Lk,b}{}^{(1R)}(t)$	Introduced state for quadratization, phase B current through inductance times $l_f(t)$
22	$y_{Lk,c}{}^{(1R)}(t)$	Introduced state for quadratization, phase C current through inductance times $l_f(t)$
23	$y_{Lk,n}{}^{(1R)}(t)$	Introduced state for quadratization, phase N current through inductance times $l_f(t)$

Table B.6. Parameters of section *k*, two-terminal transmission line model with fault, right part

Index	Variable	Description
0	$l_f(t)$	Length between the fault and left terminal of the line

Table B.7. Through variables of section *k*, two-terminal transmission line model with fault, right part

Index	Variable	Description
0	$i_{ak,a}^{(1R)}(t)$	phase A current, left terminal
1	$i_{ak,b}^{(1R)}(t)$	phase B current, left terminal
2	$i_{ak,c}^{(1R)}(t)$	phase C current, left terminal
3	$i_{ak,n}^{(1R)}(t)$	phase N current, left terminal
4	$i_{bk,a}^{(1R)}(t)$	phase A current, left terminal
5	$i_{bk,b}^{(1R)}(t)$	phase B current, left terminal
6	$i_{bk,c}^{(1R)}(t)$	phase C current, left terminal
7	$i_{bk,n}^{(1R)}(t)$	phase N current, left terminal

Define $\mathbf{i}_{Lk}^{(1R)}(t)$ as the three phase and neutral current through the series inductance; $\boldsymbol{y}_{vk}^{(1R)}(t)$, $\boldsymbol{y}_{v(k+1)}^{(1R)}(t)$, and $\boldsymbol{y}_{Lk}^{(1R)}(t)$ are introduced states for quadratization; recall the definitions of $\mathbf{i}_{ak}^{(1R)}(t)$, $\mathbf{v}_{k}^{(1R)}(t)$, $\mathbf{i}_{bk}^{(1R)}(t)$ and $\mathbf{v}_{k+1}^{(1R)}(t)$: three phase and neutral current and voltage vectors at each terminal of section *k*. That means,

$$\mathbf{v}_k^{(1R)}(t)=\begin{bmatrix} v_{k,a}^{(1R)}(t)\\ v_{k,b}^{(1R)}(t)\\ v_{k,c}^{(1R)}(t)\\ v_{k,n}^{(1R)}(t)\end{bmatrix},\quad \mathbf{v}_{k+1}^{(1R)}(t)=\begin{bmatrix} v_{k+1,a}^{(1R)}(t)\\ v_{k+1,b}^{(1R)}(t)\\ v_{k+1,c}^{(1R)}(t)\\ v_{k+1,n}^{(1R)}(t)\end{bmatrix},\quad \mathbf{i}_{Lk}^{(1R)}(t)=\begin{bmatrix} i_{Lk,a}^{(1R)}(t)\\ i_{Lk,b}^{(1R)}(t)\\ i_{Lk,c}^{(1R)}(t)\\ i_{Lk,n}^{(1R)}(t)\end{bmatrix},$$

$$\mathbf{y}_{vk}^{(1R)}(t)=\begin{bmatrix} y_{vk,a}^{(1R)}(t)\\ y_{vk,b}^{(1R)}(t)\\ y_{vk,c}^{(1R)}(t)\\ y_{vk,n}^{(1R)}(t)\end{bmatrix},\quad \mathbf{y}_{v(k+1)}^{(1R)}(t)=\begin{bmatrix} y_{v(k+1),a}^{(1R)}(t)\\ y_{v(k+1),b}^{(1R)}(t)\\ y_{v(k+1),c}^{(1R)}(t)\\ y_{v(k+1),n}^{(1R)}(t)\end{bmatrix},\quad \mathbf{y}_{Lk}^{(1R)}(t)=\begin{bmatrix} y_{Lk,a}^{(1R)}(t)\\ y_{Lk,b}^{(1R)}(t)\\ y_{Lk,c}^{(1R)}(t)\\ y_{Lk,n}^{(1R)}(t)\end{bmatrix},$$

$$\mathbf{i}_{ak}{}^{(1R)}(t)=\begin{bmatrix} i_{ak,a}{}^{(1R)}(t) \\ i_{ak,b}{}^{(1R)}(t) \\ i_{ak,c}{}^{(1R)}(t) \\ i_{ak,n}{}^{(1R)}(t) \end{bmatrix}, \ \mathbf{i}_{bk}{}^{(1R)}(t)=\begin{bmatrix} i_{bk,a}{}^{(1R)}(t) \\ i_{bk,b}{}^{(1R)}(t) \\ i_{bk,c}{}^{(1R)}(t) \\ i_{bk,n}{}^{(1R)}(t) \end{bmatrix}.$$

The transmission line section k model can be formulated in compact form as follows:

$$\mathbf{i}_{ak}{}^{(1R)}(t)=\frac{\mathbf{G}_1\cdot l_1}{n}\cdot\mathbf{v}_k{}^{(1R)}(t)-\frac{\mathbf{G}_1}{n}\cdot\mathbf{y}_{vk}{}^{(1R)}(t)+\frac{\mathbf{C}_1\cdot l_1}{n}\cdot\frac{d\mathbf{v}_k{}^{(1R)}(t)}{dt}-\frac{\mathbf{C}_1}{n}\cdot\frac{d\mathbf{y}_{vk}{}^{(1R)}(t)}{dt}+\mathbf{i}_{Lk}{}^{(1R)}(t) \quad \text{(B.7)}$$

$$\mathbf{i}_{bk}{}^{(1R)}(t)=\frac{\mathbf{G}_1\cdot l_1}{n}\cdot\mathbf{v}_{k+1}{}^{(1R)}(t)-\frac{\mathbf{G}_1}{n}\cdot\mathbf{y}_{v(k+1)}{}^{(1R)}(t)+\frac{\mathbf{C}_1\cdot l_1}{n}\cdot\frac{d\mathbf{v}_{k+1}{}^{(1R)}(t)}{dt}-\frac{\mathbf{C}_1}{n}\cdot\frac{d\mathbf{y}_{v(k+1)}{}^{(1R)}(t)}{dt}-\mathbf{i}_{Lk}{}^{(1R)}(t) \quad \text{(B.8)}$$

$$\mathbf{0}=-\mathbf{v}_k{}^{(1R)}(t)+\mathbf{v}_{k+1}{}^{(1R)}(t)+\frac{\mathbf{R}_1\cdot l_1}{n}\cdot\mathbf{i}_{Lk}{}^{(1R)}(t)-\frac{\mathbf{R}_1}{n}\cdot\mathbf{y}_{Lk}{}^{(1R)}(t)+\frac{\mathbf{L}_1\cdot l_1}{n}\cdot\frac{d\mathbf{i}_{Lk}{}^{(1R)}(t)}{dt}-\frac{\mathbf{L}_1}{n}\cdot\frac{d\mathbf{y}_{Lk}{}^{(1R)}(t)}{dt} \quad \text{(B.9)}$$

$$\mathbf{0}=\mathbf{y}_{vk}{}^{(1R)}(t)-\mathbf{v}_k{}^{(1R)}(t)\cdot l_f(t) \quad \text{(B.10)}$$

$$\mathbf{0}=\mathbf{y}_{v(k+1)}{}^{(1R)}(t)-\mathbf{v}_{k+1}{}^{(1R)}(t)\cdot l_f(t) \quad \text{(B.11)}$$

$$\mathbf{0}=\mathbf{y}_{Lk}{}^{(1R)}(t)-\mathbf{i}_{Lk}{}^{(1R)}(t)\cdot l_f(t) \quad \text{(B.12)}$$

The matrices corresponding to the SCPQDM of section k, two-terminal transmission line model with fault, right part are:

$$\boldsymbol{x}(t)=\left[\boldsymbol{v}_k^{(1R)}(t) \quad \boldsymbol{v}_{k+1}^{(1R)}(t) \quad \boldsymbol{i}_{Lk}^{(1R)}(t) \quad \boldsymbol{y}_{vk}^{(1R)}(t) \quad \boldsymbol{y}_{v(k+1)}^{(1R)}(t) \quad \boldsymbol{y}_{Lk}^{(1R)}(t)\right]^T;$$

$$\boldsymbol{i}(t)=\left[\boldsymbol{i}_{ak}{}^{(1R)}(t) \quad \boldsymbol{i}_{bk}{}^{(1R)}(t)\right]^{\mathrm{T}}; \ \boldsymbol{p}(t)=l_f(t);$$

$$\boldsymbol{Y}_{eqx1}=\begin{bmatrix} \boldsymbol{G}_1\cdot l_1/n & \mathbf{0} & \boldsymbol{I}_4 & -\boldsymbol{G}_1/n & \mathbf{0} & \mathbf{0} \\ \mathbf{0} & \boldsymbol{G}_1\cdot l_1/n & -\boldsymbol{I}_4 & \mathbf{0} & -\boldsymbol{G}_1/n & \mathbf{0} \end{bmatrix};$$

$$\boldsymbol{D}_{eqxd1}=\begin{bmatrix} \boldsymbol{C}_1\cdot l_1/n & \mathbf{0} & \mathbf{0} & -\boldsymbol{C}_1/n & \mathbf{0} & \mathbf{0} \\ \mathbf{0} & \boldsymbol{C}_1\cdot l_1/n & \mathbf{0} & \mathbf{0} & -\boldsymbol{C}_1/m & \boldsymbol{0} \end{bmatrix};$$

$$\boldsymbol{Y}_{eqx2}=\left[-\boldsymbol{I}_4 \quad \boldsymbol{I}_4 \quad \boldsymbol{R}_1\cdot l_1/n \quad \mathbf{0} \quad \mathbf{0} \quad -\boldsymbol{R}_1/n\right]; \ \boldsymbol{D}_{eqxd2}=\left[\mathbf{0} \quad \mathbf{0} \quad \boldsymbol{L}_1\cdot l_1/n \quad \mathbf{0} \quad \mathbf{0} \quad -\boldsymbol{L}_1/n\right];$$

$$\boldsymbol{Y}_{eqx3} = \begin{bmatrix} \mathbf{0} & \mathbf{0} & \mathbf{0} & \boldsymbol{I}_4 & \mathbf{0} & \mathbf{0} \\ \mathbf{0} & \mathbf{0} & \mathbf{0} & \mathbf{0} & \boldsymbol{I}_4 & \mathbf{0} \\ \mathbf{0} & \mathbf{0} & \mathbf{0} & \mathbf{0} & \mathbf{0} & \boldsymbol{I}_4 \end{bmatrix};\ \boldsymbol{F}^{i}_{eqpx3} : f_{eq[1][i]} = -1,\ others\ are\ 0,\ \ for\ i = 1 \sim 12\,;$$

$$\mathbf{Y}_{equ1} = null\,;\ \mathbf{Y}_{eqp1} = null\,;\ \mathbf{C}_{eqc1} = \mathbf{0}\,;\ \mathbf{Y}_{equ2} = null\,;\ \mathbf{Y}_{eqp2} = null\,;\ \mathbf{C}_{eqc2} = \mathbf{0}\,;\ \mathbf{Y}_{equ3} = null\,;$$

$$\mathbf{Y}_{eqp3} = null\,;\ \boldsymbol{C}_{eqc3} = \mathbf{0}\,;\ \left\langle \mathbf{F}^{i}_{eqxx3} \right\rangle = null\,;\ \left\langle \mathbf{F}^{i}_{equu3} \right\rangle = null\,;\ \left\langle \mathbf{F}^{i}_{eqpp3} \right\rangle = null\,;\ \left\langle \mathbf{F}^{i}_{eqxu3} \right\rangle = null\,;$$

$$\left\langle \mathbf{F}^{i}_{equp3} \right\rangle = null\,;$$

where $\mathbf{I}_4$ is the identity matrix with the dimension of 4.

B.3 Section *k*, Two-terminal Transmission Line Model without Fault

The model of section *k*, two-terminal transmission line model without fault is exactly the same as introduced in Appendix A, section A.1.

Appendix C: SCPQDMs of Transmission Lines with Parameters during Normal Operating Conditions

This Appendix describes SCPQDMs of transmission lines with parameters during normal operating conditions, for parameter identification application. As introduced in chapter 6, for an example tower structure provided in Figure C.1 the parameters of transmission lines include total length of the transmission line l, average distance between phase conductors d and average height of phase conductors h. Based on the combination among different parameters, here we are introducing 7 different kinds of models, including: (a) the model with the total length of the line as the only parameter; (b) the model with the average distance between phase conductors as the only parameter; (c) the model with the average height of phase conductors as the only parameter; (d) the model with the total length of the line and the average distance between phase conductors as two parameters; (e) the model with the total length of the line and the average height of phase conductors as two parameters; (f) the model with the average distance between phase conductors and the average height of phase conductors as two parameters; and (g) the model with the total length of the line, the average distance between phase conductors and the average height of phase conductors as three parameters.

For the above 7 models, here multi-section transmission models are applied, where each section is a π-equivalent model. The section number is chosen in such a way that the traveling length of electro-magnetic wave during one sampling interval is comparable to the length of each section, as shown in Figure C.2. Any of the above 7 SCPQDMs can be formed by combining SCPQDMs of all sections together. Next, the SCPQDMs of section k, for all above 7 models are introduced respectively.

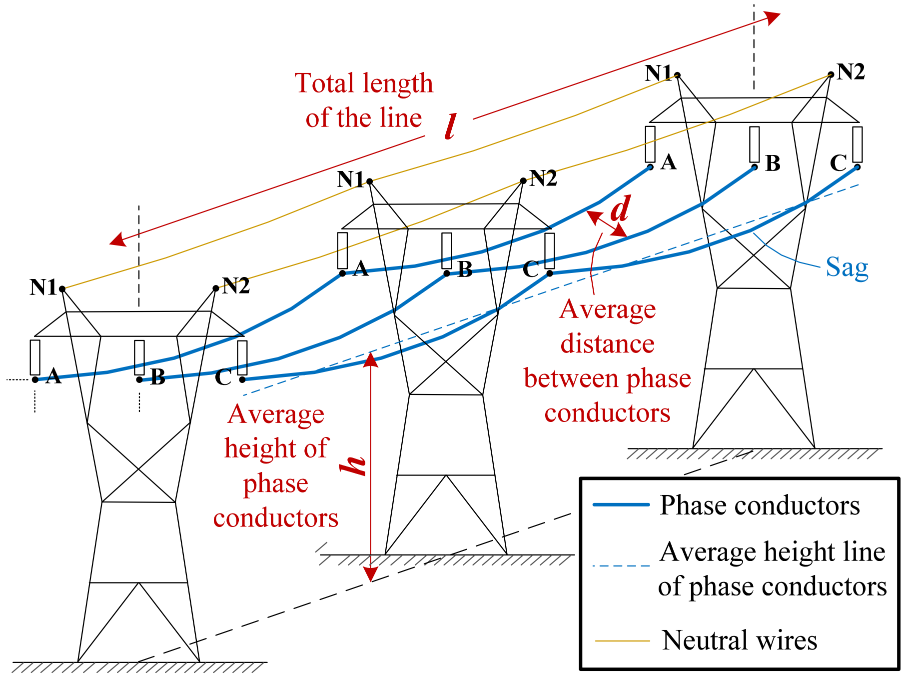

Figure C.1. Example tower structure of the transmission line

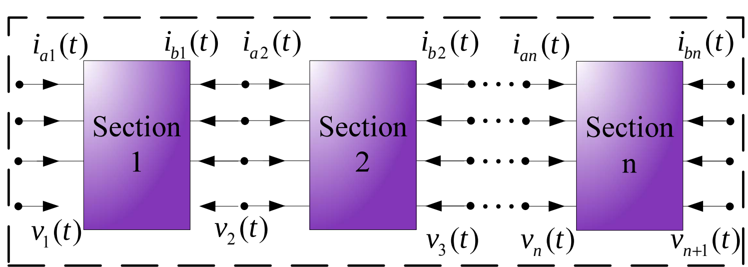

Figure C.2. Multi-section transmission line model with parameters during normal operating conditions

C.1 Section *k*, Transmission Line Model with the Total Length of the Line as the Only Parameter

The model of section k is described in Figure C.3.

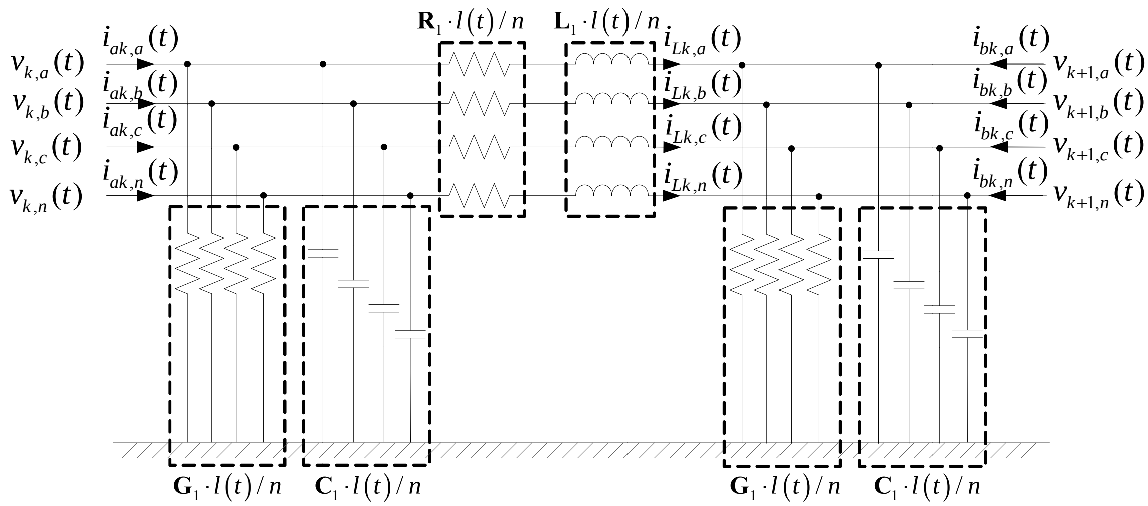

Figure C.3. Section *k* model with the total length of the line as the only parameter

where $\boldsymbol{R}_1$, $\boldsymbol{L}_1$, $\boldsymbol{G}_1$ and $\boldsymbol{C}_1$ are series resistance, series inductance, shunt conductance and shunt capacitance per mile; all states and through variables are defined in Table C.1, Table C.2 and Table C.3, respectively; $l(t)$ is the total length of the line.

Table C.1. States of section *k* model with the total length of the line as the only parameter

Index	Variable	Description
0	$v_{k,a}(t)$	phase A voltage, left terminal
1	$v_{k,b}(t)$	phase B voltage, left terminal
2	$v_{k,c}(t)$	phase C voltage, left terminal
3	$v_{k,n}(t)$	phase N voltage, left terminal
4	$v_{k+1,a}(t)$	phase A voltage, right terminal
5	$v_{k+1,b}(t)$	phase B voltage, right terminal
6	$v_{k+1,c}(t)$	phase C voltage, right terminal

Table C.1. continued

7	$v_{k+1,n}(t)$	phase N voltage, right terminal
8	$i_{Lk,a}(t)$	phase A current through inductance
9	$i_{Lk,b}(t)$	phase B current through inductance
10	$i_{Lk,c}(t)$	phase C current through inductance
11	$i_{Lk,n}(t)$	phase N current through inductance
12	$y_{vk,a}(t)$	Introduced state for quadratization, phase A voltage times $l(t)$, left terminal
13	$y_{vk,b}(t)$	Introduced state for quadratization, phase B voltage times $l(t)$, left terminal
14	$y_{vk,c}(t)$	Introduced state for quadratization, phase C voltage times $l(t)$, left terminal
15	$y_{vk,n}(t)$	Introduced state for quadratization, phase N voltage times $l(t)$, left terminal
16	$y_{v(k+1),a}(t)$	Introduced state for quadratization, phase A voltage times $l(t)$, right terminal
17	$y_{v(k+1),b}(t)$	Introduced state for quadratization, phase B voltage times $l(t)$, right terminal
18	$y_{v(k+1),c}(t)$	Introduced state for quadratization, phase C voltage times $l(t)$, right terminal
19	$y_{v(k+1),n}(t)$	Introduced state for quadratization, phase N voltage times $l(t)$, right terminal
20	$y_{Lk,a}(t)$	Introduced state for quadratization, phase A current through inductance times $l(t)$
21	$y_{Lk,b}(t)$	Introduced state for quadratization, phase B current through inductance times $l(t)$
22	$y_{Lk,c}(t)$	Introduced state for quadratization, phase C current through inductance times $l(t)$
23	$y_{Lk,n}(t)$	Introduced state for quadratization, phase N current through inductance times $l(t)$

Table C.2. Parameters of section *k* model with the total length of the line as the only parameter

Index	Variable	Description
0	$l(t)$	Total length of the line

Table C.3. Through variables of section k model with the total length of the line as the only parameter

Index	Variable	Description
0	$i_{ak,a}(t)$	phase A current, left terminal
1	$i_{ak,b}(t)$	phase B current, left terminal
2	$i_{ak,c}(t)$	phase C current, left terminal
3	$i_{ak,n}(t)$	phase N current, left terminal
4	$i_{bk,a}(t)$	phase A current, left terminal
5	$i_{bk,b}(t)$	phase B current, left terminal
6	$i_{bk,c}(t)$	phase C current, left terminal
7	$i_{bk,n}(t)$	phase N current, left terminal

Define $\mathbf{i}_{Lk}(t)$ as the three phase and neutral current through the series inductance; $\boldsymbol{y}_{vk}(t)$, $\boldsymbol{y}_{v(k+1)}(t)$, and $\boldsymbol{y}_{Lk}(t)$ are introduced states for quadratization; recall the definitions of $\mathbf{i}_{ak}(t)$, $\mathbf{v}_k(t)$, $\mathbf{i}_{bk}(t)$ and $\mathbf{v}_{k+1}(t)$: three phase and neutral current and voltage vectors at each terminal of section k. That means,

$$\mathbf{v}_k(t)=\begin{bmatrix} v_{k,a}(t) \\ v_{k,b}(t) \\ v_{k,c}(t) \\ v_{k,n}(t) \end{bmatrix},\quad \mathbf{v}_{k+1}(t)=\begin{bmatrix} v_{k+1,a}(t) \\ v_{k+1,b}(t) \\ v_{k+1,c}(t) \\ v_{k+1,n}(t) \end{bmatrix},\quad \mathbf{i}_{Lk}(t)=\begin{bmatrix} i_{Lk,a}(t) \\ i_{Lk,b}(t) \\ i_{Lk,c}(t) \\ i_{Lk,n}(t) \end{bmatrix},$$

$$\mathbf{y}_{vk}(t)=\begin{bmatrix} y_{vk,a}(t) \\ y_{vk,b}(t) \\ y_{vk,c}(t) \\ y_{vk,n}(t) \end{bmatrix},\quad \mathbf{y}_{v(k+1)}(t)=\begin{bmatrix} y_{v(k+1),a}(t) \\ y_{v(k+1),b}(t) \\ y_{v(k+1),c}(t) \\ y_{v(k+1),n}(t) \end{bmatrix},\quad \mathbf{y}_{Lk}(t)=\begin{bmatrix} y_{Lk,a}(t) \\ y_{Lk,b}(t) \\ y_{Lk,c}(t) \\ y_{Lk,n}(t) \end{bmatrix},$$

$$\mathbf{i}_{ak}(t)=\begin{bmatrix} i_{ak,a}(t) \\ i_{ak,b}(t) \\ i_{ak,c}(t) \\ i_{ak,n}(t) \end{bmatrix},\quad \mathbf{i}_{bk}(t)=\begin{bmatrix} i_{bk,a}(t) \\ i_{bk,b}(t) \\ i_{bk,c}(t) \\ i_{bk,n}(t) \end{bmatrix}.$$

The transmission line section *k* model can be formulated in compact form as follows:

$$\mathbf{i}_{ak}(t) = \frac{\mathbf{G}_1}{n} \cdot \mathbf{y}_{vk}(t) + \frac{\mathbf{C}_1}{n} \cdot \frac{d\mathbf{y}_{vk}(t)}{dt} + \mathbf{i}_{Lk}(t) \tag{C.1}$$

$$\mathbf{i}_{bk}(t) = \frac{\mathbf{G}_1}{n} \cdot \mathbf{y}_{v(k+1)}(t) + \frac{\mathbf{C}_1}{n} \cdot \frac{d\mathbf{y}_{v(k+1)}(t)}{dt} - \mathbf{i}_{Lk}(t) \tag{C.2}$$

$$\mathbf{0} = -\mathbf{v}_k(t) + \mathbf{v}_{k+1}(t) + \frac{\mathbf{R}_1}{n} \cdot \mathbf{y}_{Lk}(t) + \frac{\mathbf{L}_1}{n} \cdot \frac{d\mathbf{y}_{Lk}(t)}{dt} \tag{C.3}$$

$$\mathbf{0} = \mathbf{y}_{vk}(t) - \mathbf{v}_k(t) \cdot l(t) \tag{C.4}$$

$$\mathbf{0} = \mathbf{y}_{v(k+1)}(t) - \mathbf{v}_{k+1}(t) \cdot l(t) \tag{C.5}$$

$$\mathbf{0} = \mathbf{y}_{Lk}(t) - \mathbf{i}_{Lk}(t) \cdot l(t) \tag{C.6}$$

The matrices corresponding to the SCPQDM of section *k*, transmission line model with the total length of the line as the only parameter are:

$$\boldsymbol{x}(t) = \begin{bmatrix} \boldsymbol{v}_k(t) & \boldsymbol{v}_{k+1}(t) & \boldsymbol{i}_{Lk}(t) & \boldsymbol{y}_{vk}(t) & \boldsymbol{y}_{v(k+1)}(t) & \boldsymbol{y}_{Lk}(t) \end{bmatrix}^T;$$

$$\boldsymbol{i}(t) = \begin{bmatrix} \boldsymbol{i}_{ak}(t) & \boldsymbol{i}_{bk}(t) \end{bmatrix}^{\mathrm{T}}; \ \boldsymbol{p}(t) = l(t);$$

$$\boldsymbol{Y}_{eqx1} = \begin{bmatrix} \mathbf{0} & \mathbf{0} & \boldsymbol{I}_4 & \boldsymbol{G}_1/n & \mathbf{0} & \mathbf{0} \\ \mathbf{0} & \mathbf{0} & -\boldsymbol{I}_4 & \mathbf{0} & \boldsymbol{G}_1/n & \mathbf{0} \end{bmatrix}; \ \boldsymbol{D}_{eqxd1} = \begin{bmatrix} \mathbf{0} & \mathbf{0} & \mathbf{0} & \boldsymbol{C}_1/n & \mathbf{0} & \mathbf{0} \\ \mathbf{0} & \mathbf{0} & \mathbf{0} & \boldsymbol{0} & \boldsymbol{C}_1/n & \mathbf{0} \end{bmatrix};$$

$$\boldsymbol{Y}_{eqx2} = \begin{bmatrix} -\boldsymbol{I}_4 & \boldsymbol{I}_4 & \mathbf{0} & \mathbf{0} & \mathbf{0} & \boldsymbol{R}_1/n \end{bmatrix}; \ \boldsymbol{D}_{eqxd2} = \begin{bmatrix} \mathbf{0} & \mathbf{0} & \mathbf{0} & \mathbf{0} & \mathbf{0} & \boldsymbol{L}_1/n \end{bmatrix};$$

$$\boldsymbol{Y}_{eqx3} = \begin{bmatrix} \mathbf{0} & \mathbf{0} & \mathbf{0} & \boldsymbol{I}_4 & \mathbf{0} & \mathbf{0} \\ \mathbf{0} & \mathbf{0} & \mathbf{0} & \mathbf{0} & \boldsymbol{I}_4 & \mathbf{0} \\ \mathbf{0} & \mathbf{0} & \mathbf{0} & \mathbf{0} & \mathbf{0} & \boldsymbol{I}_4 \end{bmatrix}; \ \boldsymbol{F}^i_{eqpx3} : f_{eq[1][i]} = -1, \ \mathit{others\ are}\ 0, \ \mathit{for}\ i = 1 \sim 12;$$

$$\mathbf{Y}_{equ1} = null; \ \mathbf{Y}_{eqp1} = null; \ \mathbf{C}_{eqc1} = \mathbf{0}; \ \mathbf{Y}_{equ2} = null; \ \mathbf{Y}_{eqp2} = null; \ \mathbf{C}_{eqc2} = \mathbf{0}; \ \mathbf{Y}_{equ3} = null;$$

$$\mathbf{Y}_{eqp3} = null; \ \boldsymbol{C}_{eqc3} = \mathbf{0}; \ \left\langle \mathbf{F}^i_{eqxx3} \right\rangle = null; \ \left\langle \mathbf{F}^i_{equu3} \right\rangle = null; \ \left\langle \mathbf{F}^i_{eqpp3} \right\rangle = null; \ \left\langle \mathbf{F}^i_{eqxu3} \right\rangle = null; \left\langle \mathbf{F}^i_{equp3} \right\rangle = null;$$

where $\mathbf{I}_4$ is the identity matrix with the dimension of 4.

C.2 Section *k*, Transmission Line Model with the Average Distance between Phase Conductors as the Only Parameter

The model of section *k* is described in Figure C.4.

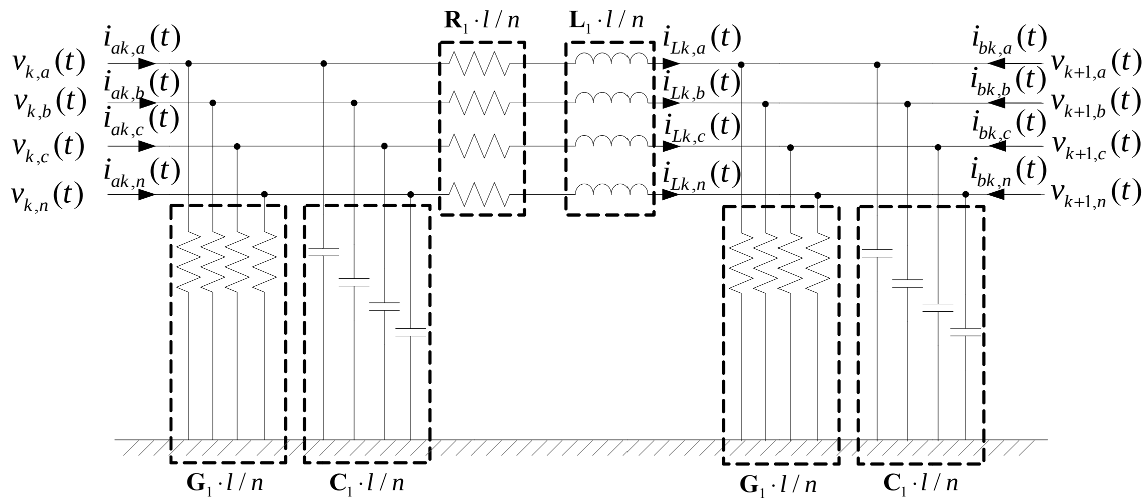

Figure C.4. Section *k* model with average distance between phase conductors as the only parameter

where $\boldsymbol{R}_1$, $\boldsymbol{L}_1$, $\boldsymbol{G}_1$ and $\boldsymbol{C}_1$ are series resistance, series inductance, shunt conductance and shunt capacitance per mile; *l* is the total length of the line; $d(t)$ is the average distance between phase conductors.

In addition, linearize the above $\boldsymbol{R}_1$, $\boldsymbol{L}_1$, $\boldsymbol{G}_1$ and $\boldsymbol{C}_1$ matrices around the initial value of the average distance between phase conductors d_0 (the value of the above matrices with distance d_0 are $\boldsymbol{R}_1^{(0)}$, $\boldsymbol{L}_1^{(0)}$, $\boldsymbol{G}_1^{(0)}$ and $\boldsymbol{C}_1^{(0)}$).

$$\mathbf{R}_1 = \mathbf{R}_1^{(0)} + \boldsymbol{\beta}_R \cdot \left(d(t) - d_0\right) \tag{C.7}$$

$$\mathbf{L}_1 = \mathbf{L}_1^{(0)} + \boldsymbol{\beta}_L \cdot \left(d(t) - d_0\right) \tag{C.8}$$

$$\mathbf{C}_1 = \mathbf{C}_1^{(0)} + \boldsymbol{\beta}_C \cdot \left(d(t) - d_0\right) \tag{C.9}$$

$$\mathbf{G}_1 = \mathbf{G}_1^{(0)} + \boldsymbol{\beta}_G \cdot \left(d\left(t\right) - d_0\right) \tag{C.10}$$

All states and through variables are defined in Table C.4, Table C.5 and Table C.6, respectively.

Table C.4. States of section *k* model with average distance between phase conductors as the only parameter

Index	Variable	Description
0	$v_{k,a}(t)$	phase A voltage, left terminal
1	$v_{k,b}(t)$	phase B voltage, left terminal
2	$v_{k,c}(t)$	phase C voltage, left terminal
3	$v_{k,n}(t)$	phase N voltage, left terminal
4	$v_{k+1,a}(t)$	phase A voltage, right terminal
5	$v_{k+1,b}(t)$	phase B voltage, right terminal
6	$v_{k+1,c}(t)$	phase C voltage, right terminal
7	$v_{k+1,n}(t)$	phase N voltage, right terminal
8	$i_{Lk,a}(t)$	phase A current through inductance
9	$i_{Lk,b}(t)$	phase B current through inductance
10	$i_{Lk,c}(t)$	phase C current through inductance
11	$i_{Lk,n}(t)$	phase N current through inductance
12	$y_{vk,a}(t)$	Introduced state for quadratization, phase A voltage times $d(t)$, left terminal
13	$y_{vk,b}(t)$	Introduced state for quadratization, phase B voltage times $d\left(t\right)$, left terminal
14	$y_{vk,c}(t)$	Introduced state for quadratization, phase C voltage times $d\left(t\right)$, left terminal
15	$y_{vk,n}(t)$	Introduced state for quadratization, phase N voltage times $d\left(t\right)$, left terminal
16	$y_{v(k+1),a}(t)$	Introduced state for quadratization, phase A voltage times $d\left(t\right)$, right terminal
17	$y_{v(k+1),b}(t)$	Introduced state for quadratization, phase B voltage times $d\left(t\right)$, right terminal
18	$y_{v(k+1),c}(t)$	Introduced state for quadratization, phase C voltage times $d\left(t\right)$, right terminal

Table C.4. continued

19	$y_{v(k+1),n}(t)$	Introduced state for quadratization, phase N voltage times $d(t)$, right terminal
20	$y_{Lk,a}(t)$	Introduced state for quadratization, phase A current through inductance times $d(t)$
21	$y_{Lk,b}(t)$	Introduced state for quadratization, phase B current through inductance times $d(t)$
22	$y_{Lk,c}(t)$	Introduced state for quadratization, phase C current through inductance times $d(t)$
23	$y_{Lk,n}(t)$	Introduced state for quadratization, phase N current through inductance times $d(t)$

Table C.5. Parameters of section *k* model with average distance between phase conductors as the only parameter

Index	Variable	Description
0	$d(t)$	Average distance between phase conductors

Table C.6. Through variables of section *k* model average distance between phase conductors as the only parameter

Index	Variable	Description
0	$i_{ak,a}(t)$	phase A current, left terminal
1	$i_{ak,b}(t)$	phase B current, left terminal
2	$i_{ak,c}(t)$	phase C current, left terminal
3	$i_{ak,n}(t)$	phase N current, left terminal
4	$i_{bk,a}(t)$	phase A current, left terminal
5	$i_{bk,b}(t)$	phase B current, left terminal
6	$i_{bk,c}(t)$	phase C current, left terminal
7	$i_{bk,n}(t)$	phase N current, left terminal

Define $\mathbf{i}_{Lk}(t)$ as the three phase and neutral current through the series inductance; $\boldsymbol{y}_{vk}(t)$, $\boldsymbol{y}_{v(k+1)}(t)$, and $\boldsymbol{y}_{Lk}(t)$ are introduced states for quadratization; recall the definitions of $\mathbf{i}_{ak}(t)$, $\mathbf{v}_k(t)$, $\mathbf{i}_{bk}(t)$ and $\mathbf{v}_{k+1}(t)$: three phase and neutral current and voltage vectors at each terminal of section *k*. That means,

$$\mathbf{v}_k(t)=\begin{bmatrix} v_{k,a}(t) \\ v_{k,b}(t) \\ v_{k,c}(t) \\ v_{k,n}(t) \end{bmatrix},\ \ \mathbf{v}_{k+1}(t)=\begin{bmatrix} v_{k+1,a}(t) \\ v_{k+1,b}(t) \\ v_{k+1,c}(t) \\ v_{k+1,n}(t) \end{bmatrix},\ \ \mathbf{i}_{Lk}(t)=\begin{bmatrix} i_{Lk,a}(t) \\ i_{Lk,b}(t) \\ i_{Lk,c}(t) \\ i_{Lk,n}(t) \end{bmatrix},$$

$$\mathbf{y}_{vk}(t)=\begin{bmatrix} y_{vk,a}(t) \\ y_{vk,b}(t) \\ y_{vk,c}(t) \\ y_{vk,n}(t) \end{bmatrix},\ \ \mathbf{y}_{v(k+1)}(t)=\begin{bmatrix} y_{v(k+1),a}(t) \\ y_{v(k+1),b}(t) \\ y_{v(k+1),c}(t) \\ y_{v(k+1),n}(t) \end{bmatrix},\ \ \mathbf{y}_{Lk}(t)=\begin{bmatrix} y_{Lk,a}(t) \\ y_{Lk,b}(t) \\ y_{Lk,c}(t) \\ y_{Lk,n}(t) \end{bmatrix},$$

$$\mathbf{i}_{ak}(t)=\begin{bmatrix} i_{ak,a}(t) \\ i_{ak,b}(t) \\ i_{ak,c}(t) \\ i_{ak,n}(t) \end{bmatrix},\ \ \mathbf{i}_{bk}(t)=\begin{bmatrix} i_{bk,a}(t) \\ i_{bk,b}(t) \\ i_{bk,c}(t) \\ i_{bk,n}(t) \end{bmatrix}.$$

The transmission line section *k* model can be formulated in compact form as follows:

$$\mathbf{i}_{ak}(t)=\frac{\left(\mathbf{G}_1^{(0)}-\boldsymbol{\beta}_G d_0\right)l}{n}\cdot\mathbf{v}_k(t)+\frac{\boldsymbol{\beta}_G l}{n}\cdot\mathbf{y}_{vk}(t)+\frac{\left(\mathbf{C}_1^{(0)}-\boldsymbol{\beta}_C d_0\right)l}{n}\cdot\frac{d\mathbf{v}_k(t)}{dt}+\frac{\boldsymbol{\beta}_C l}{n}\cdot\frac{d\mathbf{y}_{vk}(t)}{dt}+\mathbf{i}_{Lk}(t) \quad (\text{C.11})$$

$$\mathbf{i}_{bk}(t)=\frac{\left(\mathbf{G}_1^{(0)}-\boldsymbol{\beta}_G d_0\right)l}{n}\cdot\mathbf{v}_{k+1}(t)+\frac{\boldsymbol{\beta}_G l}{n}\cdot\mathbf{y}_{v(k+1)}(t)+\frac{\left(\mathbf{C}_1^{(0)}-\boldsymbol{\beta}_C d_0\right)l}{n}\cdot\frac{d\mathbf{v}_{k+1}(t)}{dt}+\frac{\boldsymbol{\beta}_C l}{n}\cdot\frac{d\mathbf{y}_{v(k+1)}(t)}{dt}-\mathbf{i}_{Lk}(t) \quad (\text{C.12})$$

$$\mathbf{0}=-\mathbf{v}_k(t)+\mathbf{v}_{k+1}(t)+\frac{\left(\mathbf{R}_1^{(0)}-\boldsymbol{\beta}_R d_0\right)l}{n}\cdot\mathbf{i}_{Lk}(t)+\frac{\boldsymbol{\beta}_R l}{n}\cdot\mathbf{y}_{Lk}(t)+\frac{\left(\mathbf{L}_1^{(0)}-\boldsymbol{\beta}_L d_0\right)l}{n}\cdot\frac{d\mathbf{i}_{Lk}(t)}{dt}+\frac{\boldsymbol{\beta}_L l}{n}\cdot\frac{d\mathbf{y}_{Lk}(t)}{dt} \quad (\text{C.13})$$

$$\mathbf{0}=\mathbf{y}_{vk}(t)-\mathbf{v}_k(t)\cdot d(t) \quad (\text{C.14})$$

$$\mathbf{0}=\mathbf{y}_{v(k+1)}(t)-\mathbf{v}_{k+1}(t)\cdot d(t) \quad (\text{C.15})$$

$$\mathbf{0}=\mathbf{y}_{Lk}(t)-\mathbf{i}_{Lk}(t)\cdot d(t) \quad (\text{C.16})$$

The matrices corresponding to the SCPQDM of section k, transmission line model with average distance between phase conductors as the only parameter are:

$$\boldsymbol{x}(t)=\left[\boldsymbol{v}_k(t) \quad \boldsymbol{v}_{k+1}(t) \quad \boldsymbol{i}_{Lk}(t) \quad \boldsymbol{y}_{vk}(t) \quad \boldsymbol{y}_{v(k+1)}(t) \quad \boldsymbol{y}_{Lk}(t)\right]^T;\ \boldsymbol{i}(t)=\left[\boldsymbol{i}_{ak}(t) \quad \boldsymbol{i}_{bk}(t)\right]^{\mathrm{T}};\ \boldsymbol{p}(t)=d(t);$$

$$\boldsymbol{Y}_{eqx1}=\begin{bmatrix} \dfrac{\left(\boldsymbol{G}_1^{(0)}-\boldsymbol{\beta}_G d_0\right)l}{n} & \mathbf{0} & \boldsymbol{I}_4 & \dfrac{\boldsymbol{\beta}_G l}{n} & \mathbf{0} & \mathbf{0} \\ \mathbf{0} & \dfrac{\left(\boldsymbol{G}_1^{(0)}-\boldsymbol{\beta}_G d_0\right)l}{n} & -\boldsymbol{I}_4 & \mathbf{0} & \dfrac{\boldsymbol{\beta}_G l}{n} & \mathbf{0} \end{bmatrix};$$

$$\boldsymbol{D}_{eqxd1}=\begin{bmatrix} \dfrac{\left(\boldsymbol{C}_1^{(0)}-\boldsymbol{\beta}_C d_0\right)l}{n} & \mathbf{0} & \mathbf{0} & \dfrac{\boldsymbol{\beta}_C l}{n} & \mathbf{0} & \mathbf{0} \\ \mathbf{0} & \dfrac{\left(\boldsymbol{C}_1^{(0)}-\boldsymbol{\beta}_C d_0\right)l}{n} & \mathbf{0} & \boldsymbol{0} & \dfrac{\boldsymbol{\beta}_C l}{n} & \mathbf{0} \end{bmatrix};$$

$$\boldsymbol{Y}_{eqx2}=\begin{bmatrix} -\boldsymbol{I}_4 & \boldsymbol{I}_4 & \dfrac{\left(\boldsymbol{R}_1^{(0)}-\boldsymbol{\beta}_R d_0\right)l}{n} & \mathbf{0} & \mathbf{0} & \dfrac{\boldsymbol{\beta}_R l}{n} \end{bmatrix};$$

$$\boldsymbol{D}_{eqxd2}=\begin{bmatrix} \mathbf{0} & \mathbf{0} & \dfrac{\left(\boldsymbol{L}_1^{(0)}-\boldsymbol{\beta}_L d_0\right)l}{n} & \mathbf{0} & \mathbf{0} & \dfrac{\boldsymbol{\beta}_L l}{n} \end{bmatrix};$$

$$\boldsymbol{Y}_{eqx3}=\begin{bmatrix} \mathbf{0} & \mathbf{0} & \mathbf{0} & \boldsymbol{I}_4 & \mathbf{0} & \mathbf{0} \\ \mathbf{0} & \mathbf{0} & \mathbf{0} & \mathbf{0} & \boldsymbol{I}_4 & \mathbf{0} \\ \mathbf{0} & \mathbf{0} & \mathbf{0} & \mathbf{0} & \mathbf{0} & \boldsymbol{I}_4 \end{bmatrix};\ \boldsymbol{F}_{eqpx3}^i : f_{eq[1][i]}=-1,\ others\ are\ 0,\ for\ i=1\sim 12;$$

$$\mathbf{Y}_{equ1}=null;\ \mathbf{Y}_{eqp1}=null;\ \mathbf{C}_{eqc1}=\mathbf{0};\ \mathbf{Y}_{equ2}=null;\ \mathbf{Y}_{eqp2}=null;\ \mathbf{C}_{eqc2}=\mathbf{0};\ \mathbf{Y}_{equ3}=null;$$

$$\mathbf{Y}_{eqp3}=null;\ \boldsymbol{C}_{eqc3}=\mathbf{0};\ \left\langle \mathbf{F}_{eqxx3}^i \right\rangle = null;\ \left\langle \mathbf{F}_{equu3}^i \right\rangle = null;\ \left\langle \mathbf{F}_{eqpp3}^i \right\rangle = null;\ \left\langle \mathbf{F}_{eqxu3}^i \right\rangle = null;$$

$$\left\langle \mathbf{F}_{equp3}^i \right\rangle = null;$$

where $\mathbf{I}_4$ is the identity matrix with the dimension of 4.

C.3 Section *k*, Transmission Line Model with the Average Height of Phase Conductors as the Only Parameter

The model of section *k* is described in Figure C.5.

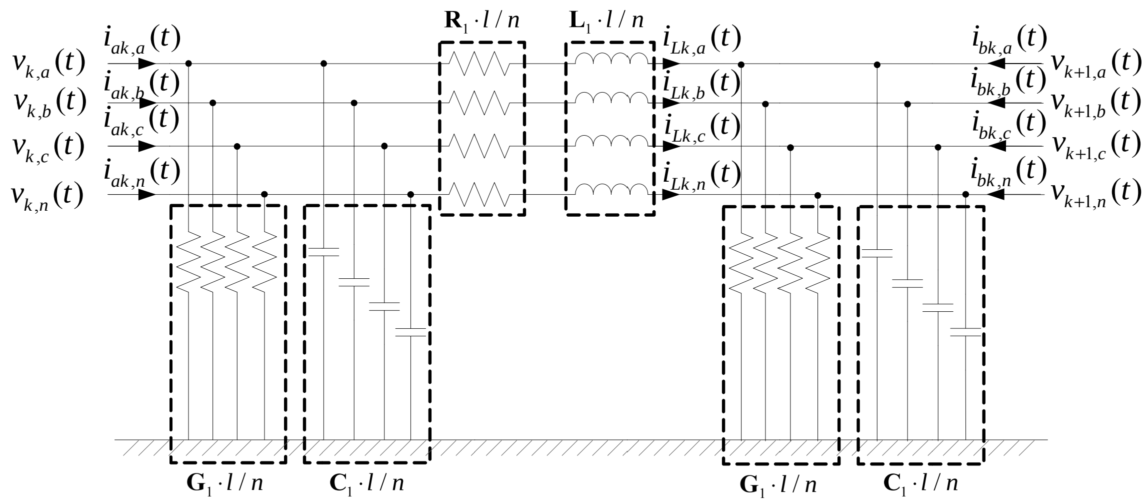

Figure C.5. Section *k* model with average height of phase conductors as the only parameter

where $\boldsymbol{R}_1$, $\boldsymbol{L}_1$, $\boldsymbol{G}_1$ and $\boldsymbol{C}_1$ are series resistance, series inductance, shunt conductance and shunt capacitance per mile; l is the total length of the line; $h(t)$ is the average height of phase conductors.

In addition, linearize the above $\boldsymbol{R}_1$, $\boldsymbol{L}_1$, $\boldsymbol{G}_1$ and $\boldsymbol{C}_1$ matrices around the initial value of the average height of phase conductors h_0 (the value of the above matrices with height h_0 are $\boldsymbol{R}_1^{(0)}$, $\boldsymbol{L}_1^{(0)}$, $\boldsymbol{G}_1^{(0)}$ and $\boldsymbol{C}_1^{(0)}$).

$$\mathbf{R}_1 = \mathbf{R}_1^{(0)} + \boldsymbol{\alpha}_R \cdot \left(h(t) - h_0\right) \tag{C.17}$$

$$\mathbf{L}_1 = \mathbf{L}_1^{(0)} + \boldsymbol{\alpha}_L \cdot \left(h(t) - h_0\right) \tag{C.18}$$

$$\mathbf{C}_1 = \mathbf{C}_1^{(0)} + \boldsymbol{\alpha}_C \cdot \left(h(t) - h_0\right) \tag{C.19}$$

$$\mathbf{G}_1 = \mathbf{G}_1^{(0)} + \boldsymbol{\alpha}_G \cdot \left(h(t) - h_0\right) \tag{C.20}$$

All states and through variables are defined in Table C.7, Table C.8 and Table C.9, respectively.

Table C.7. States of section *k* model with average height of phase conductors as the only parameter

Index	Variable	Description
0	$v_{k,a}(t)$	phase A voltage, left terminal
1	$v_{k,b}(t)$	phase B voltage, left terminal
2	$v_{k,c}(t)$	phase C voltage, left terminal
3	$v_{k,n}(t)$	phase N voltage, left terminal
4	$v_{k+1,a}(t)$	phase A voltage, right terminal
5	$v_{k+1,b}(t)$	phase B voltage, right terminal
6	$v_{k+1,c}(t)$	phase C voltage, right terminal
7	$v_{k+1,n}(t)$	phase N voltage, right terminal
8	$i_{Lk,a}(t)$	phase A current through inductance
9	$i_{Lk,b}(t)$	phase B current through inductance
10	$i_{Lk,c}(t)$	phase C current through inductance
11	$i_{Lk,n}(t)$	phase N current through inductance
12	$y_{vk,a}(t)$	Introduced state for quadratization, phase A voltage times $h(t)$, left terminal
13	$y_{vk,b}(t)$	Introduced state for quadratization, phase B voltage times $h(t)$, left terminal
14	$y_{vk,c}(t)$	Introduced state for quadratization, phase C voltage times $h(t)$, left terminal
15	$y_{vk,n}(t)$	Introduced state for quadratization, phase N voltage times $h(t)$, left terminal
16	$y_{v(k+1),a}(t)$	Introduced state for quadratization, phase A voltage times $h(t)$, right terminal
17	$y_{v(k+1),b}(t)$	Introduced state for quadratization, phase B voltage times $h(t)$, right terminal

Table C.7. continued

18	$y_{v(k+1),c}(t)$	Introduced state for quadratization, phase C voltage times $h(t)$, right terminal
19	$y_{v(k+1),n}(t)$	Introduced state for quadratization, phase N voltage times $h(t)$, right terminal
20	$y_{Lk,a}(t)$	Introduced state for quadratization, phase A current through inductance times $h(t)$
21	$y_{Lk,b}(t)$	Introduced state for quadratization, phase B current through inductance times $h(t)$
22	$y_{Lk,c}(t)$	Introduced state for quadratization, phase C current through inductance times $h(t)$
23	$y_{Lk,n}(t)$	Introduced state for quadratization, phase N current through inductance times $h(t)$

Table C.8. Parameters of section *k* model with average height of phase conductors as the only parameter

Index	Variable	Description
0	$d(t)$	Average distance between phase conductors

Table C.9. Through variables of section *k* model with average height of phase conductors as the only parameter

Index	Variable	Description
0	$i_{ak,a}(t)$	phase A current, left terminal
1	$i_{ak,b}(t)$	phase B current, left terminal
2	$i_{ak,c}(t)$	phase C current, left terminal
3	$i_{ak,n}(t)$	phase N current, left terminal
4	$i_{bk,a}(t)$	phase A current, left terminal
5	$i_{bk,b}(t)$	phase B current, left terminal
6	$i_{bk,c}(t)$	phase C current, left terminal
7	$i_{bk,n}(t)$	phase N current, left terminal

Define $\mathbf{i}_{Lk}(t)$ as the three phase and neutral current through the series inductance; $\boldsymbol{y}_{vk}(t)$, $\boldsymbol{y}_{v(k+1)}(t)$, and $\boldsymbol{y}_{Lk}(t)$ are introduced states for quadratization; recall the definitions of $\mathbf{i}_{ak}(t)$, $\mathbf{v}_{k}(t)$, $\mathbf{i}_{bk}(t)$ and $\mathbf{v}_{k+1}(t)$: three phase and neutral current and voltage vectors at each terminal of section k. That means,

$$\mathbf{v}_k(t)=\begin{bmatrix} v_{k,a}(t) \\ v_{k,b}(t) \\ v_{k,c}(t) \\ v_{k,n}(t) \end{bmatrix},\ \ \mathbf{v}_{k+1}(t)=\begin{bmatrix} v_{k+1,a}(t) \\ v_{k+1,b}(t) \\ v_{k+1,c}(t) \\ v_{k+1,n}(t) \end{bmatrix},\ \ \mathbf{i}_{Lk}(t)=\begin{bmatrix} i_{Lk,a}(t) \\ i_{Lk,b}(t) \\ i_{Lk,c}(t) \\ i_{Lk,n}(t) \end{bmatrix},$$

$$\mathbf{y}_{vk}(t)=\begin{bmatrix} y_{vk,a}(t) \\ y_{vk,b}(t) \\ y_{vk,c}(t) \\ y_{vk,n}(t) \end{bmatrix},\ \ \mathbf{y}_{v(k+1)}(t)=\begin{bmatrix} y_{v(k+1),a}(t) \\ y_{v(k+1),b}(t) \\ y_{v(k+1),c}(t) \\ y_{v(k+1),n}(t) \end{bmatrix},\ \ \mathbf{y}_{Lk}(t)=\begin{bmatrix} y_{Lk,a}(t) \\ y_{Lk,b}(t) \\ y_{Lk,c}(t) \\ y_{Lk,n}(t) \end{bmatrix},$$

$$\mathbf{i}_{ak}(t)=\begin{bmatrix} i_{ak,a}(t) \\ i_{ak,b}(t) \\ i_{ak,c}(t) \\ i_{ak,n}(t) \end{bmatrix},\ \ \mathbf{i}_{bk}(t)=\begin{bmatrix} i_{bk,a}(t) \\ i_{bk,b}(t) \\ i_{bk,c}(t) \\ i_{bk,n}(t) \end{bmatrix}.$$

The transmission line section k model can be formulated in compact form as follows:

$$\mathbf{i}_{ak}(t)=\frac{\left(\mathbf{G}_1^{(0)}-\boldsymbol{\alpha}_G h_0\right)l}{n}\cdot\mathbf{v}_k(t)+\frac{\boldsymbol{\alpha}_G l}{n}\cdot\mathbf{y}_{vk}(t)+\frac{\left(\mathbf{C}_1^{(0)}-\boldsymbol{\alpha}_C h_0\right)l}{n}\cdot\frac{d\mathbf{v}_k(t)}{dt}+\frac{\boldsymbol{\alpha}_C l}{n}\cdot\frac{d\mathbf{y}_{vk}(t)}{dt}+\mathbf{i}_{Lk}(t) \tag{C.21}$$

$$\mathbf{i}_{bk}(t)=\frac{\left(\mathbf{G}_1^{(0)}-\boldsymbol{\alpha}_G h_0\right)l}{n}\cdot\mathbf{v}_{k+1}(t)+\frac{\boldsymbol{\alpha}_G l}{n}\cdot\mathbf{y}_{v(k+1)}(t)+\frac{\left(\mathbf{C}_1^{(0)}-\boldsymbol{\alpha}_C h_0\right)l}{n}\cdot\frac{d\mathbf{v}_{k+1}(t)}{dt}+\frac{\boldsymbol{\alpha}_C l}{n}\cdot\frac{d\mathbf{y}_{v(k+1)}(t)}{dt}-\mathbf{i}_{Lk}(t) \tag{C.22}$$

$$\mathbf{0}=-\mathbf{v}_k(t)+\mathbf{v}_{k+1}(t)+\frac{\left(\mathbf{R}_1^{(0)}-\boldsymbol{\alpha}_R h_0\right)l}{n}\cdot\mathbf{i}_{Lk}(t)+\frac{\boldsymbol{\alpha}_R l}{n}\cdot\mathbf{y}_{Lk}(t)+\frac{\left(\mathbf{L}_1^{(0)}-\boldsymbol{\alpha}_L h_0\right)l}{n}\cdot\frac{d\mathbf{i}_{Lk}(t)}{dt}+\frac{\boldsymbol{\alpha}_L l}{n}\cdot\frac{d\mathbf{y}_{Lk}(t)}{dt} \tag{C.23}$$

$$\mathbf{0}=\mathbf{y}_{vk}(t)-\mathbf{v}_k(t)\cdot h(t) \tag{C.24}$$

$$\mathbf{0}=\mathbf{y}_{v(k+1)}(t)-\mathbf{v}_{k+1}(t)\cdot h(t) \tag{C.25}$$

$$\mathbf{0} = \mathbf{y}_{Lk}(t) - \mathbf{i}_{Lk}(t) \cdot h(t) \tag{C.26}$$

The matrices corresponding to the SCPQDM of section k, transmission line model with average distance between phase conductors as the only parameter are:

$$\boldsymbol{x}(t) = \begin{bmatrix} \boldsymbol{v}_k(t) & \boldsymbol{v}_{k+1}(t) & \boldsymbol{i}_{Lk}(t) & \boldsymbol{y}_{vk}(t) & \boldsymbol{y}_{v(k+1)}(t) & \boldsymbol{y}_{Lk}(t) \end{bmatrix}^T;\ \boldsymbol{i}(t) = \begin{bmatrix} \boldsymbol{i}_{ak}(t) & \boldsymbol{i}_{bk}(t) \end{bmatrix}^{\mathrm{T}};$$

$$\boldsymbol{p}(t) = h(t);\ \ \boldsymbol{Y}_{eqx1} = \begin{bmatrix} \dfrac{\left(\boldsymbol{G}_1^{(0)} - \boldsymbol{\alpha}_G h_0\right) l}{n} & \mathbf{0} & \boldsymbol{I}_4 & \dfrac{\boldsymbol{\alpha}_G l}{n} & \mathbf{0} & \mathbf{0} \\ \mathbf{0} & \dfrac{\left(\boldsymbol{G}_1^{(0)} - \boldsymbol{\alpha}_G h_0\right) l}{n} & -\boldsymbol{I}_4 & \mathbf{0} & \dfrac{\boldsymbol{\alpha}_G l}{n} & \mathbf{0} \end{bmatrix};$$

$$\boldsymbol{D}_{eqxd1} = \begin{bmatrix} \dfrac{\left(\boldsymbol{C}_1^{(0)} - \boldsymbol{\alpha}_C h_0\right) l}{n} & \mathbf{0} & \mathbf{0} & \dfrac{\boldsymbol{\alpha}_C l}{n} & \mathbf{0} & \mathbf{0} \\ \mathbf{0} & \dfrac{\left(\boldsymbol{C}_1^{(0)} - \boldsymbol{\alpha}_C h_0\right) l}{n} & \mathbf{0} & \boldsymbol{0} & \dfrac{\boldsymbol{\alpha}_C l}{n} & \mathbf{0} \end{bmatrix};$$

$$\boldsymbol{Y}_{eqx2} = \begin{bmatrix} -\boldsymbol{I}_4 & \boldsymbol{I}_4 & \dfrac{\left(\boldsymbol{R}_1^{(0)} - \boldsymbol{\alpha}_R h_0\right) l}{n} & \mathbf{0} & \mathbf{0} & \dfrac{\boldsymbol{\alpha}_R l}{n} \end{bmatrix};$$

$$\boldsymbol{D}_{eqxd2} = \begin{bmatrix} \mathbf{0} & \mathbf{0} & \dfrac{\left(\boldsymbol{L}_1^{(0)} - \boldsymbol{\alpha}_L h_0\right) l}{n} & \mathbf{0} & \mathbf{0} & \dfrac{\boldsymbol{\alpha}_L l}{n} \end{bmatrix};$$

$$\boldsymbol{Y}_{eqx3} = \begin{bmatrix} \mathbf{0} & \mathbf{0} & \mathbf{0} & \boldsymbol{I}_4 & \mathbf{0} & \mathbf{0} \\ \mathbf{0} & \mathbf{0} & \mathbf{0} & \mathbf{0} & \boldsymbol{I}_4 & \mathbf{0} \\ \mathbf{0} & \mathbf{0} & \mathbf{0} & \mathbf{0} & \mathbf{0} & \boldsymbol{I}_4 \end{bmatrix};\ \boldsymbol{F}_{eqpx3}^i : f_{eq[1][i]} = -1,\ others\ are\ 0,\ \ for\ \ i = 1 \sim 12;$$

$$\mathbf{Y}_{equ1} = null;\ \mathbf{Y}_{eqp1} = null;\ \mathbf{C}_{eqc1} = \mathbf{0};\ \mathbf{Y}_{equ2} = null;\ \mathbf{Y}_{eqp2} = null;\ \mathbf{C}_{eqc2} = \mathbf{0};\ \mathbf{Y}_{equ3} = null;$$

$$\mathbf{Y}_{eqp3} = null;\ \boldsymbol{C}_{eqc3} = \mathbf{0};\ \left\langle \mathbf{F}_{eqxx3}^i \right\rangle = null;\ \left\langle \mathbf{F}_{equu3}^i \right\rangle = null;\ \left\langle \mathbf{F}_{eqpp3}^i \right\rangle = null;\ \left\langle \mathbf{F}_{eqxu3}^i \right\rangle = null;$$

$$\left\langle \mathbf{F}_{equp3}^i \right\rangle = null;$$

where $\mathbf{I}_4$ is the identity matrix with the dimension of 4.

C.4 Section *k*, Transmission Line Model with the Total Length of the Line and the Average Distance between Phase Conductors as Two Parameters

The model of section *k* is described in Figure C.6.

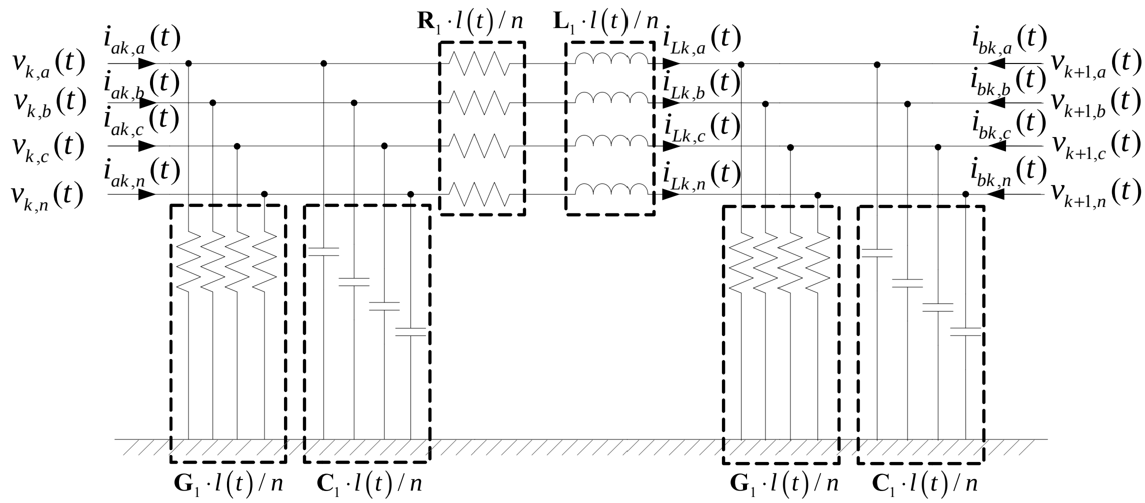

Figure C.6. Section *k* model with the total length of the line and the average distance between phase conductors as two parameters

where $\boldsymbol{R}_1$, $\boldsymbol{L}_1$, $\boldsymbol{G}_1$ and $\boldsymbol{C}_1$ are series resistance, series inductance, shunt conductance and shunt capacitance per mile; $l(t)$ is the total length of the line; $d(t)$ is the average distance between phase conductors.

In addition, linearize the above $\boldsymbol{R}_1$, $\boldsymbol{L}_1$, $\boldsymbol{G}_1$ and $\boldsymbol{C}_1$ matrices around the initial value of the average distance between phase conductors d_0 (the value of the above matrices with distance d_0 are $\boldsymbol{R}_1^{(0)}$, $\boldsymbol{L}_1^{(0)}$, $\boldsymbol{G}_1^{(0)}$ and $\boldsymbol{C}_1^{(0)}$).

$$\mathbf{R}_1 = \mathbf{R}_1^{(0)} + \boldsymbol{\beta}_R \cdot \left(d\left(t\right) - d_0\right) \tag{C.27}$$

$$\mathbf{L}_1 = \mathbf{L}_1^{(0)} + \boldsymbol{\beta}_L \cdot \left(d\left(t\right) - d_0\right) \tag{C.28}$$

$$\mathbf{C}_1 = \mathbf{C}_1^{(0)} + \boldsymbol{\beta}_C \cdot \left(d\left(t\right) - d_0\right) \tag{C.29}$$

$$\mathbf{G}_1 = \mathbf{G}_1^{(0)} + \boldsymbol{\beta}_G \cdot \left(d(t) - d_0\right) \tag{C.30}$$

All states and through variables are defined in Table C.10, Table C.11 and Table C.12, respectively.

Table C.10. States of section *k* model with the total length of the line and the average distance between phase conductors as two parameters

Index	Variable	Description
0	$v_{k,a}(t)$	phase A voltage, left terminal
1	$v_{k,b}(t)$	phase B voltage, left terminal
2	$v_{k,c}(t)$	phase C voltage, left terminal
3	$v_{k,n}(t)$	phase N voltage, left terminal
4	$v_{k+1,a}(t)$	phase A voltage, right terminal
5	$v_{k+1,b}(t)$	phase B voltage, right terminal
6	$v_{k+1,c}(t)$	phase C voltage, right terminal
7	$v_{k+1,n}(t)$	phase N voltage, right terminal
8	$i_{Lk,a}(t)$	phase A current through inductance
9	$i_{Lk,b}(t)$	phase B current through inductance
10	$i_{Lk,c}(t)$	phase C current through inductance
11	$i_{Lk,n}(t)$	phase N current through inductance
12	$y_{vk,a}(t)$	Introduced state for quadratization, phase A voltage times $l(t)$, left terminal
13	$y_{vk,b}(t)$	Introduced state for quadratization, phase B voltage times $l(t)$, left terminal
14	$y_{vk,c}(t)$	Introduced state for quadratization, phase C voltage times $l(t)$, left terminal
15	$y_{vk,n}(t)$	Introduced state for quadratization, phase N voltage times $l(t)$, left terminal
16	$y_{v(k+1),a}(t)$	Introduced state for quadratization, phase A voltage times $l(t)$, right terminal
17	$y_{v(k+1),b}(t)$	Introduced state for quadratization, phase B voltage times $l(t)$, right terminal
18	$y_{v(k+1),c}(t)$	Introduced state for quadratization, phase C voltage times $l(t)$, right terminal

Table C.10. continued

19	$y_{v(k+1),n}(t)$	Introduced state for quadratization, phase N voltage times $l(t)$, right terminal
20	$y_{Lk,a}(t)$	Introduced state for quadratization, phase A current through inductance times $l(t)$
21	$y_{Lk,b}(t)$	Introduced state for quadratization, phase B current through inductance times $l(t)$
22	$y_{Lk,c}(t)$	Introduced state for quadratization, phase C current through inductance times $l(t)$
23	$y_{Lk,n}(t)$	Introduced state for quadratization, phase N current through inductance times $l(t)$
24	$z_{vk,a}(t)$	Introduced state for quadratization, phase A voltage times $l(t)$ times $d(t)$, left terminal
25	$z_{vk,b}(t)$	Introduced state for quadratization, phase B voltage times $l(t)$ times $d(t)$, left terminal
26	$z_{vk,c}(t)$	Introduced state for quadratization, phase C voltage times $l(t)$ times $d(t)$, left terminal
27	$z_{vk,n}(t)$	Introduced state for quadratization, phase N voltage times $l(t)$ times $d(t)$, left terminal
28	$z_{v(k+1),a}(t)$	Introduced state for quadratization, phase A voltage times $l(t)$ times $d(t)$, right terminal
29	$z_{v(k+1),b}(t)$	Introduced state for quadratization, phase B voltage times $l(t)$ times $d(t)$, right terminal
30	$z_{v(k+1),c}(t)$	Introduced state for quadratization, phase C voltage times $l(t)$ times $d(t)$, right terminal
31	$z_{v(k+1),n}(t)$	Introduced state for quadratization, phase N voltage times $l(t)$ times $d(t)$, right terminal
32	$z_{Lk,a}(t)$	Introduced state for quadratization, phase A current through inductance times $l(t)$ times $d(t)$
33	$z_{Lk,b}(t)$	Introduced state for quadratization, phase B current through inductance times $l(t)$ times $d(t)$
34	$z_{Lk,c}(t)$	Introduced state for quadratization, phase C current through inductance times $l(t)$ times $d(t)$
35	$z_{Lk,n}(t)$	Introduced state for quadratization, phase N current through inductance times $l(t)$ times $d(t)$

Table C.11. Parameters of section *k* model with the total length of the line and the average distance between phase conductors as two parameters

Index	Variable	Description
0	$l(t)$	Total length of the line
0	$d(t)$	Average distance between phase conductors

Table C.12. Through variables of section *k* model with the total length of the line and the average distance between phase conductors as two parameters

Index	Variable	Description
0	$i_{ak,a}(t)$	phase A current, left terminal
1	$i_{ak,b}(t)$	phase B current, left terminal
2	$i_{ak,c}(t)$	phase C current, left terminal
3	$i_{ak,n}(t)$	phase N current, left terminal
4	$i_{bk,a}(t)$	phase A current, left terminal
5	$i_{bk,b}(t)$	phase B current, left terminal
6	$i_{bk,c}(t)$	phase C current, left terminal
7	$i_{bk,n}(t)$	phase N current, left terminal

Define $\mathbf{i}_{Lk}(t)$ as the three phase and neutral current through the series inductance; $\boldsymbol{y}_{vk}(t)$, $\boldsymbol{y}_{v(k+1)}(t)$, $\boldsymbol{y}_{Lk}(t)$, $\boldsymbol{z}_{vk}(t)$, $\boldsymbol{z}_{v(k+1)}(t)$, and $\boldsymbol{z}_{Lk}(t)$ are introduced states for quadratization; recall the definitions of $\mathbf{i}_{ak}(t)$, $\mathbf{v}_k(t)$, $\mathbf{i}_{bk}(t)$ and $\mathbf{v}_{k+1}(t)$: three phase and neutral current and voltage vectors at each terminal of section *k*. That means,

$$\mathbf{v}_k(t) = \begin{bmatrix} v_{k,a}(t) \\ v_{k,b}(t) \\ v_{k,c}(t) \\ v_{k,n}(t) \end{bmatrix}, \quad \mathbf{v}_{k+1}(t) = \begin{bmatrix} v_{k+1,a}(t) \\ v_{k+1,b}(t) \\ v_{k+1,c}(t) \\ v_{k+1,n}(t) \end{bmatrix}, \quad \mathbf{i}_{Lk}(t) = \begin{bmatrix} i_{Lk,a}(t) \\ i_{Lk,b}(t) \\ i_{Lk,c}(t) \\ i_{Lk,n}(t) \end{bmatrix},$$

$$\mathbf{y}_{vk}(t)=\begin{bmatrix} y_{vk,a}(t) \\ y_{vk,b}(t) \\ y_{vk,c}(t) \\ y_{vk,n}(t) \end{bmatrix},\ \mathbf{y}_{v(k+1)}(t)=\begin{bmatrix} y_{v(k+1),a}(t) \\ y_{v(k+1),b}(t) \\ y_{v(k+1),c}(t) \\ y_{v(k+1),n}(t) \end{bmatrix},\ \mathbf{y}_{Lk}(t)=\begin{bmatrix} y_{Lk,a}(t) \\ y_{Lk,b}(t) \\ y_{Lk,c}(t) \\ y_{Lk,n}(t) \end{bmatrix},$$

$$\mathbf{z}_{vk}(t)=\begin{bmatrix} z_{vk,a}(t) \\ z_{vk,b}(t) \\ z_{vk,c}(t) \\ z_{vk,n}(t) \end{bmatrix},\ \mathbf{z}_{v(k+1)}(t)=\begin{bmatrix} z_{v(k+1),a}(t) \\ z_{v(k+1),b}(t) \\ z_{v(k+1),c}(t) \\ z_{v(k+1),n}(t) \end{bmatrix},\ \mathbf{z}_{Lk}(t)=\begin{bmatrix} z_{Lk,a}(t) \\ z_{Lk,b}(t) \\ z_{Lk,c}(t) \\ z_{Lk,n}(t) \end{bmatrix},$$

$$\mathbf{i}_{ak}(t)=\begin{bmatrix} i_{ak,a}(t) \\ i_{ak,b}(t) \\ i_{ak,c}(t) \\ i_{ak,n}(t) \end{bmatrix},\ \mathbf{i}_{bk}(t)=\begin{bmatrix} i_{bk,a}(t) \\ i_{bk,b}(t) \\ i_{bk,c}(t) \\ i_{bk,n}(t) \end{bmatrix}.$$

The transmission line section k model can be formulated in compact form as follows:

$$\mathbf{i}_{ak}(t)=\frac{\mathbf{G}_1^{(0)}-\boldsymbol{\beta}_G d_0}{n}\cdot\mathbf{y}_{vk}(t)+\frac{\boldsymbol{\beta}_G}{n}\cdot\mathbf{z}_{vk}(t)+\frac{\mathbf{C}_1^{(0)}-\boldsymbol{\beta}_C d_0}{n}\cdot\frac{d\mathbf{y}_{vk}(t)}{dt}+\frac{\boldsymbol{\beta}_C}{n}\cdot\frac{d\mathbf{z}_{vk}(t)}{dt}+\mathbf{i}_{Lk}(t) \quad \text{(C.31)}$$

$$\mathbf{i}_{bk}(t)=\frac{\mathbf{G}_1^{(0)}-\boldsymbol{\beta}_G d_0}{n}\cdot\mathbf{y}_{v(k+1)}(t)+\frac{\boldsymbol{\beta}_G}{n}\cdot\mathbf{z}_{v(k+1)}(t)+\frac{\mathbf{C}_1^{(0)}-\boldsymbol{\beta}_C d_0}{n}\cdot\frac{d\mathbf{y}_{v(k+1)}(t)}{dt}+\frac{\boldsymbol{\beta}_C}{n}\frac{d\mathbf{z}_{v(k+1)}(t)}{dt}-\mathbf{i}_{Lk}(t) \quad \text{(C.32)}$$

$$\mathbf{0}=-\mathbf{v}_k(t)+\mathbf{v}_{k+1}(t)+\frac{\mathbf{R}_1^{(0)}-\boldsymbol{\beta}_R d_0}{n}\cdot\mathbf{y}_{Lk}(t)+\frac{\boldsymbol{\beta}_R}{n}\cdot\mathbf{z}_{Lk}(t)+\frac{\mathbf{L}_1^{(0)}-\boldsymbol{\beta}_L d_0}{n}\cdot\frac{d\mathbf{y}_{Lk}(t)}{dt}+\frac{\boldsymbol{\beta}_L}{n}\cdot\frac{d\mathbf{z}_{Lk}(t)}{dt} \quad \text{(C.33)}$$

$$\mathbf{0}=\mathbf{y}_{vk}(t)-\mathbf{v}_k(t)\cdot l(t) \quad \text{(C.34)}$$

$$\mathbf{0}=\mathbf{y}_{v(k+1)}(t)-\mathbf{v}_{k+1}(t)\cdot l(t) \quad \text{(C.35)}$$

$$\mathbf{0}=\mathbf{y}_{Lk}(t)-\mathbf{i}_{Lk}(t)\cdot l(t) \quad \text{(C.36)}$$

$$\mathbf{0}=\mathbf{z}_{vk}(t)-\mathbf{y}_{vk}(t)\cdot d(t) \quad \text{(C.37)}$$

$$\mathbf{0}=\mathbf{z}_{v(k+1)}(t)-\mathbf{y}_{v(k+1)}(t)\cdot d(t) \quad \text{(C.38)}$$

$$\mathbf{0}=\mathbf{z}_{Lk}(t)-\mathbf{y}_{Lk}(t)\cdot d(t) \quad \text{(C.39)}$$

The matrices corresponding to the SCPQDM of section k, transmission line model with the total length of the line and the average distance between phase conductors as parameters are:

$$\boldsymbol{x}(t)=\begin{bmatrix}\boldsymbol{v}_k(t) & \boldsymbol{v}_{k+1}(t) & \boldsymbol{i}_{Lk}(t) & \boldsymbol{y}_{vk}(t) & \boldsymbol{y}_{v(k+1)}(t) & \boldsymbol{y}_{Lk}(t) & \boldsymbol{z}_{vk}(t) & \boldsymbol{z}_{v(k+1)}(t) & \boldsymbol{z}_{Lk}(t)\end{bmatrix}^T;$$

$$\boldsymbol{i}(t)=\begin{bmatrix}\boldsymbol{i}_{ak}(t) & \boldsymbol{i}_{bk}(t)\end{bmatrix}^{\mathrm{T}};\ \boldsymbol{p}(t)=\begin{bmatrix}l(t) & d(t)\end{bmatrix}^T;$$

$$\boldsymbol{Y}_{eqx1}=\begin{bmatrix}\mathbf{0} & \mathbf{0} & \boldsymbol{I}_4 & \dfrac{\boldsymbol{G}_1^{(0)}-\boldsymbol{\beta}_G d_0}{n} & \mathbf{0} & \mathbf{0} & \dfrac{\boldsymbol{\beta}_G}{n} & \mathbf{0} & \mathbf{0}\\ \mathbf{0} & \mathbf{0} & -\boldsymbol{I}_4 & \mathbf{0} & \dfrac{\boldsymbol{G}_1^{(0)}-\boldsymbol{\beta}_G d_0}{n} & \mathbf{0} & \mathbf{0} & \dfrac{\boldsymbol{\beta}_G}{n} & \mathbf{0}\end{bmatrix};$$

$$\boldsymbol{D}_{eqxd1}=\begin{bmatrix}\mathbf{0} & \mathbf{0} & \mathbf{0} & \dfrac{\boldsymbol{C}_1^{(0)}-\boldsymbol{\beta}_C d_0}{n} & \mathbf{0} & \mathbf{0} & \dfrac{\boldsymbol{\beta}_C}{n} & \mathbf{0} & \mathbf{0}\\ \mathbf{0} & \mathbf{0} & \mathbf{0} & \mathbf{0} & \dfrac{\boldsymbol{C}_1^{(0)}-\boldsymbol{\beta}_C d_0}{n} & \mathbf{0} & \mathbf{0} & \dfrac{\boldsymbol{\beta}_C}{n} & \mathbf{0}\end{bmatrix};$$

$$\boldsymbol{Y}_{eqx2}=\begin{bmatrix}-\boldsymbol{I}_4 & \boldsymbol{I}_4 & \mathbf{0} & \mathbf{0} & \mathbf{0} & \dfrac{\boldsymbol{R}_1^{(0)}-\boldsymbol{\beta}_R d_0}{n} & \mathbf{0} & \mathbf{0} & \dfrac{\boldsymbol{\beta}_R}{n}\end{bmatrix};$$

$$\boldsymbol{D}_{eqxd2}==\begin{bmatrix}\mathbf{0} & \mathbf{0} & \mathbf{0} & \mathbf{0} & \mathbf{0} & \dfrac{\boldsymbol{L}_1^{(0)}-\boldsymbol{\beta}_L d_0}{n} & \mathbf{0} & \mathbf{0} & \dfrac{\boldsymbol{\beta}_L}{n}\end{bmatrix};$$

$$\boldsymbol{Y}_{eqx3}=\begin{bmatrix}\mathbf{0} & \mathbf{0} & \mathbf{0} & \boldsymbol{I}_4 & \mathbf{0} & \mathbf{0} & \mathbf{0} & \mathbf{0} & \mathbf{0}\\ \mathbf{0} & \mathbf{0} & \mathbf{0} & \mathbf{0} & \boldsymbol{I}_4 & \mathbf{0} & \mathbf{0} & \mathbf{0} & \mathbf{0}\\ \mathbf{0} & \mathbf{0} & \mathbf{0} & \mathbf{0} & \mathbf{0} & \boldsymbol{I}_4 & \mathbf{0} & \mathbf{0} & \mathbf{0}\\ \mathbf{0} & \mathbf{0} & \mathbf{0} & \mathbf{0} & \mathbf{0} & \mathbf{0} & \boldsymbol{I}_4 & \mathbf{0} & \mathbf{0}\\ \mathbf{0} & \mathbf{0} & \mathbf{0} & \mathbf{0} & \mathbf{0} & \mathbf{0} & \mathbf{0} & \boldsymbol{I}_4 & \mathbf{0}\\ \mathbf{0} & \mathbf{0} & \mathbf{0} & \mathbf{0} & \mathbf{0} & \mathbf{0} & \mathbf{0} & \mathbf{0} & \boldsymbol{I}_4\end{bmatrix};$$

$$\boldsymbol{F}_{eqpx3}^{i}: f_{eq[1][i]}=-1,\ \textit{others are}\ 0,\ \textit{for}\ i=1\sim 12;$$

$$\boldsymbol{F}_{eqpx3}^{i}: f_{eq[2][i]}=-1,\ \textit{others are}\ 0,\ \textit{for}\ i=13\sim 24$$

$$\mathbf{Y}_{equ1} = null;\ \mathbf{Y}_{eqp1} = null;\ \mathbf{C}_{eqc1} = \mathbf{0};\ \mathbf{Y}_{equ2} = null;\ \mathbf{Y}_{eqp2} = null;\ \mathbf{C}_{eqc2} = \mathbf{0};\ \mathbf{Y}_{equ3} = null;$$

$$\mathbf{Y}_{eqp3} = null;\ \boldsymbol{C}_{eqc3} = \mathbf{0};\ \left\langle \mathbf{F}^{i}_{eqxx3} \right\rangle = null;\ \left\langle \mathbf{F}^{i}_{equu3} \right\rangle = null;\ \left\langle \mathbf{F}^{i}_{eqpp3} \right\rangle = null;\ \left\langle \mathbf{F}^{i}_{eqxu3} \right\rangle = null;$$

$$\left\langle \mathbf{F}^{i}_{equp3} \right\rangle = null;$$

where $\mathbf{I}_4$ is the identity matrix with the dimension of 4.

C.5 Section *k*, Transmission Line Model with the Total Length of the Line and the Average Height of Phase Conductors as Two Parameters

The model of section *k* is described in Figure C.7.

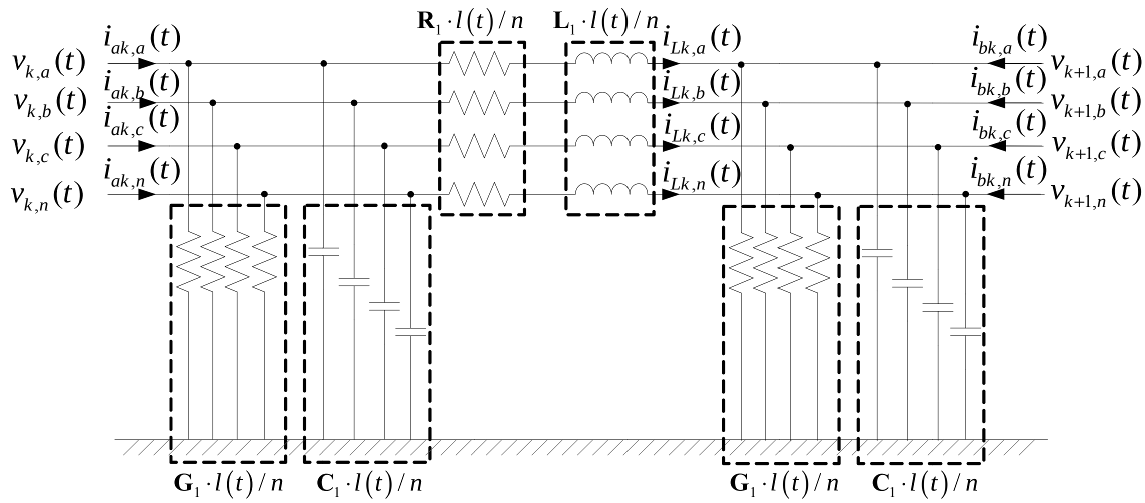

Figure C.7. Section *k* model with the total length of the line and the average height of phase conductors as two parameters

where $\boldsymbol{R}_1$, $\boldsymbol{L}_1$, $\boldsymbol{G}_1$ and $\boldsymbol{C}_1$ are series resistance, series inductance, shunt conductance and shunt capacitance per mile; $l(t)$ is the total length of the line; $h(t)$ is the average height of phase conductors.

In addition, linearize the above $\boldsymbol{R}_1$, $\boldsymbol{L}_1$, $\boldsymbol{G}_1$ and $\boldsymbol{C}_1$ matrices around the initial value of the average height of phase conductors h_0 (the value of the above matrices with height h_0 are $\boldsymbol{R}_1^{(0)}$, $\boldsymbol{L}_1^{(0)}$, $\boldsymbol{G}_1^{(0)}$ and $\boldsymbol{C}_1^{(0)}$).

$$\mathbf{R}_1 = \mathbf{R}_1^{(0)} + \boldsymbol{\alpha}_R \cdot \left(h(t) - h_0\right) \tag{C.40}$$

$$\mathbf{L}_1 = \mathbf{L}_1^{(0)} + \boldsymbol{\alpha}_L \cdot \left(h(t) - h_0\right) \tag{C.41}$$

$$\mathbf{C}_1 = \mathbf{C}_1^{(0)} + \boldsymbol{\alpha}_C \cdot \left(h(t) - h_0\right) \tag{C.42}$$

$$\mathbf{G}_1 = \mathbf{G}_1^{(0)} + \boldsymbol{\alpha}_G \cdot \left(h(t) - h_0\right) \tag{C.43}$$

All states and through variables are defined in Table C.13, Table C.14 and Table C.15, respectively.

Table C.13. States of section *k* model with the total length of the line and the average height of phase conductors as two parameters

Index	Variable	Description
0	$v_{k,a}(t)$	phase A voltage, left terminal
1	$v_{k,b}(t)$	phase B voltage, left terminal
2	$v_{k,c}(t)$	phase C voltage, left terminal
3	$v_{k,n}(t)$	phase N voltage, left terminal
4	$v_{k+1,a}(t)$	phase A voltage, right terminal
5	$v_{k+1,b}(t)$	phase B voltage, right terminal
6	$v_{k+1,c}(t)$	phase C voltage, right terminal
7	$v_{k+1,n}(t)$	phase N voltage, right terminal
8	$i_{Lk,a}(t)$	phase A current through inductance
9	$i_{Lk,b}(t)$	phase B current through inductance
10	$i_{Lk,c}(t)$	phase C current through inductance
11	$i_{Lk,n}(t)$	phase N current through inductance
12	$y_{vk,a}(t)$	Introduced state for quadratization, phase A voltage times $l(t)$, left terminal
13	$y_{vk,b}(t)$	Introduced state for quadratization, phase B voltage times $l(t)$, left terminal
14	$y_{vk,c}(t)$	Introduced state for quadratization, phase C voltage times $l(t)$, left terminal
15	$y_{vk,n}(t)$	Introduced state for quadratization, phase N voltage times $l(t)$, left terminal
16	$y_{v(k+1),a}(t)$	Introduced state for quadratization, phase A voltage times $l(t)$, right terminal
17	$y_{v(k+1),b}(t)$	Introduced state for quadratization, phase B voltage times $l(t)$, right terminal
18	$y_{v(k+1),c}(t)$	Introduced state for quadratization, phase C voltage times $l(t)$, right terminal

Table C.13. continued

19	$y_{v(k+1),n}(t)$	Introduced state for quadratization, phase N voltage times $l(t)$, right terminal
20	$y_{Lk,a}(t)$	Introduced state for quadratization, phase A current through inductance times $l(t)$
21	$y_{Lk,b}(t)$	Introduced state for quadratization, phase B current through inductance times $l(t)$
22	$y_{Lk,c}(t)$	Introduced state for quadratization, phase C current through inductance times $l(t)$
23	$y_{Lk,n}(t)$	Introduced state for quadratization, phase N current through inductance times $l(t)$
24	$z_{vk,a}(t)$	Introduced state for quadratization, phase A voltage times $l(t)$ times $h(t)$, left terminal
25	$z_{vk,b}(t)$	Introduced state for quadratization, phase B voltage times $l(t)$ times $h(t)$, left terminal
26	$z_{vk,c}(t)$	Introduced state for quadratization, phase C voltage times $l(t)$ times $h(t)$, left terminal
27	$z_{vk,n}(t)$	Introduced state for quadratization, phase N voltage times $l(t)$ times $h(t)$, left terminal
28	$z_{v(k+1),a}(t)$	Introduced state for quadratization, phase A voltage times $l(t)$ times $h(t)$, right terminal
29	$z_{v(k+1),b}(t)$	Introduced state for quadratization, phase B voltage times $l(t)$ times $h(t)$, right terminal
30	$z_{v(k+1),c}(t)$	Introduced state for quadratization, phase C voltage times $l(t)$ times $h(t)$, right terminal
31	$z_{v(k+1),n}(t)$	Introduced state for quadratization, phase N voltage times $l(t)$ times $h(t)$, right terminal
32	$z_{Lk,a}(t)$	Introduced state for quadratization, phase A current through inductance times $l(t)$ times $h(t)$
33	$z_{Lk,b}(t)$	Introduced state for quadratization, phase B current through inductance times $l(t)$ times $h(t)$
34	$z_{Lk,c}(t)$	Introduced state for quadratization, phase C current through inductance times $l(t)$ times $h(t)$
35	$z_{Lk,n}(t)$	Introduced state for quadratization, phase N current through inductance times $l(t)$ times $h(t)$

Table C.14. Parameters of section *k* model with the total length of the line and the average height of phase conductors as two parameters

Index	Variable	Description
0	$l(t)$	Total length of the line
0	$h(t)$	Average height of phase conductors

Table C.15. Through variables of section *k* model with the total length of the line and the average height of phase conductors as two parameters

Index	Variable	Description
0	$i_{ak,a}(t)$	phase A current, left terminal
1	$i_{ak,b}(t)$	phase B current, left terminal
2	$i_{ak,c}(t)$	phase C current, left terminal
3	$i_{ak,n}(t)$	phase N current, left terminal
4	$i_{bk,a}(t)$	phase A current, left terminal
5	$i_{bk,b}(t)$	phase B current, left terminal
6	$i_{bk,c}(t)$	phase C current, left terminal
7	$i_{bk,n}(t)$	phase N current, left terminal

Define $\mathbf{i}_{Lk}(t)$ as the three phase and neutral current through the series inductance; $\boldsymbol{y}_{vk}(t)$, $\boldsymbol{y}_{v(k+1)}(t)$, $\boldsymbol{y}_{Lk}(t)$, $\boldsymbol{z}_{vk}(t)$, $\boldsymbol{z}_{v(k+1)}(t)$, and $\boldsymbol{z}_{Lk}(t)$ are introduced states for quadratization; recall the definitions of $\mathbf{i}_{ak}(t)$, $\mathbf{v}_k(t)$, $\mathbf{i}_{bk}(t)$ and $\mathbf{v}_{k+1}(t)$: three phase and neutral current and voltage vectors at each terminal of section k. That means,

$$\mathbf{v}_k(t) = \begin{bmatrix} v_{k,a}(t) \\ v_{k,b}(t) \\ v_{k,c}(t) \\ v_{k,n}(t) \end{bmatrix}, \quad \mathbf{v}_{k+1}(t) = \begin{bmatrix} v_{k+1,a}(t) \\ v_{k+1,b}(t) \\ v_{k+1,c}(t) \\ v_{k+1,n}(t) \end{bmatrix}, \quad \mathbf{i}_{Lk}(t) = \begin{bmatrix} i_{Lk,a}(t) \\ i_{Lk,b}(t) \\ i_{Lk,c}(t) \\ i_{Lk,n}(t) \end{bmatrix},$$

$$\mathbf{y}_{vk}(t)=\begin{bmatrix} y_{vk,a}(t)\\ y_{vk,b}(t)\\ y_{vk,c}(t)\\ y_{vk,n}(t)\end{bmatrix},\ \ \mathbf{y}_{v(k+1)}(t)=\begin{bmatrix} y_{v(k+1),a}(t)\\ y_{v(k+1),b}(t)\\ y_{v(k+1),c}(t)\\ y_{v(k+1),n}(t)\end{bmatrix},\ \ \mathbf{y}_{Lk}(t)=\begin{bmatrix} y_{Lk,a}(t)\\ y_{Lk,b}(t)\\ y_{Lk,c}(t)\\ y_{Lk,n}(t)\end{bmatrix},$$

$$\mathbf{z}_{vk}(t)=\begin{bmatrix} z_{vk,a}(t)\\ z_{vk,b}(t)\\ z_{vk,c}(t)\\ z_{vk,n}(t)\end{bmatrix},\ \ \mathbf{z}_{v(k+1)}(t)=\begin{bmatrix} z_{v(k+1),a}(t)\\ z_{v(k+1),b}(t)\\ z_{v(k+1),c}(t)\\ z_{v(k+1),n}(t)\end{bmatrix},\ \ \mathbf{z}_{Lk}(t)=\begin{bmatrix} z_{Lk,a}(t)\\ z_{Lk,b}(t)\\ z_{Lk,c}(t)\\ z_{Lk,n}(t)\end{bmatrix},$$

$$\mathbf{i}_{ak}(t)=\begin{bmatrix} i_{ak,a}(t)\\ i_{ak,b}(t)\\ i_{ak,c}(t)\\ i_{ak,n}(t)\end{bmatrix},\ \ \mathbf{i}_{bk}(t)=\begin{bmatrix} i_{bk,a}(t)\\ i_{bk,b}(t)\\ i_{bk,c}(t)\\ i_{bk,n}(t)\end{bmatrix}.$$

The transmission line section k model can be formulated in compact form as follows:

$$\mathbf{i}_{ak}(t)=\frac{\mathbf{G}_1^{(0)}-\boldsymbol{\alpha}_G h_0}{n}\cdot\mathbf{y}_{vk}(t)+\frac{\boldsymbol{\alpha}_G}{n}\cdot\mathbf{z}_{vk}(t)+\frac{\mathbf{C}_1^{(0)}-\boldsymbol{\alpha}_C h_0}{n}\cdot\frac{d\mathbf{y}_{vk}(t)}{dt}+\frac{\boldsymbol{\alpha}_C}{n}\cdot\frac{d\mathbf{z}_{vk}(t)}{dt}+\mathbf{i}_{Lk}(t)\quad\text{(C.44)}$$

$$\mathbf{i}_{bk}(t)=\frac{\mathbf{G}_1^{(0)}-\boldsymbol{\alpha}_G h_0}{n}\cdot\mathbf{y}_{v(k+1)}(t)+\frac{\boldsymbol{\alpha}_G}{n}\cdot\mathbf{z}_{v(k+1)}(t)+\frac{\mathbf{C}_1^{(0)}-\boldsymbol{\alpha}_C h_0}{n}\cdot\frac{d\mathbf{y}_{v(k+1)}(t)}{dt}+\frac{\boldsymbol{\alpha}_C}{n}\frac{d\mathbf{z}_{v(k+1)}(t)}{dt}-\mathbf{i}_{Lk}(t)\quad\text{(C.45)}$$

$$\mathbf{0}=-\mathbf{v}_k(t)+\mathbf{v}_{k+1}(t)+\frac{\mathbf{R}_1^{(0)}-\boldsymbol{\alpha}_R h_0}{n}\cdot\mathbf{y}_{Lk}(t)+\frac{\boldsymbol{\alpha}_R}{n}\cdot\mathbf{z}_{Lk}(t)+\frac{\mathbf{L}_1^{(0)}-\boldsymbol{\alpha}_L h_0}{n}\cdot\frac{d\mathbf{y}_{Lk}(t)}{dt}+\frac{\boldsymbol{\alpha}_L}{n}\cdot\frac{d\mathbf{z}_{Lk}(t)}{dt}\quad\text{(C.46)}$$

$$\mathbf{0}=\mathbf{y}_{vk}(t)-\mathbf{v}_k(t)\cdot l(t)\quad\text{(C.47)}$$

$$\mathbf{0}=\mathbf{y}_{v(k+1)}(t)-\mathbf{v}_{k+1}(t)\cdot l(t)\quad\text{(C.48)}$$

$$\mathbf{0}=\mathbf{y}_{Lk}(t)-\mathbf{i}_{Lk}(t)\cdot l(t)\quad\text{(C.49)}$$

$$\mathbf{0}=\mathbf{z}_{vk}(t)-\mathbf{y}_{vk}(t)\cdot h(t)\quad\text{(C.50)}$$

$$\mathbf{0}=\mathbf{z}_{v(k+1)}(t)-\mathbf{y}_{v(k+1)}(t)\cdot h(t)\quad\text{(C.51)}$$

$$\mathbf{0}=\mathbf{z}_{Lk}(t)-\mathbf{y}_{Lk}(t)\cdot h(t)\quad\text{(C.52)}$$

The matrices corresponding to the SCPQDM of section k, transmission line model with the total length of the line and the average height of phase conductors as parameters are:

$$\boldsymbol{x}(t)=\left[\boldsymbol{v}_k(t)\quad \boldsymbol{v}_{k+1}(t)\quad \boldsymbol{i}_{Lk}(t)\quad \boldsymbol{y}_{vk}(t)\quad \boldsymbol{y}_{v(k+1)}(t)\quad \boldsymbol{y}_{Lk}(t)\quad \boldsymbol{z}_{vk}(t)\quad \boldsymbol{z}_{v(k+1)}(t)\quad \boldsymbol{z}_{Lk}(t)\right]^T;$$

$$\boldsymbol{i}(t)=\left[\boldsymbol{i}_{ak}(t)\quad \boldsymbol{i}_{bk}(t)\right]^{\mathrm{T}};\ \boldsymbol{p}(t)=\left[l(t)\quad h(t)\right]^T;$$

$$\boldsymbol{Y}_{eqx1}=\begin{bmatrix} \mathbf{0} & \mathbf{0} & \boldsymbol{I}_4 & \dfrac{\boldsymbol{G}_1^{(0)}-\boldsymbol{\alpha}_G h_0}{n} & \mathbf{0} & \mathbf{0} & \dfrac{\boldsymbol{\alpha}_G}{n} & \mathbf{0} & \mathbf{0} \\ \mathbf{0} & \mathbf{0} & -\boldsymbol{I}_4 & \mathbf{0} & \dfrac{\boldsymbol{G}_1^{(0)}-\boldsymbol{\alpha}_G h_0}{n} & \mathbf{0} & \mathbf{0} & \dfrac{\boldsymbol{\alpha}_G}{n} & \mathbf{0} \end{bmatrix};$$

$$\boldsymbol{D}_{eqxd1}=\begin{bmatrix} \mathbf{0} & \mathbf{0} & \mathbf{0} & \dfrac{\boldsymbol{C}_1^{(0)}-\boldsymbol{\alpha}_C h_0}{n} & \mathbf{0} & \mathbf{0} & \dfrac{\boldsymbol{\alpha}_C}{n} & \mathbf{0} & \mathbf{0} \\ \mathbf{0} & \mathbf{0} & \mathbf{0} & \mathbf{0} & \dfrac{\boldsymbol{C}_1^{(0)}-\boldsymbol{\alpha}_C h_0}{n} & \mathbf{0} & \mathbf{0} & \dfrac{\boldsymbol{\alpha}_C}{n} & \mathbf{0} \end{bmatrix};$$

$$\boldsymbol{Y}_{eqx2}=\begin{bmatrix} -\boldsymbol{I}_4 & \boldsymbol{I}_4 & \mathbf{0} & \mathbf{0} & \mathbf{0} & \dfrac{\boldsymbol{R}_1^{(0)}-\boldsymbol{\alpha}_R h_0}{n} & \mathbf{0} & \mathbf{0} & \dfrac{\boldsymbol{\alpha}_R}{n} \end{bmatrix};$$

$$\boldsymbol{D}_{eqxd2}==\begin{bmatrix} \mathbf{0} & \mathbf{0} & \mathbf{0} & \mathbf{0} & \mathbf{0} & \dfrac{\boldsymbol{L}_1^{(0)}-\boldsymbol{\alpha}_L h_0}{n} & \mathbf{0} & \mathbf{0} & \dfrac{\boldsymbol{\alpha}_L}{n} \end{bmatrix};$$

$$\boldsymbol{Y}_{eqx3}=\begin{bmatrix} \mathbf{0} & \mathbf{0} & \mathbf{0} & \boldsymbol{I}_4 & \mathbf{0} & \mathbf{0} & \mathbf{0} & \mathbf{0} & \mathbf{0} \\ \mathbf{0} & \mathbf{0} & \mathbf{0} & \mathbf{0} & \boldsymbol{I}_4 & \mathbf{0} & \mathbf{0} & \mathbf{0} & \mathbf{0} \\ \mathbf{0} & \mathbf{0} & \mathbf{0} & \mathbf{0} & \mathbf{0} & \boldsymbol{I}_4 & \mathbf{0} & \mathbf{0} & \mathbf{0} \\ \mathbf{0} & \mathbf{0} & \mathbf{0} & \mathbf{0} & \mathbf{0} & \mathbf{0} & \boldsymbol{I}_4 & \mathbf{0} & \mathbf{0} \\ \mathbf{0} & \mathbf{0} & \mathbf{0} & \mathbf{0} & \mathbf{0} & \mathbf{0} & \mathbf{0} & \boldsymbol{I}_4 & \mathbf{0} \\ \mathbf{0} & \mathbf{0} & \mathbf{0} & \mathbf{0} & \mathbf{0} & \mathbf{0} & \mathbf{0} & \mathbf{0} & \boldsymbol{I}_4 \end{bmatrix};$$

$$\boldsymbol{F}_{eqpx3}^i: f_{eq[1][i]}=-1,\ \textit{others are } 0,\ \textit{for } i=1\sim 12;$$

$$\boldsymbol{F}_{eqpx3}^i: f_{eq[2][i]}=-1,\ \textit{others are } 0,\ \textit{for } i=13\sim 24$$

$$\mathbf{Y}_{equ1} = null\ ;\ \mathbf{Y}_{eqp1} = null\ ;\ \mathbf{C}_{eqc1} = \mathbf{0}\ ;\ \mathbf{Y}_{equ2} = null\ ;\ \mathbf{Y}_{eqp2} = null\ ;\ \mathbf{C}_{eqc2} = \mathbf{0}\ ;\ \mathbf{Y}_{equ3} = null\ ;$$

$$\mathbf{Y}_{eqp3} = null\ ;\ \boldsymbol{C}_{eqc3} = \mathbf{0}\ ;\ \left\langle \mathbf{F}^{i}_{eqxx3} \right\rangle = null\ ;\ \left\langle \mathbf{F}^{i}_{equu3} \right\rangle = null\ ;\ \left\langle \mathbf{F}^{i}_{eqpp3} \right\rangle = null\ ;\ \left\langle \mathbf{F}^{i}_{eqxu3} \right\rangle = null\ ;$$

$$\left\langle \mathbf{F}^{i}_{equp3} \right\rangle = null\ ;$$

where $\mathbf{I}_4$ is the identity matrix with the dimension of 4.

C.6 Section *k*, Transmission Line Model with the Average Distance between Phase Conductors and the Average Height of Phase Conductors as Two Parameters

The model of section *k* is described in Figure C.8.

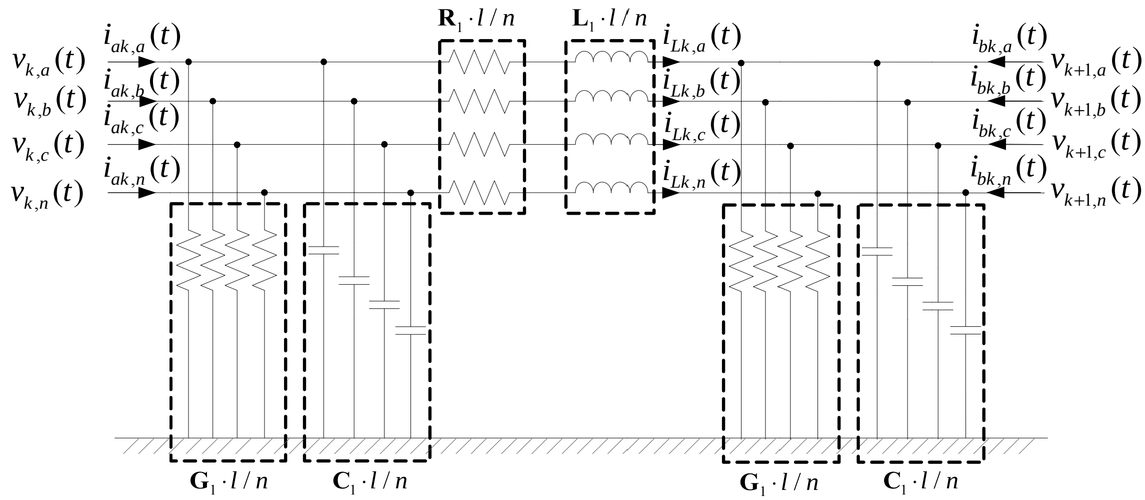

Figure C.8. Section *k* model with the average distance between phase conductors and the average height of phase conductors as two parameters

where $\boldsymbol{R}_1$, $\boldsymbol{L}_1$, $\boldsymbol{G}_1$ and $\boldsymbol{C}_1$ are series resistance, series inductance, shunt conductance and shunt capacitance per mile; *l* is the total length of the line; $d(t)$ is the average distance between phase conductors; $h(t)$ is the average height of phase conductors.

In addition, linearize the above $\boldsymbol{R}_1$, $\boldsymbol{L}_1$, $\boldsymbol{G}_1$ and $\boldsymbol{C}_1$ matrices around the initial value of the average distance between phase conductors d_0 and the average height of phase conductors h_0 (the value of the above matrices with distance d_0 and height h_0 are $\boldsymbol{R}_1^{(0)}$, $\boldsymbol{L}_1^{(0)}$, $\boldsymbol{G}_1^{(0)}$ and $\boldsymbol{C}_1^{(0)}$).

$$\mathbf{R}_1 = \mathbf{R}_1^{(0)} + \boldsymbol{\alpha}_R \cdot \left(h(t) - h_0\right) + \boldsymbol{\beta}_R \cdot \left(d(t) - d_0\right) \tag{C.53}$$

$$\mathbf{L}_1 = \mathbf{L}_1^{(0)} + \boldsymbol{\alpha}_L \cdot \left(h(t) - h_0\right) + \boldsymbol{\beta}_L \cdot \left(d(t) - d_0\right) \tag{C.54}$$

$$\mathbf{C}_1 = \mathbf{C}_1^{(0)} + \boldsymbol{\alpha}_C \cdot \left(h(t) - h_0\right) + \boldsymbol{\beta}_C \cdot \left(d(t) - d_0\right) \tag{C.55}$$

$$\mathbf{G}_1 = \mathbf{G}_1^{(0)} + \boldsymbol{\alpha}_G \cdot \left(h(t) - h_0\right) + \boldsymbol{\beta}_G \cdot \left(d(t) - d_0\right) \tag{C.56}$$

All states and through variables are defined in Table C.16, Table C.17 and Table C.18, respectively.

Table C.16. States of section *k* model with the average distance between phase conductors and the average height of phase conductors as two parameters

Index	Variable	Description
0	$v_{k,a}(t)$	phase A voltage, left terminal
1	$v_{k,b}(t)$	phase B voltage, left terminal
2	$v_{k,c}(t)$	phase C voltage, left terminal
3	$v_{k,n}(t)$	phase N voltage, left terminal
4	$v_{k+1,a}(t)$	phase A voltage, right terminal
5	$v_{k+1,b}(t)$	phase B voltage, right terminal
6	$v_{k+1,c}(t)$	phase C voltage, right terminal
7	$v_{k+1,n}(t)$	phase N voltage, right terminal
8	$i_{Lk,a}(t)$	phase A current through inductance
9	$i_{Lk,b}(t)$	phase B current through inductance
10	$i_{Lk,c}(t)$	phase C current through inductance
11	$i_{Lk,n}(t)$	phase N current through inductance
12	$y_{vk,a}(t)$	Introduced state for quadratization, phase A voltage times $d(t)$, left terminal
13	$y_{vk,b}(t)$	Introduced state for quadratization, phase B voltage times $d(t)$, left terminal
14	$y_{vk,c}(t)$	Introduced state for quadratization, phase C voltage times $d(t)$, left terminal
15	$y_{vk,n}(t)$	Introduced state for quadratization, phase N voltage times $d(t)$, left terminal
16	$y_{v(k+1),a}(t)$	Introduced state for quadratization, phase A voltage times $d(t)$, right terminal

Table C.16. continued

17	$y_{v(k+1),b}(t)$	Introduced state for quadratization, phase B voltage times $d(t)$, right terminal
18	$y_{v(k+1),c}(t)$	Introduced state for quadratization, phase C voltage times $d(t)$, right terminal
19	$y_{v(k+1),n}(t)$	Introduced state for quadratization, phase N voltage times $d(t)$, right terminal
20	$y_{Lk,a}(t)$	Introduced state for quadratization, phase A current through inductance times $d(t)$
21	$y_{Lk,b}(t)$	Introduced state for quadratization, phase B current through inductance times $d(t)$
22	$y_{Lk,c}(t)$	Introduced state for quadratization, phase C current through inductance times $d(t)$
23	$y_{Lk,n}(t)$	Introduced state for quadratization, phase N current through inductance times $d(t)$
24	$z_{vk,a}(t)$	Introduced state for quadratization, phase A voltage times $h(t)$, left terminal
25	$z_{vk,b}(t)$	Introduced state for quadratization, phase B voltage times $h(t)$, left terminal
26	$z_{vk,c}(t)$	Introduced state for quadratization, phase C voltage times $h(t)$, left terminal
27	$z_{vk,n}(t)$	Introduced state for quadratization, phase N voltage times $h(t)$, left terminal
28	$z_{v(k+1),a}(t)$	Introduced state for quadratization, phase A voltage times $h(t)$, right terminal
29	$z_{v(k+1),b}(t)$	Introduced state for quadratization, phase B voltage times $h(t)$, right terminal
30	$z_{v(k+1),c}(t)$	Introduced state for quadratization, phase C voltage times $h(t)$, right terminal
31	$z_{v(k+1),n}(t)$	Introduced state for quadratization, phase N voltage times $h(t)$, right terminal
32	$z_{Lk,a}(t)$	Introduced state for quadratization, phase A current through inductance times $h(t)$
33	$z_{Lk,b}(t)$	Introduced state for quadratization, phase B current through inductance times $h(t)$
34	$z_{Lk,c}(t)$	Introduced state for quadratization, phase C current through inductance times $h(t)$
35	$z_{Lk,n}(t)$	Introduced state for quadratization, phase N current through inductance times $h(t)$

Table C.17. Parameters of section *k* model with the average distance between phase conductors and the average height of phase conductors as two parameters

Index	Variable	Description
0	$d(t)$	Average distance between phase conductors
0	$h(t)$	Average height of phase conductors

Table C.18. Through variables of section *k* model with the average distance between phase conductors and the average height of phase conductors as two parameters

Index	Variable	Description
0	$i_{ak,a}(t)$	phase A current, left terminal
1	$i_{ak,b}(t)$	phase B current, left terminal
2	$i_{ak,c}(t)$	phase C current, left terminal
3	$i_{ak,n}(t)$	phase N current, left terminal
4	$i_{bk,a}(t)$	phase A current, left terminal
5	$i_{bk,b}(t)$	phase B current, left terminal
6	$i_{bk,c}(t)$	phase C current, left terminal
7	$i_{bk,n}(t)$	phase N current, left terminal

Define $\mathbf{i}_{Lk}(t)$ as the three phase and neutral current through the series inductance; $\boldsymbol{y}_{vk}(t)$, $\boldsymbol{y}_{v(k+1)}(t)$, $\boldsymbol{y}_{Lk}(t)$, $\boldsymbol{z}_{vk}(t)$, $\boldsymbol{z}_{v(k+1)}(t)$, and $\boldsymbol{z}_{Lk}(t)$ are introduced states for quadratization; recall the definitions of $\mathbf{i}_{ak}(t)$, $\mathbf{v}_k(t)$, $\mathbf{i}_{bk}(t)$ and $\mathbf{v}_{k+1}(t)$: three phase and neutral current and voltage vectors at each terminal of section *k*. That means,

$$\mathbf{v}_k(t)=\begin{bmatrix} v_{k,a}(t) \\ v_{k,b}(t) \\ v_{k,c}(t) \\ v_{k,n}(t) \end{bmatrix},\quad \mathbf{v}_{k+1}(t)=\begin{bmatrix} v_{k+1,a}(t) \\ v_{k+1,b}(t) \\ v_{k+1,c}(t) \\ v_{k+1,n}(t) \end{bmatrix},\quad \mathbf{i}_{Lk}(t)=\begin{bmatrix} i_{Lk,a}(t) \\ i_{Lk,b}(t) \\ i_{Lk,c}(t) \\ i_{Lk,n}(t) \end{bmatrix},$$

$$\mathbf{y}_{vk}(t)=\begin{bmatrix} y_{vk,a}(t) \\ y_{vk,b}(t) \\ y_{vk,c}(t) \\ y_{vk,n}(t) \end{bmatrix},\ \ \mathbf{y}_{v(k+1)}(t)=\begin{bmatrix} y_{v(k+1),a}(t) \\ y_{v(k+1),b}(t) \\ y_{v(k+1),c}(t) \\ y_{v(k+1),n}(t) \end{bmatrix},\ \ \mathbf{y}_{Lk}(t)=\begin{bmatrix} y_{Lk,a}(t) \\ y_{Lk,b}(t) \\ y_{Lk,c}(t) \\ y_{Lk,n}(t) \end{bmatrix},$$

$$\mathbf{z}_{vk}(t)=\begin{bmatrix} z_{vk,a}(t) \\ z_{vk,b}(t) \\ z_{vk,c}(t) \\ z_{vk,n}(t) \end{bmatrix},\ \ \mathbf{z}_{v(k+1)}(t)=\begin{bmatrix} z_{v(k+1),a}(t) \\ z_{v(k+1),b}(t) \\ z_{v(k+1),c}(t) \\ z_{v(k+1),n}(t) \end{bmatrix},\ \ \mathbf{z}_{Lk}(t)=\begin{bmatrix} z_{Lk,a}(t) \\ z_{Lk,b}(t) \\ z_{Lk,c}(t) \\ z_{Lk,n}(t) \end{bmatrix},$$

$$\mathbf{i}_{ak}(t)=\begin{bmatrix} i_{ak,a}(t) \\ i_{ak,b}(t) \\ i_{ak,c}(t) \\ i_{ak,n}(t) \end{bmatrix},\ \ \mathbf{i}_{bk}(t)=\begin{bmatrix} i_{bk,a}(t) \\ i_{bk,b}(t) \\ i_{bk,c}(t) \\ i_{bk,n}(t) \end{bmatrix}.$$

The transmission line section k model can be formulated in compact form as follows:

$$\begin{aligned}\mathbf{i}_{ak}(t)=&\frac{\left(\mathbf{G}_1^{(0)}-\boldsymbol{\alpha}_G h_0-\boldsymbol{\beta}_G d_0\right)l}{n}\cdot\mathbf{v}_k(t)+\frac{\boldsymbol{\beta}_G l}{n}\cdot\mathbf{y}_{vk}(t)+\frac{\boldsymbol{\alpha}_G l}{n}\cdot\mathbf{z}_{vk}(t)\\&+\frac{\left(\mathbf{C}_1^{(0)}-\boldsymbol{\alpha}_C h_0-\boldsymbol{\beta}_C d_0\right)l}{n}\cdot\frac{d\mathbf{v}_k(t)}{dt}+\frac{\boldsymbol{\beta}_C l}{n}\cdot\frac{d\mathbf{y}_{vk}(t)}{dt}+\frac{\boldsymbol{\alpha}_C l}{n}\cdot\frac{d\mathbf{z}_{vk}(t)}{dt}+\mathbf{i}_{Lk}(t)\end{aligned} \tag{C.57}$$

$$\begin{aligned}\mathbf{i}_{bk}(t)=&\frac{\left(\mathbf{G}_1^{(0)}-\boldsymbol{\alpha}_G h_0-\boldsymbol{\beta}_G d_0\right)l}{n}\cdot\mathbf{v}_{k+1}(t)+\frac{\boldsymbol{\beta}_G l}{n}\cdot\mathbf{y}_{v(k+1)}(t)+\frac{\boldsymbol{\alpha}_G l}{n}\cdot\mathbf{z}_{v(k+1)}(t)\\&+\frac{\left(\mathbf{C}_1^{(0)}-\boldsymbol{\alpha}_C h_0-\boldsymbol{\beta}_C d_0\right)l}{n}\cdot\frac{d\mathbf{v}_{k+1}(t)}{dt}+\frac{\boldsymbol{\beta}_C l}{n}\cdot\frac{d\mathbf{y}_{v(k+1)}(t)}{dt}+\frac{\boldsymbol{\alpha}_C l}{n}\cdot\frac{d\mathbf{z}_{v(k+1)}(t)}{dt}-\mathbf{i}_{Lk}(t)\end{aligned} \tag{C.58}$$

$$\begin{aligned}\mathbf{0}=&-\mathbf{v}_k(t)+\mathbf{v}_{k+1}(t)+\frac{\left(\mathbf{R}_1^{(0)}-\boldsymbol{\alpha}_R h_0-\boldsymbol{\beta}_R d_0\right)l}{n}\cdot\mathbf{i}_{Lk}(t)+\frac{\boldsymbol{\beta}_R l}{n}\cdot\mathbf{y}_{Lk}(t)+\frac{\boldsymbol{\alpha}_R l}{n}\cdot\mathbf{z}_{Lk}(t)\\&+\frac{\left(\mathbf{L}_1^{(0)}-\boldsymbol{\alpha}_L h_0-\boldsymbol{\beta}_L d_0\right)l}{n}\cdot\frac{d\mathbf{i}_{Lk}(t)}{dt}+\frac{\boldsymbol{\beta}_L l}{n}\cdot\frac{d\mathbf{y}_{Lk}(t)}{dt}+\frac{\boldsymbol{\alpha}_L l}{n}\cdot\frac{d\mathbf{z}_{Lk}(t)}{dt}\end{aligned} \tag{C.59}$$

$$\mathbf{0}=\mathbf{y}_{vk}(t)-\mathbf{v}_k(t)\cdot d(t) \tag{C.60}$$

$$\mathbf{0}=\mathbf{y}_{v(k+1)}(t)-\mathbf{v}_{k+1}(t)\cdot d(t) \tag{C.61}$$

$$\mathbf{0} = \mathbf{y}_{Lk}(t) - \mathbf{i}_{Lk}(t) \cdot d(t) \tag{C.62}$$

$$\mathbf{0} = \mathbf{z}_{vk}(t) - \mathbf{v}_{k}(t) \cdot h(t) \tag{C.63}$$

$$\mathbf{0} = \mathbf{z}_{v(k+1)}(t) - \mathbf{v}_{k+1}(t) \cdot h(t) \tag{C.64}$$

$$\mathbf{0} = \mathbf{z}_{Lk}(t) - \mathbf{i}_{Lk}(t) \cdot h(t) \tag{C.65}$$

The matrices corresponding to the SCPQDM of section k, transmission line model with the average distance between phase conductors and the average height of phase conductors as parameters are:

$$\boldsymbol{x}(t) = \begin{bmatrix} \boldsymbol{v}_k(t) & \boldsymbol{v}_{k+1}(t) & \boldsymbol{i}_{Lk}(t) & \boldsymbol{y}_{vk}(t) & \boldsymbol{y}_{v(k+1)}(t) & \boldsymbol{y}_{Lk}(t) & \boldsymbol{z}_{vk}(t) & \boldsymbol{z}_{v(k+1)}(t) & \boldsymbol{z}_{Lk}(t) \end{bmatrix}^T;$$

$$\boldsymbol{i}(t) = \begin{bmatrix} \boldsymbol{i}_{ak}(t) & \boldsymbol{i}_{bk}(t) \end{bmatrix}^{\mathrm{T}}; \ \boldsymbol{p}(t) = \begin{bmatrix} d(t) & h(t) \end{bmatrix}^T;$$

$$\boldsymbol{Y}_{eqx1} = \begin{bmatrix} \frac{\left(\boldsymbol{G}_1^{(0)} - \boldsymbol{\alpha}_G h_0 - \boldsymbol{\beta}_G d_0\right) l}{n} & \mathbf{0} & \boldsymbol{I}_4 & \frac{\boldsymbol{\beta}_G l}{n} & \mathbf{0} & \mathbf{0} & \frac{\boldsymbol{\alpha}_G l}{n} & \mathbf{0} & \mathbf{0} \\ \mathbf{0} & \frac{\left(\boldsymbol{G}_1^{(0)} - \boldsymbol{\alpha}_G h_0 - \boldsymbol{\beta}_G d_0\right) l}{n} & -\boldsymbol{I}_4 & \mathbf{0} & \frac{\boldsymbol{\beta}_G l}{n} & \mathbf{0} & \mathbf{0} & \frac{\boldsymbol{\alpha}_G l}{n} & \mathbf{0} \end{bmatrix};$$

$$\boldsymbol{D}_{eqxd1} = \begin{bmatrix} \frac{\left(\boldsymbol{C}_1^{(0)} - \boldsymbol{\alpha}_C h_0 - \boldsymbol{\beta}_C d_0\right) l}{n} & \mathbf{0} & \mathbf{0} & \frac{\boldsymbol{\beta}_C l}{n} & \mathbf{0} & \mathbf{0} & \frac{\boldsymbol{\alpha}_C l}{n} & \mathbf{0} & \mathbf{0} \\ \mathbf{0} & \frac{\left(\boldsymbol{C}_1^{(0)} - \boldsymbol{\alpha}_C h_0 - \boldsymbol{\beta}_C d_0\right) l}{n} & \mathbf{0} & \mathbf{0} & \frac{\boldsymbol{\beta}_C l}{n} & \mathbf{0} & \mathbf{0} & \frac{\boldsymbol{\alpha}_C l}{n} & \mathbf{0} \end{bmatrix};$$

$$\boldsymbol{Y}_{eqx2} = \begin{bmatrix} -\boldsymbol{I}_4 & \boldsymbol{I}_4 & \frac{\left(\boldsymbol{R}_1^{(0)} - \boldsymbol{\alpha}_R h_0 - \boldsymbol{\beta}_R d_0\right) l}{n} & \mathbf{0} & \mathbf{0} & \frac{\boldsymbol{\beta}_R l}{n} & \mathbf{0} & \mathbf{0} & \frac{\boldsymbol{\alpha}_R l}{n} \end{bmatrix};$$

$$\boldsymbol{D}_{eqxd2} == \begin{bmatrix} \mathbf{0} & \mathbf{0} & \frac{\left(\boldsymbol{L}_1^{(0)} - \boldsymbol{\alpha}_L h_0 - \boldsymbol{\beta}_L d_0\right) l}{n} & \mathbf{0} & \mathbf{0} & \frac{\boldsymbol{\beta}_L l}{n} & \mathbf{0} & \mathbf{0} & \frac{\boldsymbol{\alpha}_L l}{n} \end{bmatrix};$$

$$
\boldsymbol{Y}_{eqx3} = \begin{bmatrix} \mathbf{0} & \mathbf{0} & \mathbf{0} & \boldsymbol{I}_4 & \mathbf{0} & \mathbf{0} & \mathbf{0} & \mathbf{0} & \mathbf{0} \\ \mathbf{0} & \mathbf{0} & \mathbf{0} & \mathbf{0} & \boldsymbol{I}_4 & \mathbf{0} & \mathbf{0} & \mathbf{0} & \mathbf{0} \\ \mathbf{0} & \mathbf{0} & \mathbf{0} & \mathbf{0} & \mathbf{0} & \boldsymbol{I}_4 & \mathbf{0} & \mathbf{0} & \mathbf{0} \\ \mathbf{0} & \mathbf{0} & \mathbf{0} & \mathbf{0} & \mathbf{0} & \mathbf{0} & \boldsymbol{I}_4 & \mathbf{0} & \mathbf{0} \\ \mathbf{0} & \mathbf{0} & \mathbf{0} & \mathbf{0} & \mathbf{0} & \mathbf{0} & \mathbf{0} & \boldsymbol{I}_4 & \mathbf{0} \\ \mathbf{0} & \mathbf{0} & \mathbf{0} & \mathbf{0} & \mathbf{0} & \mathbf{0} & \mathbf{0} & \mathbf{0} & \boldsymbol{I}_4 \end{bmatrix};
$$

$$
\boldsymbol{F}^i_{eqpx3} : f_{eq[1][i]} = -1,\ \textit{others are}\ 0,\ \textit{for}\ i = 1 \sim 12;
$$

$$
\boldsymbol{F}^i_{eqpx3} : f_{eq[2][i-12]} = -1,\ \textit{others are}\ 0,\ \textit{for}\ i = 13 \sim 24
$$

$$
\mathbf{Y}_{equ1} = null;\ \mathbf{Y}_{eqp1} = null;\ \mathbf{C}_{eqc1} = \mathbf{0};\ \mathbf{Y}_{equ2} = null;\ \mathbf{Y}_{eqp2} = null;\ \mathbf{C}_{eqc2} = \mathbf{0};\ \mathbf{Y}_{equ3} = null;
$$

$$
\mathbf{Y}_{eqp3} = null;\ \boldsymbol{C}_{eqc3} = \mathbf{0};\ \left\langle \mathbf{F}^i_{eqxx3} \right\rangle = null;\ \left\langle \mathbf{F}^i_{equu3} \right\rangle = null;\ \left\langle \mathbf{F}^i_{eqpp3} \right\rangle = null;\ \left\langle \mathbf{F}^i_{eqxu3} \right\rangle = null;
$$

$$
\left\langle \mathbf{F}^i_{equp3} \right\rangle = null;
$$

where $\mathbf{I}_4$ is the identity matrix with the dimension of 4.

C.7 Section *k*, Transmission Line Model with the Total Length of the Line, the Average Distance between Phase Conductors and the Average Height of Phase Conductors as Three Parameters

The model of section *k* is described in Figure C.9.

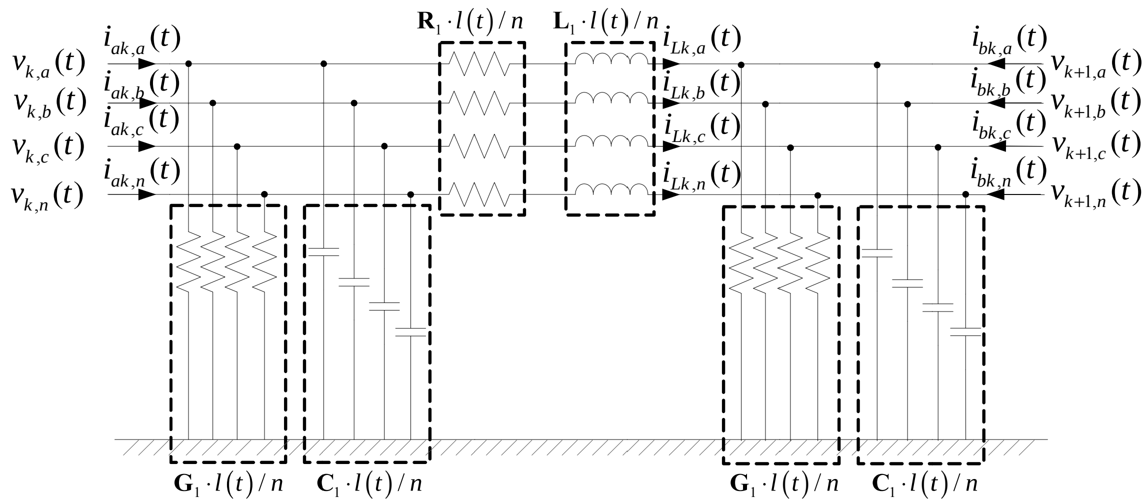

Figure C.9. Section *k* model with the total length of the line, the average distance between phase conductors and the average height of phase conductors as three parameters

where $\boldsymbol{R}_1$, $\boldsymbol{L}_1$, $\boldsymbol{G}_1$ and $\boldsymbol{C}_1$ are series resistance, series inductance, shunt conductance and shunt capacitance per mile; $l(t)$ is the total length of the line; $d(t)$ is the average distance between phase conductors; $h(t)$ is the average height of phase conductors.

In addition, linearize the above $\boldsymbol{R}_1$, $\boldsymbol{L}_1$, $\boldsymbol{G}_1$ and $\boldsymbol{C}_1$ matrices around the initial value of the average distance between phase conductors d_0 and the average height of phase conductors h_0 (the value of the above matrices with distance d_0 and height h_0 are $\boldsymbol{R}_1^{(0)}$, $\boldsymbol{L}_1^{(0)}$, $\boldsymbol{G}_1^{(0)}$ and $\boldsymbol{C}_1^{(0)}$).

$$\mathbf{R}_1 = \mathbf{R}_1^{(0)} + \boldsymbol{\alpha}_R \cdot \left(h(t) - h_0\right) + \boldsymbol{\beta}_R \cdot \left(d(t) - d_0\right) \tag{C.66}$$

$$\mathbf{L}_1 = \mathbf{L}_1^{(0)} + \boldsymbol{\alpha}_L \cdot \left(h(t) - h_0\right) + \boldsymbol{\beta}_L \cdot \left(d(t) - d_0\right) \tag{C.67}$$

$$\mathbf{C}_1 = \mathbf{C}_1^{(0)} + \boldsymbol{\alpha}_C \cdot \left(h(t) - h_0\right) + \boldsymbol{\beta}_C \cdot \left(d(t) - d_0\right) \tag{C.68}$$

$$\mathbf{G}_1 = \mathbf{G}_1^{(0)} + \boldsymbol{\alpha}_G \cdot \left(h(t) - h_0\right) + \boldsymbol{\beta}_G \cdot \left(d(t) - d_0\right) \tag{C.69}$$

All states and through variables are defined in Table C.19, Table C.20 and Table C.21, respectively.

Table C.19. States of section *k* model with the length, the average distance between phase conductors and the average height of phase conductors as three parameters

Index	Variable	Description
0	$v_{k,a}(t)$	phase A voltage, left terminal
1	$v_{k,b}(t)$	phase B voltage, left terminal
2	$v_{k,c}(t)$	phase C voltage, left terminal
3	$v_{k,n}(t)$	phase N voltage, left terminal
4	$v_{k+1,a}(t)$	phase A voltage, right terminal
5	$v_{k+1,b}(t)$	phase B voltage, right terminal
6	$v_{k+1,c}(t)$	phase C voltage, right terminal
7	$v_{k+1,n}(t)$	phase N voltage, right terminal
8	$i_{Lk,a}(t)$	phase A current through inductance
9	$i_{Lk,b}(t)$	phase B current through inductance
10	$i_{Lk,c}(t)$	phase C current through inductance
11	$i_{Lk,n}(t)$	phase N current through inductance
12	$y_{vk,a}(t)$	Introduced state for quadratization, phase A voltage times $l(t)$, left terminal
13	$y_{vk,b}(t)$	Introduced state for quadratization, phase B voltage times $l(t)$, left terminal

Table C.19. continued

14	$y_{vk,c}(t)$	Introduced state for quadratization, phase C voltage times $l(t)$, left terminal
15	$y_{vk,n}(t)$	Introduced state for quadratization, phase N voltage times $l(t)$, left terminal
16	$y_{v(k+1),a}(t)$	Introduced state for quadratization, phase A voltage times $l(t)$, right terminal
17	$y_{v(k+1),b}(t)$	Introduced state for quadratization, phase B voltage times $l(t)$, right terminal
18	$y_{v(k+1),c}(t)$	Introduced state for quadratization, phase C voltage times $l(t)$, right terminal
19	$y_{v(k+1),n}(t)$	Introduced state for quadratization, phase N voltage times $l(t)$, right terminal
20	$y_{Lk,a}(t)$	Introduced state for quadratization, phase A current through inductance times $l(t)$
21	$y_{Lk,b}(t)$	Introduced state for quadratization, phase B current through inductance times $l(t)$
22	$y_{Lk,c}(t)$	Introduced state for quadratization, phase C current through inductance times $l(t)$
23	$y_{Lk,n}(t)$	Introduced state for quadratization, phase N current through inductance times $l(t)$
24	$z_{vk,a}(t)$	Introduced state for quadratization, phase A voltage times $l(t)$ times $d(t)$, left terminal
25	$z_{vk,b}(t)$	Introduced state for quadratization, phase B voltage times $l(t)$ times $d(t)$, left terminal
26	$z_{vk,c}(t)$	Introduced state for quadratization, phase C voltage times $l(t)$ times $d(t)$, left terminal
27	$z_{vk,n}(t)$	Introduced state for quadratization, phase N voltage times $l(t)$ times $d(t)$, left terminal
28	$z_{v(k+1),a}(t)$	Introduced state for quadratization, phase A voltage times $l(t)$ times $d(t)$, right terminal
29	$z_{v(k+1),b}(t)$	Introduced state for quadratization, phase B voltage times $l(t)$ times $d(t)$, right terminal
30	$z_{v(k+1),c}(t)$	Introduced state for quadratization, phase C voltage times $l(t)$ times $d(t)$, right terminal
31	$z_{v(k+1),n}(t)$	Introduced state for quadratization, phase N voltage times $l(t)$ times $d(t)$, right terminal
32	$z_{Lk,a}(t)$	Introduced state for quadratization, phase A current through inductance times $l(t)$ times $d(t)$
33	$z_{Lk,b}(t)$	Introduced state for quadratization, phase B current through inductance times $l(t)$ times $d(t)$

Table C.19. continued

34	$z_{Lk,c}(t)$	Introduced state for quadratization, phase C current through inductance times $l(t)$ times $d(t)$
35	$z_{Lk,n}(t)$	Introduced state for quadratization, phase N current through inductance times $l(t)$ times $d(t)$
36	$w_{vk,a}(t)$	Introduced state for quadratization, phase A voltage times $l(t)$ times $h(t)$, left terminal
37	$w_{vk,b}(t)$	Introduced state for quadratization, phase B voltage times $l(t)$ times $h(t)$, left terminal
38	$w_{vk,c}(t)$	Introduced state for quadratization, phase C voltage times $l(t)$ times $h(t)$, left terminal
39	$w_{vk,n}(t)$	Introduced state for quadratization, phase N voltage times $l(t)$ times $h(t)$, left terminal
40	$w_{v(k+1),a}(t)$	Introduced state for quadratization, phase A voltage times $l(t)$ times $h(t)$, right terminal
41	$w_{v(k+1),b}(t)$	Introduced state for quadratization, phase B voltage times $l(t)$ times $h(t)$, right terminal
42	$w_{v(k+1),c}(t)$	Introduced state for quadratization, phase C voltage times $l(t)$ times $h(t)$, right terminal
43	$w_{v(k+1),n}(t)$	Introduced state for quadratization, phase N voltage times $l(t)$ times $h(t)$, right terminal
44	$w_{Lk,a}(t)$	Introduced state for quadratization, phase A current through inductance times $l(t)$ times $h(t)$
45	$w_{Lk,b}(t)$	Introduced state for quadratization, phase B current through inductance times $l(t)$ times $h(t)$
46	$w_{Lk,c}(t)$	Introduced state for quadratization, phase C current through inductance times $l(t)$ times $h(t)$
47	$w_{Lk,n}(t)$	Introduced state for quadratization, phase N current through inductance times $l(t)$ times $h(t)$

Table C.20. Parameters of section *k* model with the length, the average distance between phase conductors and the average height of phase conductors as three parameters

Index	Variable	Description
0	$d(t)$	Average distance between phase conductors
0	$h(t)$	Average height of phase conductors

Table C.21. Through variables of section k model with the length, the average distance between phase conductors and the average height of phase conductors as three parameters

Index	Variable	Description
0	$i_{ak,a}(t)$	phase A current, left terminal
1	$i_{ak,b}(t)$	phase B current, left terminal
2	$i_{ak,c}(t)$	phase C current, left terminal
3	$i_{ak,n}(t)$	phase N current, left terminal
4	$i_{bk,a}(t)$	phase A current, left terminal
5	$i_{bk,b}(t)$	phase B current, left terminal
6	$i_{bk,c}(t)$	phase C current, left terminal
7	$i_{bk,n}(t)$	phase N current, left terminal

Define $\mathbf{i}_{Lk}(t)$ as the three phase and neutral current through the series inductance; $\boldsymbol{y}_{vk}(t)$, $\boldsymbol{y}_{v(k+1)}(t)$, $\boldsymbol{y}_{Lk}(t)$, $\boldsymbol{z}_{vk}(t)$, $\boldsymbol{z}_{v(k+1)}(t)$, $\boldsymbol{z}_{Lk}(t)$, $\boldsymbol{w}_{vk}(t)$, $\boldsymbol{w}_{v(k+1)}(t)$, and $\boldsymbol{w}_{Lk}(t)$ are introduced states for quadratization; recall the definitions of $\mathbf{i}_{ak}(t)$, $\mathbf{v}_k(t)$, $\mathbf{i}_{bk}(t)$ and $\mathbf{v}_{k+1}(t)$: three phase and neutral current and voltage vectors at each terminal of section k. That means,

$$\mathbf{v}_k(t)=\begin{bmatrix} v_{k,a}(t) \\ v_{k,b}(t) \\ v_{k,c}(t) \\ v_{k,n}(t) \end{bmatrix},\quad \mathbf{v}_{k+1}(t)=\begin{bmatrix} v_{k+1,a}(t) \\ v_{k+1,b}(t) \\ v_{k+1,c}(t) \\ v_{k+1,n}(t) \end{bmatrix},\quad \mathbf{i}_{Lk}(t)=\begin{bmatrix} i_{Lk,a}(t) \\ i_{Lk,b}(t) \\ i_{Lk,c}(t) \\ i_{Lk,n}(t) \end{bmatrix},$$

$$\mathbf{y}_{vk}(t)=\begin{bmatrix} y_{vk,a}(t) \\ y_{vk,b}(t) \\ y_{vk,c}(t) \\ y_{vk,n}(t) \end{bmatrix},\quad \mathbf{y}_{v(k+1)}(t)=\begin{bmatrix} y_{v(k+1),a}(t) \\ y_{v(k+1),b}(t) \\ y_{v(k+1),c}(t) \\ y_{v(k+1),n}(t) \end{bmatrix},\quad \mathbf{y}_{Lk}(t)=\begin{bmatrix} y_{Lk,a}(t) \\ y_{Lk,b}(t) \\ y_{Lk,c}(t) \\ y_{Lk,n}(t) \end{bmatrix},$$

$$\mathbf{z}_{vk}(t)=\begin{bmatrix} z_{vk,a}(t)\\ z_{vk,b}(t)\\ z_{vk,c}(t)\\ z_{vk,n}(t)\end{bmatrix},\quad \mathbf{z}_{v(k+1)}(t)=\begin{bmatrix} z_{v(k+1),a}(t)\\ z_{v(k+1),b}(t)\\ z_{v(k+1),c}(t)\\ z_{v(k+1),n}(t)\end{bmatrix},\quad \mathbf{z}_{Lk}(t)=\begin{bmatrix} z_{Lk,a}(t)\\ z_{Lk,b}(t)\\ z_{Lk,c}(t)\\ z_{Lk,n}(t)\end{bmatrix},$$

$$\mathbf{w}_{vk}(t)=\begin{bmatrix} w_{vk,a}(t)\\ w_{vk,b}(t)\\ w_{vk,c}(t)\\ w_{vk,n}(t)\end{bmatrix},\quad \mathbf{w}_{v(k+1)}(t)=\begin{bmatrix} w_{v(k+1),a}(t)\\ w_{v(k+1),b}(t)\\ w_{v(k+1),c}(t)\\ w_{v(k+1),n}(t)\end{bmatrix},\quad \mathbf{w}_{Lk}(t)=\begin{bmatrix} w_{Lk,a}(t)\\ w_{Lk,b}(t)\\ w_{Lk,c}(t)\\ w_{Lk,n}(t)\end{bmatrix},$$

$$\mathbf{i}_{ak}(t)=\begin{bmatrix} i_{ak,a}(t)\\ i_{ak,b}(t)\\ i_{ak,c}(t)\\ i_{ak,n}(t)\end{bmatrix},\quad \mathbf{i}_{bk}(t)=\begin{bmatrix} i_{bk,a}(t)\\ i_{bk,b}(t)\\ i_{bk,c}(t)\\ i_{bk,n}(t)\end{bmatrix}.$$

The transmission line section k model can be formulated in compact form as follows:

$$\begin{aligned}\mathbf{i}_{ak}(t)=&\frac{\mathbf{G}_1^{(0)}-\boldsymbol{\alpha}_G h_0-\boldsymbol{\beta}_G d_0}{n}\cdot\mathbf{y}_{vk}(t)+\frac{\boldsymbol{\beta}_G}{n}\cdot\mathbf{z}_{vk}(t)+\frac{\boldsymbol{\alpha}_G}{n}\cdot\mathbf{w}_{vk}(t)\\ &+\frac{\mathbf{C}_1^{(0)}-\boldsymbol{\alpha}_C h_0-\boldsymbol{\beta}_C d_0}{n}\cdot\frac{d\mathbf{y}_{vk}(t)}{dt}+\frac{\boldsymbol{\beta}_C}{n}\cdot\frac{d\mathbf{z}_{vk}(t)}{dt}+\frac{\boldsymbol{\alpha}_C}{n}\cdot\frac{d\mathbf{w}_{vk}(t)}{dt}+\mathbf{i}_{Lk}(t)\end{aligned}\tag{C.70}$$

$$\begin{aligned}\mathbf{i}_{bk}(t)=&\frac{\mathbf{G}_1^{(0)}-\boldsymbol{\alpha}_G h_0-\boldsymbol{\beta}_G d_0}{n}\cdot\mathbf{y}_{v(k+1)}(t)+\frac{\boldsymbol{\beta}_G}{n}\cdot\mathbf{z}_{v(k+1)}(t)+\frac{\boldsymbol{\alpha}_G}{n}\cdot\mathbf{w}_{v(k+1)}(t)\\ &+\frac{\mathbf{C}_1^{(0)}-\boldsymbol{\alpha}_C h_0-\boldsymbol{\beta}_C d_0}{n}\cdot\frac{d\mathbf{y}_{v(k+1)}(t)}{dt}+\frac{\boldsymbol{\beta}_C}{n}\cdot\frac{d\mathbf{z}_{v(k+1)}(t)}{dt}+\frac{\boldsymbol{\alpha}_C}{n}\cdot\frac{d\mathbf{w}_{v(k+1)}(t)}{dt}-\mathbf{i}_{Lk}(t)\end{aligned}\tag{C.71}$$

$$\begin{aligned}\mathbf{0}=&-\mathbf{v}_k(t)+\mathbf{v}_{k+1}(t)+\frac{\mathbf{R}_1^{(0)}-\boldsymbol{\alpha}_R h_0-\boldsymbol{\beta}_R d_0}{n}\cdot\mathbf{y}_{Lk}(t)+\frac{\boldsymbol{\beta}_R}{n}\cdot\mathbf{z}_{Lk}(t)+\frac{\boldsymbol{\alpha}_R}{n}\cdot\mathbf{w}_{Lk}(t)\\ &+\frac{\mathbf{L}_1^{(0)}-\boldsymbol{\alpha}_L h_0-\boldsymbol{\beta}_L d_0}{n}\cdot\frac{d\mathbf{y}_{Lk}(t)}{dt}+\frac{\boldsymbol{\beta}_L l}{n}\cdot\frac{d\mathbf{z}_{Lk}(t)}{dt}+\frac{\boldsymbol{\alpha}_L l}{n}\cdot\frac{d\mathbf{w}_{Lk}(t)}{dt}\end{aligned}\tag{C.72}$$

$$\mathbf{0}=\mathbf{y}_{vk}(t)-\mathbf{v}_k(t)\cdot l(t)\tag{C.73}$$

$$\mathbf{0}=\mathbf{y}_{v(k+1)}(t)-\mathbf{v}_{k+1}(t)\cdot l(t)\tag{C.74}$$

$$\mathbf{0} = \mathbf{y}_{Lk}(t) - \mathbf{i}_{Lk}(t) \cdot l(t) \tag{C.75}$$

$$\mathbf{0} = \mathbf{z}_{vk}(t) - \mathbf{y}_{vk}(t) \cdot d(t) \tag{C.76}$$

$$\mathbf{0} = \mathbf{z}_{v(k+1)}(t) - \mathbf{y}_{v(k+1)}(t) \cdot d(t) \tag{C.77}$$

$$\mathbf{0} = \mathbf{z}_{Lk}(t) - \mathbf{y}_{Lk}(t) \cdot d(t) \tag{C.78}$$

$$\mathbf{0} = \mathbf{w}_{vk}(t) - \mathbf{y}_{vk}(t) \cdot h(t) \tag{C.79}$$

$$\mathbf{0} = \mathbf{w}_{v(k+1)}(t) - \mathbf{y}_{v(k+1)}(t) \cdot h(t) \tag{C.80}$$

$$\mathbf{0} = \mathbf{w}_{Lk}(t) - \mathbf{y}_{Lk}(t) \cdot h(t) \tag{C.81}$$

The matrices corresponding to the SCPQDM of section k, transmission line model with the total length of the line, the average distance between phase conductors and the average height of phase conductors as parameters are:

$$\boldsymbol{x}(t) = \begin{bmatrix} \boldsymbol{v}_k(t) & \boldsymbol{v}_{k+1}(t) & \boldsymbol{i}_{Lk}(t) & \boldsymbol{y}_{vk}(t) & \boldsymbol{y}_{v(k+1)}(t) & \boldsymbol{y}_{Lk}(t) & \boldsymbol{z}_{vk}(t) & \boldsymbol{z}_{v(k+1)}(t) & \boldsymbol{z}_{Lk}(t) & \boldsymbol{w}_{vk}(t) & \boldsymbol{w}_{v(k+1)}(t) & \boldsymbol{w}_{Lk}(t) \end{bmatrix}^T;$$

$$\boldsymbol{i}(t) = \begin{bmatrix} \boldsymbol{i}_{ak}(t) & \boldsymbol{i}_{bk}(t) \end{bmatrix}^{\mathrm{T}}; \ \boldsymbol{p}(t) = \begin{bmatrix} l(t) & d(t) & h(t) \end{bmatrix}^T;$$

$$\boldsymbol{Y}_{eqx1} = \begin{bmatrix} \mathbf{0} & \mathbf{0} & \boldsymbol{I}_4 & \dfrac{\boldsymbol{G}_1^{(0)} - \boldsymbol{\alpha}_G h_0 - \boldsymbol{\beta}_G d_0}{n} & \mathbf{0} & \mathbf{0} & \dfrac{\boldsymbol{\beta}_G}{n} & \mathbf{0} & \mathbf{0} & \dfrac{\boldsymbol{\alpha}_G}{n} & \mathbf{0} & \mathbf{0} \\ \mathbf{0} & \mathbf{0} & -\boldsymbol{I}_4 & \mathbf{0} & \dfrac{\boldsymbol{G}_1^{(0)} - \boldsymbol{\alpha}_G h_0 - \boldsymbol{\beta}_G d_0}{n} & \mathbf{0} & \mathbf{0} & \dfrac{\boldsymbol{\beta}_G}{n} & \mathbf{0} & \mathbf{0} & \dfrac{\boldsymbol{\alpha}_G}{n} & \mathbf{0} \end{bmatrix};$$

$$\boldsymbol{D}_{eqxd1} = \begin{bmatrix} \mathbf{0} & \mathbf{0} & \mathbf{0} & \dfrac{\boldsymbol{C}_1^{(0)} - \boldsymbol{\alpha}_C h_0 - \boldsymbol{\beta}_C d_0}{n} & \mathbf{0} & \mathbf{0} & \dfrac{\boldsymbol{\beta}_C}{n} & \mathbf{0} & \mathbf{0} & \dfrac{\boldsymbol{\alpha}_C}{n} & \mathbf{0} & \mathbf{0} \\ \mathbf{0} & \mathbf{0} & \mathbf{0} & \mathbf{0} & \dfrac{\boldsymbol{C}_1^{(0)} - \boldsymbol{\alpha}_C h_0 - \boldsymbol{\beta}_C d_0}{n} & \mathbf{0} & \mathbf{0} & \dfrac{\boldsymbol{\beta}_C}{n} & \mathbf{0} & \mathbf{0} & \dfrac{\boldsymbol{\alpha}_C}{n} & \mathbf{0} \end{bmatrix};$$

$$\boldsymbol{Y}_{eqx2}=\begin{bmatrix}-\boldsymbol{I}_4 & \boldsymbol{I}_4 & \mathbf{0} & \mathbf{0} & \mathbf{0} & \dfrac{\boldsymbol{R}_1^{(0)}-\boldsymbol{\alpha}_R h_0-\boldsymbol{\beta}_R d_0}{n} & \mathbf{0} & \mathbf{0} & \dfrac{\boldsymbol{\beta}_R}{n} & \mathbf{0} & \mathbf{0} & \dfrac{\boldsymbol{\alpha}_R}{n}\end{bmatrix};$$

$$\boldsymbol{D}_{eqxd2}==\begin{bmatrix}\mathbf{0} & \mathbf{0} & \mathbf{0} & \mathbf{0} & \mathbf{0} & \dfrac{\boldsymbol{L}_1^{(0)}-\boldsymbol{\alpha}_L h_0-\boldsymbol{\beta}_L d_0}{n} & \mathbf{0} & \mathbf{0} & \dfrac{\boldsymbol{\beta}_L}{n} & \mathbf{0} & \mathbf{0} & \dfrac{\boldsymbol{\alpha}_L}{n}\end{bmatrix};$$

$$\boldsymbol{Y}_{eqx3}=\begin{bmatrix}
\mathbf{0} & \mathbf{0} & \mathbf{0} & \boldsymbol{I}_4 & \mathbf{0} & \mathbf{0} & \mathbf{0} & \mathbf{0} & \mathbf{0} & \mathbf{0} & \mathbf{0} & \mathbf{0}\\
\mathbf{0} & \mathbf{0} & \mathbf{0} & \mathbf{0} & \boldsymbol{I}_4 & \mathbf{0} & \mathbf{0} & \mathbf{0} & \mathbf{0} & \mathbf{0} & \mathbf{0} & \mathbf{0}\\
\mathbf{0} & \mathbf{0} & \mathbf{0} & \mathbf{0} & \mathbf{0} & \boldsymbol{I}_4 & \mathbf{0} & \mathbf{0} & \mathbf{0} & \mathbf{0} & \mathbf{0} & \mathbf{0}\\
\mathbf{0} & \mathbf{0} & \mathbf{0} & \mathbf{0} & \mathbf{0} & \mathbf{0} & \boldsymbol{I}_4 & \mathbf{0} & \mathbf{0} & \mathbf{0} & \mathbf{0} & \mathbf{0}\\
\mathbf{0} & \mathbf{0} & \mathbf{0} & \mathbf{0} & \mathbf{0} & \mathbf{0} & \mathbf{0} & \boldsymbol{I}_4 & \mathbf{0} & \mathbf{0} & \mathbf{0} & \mathbf{0}\\
\mathbf{0} & \mathbf{0} & \mathbf{0} & \mathbf{0} & \mathbf{0} & \mathbf{0} & \mathbf{0} & \mathbf{0} & \boldsymbol{I}_4 & \mathbf{0} & \mathbf{0} & \mathbf{0}\\
\mathbf{0} & \mathbf{0} & \mathbf{0} & \mathbf{0} & \mathbf{0} & \mathbf{0} & \mathbf{0} & \mathbf{0} & \mathbf{0} & \boldsymbol{I}_4 & \mathbf{0} & \mathbf{0}\\
\mathbf{0} & \mathbf{0} & \mathbf{0} & \mathbf{0} & \mathbf{0} & \mathbf{0} & \mathbf{0} & \mathbf{0} & \mathbf{0} & \mathbf{0} & \boldsymbol{I}_4 & \mathbf{0}\\
\mathbf{0} & \mathbf{0} & \mathbf{0} & \mathbf{0} & \mathbf{0} & \mathbf{0} & \mathbf{0} & \mathbf{0} & \mathbf{0} & \mathbf{0} & \mathbf{0} & \boldsymbol{I}_4
\end{bmatrix};$$

$$\boldsymbol{F}_{eqpx3}^{i}: f_{eq[1][i]}=-1,\ others\ are\ 0,\ for\ i=1\sim 12;$$

$$\boldsymbol{F}_{eqpx3}^{i}: f_{eq[2][i]}=-1,\ others\ are\ 0,\ for\ i=13\sim 24;$$

$$\boldsymbol{F}_{eqpx3}^{i}: f_{eq[3][i-12]}=-1,\ others\ are\ 0,\ for\ i=25\sim 36;$$

$$\mathbf{Y}_{equ1}=null;\ \mathbf{Y}_{eqp1}=null;\ \mathbf{C}_{eqc1}=\mathbf{0};\ \mathbf{Y}_{equ2}=null;\ \mathbf{Y}_{eqp2}=null;\ \mathbf{C}_{eqc2}=\mathbf{0};\ \mathbf{Y}_{equ3}=null;$$

$$\mathbf{Y}_{eqp3}=null;\ \boldsymbol{C}_{eqc3}=\mathbf{0};\ \left\langle\mathbf{F}_{eqxx3}^{i}\right\rangle=null;\ \left\langle\mathbf{F}_{equu3}^{i}\right\rangle=null;\ \left\langle\mathbf{F}_{eqpp3}^{i}\right\rangle=null;\ \left\langle\mathbf{F}_{eqxu3}^{i}\right\rangle=null;$$

$$\left\langle\mathbf{F}_{equp3}^{i}\right\rangle=null;$$

where $\mathbf{I}_4$ is the identity matrix with the dimension of 4.

Appendix D: Quadratic Integration

When solving algebraic and differential equations, we need to eliminate the differential terms (using some integration methods) so that the original equations can be converted into pure algebraic equations. In this dissertation, the quadratic integration method [36] is adopted. This method assumes that the curve under integration varies quadratically within the integration time window.

For example, as depicted in Figure D.1. The integration time window is $[t-h, t]$. Traditional trapezoidal integration method assumes that the curve varies linearly, and calculates the integration results based on $x(t)$ and $x(t-h)$. Quadratic integration calculates the integration results based on $x(t)$, $x(t_m)$ and $x(t-h)$ (with an additional value $x(t_m)$, where $t_m = t - h/2$), which improves the accuracy and numerical stability compared to trapezoidal integration. Detail results for quadratic integration are derived as follows.

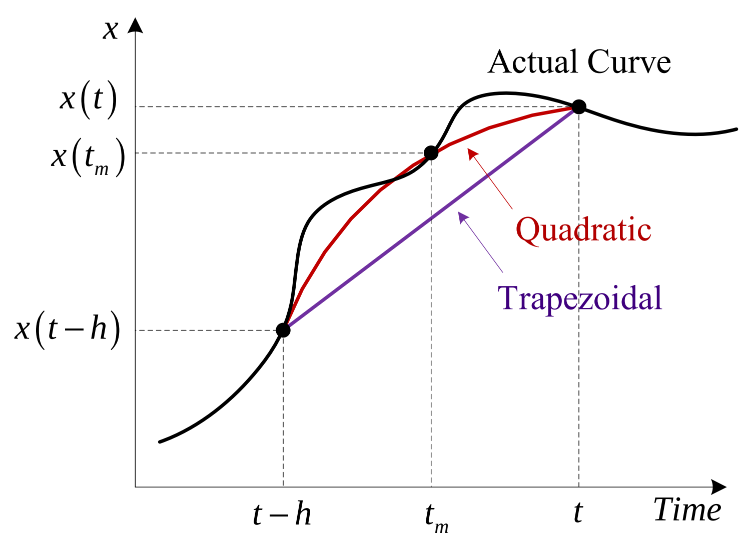

Figure D.1. Quadratic integration method

From Figure D.1, the red curve is a quadratic curve during the interval $[t-h,t]$. Therefore, the curve satisfies the following function:

$$x(\tau)=a\tau^2+b\tau+c \tag{D.1}$$

Also, the above curve passes 3 points: $\left((t-h),x(t-h)\right)$, $\left(t_m,x(t_m)\right)$, and $\left(t,\ x(t)\right)$, that means:

$$at^2+bt+c=x(t)$$

$$at^2+bt+c=x(t) \tag{D.2}$$

$$a(t-h/2)^2+b(t-h/2)+c=x(t_m) \tag{D.3}$$

$$a(t-h)^2+b(t-h)+c=x(t-h) \tag{D.4}$$

We can therefore calculate the corresponding coefficients of the quadratic curve,

$$a=-\frac{2}{h^2}\left(2x(t_m)-x(t)-x(t-h)\right) \tag{D.5}$$

$$b=\frac{2}{h}\left(\frac{3}{2}x(t)-2x(t_m)+\frac{1}{2}x(t-h)+\frac{2t}{h}\left(2x(t_m)-x(t)-x(t-h)\right)\right) \tag{D.6}$$

$$c=x(t)+\frac{t}{h}\left(4x(t_m)-3x(t)-x(t-h)\right)-\frac{2t^2}{h^2}\left(2x(t_m)-x(t)-x(t-h)\right) \tag{D.7}$$

For the integration of $x(t)$ from $[t-h,t]$,

$$\int_{t-h}^{t}x(t)dt=\left(\frac{1}{3}at^3+\frac{1}{2}bt^2+ct\right)\Bigg|_{t-h}^{t}=a(t^2h-th^2+\frac{1}{3}h^3)+b(th-\frac{1}{2}h^2)+ch \tag{D.8}$$

By substituting (D.5), (D.6) and (D.7), we have,

$$\int_{t-h}^{t}x(t)dt=\frac{1}{6}hx(t)+\frac{2}{3}hx(t_m)+\frac{1}{6}hx(t-h) \tag{D.9}$$

Similarly, for the integration of $x(t)$ from $[t-h, t_m]$,

$$\int_{t-h}^{t-\frac{h}{2}} x(t)dt = (\frac{1}{3}at^3 + \frac{1}{2}bt^2 + ct)\Bigg|_{t-h}^{t-\frac{h}{2}} = a(\frac{1}{2}t^2h - \frac{3}{4}th^2 + \frac{7}{24}h^3) + b(\frac{1}{2}th - \frac{3}{8}h^2) + c\frac{h}{2} \quad \text{(D.10)}$$

By substituting (D.5), (D.6) and (D.7), we have,

$$\int_{t-h}^{t-\frac{h}{2}} x(t)dt = -\frac{1}{24}hx(t) + \frac{1}{3}hx(t_m) + \frac{5}{24}hx(t-h) \quad \text{(D.11)}$$

Appendix E: Validation of Multi-section Transmission Line Model

This Appendix provides a comparison between the multi-section transmission line model and the fully distributed, frequency dependent line model [46]. Because of space limitations, the comparison is limited to an energization event. The test system consists of a source, a line and a load as shown in Figure E.1. The line is modelled with the multi-section model in one case and with the distributed, frequency dependent model in the other case. The results during line energization for both cases are shown for the period 0 seconds to 2 milli-seconds.

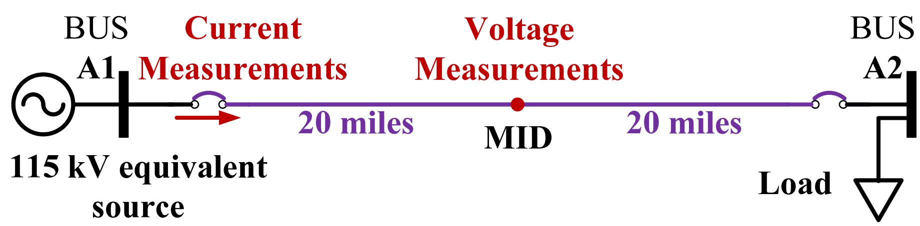

Figure E.1. Example test system for multi-section transmission line model validation

The currents at the output of the source and the voltages at the middle point of the transmission line, for both cases, are depicted in Figure. E.2 and Figure E.3. It can be observed that the currents have the maximum difference of less than 1.3% while the voltages have the maximum difference of less than 2%. It is concluded that even for this severe transient event, the accuracy of the model is very good as compared to the distributed, frequency dependent line model.

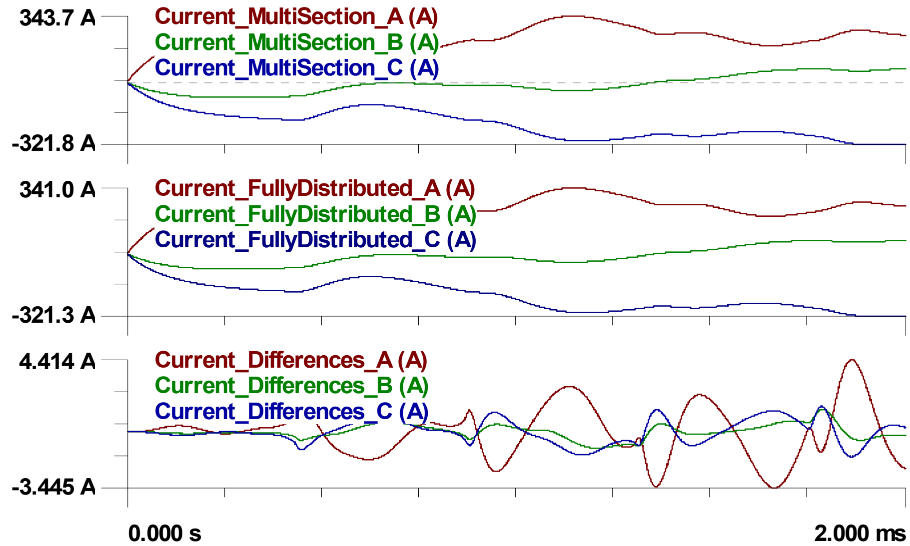

Figure E.2. Simulation results: currents at the output of the source, multi-section model, fully distributed model and their differences

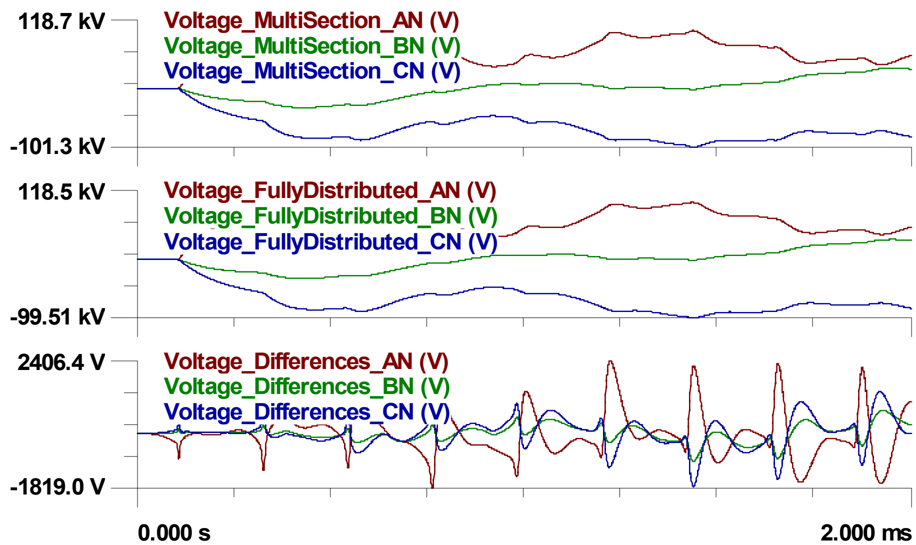

Figure E.3. Simulation results: voltages at the midpoint of the line, multi-section model, fully distributed model and their differences

REFERENCES

[1] A. J. Urdaneta, H. Restrepo, S. Marquez, and J. Sanchez," Coordination of Directional Overcurrent Relay Timing Using Linear Programming technique," in *IEEE Transactions on Power Delivery*, vol. 11, pp. 122-129, Jan. 1996.

[2] A. S. Noghabi, J. Sadeh, and H. R. Mashhadi, "Considering different network topologies in optimal overcurrent relay coordination using a hybrid ga," in *IEEE Transactions on Power Delivery*, vol. 24, no. 4, pp. 1857–1863, Oct. 2009.

[3] Mann, B.J.; Morrison, I.F. "Digital Calculation of Impedance for Transmission Line Protection" in *IEEE Transactions on Power Apparatus and Systems*, vol PAS-90, no.1 pp. 270-279, Jan. 1971.

[4] K. K. Li, L. L. Lai, and A. K. David, "Stand alone intelligent digital distance relay," in *IEEE Transactions on Power Delivery*, vol. 15, no. 1, pp. 137–142, Feb. 2000.

[5] T.F. Gallen, W.D. Breingan, M.M. Chen, "A digital system for directional - comparison relaying", in *IEEE Transactions on Power Apparatus and Systems*, vol PAS-98, no.3 pp. 948-956, May. 1979.

[6] M. Lucia, R. Cezari, D. Erwin, J.C.Theron, and M. Thakur, "Perfecting performance of distance protective relays and its associated pilot protection schemes in extra high voltage (EHV) transmission line applications", in *59th Annual Conference for Protective Relay Engineers*, College Station, TX, Apr. 2006.

[7] E. Bartosiewicz, R. Kowalik and M. Januszewski, "Overview and test results of modern pilot schemes for coordination of line distance protection relays", in *12th International Conference on Environment and Electrical Engineering (EEEIC)*, pp. 191-196, Wroclaw, Poland, May, 2013.

[8] *SEL-387L Relay Instruction Manual*, Schweitzer Engineering Laboratories, Inc., Pullman, WA, 2011.

[9] S. He, J. Suonan, Z.Q. Bo, " Integrated Impedance-Based Pilot Protection Scheme for the TCSC-Compensated EHV/UHV Transmission Lines ", in *IEEE Transactions on Power Delivery*, vol. 28, no.2, pp. 835-844, Apr. 2013.

[10] A. Newbould and I. A. Taylor, "Series compensated line protection: System modeling and relay testing," in *4th IEE International Conference on Developments in Power System Protection*, 1989, pp. 182–186.

[11] A.K. Pradhan, ; A. Routray, S. Pati, D.K. Pradhan, "Wavelet fuzzy combined approach for fault classification of a series-compensated transmission line", in *IEEE Transactions on Power Delivery*, vol. 19, no. 4, pp. 1612-1618, Oct. 2004.

[12] N. Perera and A. D. Rajapakse, "Series-compensated double-circuit transmission-line protection using directions of current transients," in *IEEE Transactions on Power Delivery*, vol. 28, no. 3, pp. 1566–1575, Jul. 2013.

[13] M. M. Saha, B. Kastenny, E. Rosolowski, and J. Izykowski, "First zone algorithm for protection of series compensated lines," in *IEEE Transactions on Power Delivery*, vol. 16, pp. 200–207, Apr. 2001.

[14] T.S.Sidhu, M. Khederzadeh, " Series compensated line protection enhancement by modified pilot relaying schemes," in *IEEE Transactions on Power Delivery*, vol.21, no. 3, pp. 1191-1198, July. 2006.

[15] H. J. Altuve, J. B. Mooney, and G. E. Alexander, "Advances in series-compensated line protection," in 62nd Annual Conference for Protective Relay Engineers, Austin, TX, Mar. 2009.

[16] *SEL-351 Protection System Instruction Manual*, Schweitzer Engineering Laboratories Inc., Pullman, WA, 2015.

[17] *GE D90^{Plus} Line Distance Protection System Instruction Manual*, General Electric Multilin, Markham, Ontario, Canada, 2012.

[18] *Siemens SIPROTEC Line Differential Protection with Distance Protection 7SD5,*

Version 4.70, Siemens, Munich, Bavaria, Germany, 2011.

[19] L. Ericson, M. M. Saha, and G. D. Rockeffeler, “An accurate fault locator with compensation for apparent reactance in the fault resistance resulting from remote-end infeed,” in *IEEE Transactions on Power Apparatus and Systems*, vol. PAS-104, pp. 424–435, July 1985.

[20] H. Ha, B. Zhang and Z. Lv, "A novel principle of single-ended fault location technique for EHV transmission lines", in *IEEE Transactions on Power Delivery*, vol.18, no.4, pp. 1147- 1151, Oct. 2003.

[21] T. Kawady and J. Stenzel, “A practical fault location approach for double circuit transmission lines using single end data,” in *IEEE Transactions on Power Delivery*, vol. 18, no. 4, pp. 1166–1173, Oct. 2003.

[22] J. Izykowski, R. Molag, E. Rosolowski, and M. M. Saha, “Accurate location of faults on power transmission lines with use of two-end unsynchronized measurements,” in *IEEE Transactions on Power Delivery*, vol. 21, no. 2, pp. 627–633, Apr. 2006.

[23] S. M. Brahma and A. A. Girgis, “Fault location on a transmission line using synchronized voltage measurements,” in *IEEE Transactions on Power Delivery*, vol. 19, no.4, pp. 1619-1622, Oct. 2004.

[24] M. M. Saha, J. Izykowski, and E. Rosolowski, “A two-ended method of fault location immune to saturation of current transformers,” in *8th IEE International Conference on Developments in Power System Protection*, pp. 172-175, 2004.

[25] D. Novosel, D.G. Hart, E.Udren, and J. Garitty, “Unsynchronized two-terminal fault location estimation,” in *IEEE Transactions on Power Delivery*, vol. 11, no. 1, pp.130-138, Jan. 1996.

[26] *SEL-411 Advanced Line Differential Protection, Automation, and Control System Instruction Manual*, Schweitzer Engineering Laboratories Inc., Pullman, WA, 2015.

[27] *Reason RPV311 Distributed Multifunction Fault Recorder Technical Manual*,

General Electric, Schenectady, NY, 2014

[28] IEEE Guide for Determining Fault Location on AC Transmission and Distribution Lines, IEEE Standard C37.114, 2014.

[29] S. Azizi, M. Sanaye-Pasand, M. Abedini, and A. Hassani, “A traveling wave-based methodology for wide-area fault location in multiterminal DC systems,” in *IEEE Transactions on Power Delivery*, vol. 29, no. 6, pp. 2552–2560, Dec. 2014.

[30] D. Spoor and J. G. Zhu, “Improved single-ended traveling-wave fault location algorithm based on experience with conventional substation transducers,” in *IEEE Transactions on Power Delivery*, vol. 21, no. 3, pp. 1714–1720, Jul. 2006.

[31] M. B. Dewe, S. Sankar, and J. Arrillaga, “The application of satellite time references to HVDC fault location,” in *IEEE Transactions on Power Delivery*, vol. 8, no. 3, pp. 1295–1302, Jul. 1993.

[32] P. Jafarian and M. Sanaye-Pasand, “A traveling wave based protection technique using wavelet/PCA analysis,” in *IEEE Transactions on Power Delivery*, vol. 25, no. 2, pp. 588–599, Apr. 2010.

[33] A. Abur and F. Magnago, “Fault location using wavelets,” in *IEEE Transactions on Power Delivery*, vol. 13, no. 4, pp. 1475–1480, Oct. 1988.

[34] C. Y. Evrenosoglu and A. Abur, “Traveling wave based fault location for teed circuits,” in *IEEE Transactions on Power Delivery*, vol. 20, no. 2, pt. 1, pp. 1115–1121, Apr. 2005.

[35] J. Suonan, S. Gao, and G. Song, “A Novel Fault-location Method for HVDC Transmission Lines,” in *IEEE Transactions on Power Delivery*, vol. 25, no. 2, pp. 1203–1209, Apr. 2010.

[36] A.P. Meliopoulos, G. Cokkinides and G. Stefopoulos, “Quadratic integration method,” in *Proceedings of the 2005 International Power System Transients Conference, pp. 19-23,* 2005.

[37] F. C. Schweppe,R. D. Masiello, "A Tracking Static State Estimator," in *IEEE Transactions on Power Apparatus and Systems*, vol. PAS-90, pp. 1025-1033, 1971.

[38] IEEE Guide for Application of Digital Line Current Differential Relays Using Digital Communication, in *IEEE Std C37.243-2015*, Aug. 7 2015.

[39] S. Das, S. Santoso, A. Gaikwad and M. Patel, "Impedance-based fault location in transmission networks: theory and application," *IEEE Access*, vol. 2, no. , pp. 537-557, 2014.

[40] Z. Y. He et al., "Dynamic fault locator for three-terminal transmission lines for phasor measurement units," *IET Generation Transmission & Distribution*, vol. 7, no. 2, pp. 183–191, Feb. 2013.

[41] R. K. Aggarwal, D. V. Coury, A. T. Johns, and A. Kalam, "A practical approach to accurate fault location on extra high voltage teed feeders," *IEEE Transactions on Power Delivery*, vol. 8, no. 3, pp. 874–883, Jul. 1993.

[42] A. A. Girgis, D. G. Hart, and W. L. Peterson, "A new fault location technique for two-and three-terminal lines," *IEEE Transactions on Power Delivery*, vol. 7, no. 1, pp. 98–107, Jan. 1992.

[43] Y. Lin, C. Liu, and C. Yu, "A new fault locator for three-terminal transmission lines using two-terminal synchronized voltage and current phasors," *IEEE Transactions on Power Delivery*, vol. 7, no. 3, pp. 452–459, Jul. 2002.

[44] J. Izykowski, E. Rosolowski, M. M. Saha, M. Fulczyk and P. Balcerek, "A Fault-Location Method for Application With Current Differential Relays of Three-Terminal Lines," *IEEE Transactions on Power Delivery*, vol. 22, no. 4, pp. 2099-2107, Oct. 2007.

[45] H. Livani and C. Y. Evrenosoglu, "A fault classification and localization method for three-terminal circuits using machine learning," *IEEE Transactions on Power Delivery*, vol. 28, no. 4, pp. 2282-2290, Oct. 2013.

[46] G. J. Cokkinides and A. P. Meliopoulos, “Transmission line modeling with explicit grounding representation,” *Electric Power Systems Research*, vol. 14, no.2, pp. 109-119, April 1988.

[47] Y. Liu, S. Meliopoulos, R. Fan and L. Sun, “Dynamic State Estimation Based Protection of Microgrid Circuits”, in *IEEE Power and Energy Society (PES) General Meeting*, 2015.

[48] S. Meliopoulos, G. J. Cokkinides, P. Myrda, Y. Liu, R. Fan, L. Sun, R. Huang and Z. Tan, “Dynamic State Estimation Based Protection: Status and Promise”, *IEEE Transactions on Power Delivery*, Vol 32, Issue 1, pp 320-330, Feb. 2017.

[49] Y. Liu, S. Meliopoulos, R. Fan, L. Sun and Z. Tan, “Dynamic State Estimation Based Protection on Series Compensated Transmission Lines”, *IEEE Transactions on Power Delivery*, in press.

[50] Y. Liu, S. Meliopoulos, L. Sun and R. Fan, “Dynamic State Estimation Based Protection on Mutually Coupled Transmission Lines”, *CSEE Journal of Power and Energy Systems*, vol.2, no.4, pp 6- 14, Dec. 2016.

[51] Y. Liu, S. Choi, S. Meliopoulos, R. Fan, L. Sun and Z. Tan, “Dynamic State Estimation Enabled Predictive Inverter Control”, in *IEEE Power and Energy Society (PES) General Meeting*, 2016.

[52] S. Meliopoulos, G. Cokkinides, Y. Liu, R. Fan, S. Choi and P. Myrda, “Protection and Control of Systems with Converter Interfaced Generation (CIG)”, in *49th Hawaii International Conference on System Sciences (HICSS)*, 2016.

[53] L. Sun, R. Fan, S. Meliopoulos, Y. Liu and Z. Tan, “Capacitor Bank Protection via Constraint WLS Dynamic State Estimation Method (CWLS-DSE) ”, in *North American Power Symposium (NAPS)*, 2016.

[54] R. Fan, S. Meliopoulos, L. Sun, Z. Tan and Y. Liu, “Transformer Inter-turn Faults Detection by Dynamic State Estimation Method”, in *North American Power Symposium (NAPS)*, 2016.

[55] R. Fan, S. Meliopoulos, G. J. Cokkinides, L, Sun and Y. Liu, "Dynamic State Estimation-based Protection of Power Transformers", in *IEEE Power and Energy Society (PES) General Meeting*, 2015.

[56] L. Sun, S. Meliopoulos, Y. Liu and B. Xie, "Dynamic State Estimation Based Synchronous Generator Model Calibration Using PMU Data", in *IEEE Power and Energy Society (PES) General Meeting*, 2017.

[57] Y. Liu, S. Meliopoulos, N. Tai, L. Sun and B. Xie, "Protection and Fault Locating Method of Series Compensated Lines by Wavelet Based Energy Traveling Wave", in *IEEE Power and Energy Society (PES) General Meeting*, 2017.